USGS
science for a changing world

Petrography and Mineralogy of Selected Pre-Middle Jurassic Basement Rocks Beneath the Atlantic and Gulf Coastal Plains in Florida

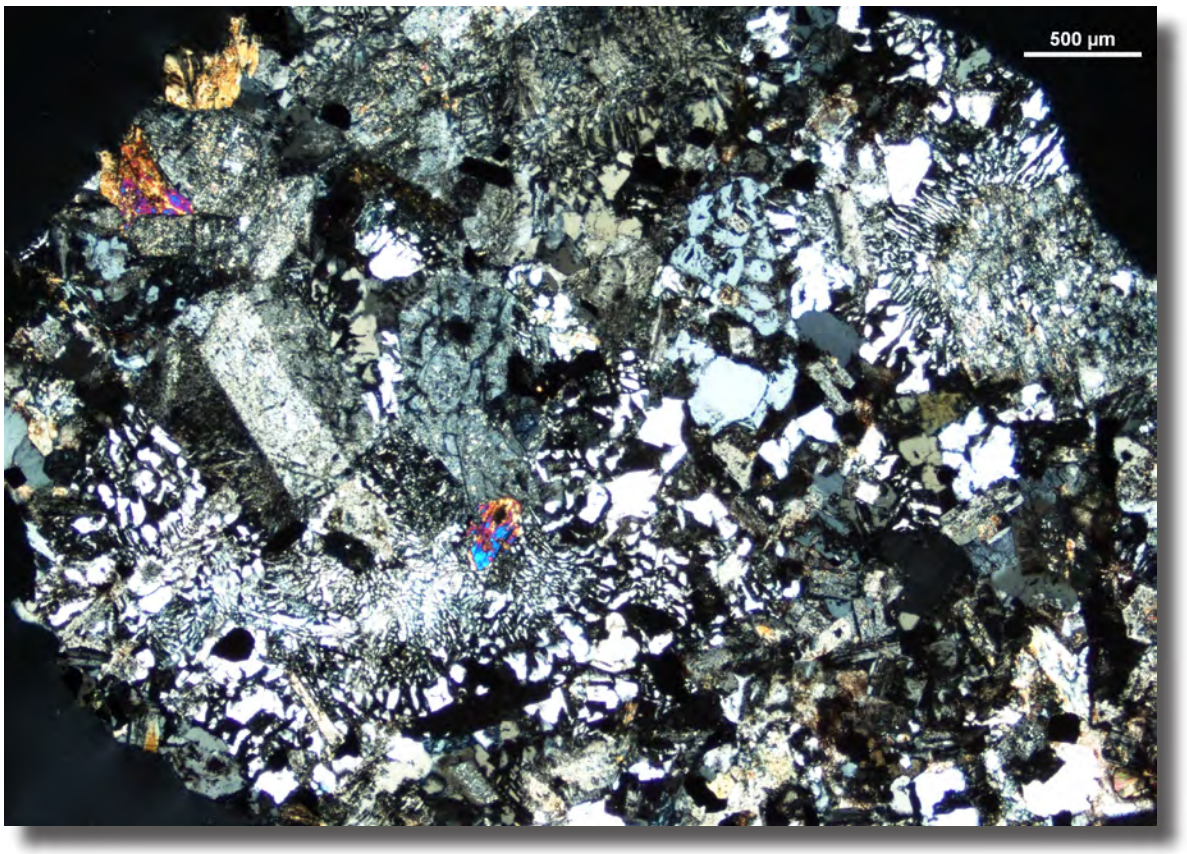

Data Report 1209

U.S. Department of the Interior
U.S. Geological Survey

Cover. Photomicrograph in cross-polarized light of a cuttings fragment of granodiorite from borehole W12497 from 12,390 to 12,400 feet depth. Term: µm, micrometer. Photomicrograph by Ryan T. Deasy, U.S. Geological Survey.

Petrography and Mineralogy of Selected Pre-Middle Jurassic Basement Rocks Beneath the Atlantic and Gulf Coastal Plains in Florida

By Ryan T. Deasy, Mary E. Lupo, Ryan J. McAleer, and J. Wright Horton, Jr.

Data Report 1209

U.S. Department of the Interior
U.S. Geological Survey

U.S. Geological Survey, Reston, Virginia: 2026

For more information on the USGS—the Federal source for science about the Earth, its natural and living resources, natural hazards, and the environment—visit https://www.usgs.gov.

For an overview of USGS information products, including maps, imagery, and publications, visit https://store.usgs.gov/ or contact the store at 1–888–275–8747.

Suggested citation:
Deasy, R.T., Lupo, M.E., McAleer, R.J., and Horton, J.W., Jr., 2026, Petrography and mineralogy of selected pre-Middle Jurassic basement rocks beneath the Atlantic and Gulf Coastal Plains in Florida: U.S. Geological Survey Data Report 1209, 150 p., https://doi.org/10.3133/dr1209.

Associated data for this publication:
Deasy, R.T., Horton, J.W., Jr., Glock, S.N., and Lupo, M.E., 2024, Geochemical data from selected pre-Middle Jurassic basement rocks beneath the Atlantic and Gulf Coastal Plains in Florida and Alabama: U.S. Geological Survey data release, https://doi.org/10.5066/P13NBKKC.

Deasy, R.T., Horton, J.W., Jr., Glock, S.N., and Lupo, M.E., 2024, Mineral abundances of selected pre-Middle Jurassic basement rocks beneath the Atlantic and Gulf Coastal Plains in Florida and Alabama from whole-rock powder X-ray diffraction analysis and the Rietveld method: U.S. Geological Survey data release, https://doi.org/10.5066/P133DRW5.

Deasy, R.T., Lupo, M.E., McAleer, R.J., and Horton, J.W., Jr., 2024, Photographs and photomicrographs of selected pre-Middle Jurassic basement rocks beneath the Atlantic and Gulf Coastal Plains in Florida (ver. 1.1, June 2026): U.S. Geological Survey data release, https://doi.org/10.5066/P13XYCUC.

Horton, J.W., Jr., Glock, S.N., Daniels, D.L., and Deasy, R.T., 2023, Borehole data for pre-Middle Jurassic basement rocks beneath the Atlantic and Gulf Coastal Plains, Florida and Alabama (ver. 1.1, June 2026): U.S. Geological Survey data release, https://doi.org/10.5066/P9VBO427.

ISSN 2771-9448 (online)

Acknowledgments

The authors thank Guy Means, David Paul, and Edward Chelette of the Florida Geological Survey for access to subsurface rock samples and information. Thanks also to Jon Arthur of the American Geosciences Institute for instructive conversations regarding sampling and analytical strategy. Much appreciation goes to David Bish and Maren Pink of the Indiana University Molecular Structure Center for help with X-ray diffraction data collection and interpretation. The manuscript benefitted from helpful reviews by Mark Carter, Arthur Merschat, and Randy Orndorff. This data report was produced as part of a U.S. Geological Survey Mendenhall Research Associateship with support of the National Cooperative Geologic Mapping Program.

Contents

Figures

Table

Conversion Factors

Multiply	By	To obtain
	Length	
inch (in.)	2.54	centimeter (cm)
inch (in.)	25.4	millimeter (mm)
foot (ft)	0.3048	meter (m)
centimeter (cm)	0.3937	inch (in.)
millimeter (mm)	0.03937	inch (in.)
micrometer (µm)	0.00003937	inch (in.)
nanometer (nm)	0.00000003937	inch (in.)
kilometer (km)	0.6214	mile (mi)
	Mass	
gram (g)	0.03527	ounce, avoirdupois (oz)

Datums

Vertical coordinate information is referenced to the National Geodetic Vertical Datum of 1929 (NGVD 29).

Horizontal coordinate information is referenced to the North American Datum of 1927 (NAD 27).

Abbreviations

~	approximately
°	degree(s)
>	greater than
<	less than
≤	less than or equal to
%	percent
Θ	theta
1M	one-layer monoclinic
2M1	two-layer monoclinic
AA	as in the interval immediately above
AD	air-dried
Ar	argon
Base_Elev	elevation of top-of-basement rock, in feet relative to mean sea level
Base_Pen	thickness of basement rock penetrated by drilling, in feet
BSE	back-scattered electron(s)
CL	cathodoluminescence
CPS	counts per second
Cu	copper
d	*d*-spacing
EDS	energy dispersive spectroscopy
EG	ethylene glycol
Fe	iron
HCl	hydrochloric acid
ICP-MS	inductively coupled plasma mass spectrometry
ICP-OES	inductively coupled plasma optical emission spectrometry
INAA	instrumental neutron activation analysis
K	potassium

LA-ICP-MS	laser ablation inductively coupled plasma mass spectrometry
Ma	mega-annum (million years ago)
Mg	magnesium
Mn	manganese
n	number (of samples)
Na	sodium
Pb	lead
PPL	plane-polarized light
Rb	rubidium
REE	rare earth element
RL	reflected light
sec	second (unit of time)
Sr	strontium
TD	total depth
Ti	titanium
U	uranium
Well_ID	Florida Geological Survey borehole number
wt. pct.	weight percent
XPL	cross-polarized light
XRD	X-ray diffraction
XRF	X-ray fluorescence
Zr	zirconium

Petrography and Mineralogy of Selected Pre-Middle Jurassic Basement Rocks Beneath the Atlantic and Gulf Coastal Plains in Florida

By Ryan T. Deasy,[1] Mary E. Lupo,[2] Ryan J. McAleer,[1] and J. Wright Horton, Jr.[3]

Abstract

Florida is covered by flat-lying sedimentary strata of the Atlantic and Gulf Coastal Plains. These strata have accumulated since Middle Jurassic time. The pre-Middle Jurassic, or basement, rocks that underlie the Coastal Plain in Florida are known only from drill cores and cuttings recovered from a relatively small number of boreholes. This data report presents petrographic observations and the results of X-ray diffraction analyses of basement rocks from 18 boreholes across Florida in support of the identification, discrimination, and correlation of units for a subcrop geologic map of pre-Middle Jurassic rocks composing Florida's sub-Coastal Plain geology.

Introduction

This data report provides petrographic and mineralogical observations (including X-ray diffraction [XRD] analyses) of core and cuttings of selected pre-Middle Jurassic basement rocks across Florida (fig. 1). These data were collected during production of a geologic map of pre-Middle Jurassic basement rocks beneath the Coastal Plain in Florida (Deasy and others, 2026). The primary targets of this investigation were the plutonic and volcanic rocks composing the basement geology of Florida. These rocks were selected for two reasons: (1) to evaluate their potential for uranium-lead (U-Pb), argon-argon ($^{40}Ar/^{39}Ar$), and other geochronological and thermochronological analyses and (2) because the textures and compositions of these rocks may yield petrologic and tectonic insight. The observations contained herein are intended to support the geologic map of the pre-Middle Jurassic basement rocks beneath the Coastal Plain in Florida (Deasy and others, 2026) and to complement geochronological, thermochronological, and geochemical studies in the development of framework models for the coastal basement geology of the southeastern United States.

Samples of basement rocks were selected from 18 boreholes across Florida for investigation (table 1). Table 1 is excerpted from Horton and others (2023), which includes additional information and documentation of these and other boreholes in Florida and Alabama. Values for elevations of top-of-basement rock (Base_Elev) are given in feet relative to mean sea level. Apparent thicknesses of basement rock penetrated by drilling (Base_Pen) are given in feet. Throughout this report, depths for samples and in logs are reported as they are recorded in original drilling logs and in the Florida Geological Survey core repository database (Florida Geological Survey, 2023); that is, as positive values in feet below a depth reference (kelly bushing, derrick floor, or ground level; see Horton and others, 2023).

Samples were first investigated in hand sample, and downhole variations in core and cuttings were documented. Polished thin sections of core chips and cuttings were studied under plane-polarized, cross-polarized, and reflected light (PPL, XPL, and RL, respectively) on a standard petrographic microscope. Further investigation by scanning electron microscopy included back-scattered electron (BSE) and cathodoluminescence (CL) imaging as well as qualitative mineral compositions and elemental abundance maps generated by energy dispersive spectroscopy (EDS). Annotated images of representative textures and structures are included in this publication; original images may be found in a companion data release (Deasy and others, 2024c). Powdered aliquots of core chips and cuttings were analyzed by XRD to characterize the mineralogy. Details of sample preparation and XRD analyses, as well as results of those experiments, are included in this data report; semi-quantitative mineral abundances determined by the Rietveld method are available in a second companion data release (Deasy and others, 2024b). Major- and trace-element compositions of most of the same powdered aliquots are available in a third companion data release (Deasy and others, 2024a).

This document is divided into sections, each of which presents the results from one borehole. Sections are headed by borehole number (Well_ID, table 1) followed by a sentence or two summarizing the basement rock(s) in that borehole. The "Previous Work" subsections summarize previously published descriptions of, and analytical work done on, the basement core or cuttings. The "Core and Cuttings Log" or "Cuttings Log"

[1]U.S. Geological Survey.

[2]Florida Geological Survey.

[3]U.S. Geological Survey, retired (emeritus).

subsections, where applicable, contain a downhole visual description of the recovered basement rock and overlying strata (both a summary description and a detailed description of each interval). The "Thin Section Petrography" subsections, where applicable, include descriptions of optical and (or) scanning electron photomicrographs. The "Notes on XRD Methods and Results" subsections, where applicable, include detailed discussions of methods and results for the preparation and analysis of samples by XRD from the borehole.

For clarity, in this document, the following terms are used only with the corresponding definitions:

fragment	individual piece of drill cuttings
clast	sedimentary particle
grain	mineral constituent of a fragment or clast

Abbreviations for minerals follow Whitney and Evans (2010). Abbreviations for mixed clays follow Warr (2020).

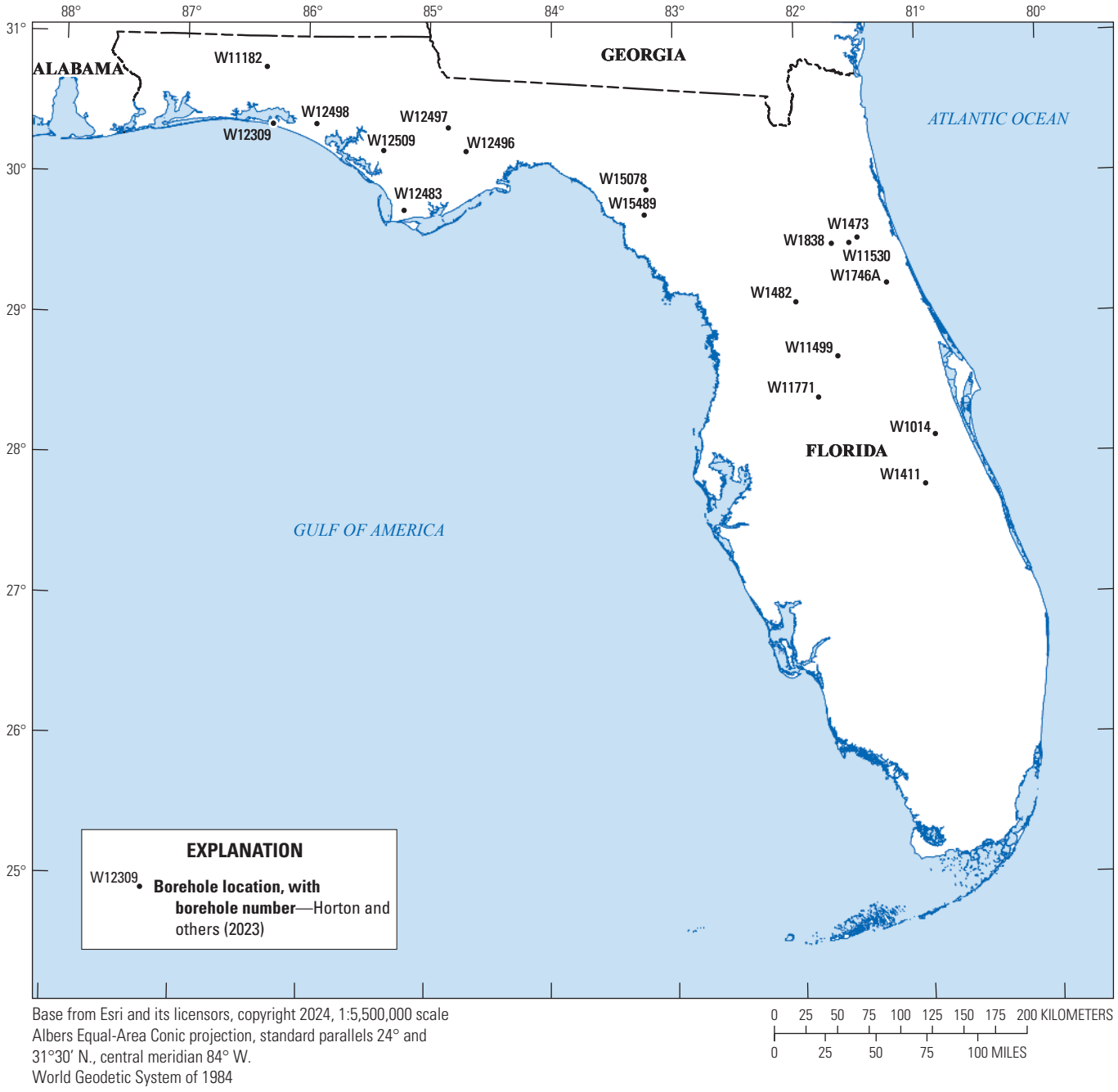

Figure 1. Map of Florida showing locations and borehole numbers of the 18 boreholes investigated in this study. Data from these and other basement-penetrating boreholes are available from Horton and others (2023).

Table 1. Information for boreholes in Florida from which pre-Middle Jurassic basement rocks are described in this report.

[Data in this table are excerpted Horton and others (2023). Terms: Well_ID, borehole number; Alt_ID, Alternate borehole designation ("OG_" indicates the Florida Oil and Gas Program permit number of the Florida Department of Environmental Protection Division of Water Resource Management); Lat, latitude; Lon, longitude; NAD27, North American Datum of 1927; Base_Elev, elevation of top-of-basement rock, in feet relative to mean sea level; Base_Pen, thickness of basement rock penetrated by drilling, in feet; Sample, type of sample reviewed in this report]

Well_ID	Alt_ID	Borehole name or location	Year	Lat_NAD27	Lon_NAD27	Base_Elev	Base_Pen	Sample
W11182	OG_519	Coastal Prod. Brady Belcher No. 1	1971	30.77482	−86.34978	−12,071	55	core
W12309	OG_721	St. Joe Paper No. 4	1974	30.37056	−86.29056	−14,436	35	cuttings
W12498	OG_690	St. Joe Paper No. 2	1973	30.37333	−85.93222	−12,191	55	cuttings
W12509	OG_746	Hunt Oil International Paper No. 30–4	1974	30.18750	−85.37889	−12,817	386	cuttings
W12497	OG_745	Placid Oil USA No. 16–3	1974	30.35285	−84.84861	−11,964	360	cuttings
W12496	OG_730	Placid Oil USA No. 26–4	1974	30.18472	−84.70139	−11,690	378	cuttings
W12483	OG_670	St. Joe Paper No. 1	1973	29.76250	−85.20667	−14,227	36	core chips
W15078	OG_1052	P.C. Crapps No. 1C	1981	29.91172	−83.22348	−4,560	5,458	cuttings
W15489	OG_1129	Buckeye 5–9 No. 1	1984	29.73167	−83.23889	−4,902	4,133	cuttings; core
W1838	OG_96	Sun Oil Co.–Westbury #1	1949	29.51428	−81.71021	−3,841	19	core
W11530	OG_607	Johnson Malphure No. 1	1972	29.51833	−81.56694	−4,392	1,146	cuttings
W1473	OG_44	J.W. Campbell No. 1	1947	29.55555	−81.49933	−4,557	44	core
W1482	OG_53	H.N. Camp No. 1	1947	29.10174	−82.00767	−4,541	22	core
W1746A	OG_78	Retail Lumber Co. No. 1 (P. Oles-De Leon Springs)	1949	29.23091	−81.26592	−5,359	21	cuttings; core
W11499	OG_574	Hamilton Bros. No. 1	1972	28.71195	−81.67382	−5,103	202	cuttings
W11771	OG_629	Arnold Indus No. 1	1972	28.42056	−81.83611	−5,620	31	cuttings
W1014	OG_8	N. Ray Carroll No. 1	1946	28.14278	−80.89861	−7,973	14	core
W1411	OG_31	W.P. Hayman No. 1	1946	27.79306	−80.98694	−8,654	58	core

Borehole W11182

Basement rock encountered in this borehole includes volcaniclastic sandstone and conglomerate, with minor phyllite, at depths of 12,285–12,340 feet (ft). Samples from 12,335 ft, 12,336 ft, and 12,338 ft depth were investigated in this study.

Previous Work

Barnett (1975, p. 138) describes approximately 55 ft of basement penetration beginning at 12,285 ft depth as "metamorphosed volcanic sandstone and granule conglomerate. Cambrian or U. Precambrian (sic)?" and adds "Core 12333 to 12340 rec[overed] 3 [ft] volcanic granule conglomerate and sandstone, 3 ft. slightly metamorphosed red and green shale, 1 ft. pebble conglomerate and sandstone." This information is also included in the compilation of Lloyd (1985).

Thin Section Petrography

Three thin sections were prepared from core chips from each of the following depths:

12,335 ft

12,336 ft

12,338 ft

The sample from 12,335 feet depth is a large, approximately (~) 1.5 centimeter (cm)×~3 cm core chip of feldspathic litharenite. Grains are subangular to well rounded and range in size from clay to granule, with a maximum clast dimension of ~0.3 cm (fig. 2). The chip preserves a bedding contact between coarser and finer grained sand. The sample contains a well-developed bedding-parallel metamorphic foliation defined by white mica (fig. 3). Lithic clasts include fine-grained, rounded sandstone pebbles and feldspar-phyric volcanic clasts (fig. 3). Detrital feldspars are commonly blocky and include perthitic alkali feldspars (fig. 3) and plagioclase with deformation twins (fig. 3, center right). Some feldspathic grains are unaltered and free of inclusions, whereas others are partially to completely sericitized or riddled with inclusions (fig. 2). Some lithic and feldspathic grains have reaction rims of white mica (fig. 3) which are probably coincident with foliation development.

The sample from 12,336 feet depth comprises cuttings ranging in size from submillimeter to ~1 cm in maximum dimension. In hand sample, the fragments have a very fine grained, lustrous foliation. Most fragments are red, but some of the larger fragments have sharp contacts with yellow-green domains and some of the smaller fragments are completely yellow-green in color. The relationship between these color domains suggests redoximorphic structures. In thin section, the phyllitic fragments have strongly hematite-stained matrices and lithic clasts, whereas quartz grains up to 0.1 cm in diameter and phyllitic clasts up to 0.2 cm in diameter with long axes aligned with bedding contain little to no hematite (figs. 4 and 5). Despite the prevalence of detrital feldspars in the litharenitic samples above and below, feldspar clasts appear to be absent in the phyllitic fragments (figs. 4 and 5). Either this sample represents a relatively muddy and more mature sediment intercalated among litharenitic beds, or all feldspars in this layer were replaced by white mica during metamorphism. The high optic density due to the prevalence of hematite in this sample impairs easy estimation of the lithic content of the phyllitic fragments.

The sample from 12,338 feet depth is a large, ~1.5×~3-cm core chip of massive feldspathic litharenite (fig. 6). Grains are subangular to well rounded and range in size from fine sand to granule, with a maximum clast size of ~0.3 cm. The matrix is overprinted by randomly oriented, fine-grained white mica, epidote (fig. 7), and chlorite (fig. 8). The clastic load comprises subangular to well-rounded mono- and polycrystalline quartz grains (figs. 6–8), blocky to subrounded feldspars (fig. 7), rounded fine-grained sandstone clasts (fig. 8, center), and subangular to rounded plagioclase-phyric volcanic clasts (for example, fig. 8, center left).

Notes on XRD Methods and Results

Hand-picked fragments of red phyllite from 12,336 ft depth were separated and placed in an automated Brinkman grinder fitted with an agate mortar and pestle. The samples were continuously lubricated with acetone during grinding. The resulting powders were further ground by hand in a corundum mortar and pestle, again lubricated with acetone, and allowed to air dry. Aliquots of the powders were placed in 3×2×0.1-cm cavities of titanium (Ti) "front-pack" mounts and scanned in a Bruker D8 diffractometer with a copper (Cu) anode and point detector from an angular range of 2–90° 2 theta (Θ) at 0.02° steps and a rate of 8 seconds (sec)/step. Semiquantitative mineral abundances (Deasy and others, 2024b) were obtained by Rietveld refinement modeling in TOPAS (Bruker AXS, 2011).

The broad shape of the 1.0-nanometer (nm) peak in diffraction results prompted re-analysis to characterize clay minerals, as follows. A small amount of the red phyllite was mixed in a slurry with distilled water on a quartz "zero background" plate, was allowed to air dry, and was then scanned on the Bruker D8 from 2 to 100° 2Θ at 8 sec/step. The mounted sample was then placed in a chamber saturated with ethylene glycol (EG) for ~24 hours before being scanned again, immediately upon removal from the EG chamber, from 2 to 40° 2Θ at 2 sec/step.

Upon EG solvation, the faint, broad peak at ~6° 2Θ, corresponding to a *d*-spacing (*d*) of ~1.4 nm, disappears (fig. 9), indicating trace amounts of chlorite/smectite. Furthermore, the broad peak at ~9° 2Θ shifts to slightly higher angles (corresponding to a *d*-spacing shift from 1.005 nm to 0.990 nm), the peak at ~18° 2Θ shifts to slightly lower angles (corresponding to a *d*-spacing shift from 0.495 nm to 0.505 nm), and the peak at ~27° 2Θ (*d*=0.33 nm) increases in intensity. This is consistent with trace amounts of illite/smectite. Interference from the illite, (modeled as a one-layer monoclinic [1M] white mica) and muscovite (modeled as a two-layer monoclinic [2M1] white mica) peaks prevent precise estimation of the fraction of smectitic layers in the illite/smectite without further investigation, but the slightness of the EG-solvation effects suggests a low (less than [<]10 percent) abundance. Notably, evidence of feldspars is absent in all XRD scans of phyllite from 12,336 ft depth, corroborating optical evidence (figs. 4 and 5).

Figure 2. Full thin section scan of feldspathic litharenite in plane-polarized light of a core chip from borehole W11182 from 12,335 feet depth. Note the bedding contact, subvertical in this view, between finer grained (left side) and coarser grained rock. Term: cm, centimeter. Photomicrograph by Ryan Deasy, U.S. Geological Survey.

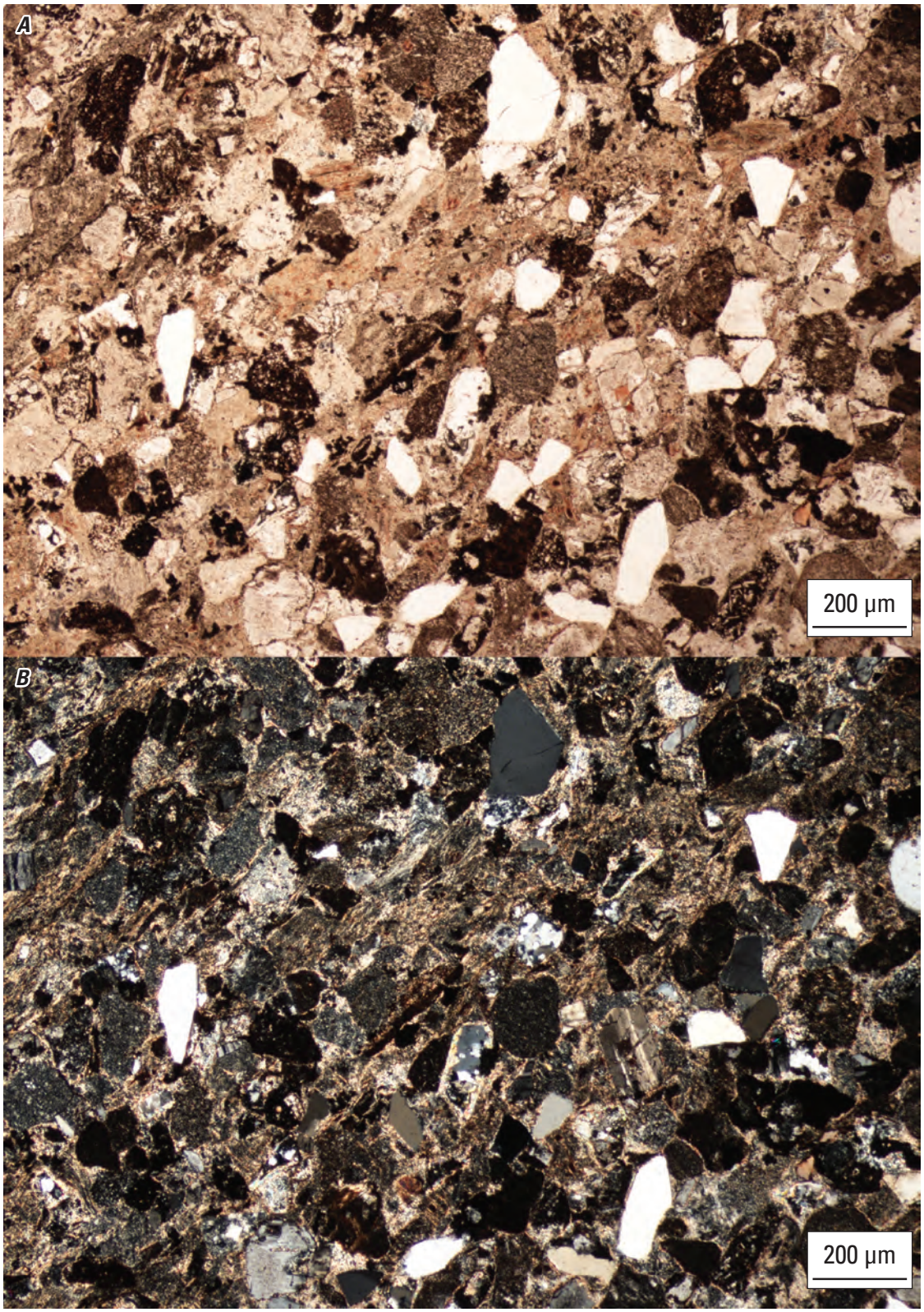

Figure 3. Pair of photomicrographs of a thin section of a core chip of feldspathic litharenite from borehole W11182 from 12,335 feet depth in plane-polarized light (*A*) and cross-polarized light (*B*). Detrital grains include quartz and feldspar clasts as well as sandstone (far left) and feldspar-phyric volcanic clasts (bottom right). A preferred orientation of metamorphic white mica is aligned from lower left to upper right in this view and is parallel to bedding. Term: µm, micrometer. Photomicrographs by Ryan Deasy, U.S. Geological Survey.

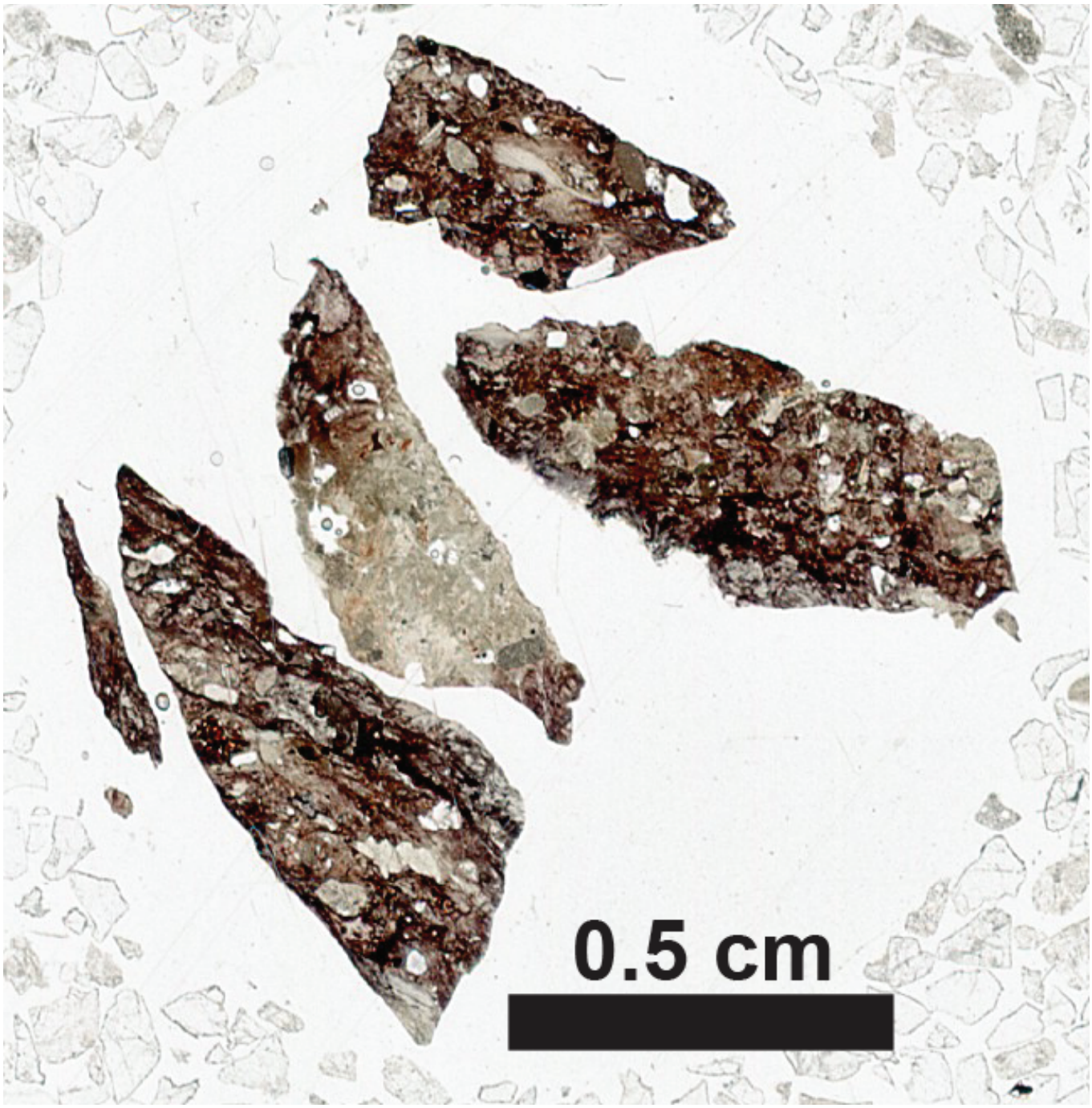

Figure 4. Full thin section scan in plane-polarized light of drill cuttings from borehole W11182 from 12,336 feet depth. Term: cm, centimeter. Photomicrograph by Ryan Deasy, U.S. Geological Survey.

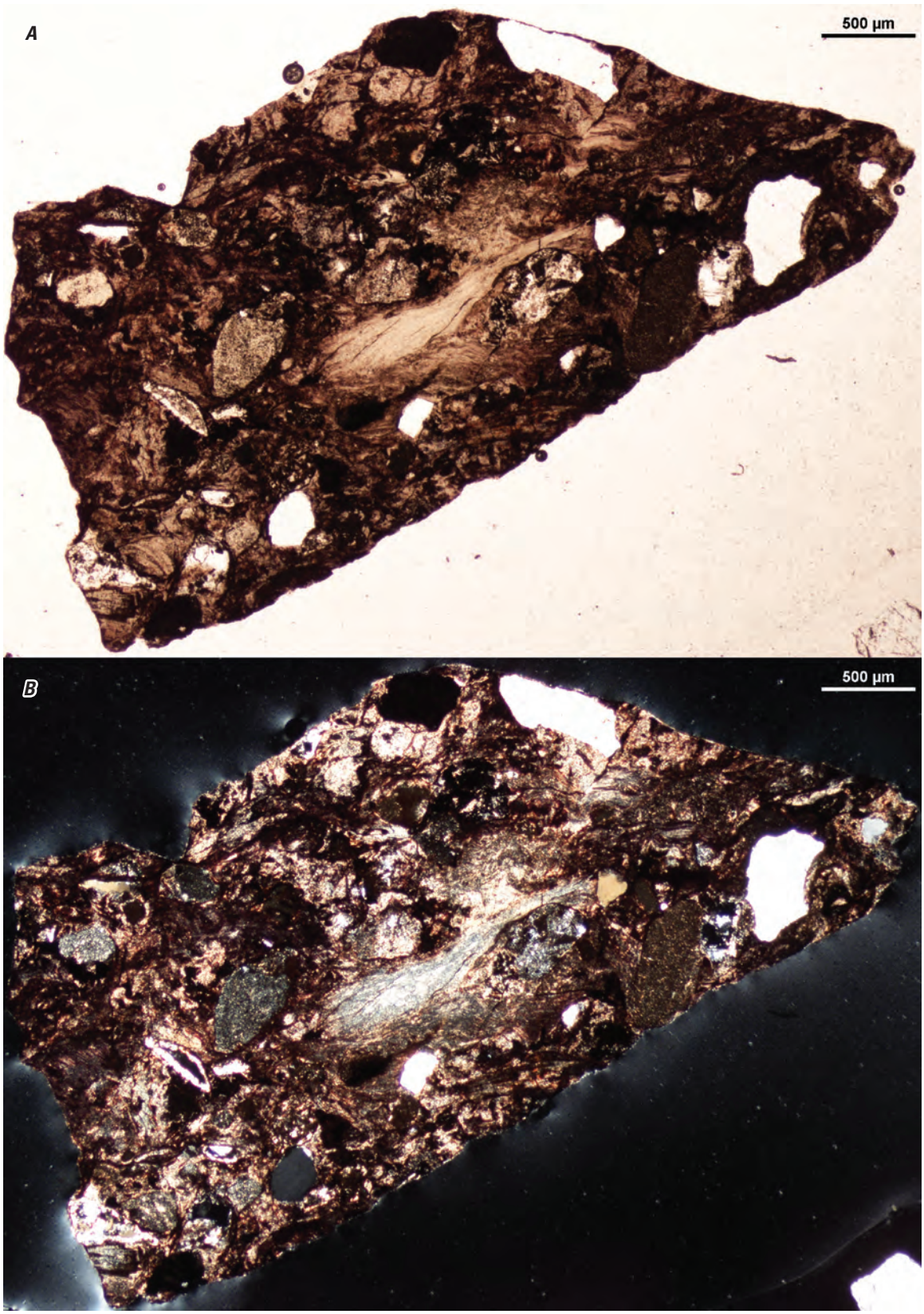

Figure 5. Pair of photomicrographs of thin section of a fragment from borehole W11182 from 12,336 feet depth in plane-polarized light (*A*) and cross-polarized light (*B*). Term: µm, micrometer. Photomicrographs by Ryan Deasy, U.S. Geological Survey.

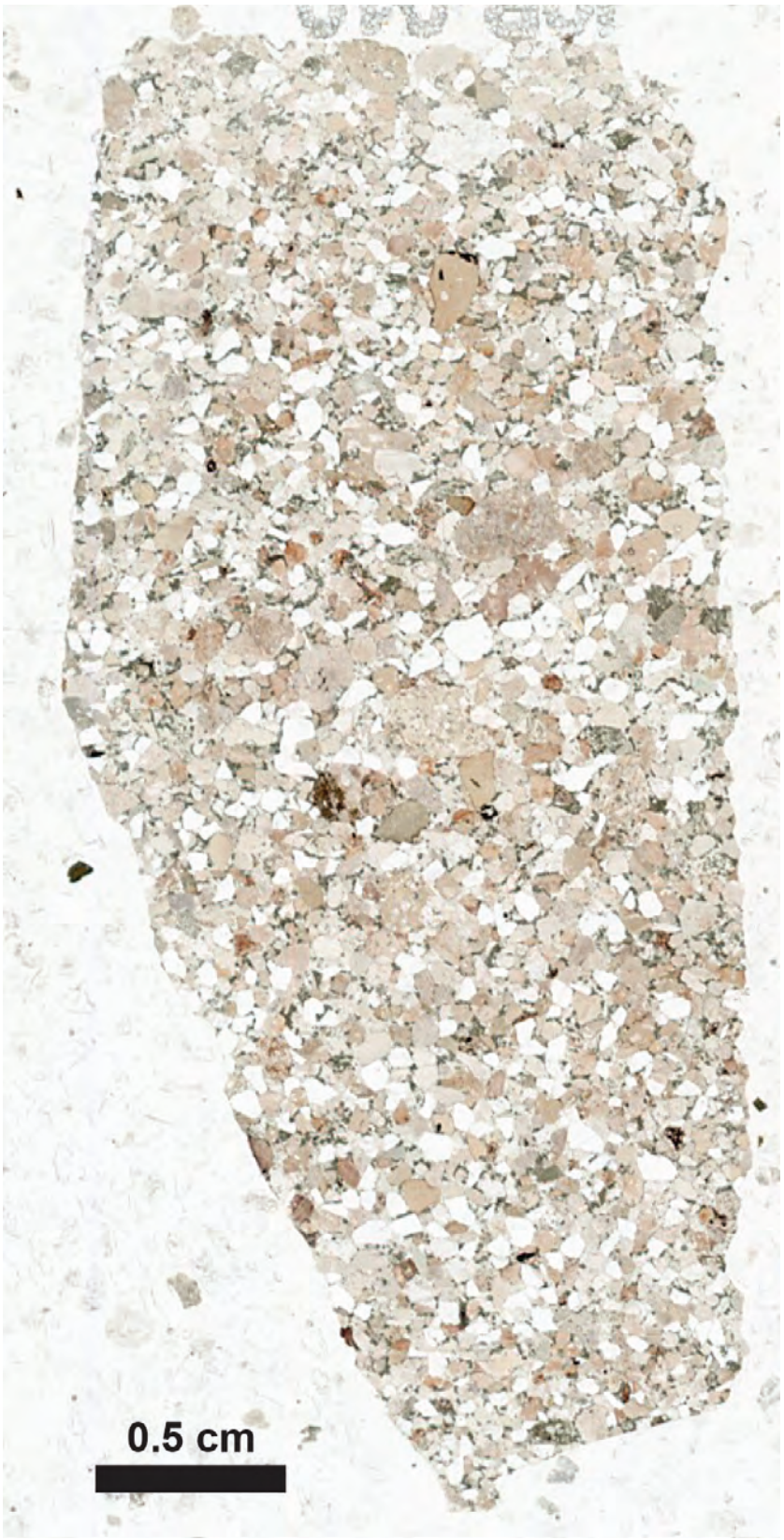

Figure 6. Full thin section scan in plane-polarized light of a core chip of feldspathic litharenite from borehole W11182 from 12,338 feet depth. Term: cm, centimeter. Photomicrograph by Ryan Deasy, U.S. Geological Survey.

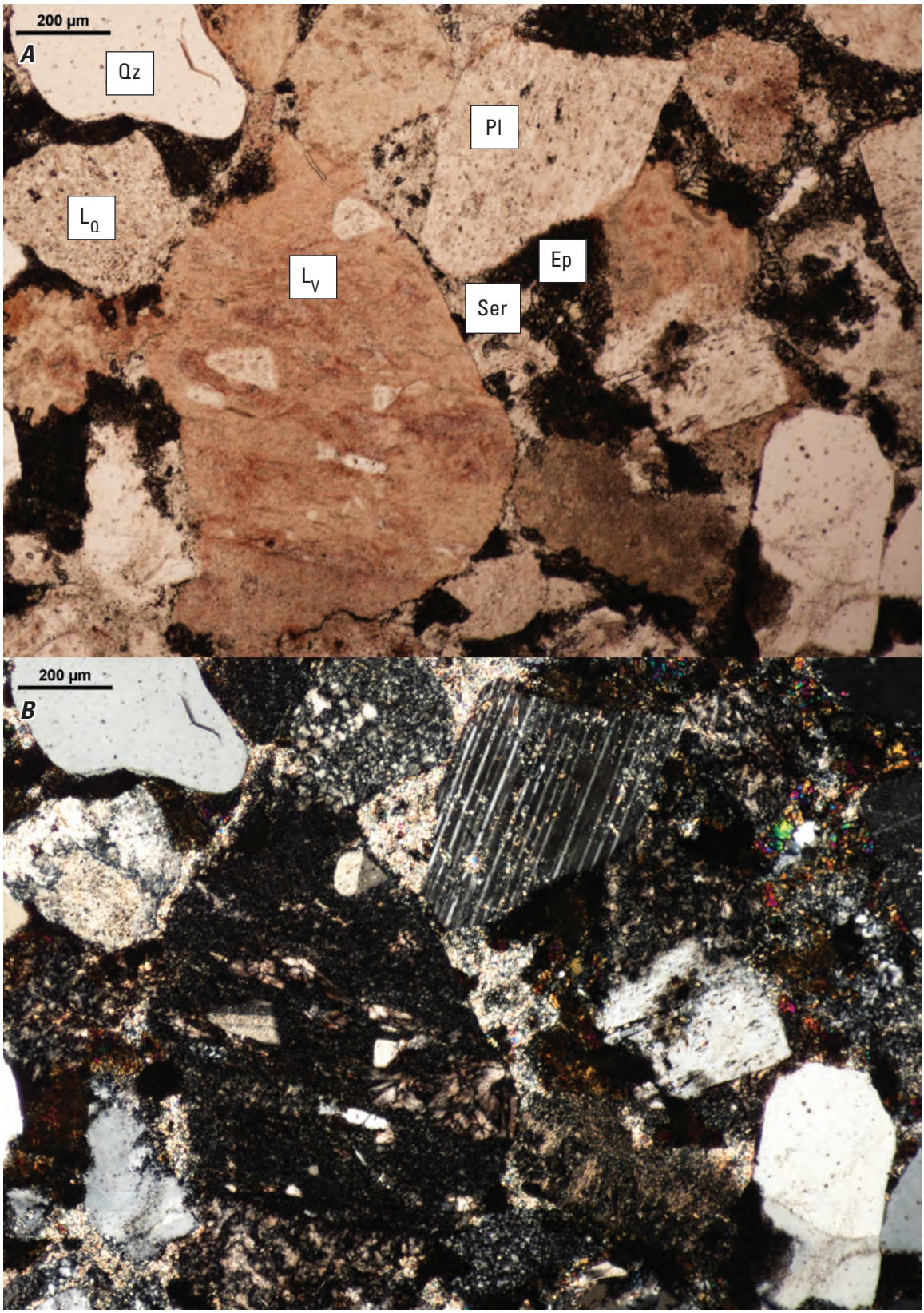

Figure 7. Pair of photomicrographs of a thin section of a feldspathic litharenite core chip from borehole W11182 from 12,338 feet depth in plane-polarized light (*A*) and cross-polarized light (*B*). Terms: µm, micrometer; Qz, quartz; Pl, plagioclase; Ep, epidote; L_V, volcanic clast; L_Q, quartzite clast; Ser, sericite. Photomicrographs by Ryan Deasy, U.S. Geological Survey.

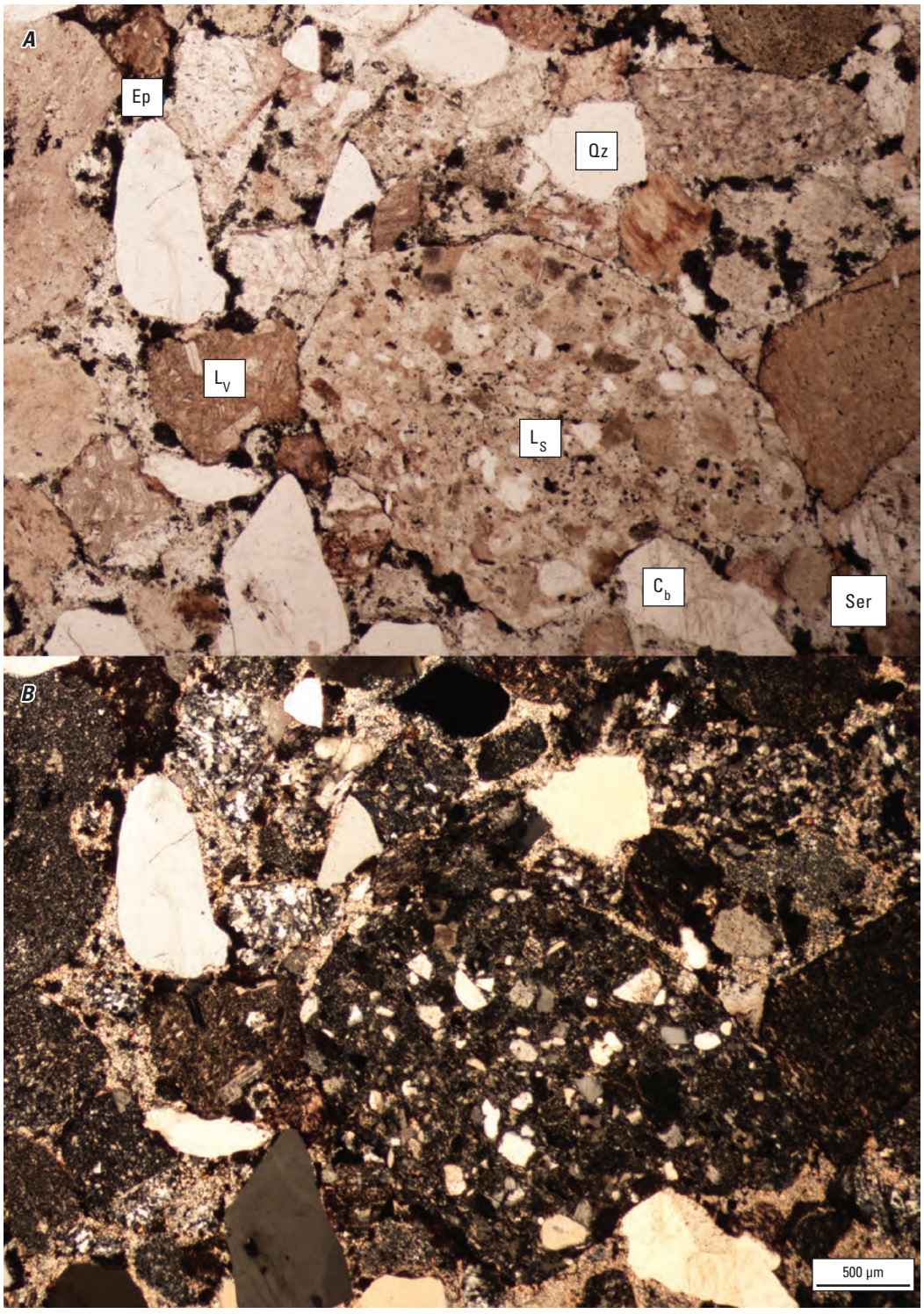

Figure 8. Pair of photomicrographs of a thin section of a feldspathic litharenite core chip from borehole W11182 from 12,338 feet depth in plane-polarized light (*A*) and cross-polarized light (*B*). Terms: µm, micrometer; Qz, quartz; Cb, carbonate mineral(s); Ep, epidote; L_V, volcanic clast; L_S, sandstone clast; Ser, sericite. Photomicrographs by Ryan Deasy, U.S. Geological Survey.

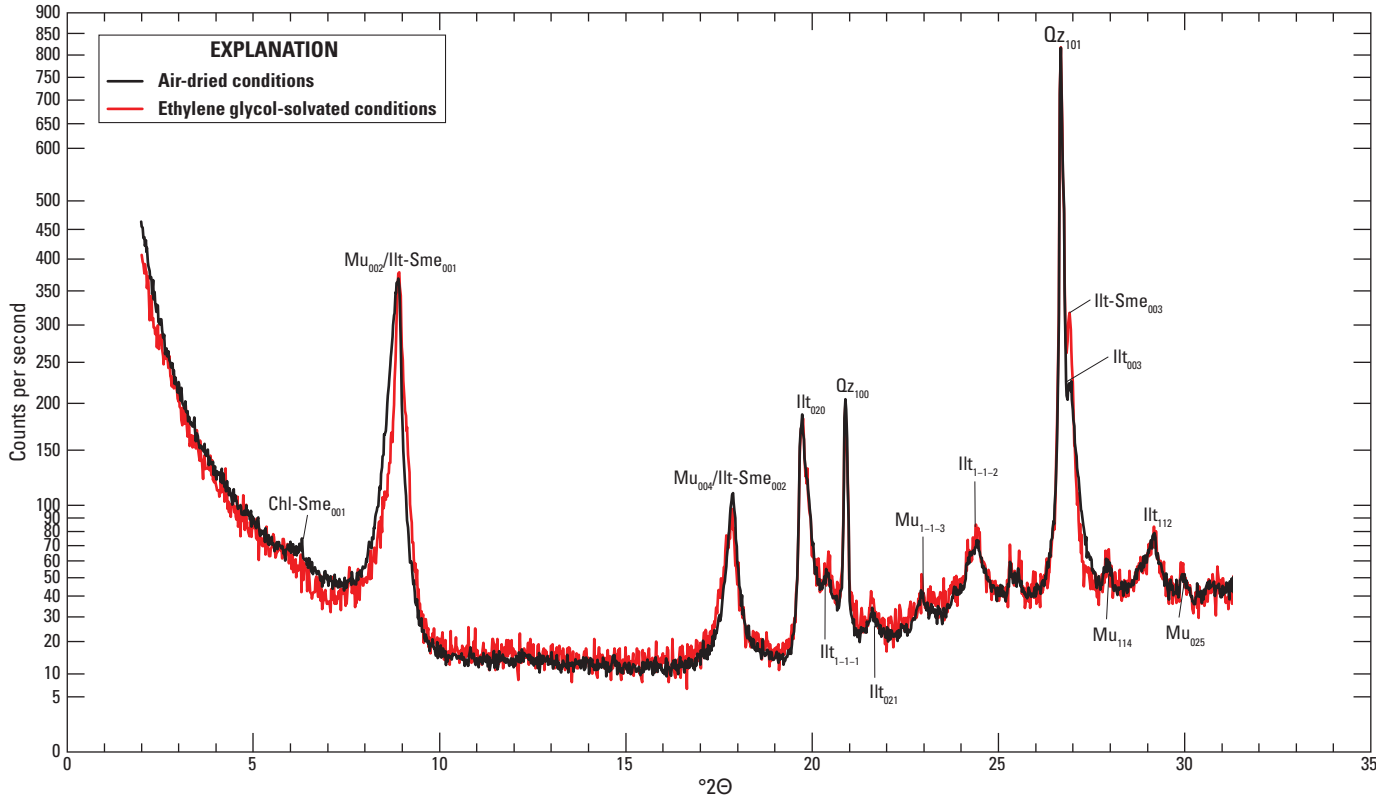

Figure 9. X-ray diffractograms of phyllite from borehole W11182 from 12,336 feet depth under air-dried and ethylene glycol-solvated conditions. The *y*-axis is in square root scale. Selected peaks are labeled with mineral abbreviations; numbers in subscript denote Miller indices. Terms: °2Θ, degrees two theta; Chl-Sme, chlorite/smectite; Mu, muscovite; Ilt-Sme, illite-smectite; Qz, quartz.

Borehole W12309

Granite and porphyritic rhyolite occur in similar proportions in cuttings from 14,480 to 14,515 ft depth. Samples from 14,490 to 14,500 ft depth were investigated in detail in this study.

Previous Work

Barnett (1975, p. 138) reports 35 ft of basement recovery from 14,480 to 14,515 ft depth, adding that the drill cuttings at 14,510–14,515 ft depth are a "coarse red granite wash and weathered biotite granite pegmatite."

Cuttings Log

Summary: Angular to subrounded granitic fragments occur in cuttings as shallow as 14,450–14,460 ft depth and, although they are more abundant with depth, do not compose a majority of cuttings in any interval. Porphyritic rhyolite fragments are also present and compose a similar proportion of the granitic fragments in each interval.

14,500–14,510 ft Cuttings are dominated by red siltstone. Granitic fragments are rare and typically comprise only potassium (K) feldspar and quartz. One granitic fragment contains euhedral muscovite and yellow apatite(?). Porphyritic fragments are as common as granitic bits and contain pink feldspar(?) and translucent quartz phenocrysts in a red to maroon, sucrosic, fine-grained matrix.

14,510–14,515 ft (total depth [TD]) Slightly higher proportion of granitic fragments than above. Feldspar cleavage identified in some phenocrysts within porphyritic fragments.

Thin Section Petrography

Thin sections were prepared of some of the coarser cuttings from borehole W12309 at 14,490–14,500 ft depth, including representative granitic and porphyritic fragments.

Granitic fragments are comprised of subequal amounts of quartz, plagioclase, and K-feldspar, with accessory chloritized biotite, magnetite, and apatite (fig. 10). Quartz grains have uniform extinction and are mostly free of inclusions. The feldspars are pervasively altered to fine-grained sericite, chlorite, and hematite, particularly along cleavages. Plagioclase grains have deformation twins. Carlsbad twins are common among K-feldspar grains. Graphic intergrowths of K-feldspar and quartz are present in some fragments (fig. 11).

Porphyritic grains have plagioclase and quartz phenocrysts in very fine grained quartzofeldspathic matrices (fig. 12). Dynamic layering at the scale of several micrometers is evident in many fragments and is interpreted as magmatic flow banding. Plagioclase phenocrysts are many times larger than the quartz grains and may exceed the size of the cuttings fragments; therefore, the maximum phenocryst size is unknown. Many plagioclase phenocrysts are euhedral, but broken grains are also present, and zoning is apparent in one grain (fig. 13). The alteration of plagioclase phenocrysts is similar to the alteration in the granitic fragments, with chlorite, sericite, and oxides growing along cleavage planes.

Notes on XRD Methods and Results

Granitic fragments were handpicked under a binocular microscope to isolate them from the sedimentary and porphyritic fragments and were separated into ~0.7-gram (g) subsamples. Each subsample was ground by hand in an agate mortar and pestle while being continuously lubricated with acetone. The resulting fine powder was allowed to air dry. Aliquots of each subsample were placed in the 2-cm-wide cavities of circular "back-pack" mounts and scanned in a Panalytical X'Pert diffractometer with a Cu anode from an angular range of 3–90° 2Θ. Semiquantitative mineral abundances (Deasy and others, 2024b) were obtained by Rietveld refinement modeling in HighScore Plus (Malvern Panalytical, 2018). Geochemical analyses were thereafter performed on the same subsamples (Deasy and others, 2024a).

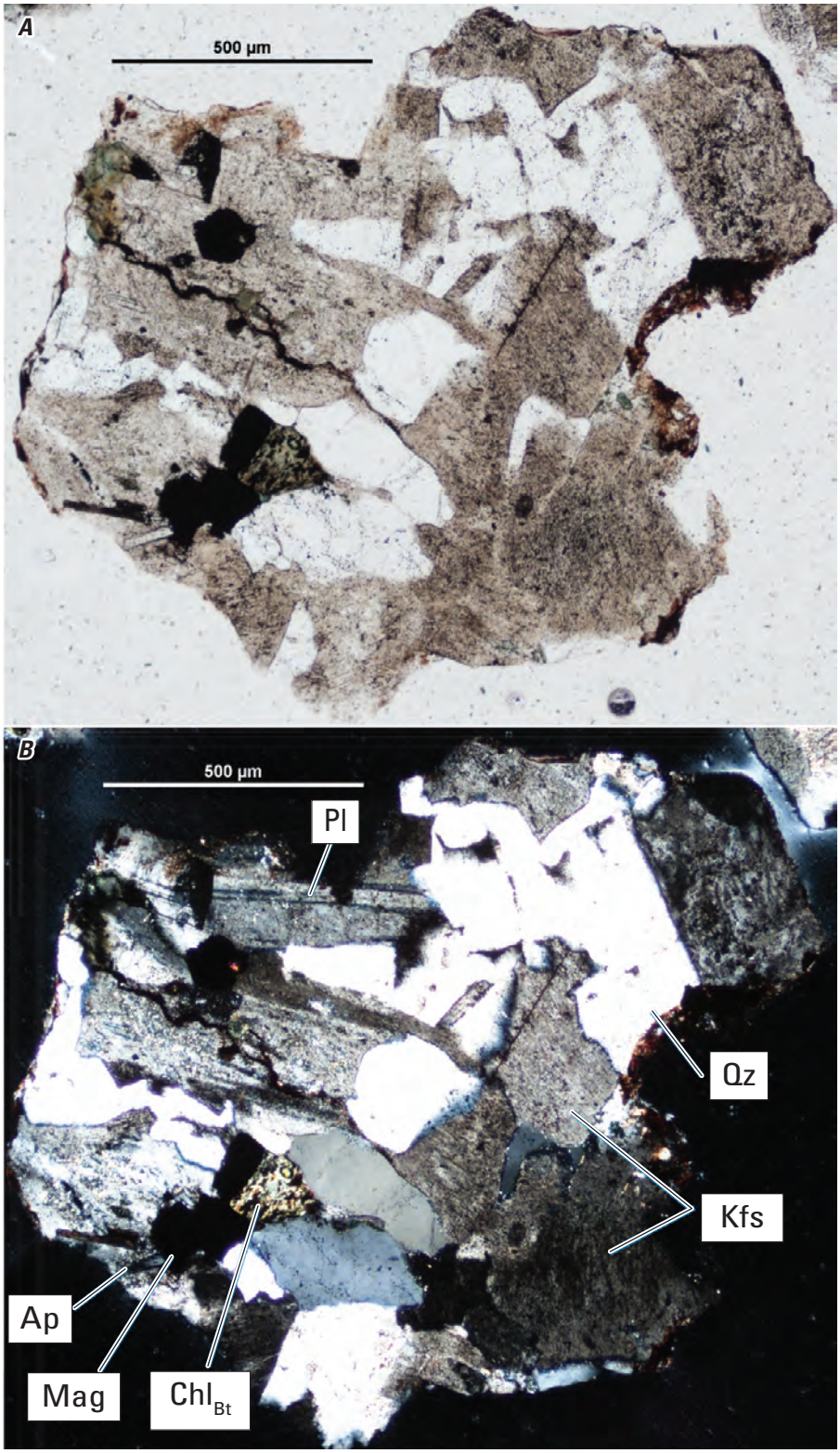

Figure 10. Pair of photomicrographs of a representative granitic fragment from borehole W12309 from 14,490 to 14,500 feet depth in plane-polarized light (*A*) and cross-polarized light (*B*). Plagioclase (Pl) and potassium feldspar (Kfs) are strongly sericitized. Quartz (Qz) occurs as graphic intergrowths with Kfs and as equant magmatic grains (center). Magmatic biotite (Bt) is pseudomorphically replaced by chlorite (Chl). Apatite (Ap) and magnetite (Mag) are accessory minerals and strongly associated with chloritized Bt. Term: µm, micrometer. Photomicrographs by Ryan Deasy, U.S. Geological Survey.

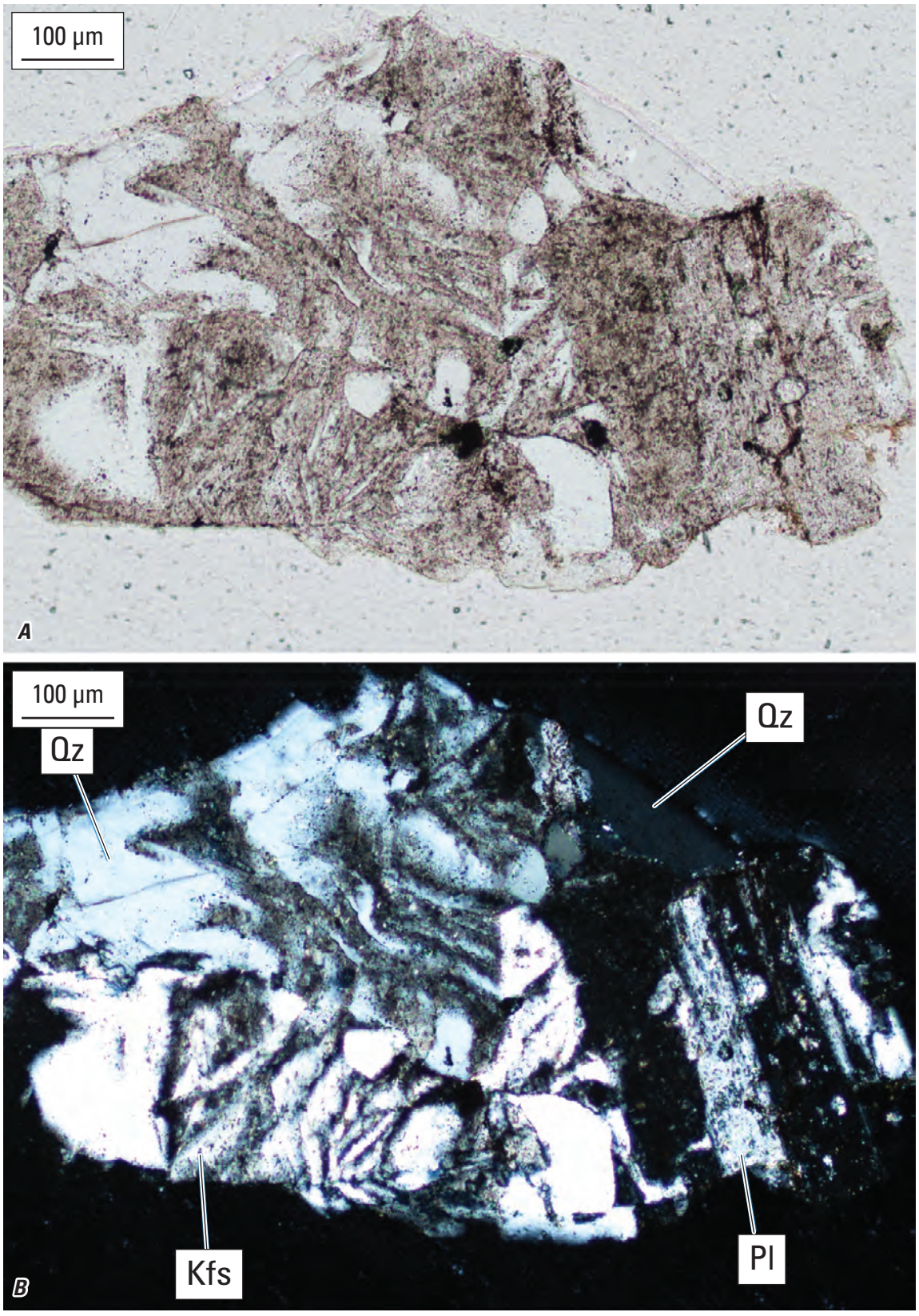

Figure 11. Pair of photomicrographs of cuttings fragment of graphic granite from borehole W12309 from 14,490 to 14,500 feet depth in plane-polarized light (*A*) and cross-polarized light (*B*). Plagioclase (Pl) and potassium feldspar (Kfs) are strongly altered. Quartz (Qz) occurs as graphic intergrowths with Kfs and as independent magmatic grains (top right). Term: µm, micrometer. Photomicrographs by Ryan Deasy, U.S. Geological Survey.

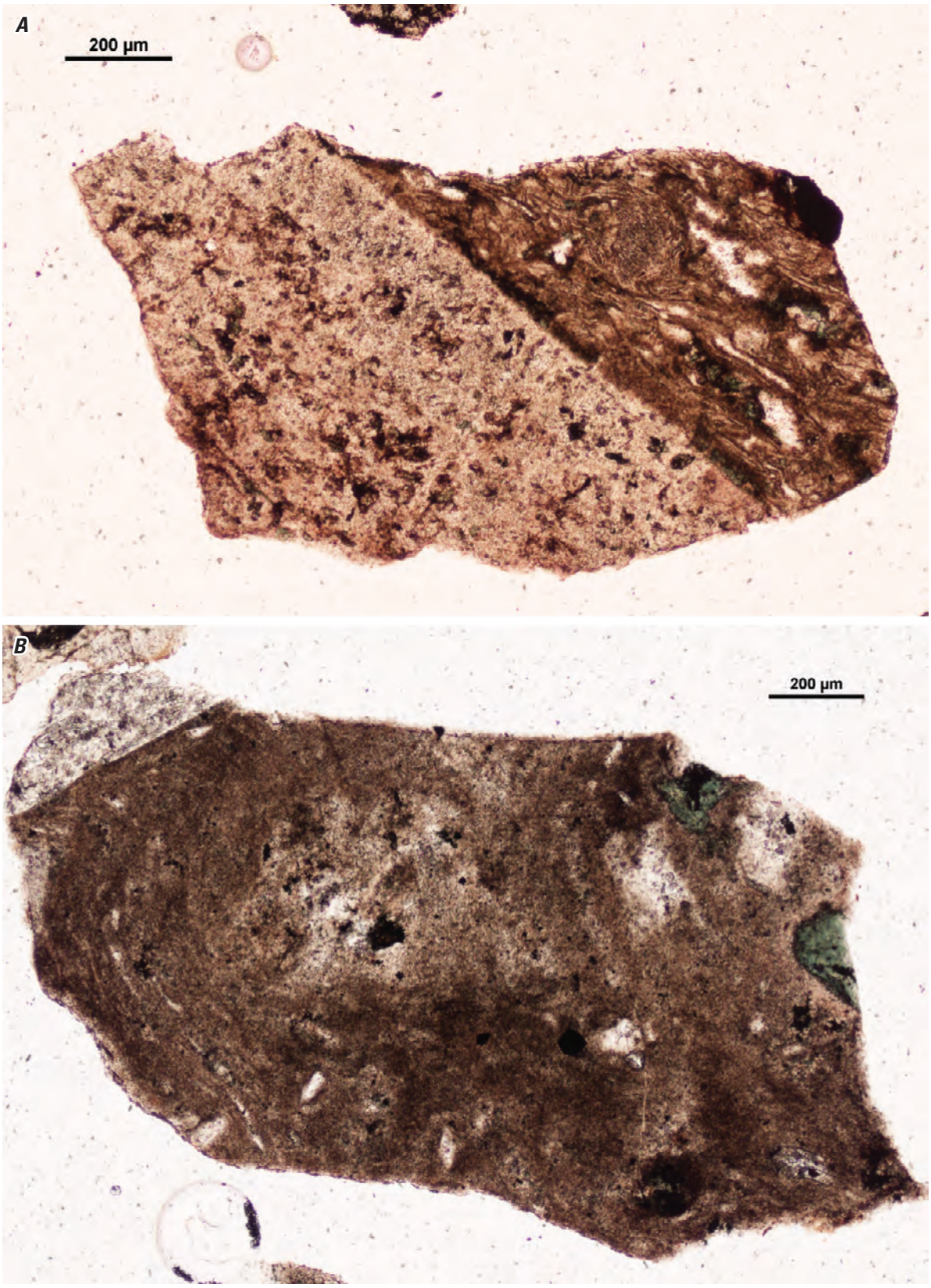

Figure 12. Photomicrographs showing plane-polarized light of representative cuttings fragments of felsic porphyry from borehole W12309 from 14,490 to 14,500 feet depth. Flow banding in the fine-grained matrix may be parallel to (*A*) or deformed against (*B*) feldspar phenocrysts. Term: µm, micrometer. Photomicrographs by Ryan Deasy, U.S. Geological Survey.

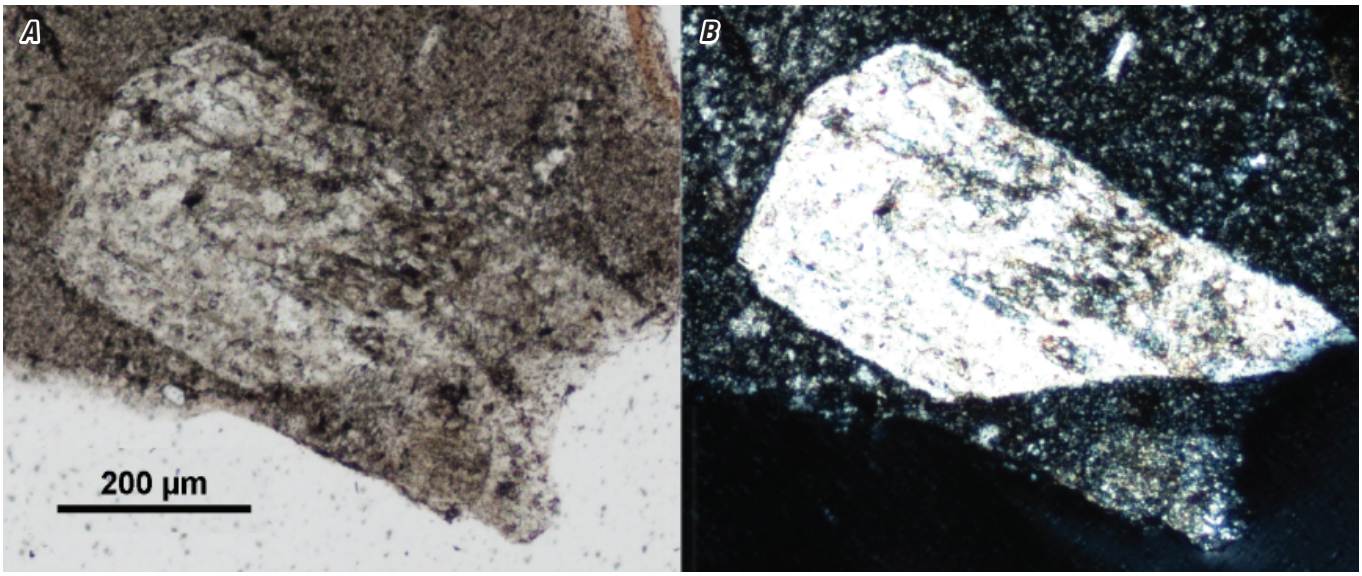

Figure 13. Photomicrographs showing plane-polarized light (*A*) and cross-polarized light (*B*) of a zoned subhedral plagioclase phenocryst, broken on its bottom edge, in a porphyritic fragment from borehole W12309 from 14,490 to 14,500 feet depth. Term: µm, micrometer. Photomicrographs by Ryan Deasy, U.S. Geological Survey.

Borehole W12498

Granitic fragments occur in cuttings from 12,258 to 12,313 ft depth. Samples from 12,290 to 12,313 ft depth were investigated in this study.

Previous Work

Barnett (1975, p. 133) reports 55 ft of granitic basement rock penetration from 12,258 to 12,313 ft depth and includes the following description of a thin section of cuttings from 12,290 to 12,313 ft depth:

> Granite to granodiorite; primarily fine to medium anhedral to subhedral orthoclase, some Carlsbad twins, fractured, sericitic, with quartz, strained and fractured, plagioclase occasionally predominant, and chlorite and magnetite replacing biotite and hornblende. Some chlorite and magnetite in fractures and seams at grain boundaries. Fine tourmaline needles in one fragment.

Thin Section Petrography

A polished thin section was prepared from granitic cuttings from 12,290 to 12,313 ft depth. This granite is coarse grained, with quartz and feldspar grains up to ~1 millimeter (mm) in maximum dimension (fig. 14). Quartz grains are equant, free of inclusions, and display undulose or patchwork extinction in XPL (figs. 14–16). Feldspars are subhedral to euhedral with aspect ratios of ~2:1 and are pervasively altered with fine-grained chlorite, epidote, or sericite, imbuing the grains with a high turbidity. Nevertheless, albite and microcline twinning remain visible in some grains. Some feldspars are broken (fig. 15). Biotite grains are pseudomorphically replaced by chlorite with inclusions of ilmenite (figs. 14 and 16). Fine-grained epidote fills sinuous fractures in some fragments (fig. 16).

Notes on XRD Methods and Results

Fragments of granite were separated from contaminants by hand under a binocular microscope. The separated fragments were then placed in an automated Brinkman grinder fitted with an agate mortar and pestle. The sample was continuously lubricated with acetone during grinding. The resulting coarse powder was further ground by hand in a corundum mortar and pestle, again lubricated with acetone, and allowed to air dry. An aliquot of powder was then mounted in the 2-cm-wide cavity of a standard "back-pack" mount and analyzed on a Panalytical Empyrean diffractometer with a Cu anode from an angular range of 3–100° 2Θ. Semiquantitative mineral abundances in this sample (Deasy and others, 2024b) were determined by Rietveld modeling in TOPAS (Bruker AXS, 2011).

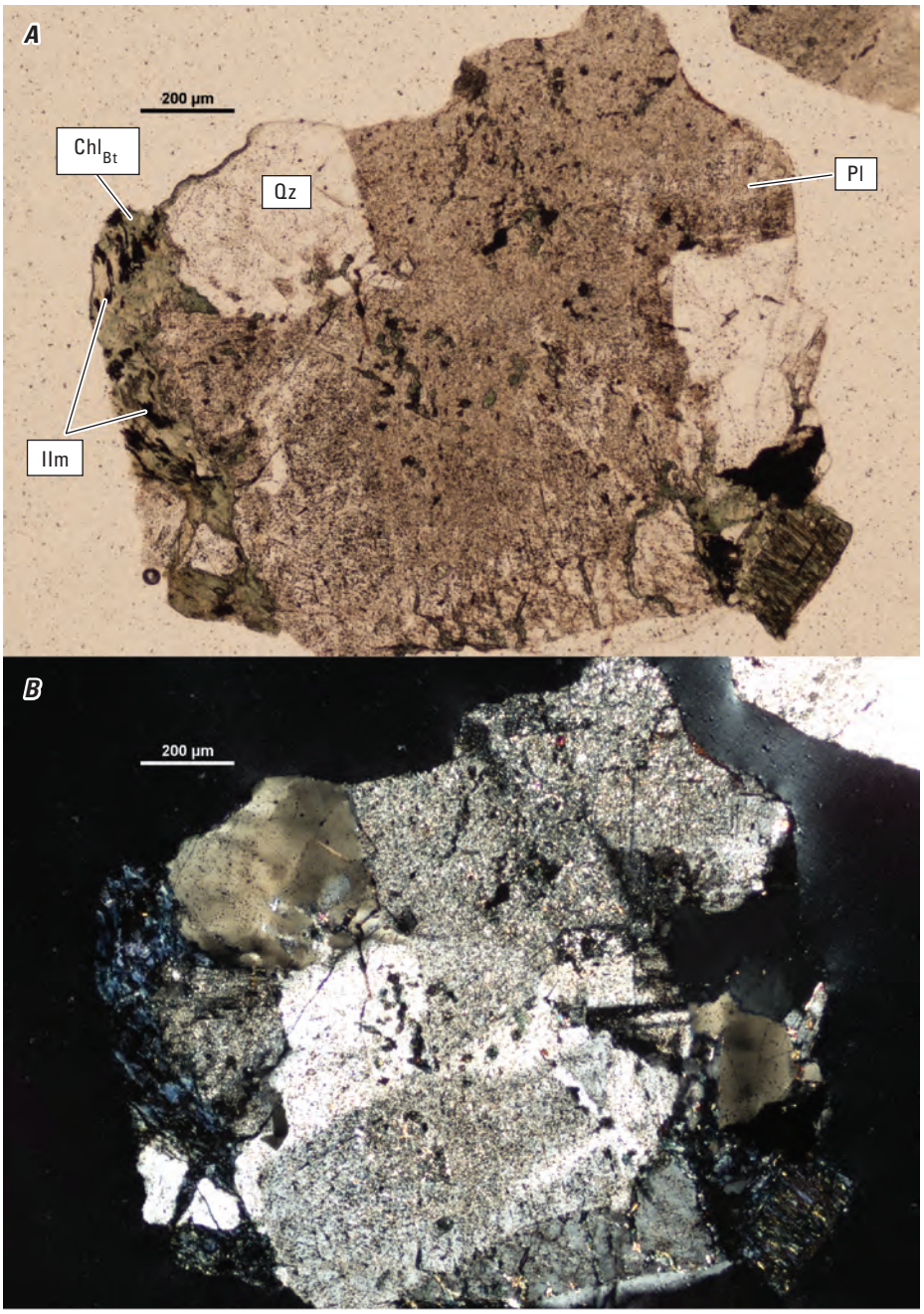

Figure 14. Pair of photomicrographs of a representative granitic cuttings fragment from borehole W12498 from 12,290 to 12,313 feet depth in plane-polarized light (*A*) and cross-polarized light (*B*). Terms: Qz, quartz; Pl, plagioclase; Chl_{Bt}, chlorite (pseudomorph after biotite [Bt]); Ilm, ilmenite; µm, micrometer. Photomicrographs by Ryan Deasy, U.S. Geological Survey.

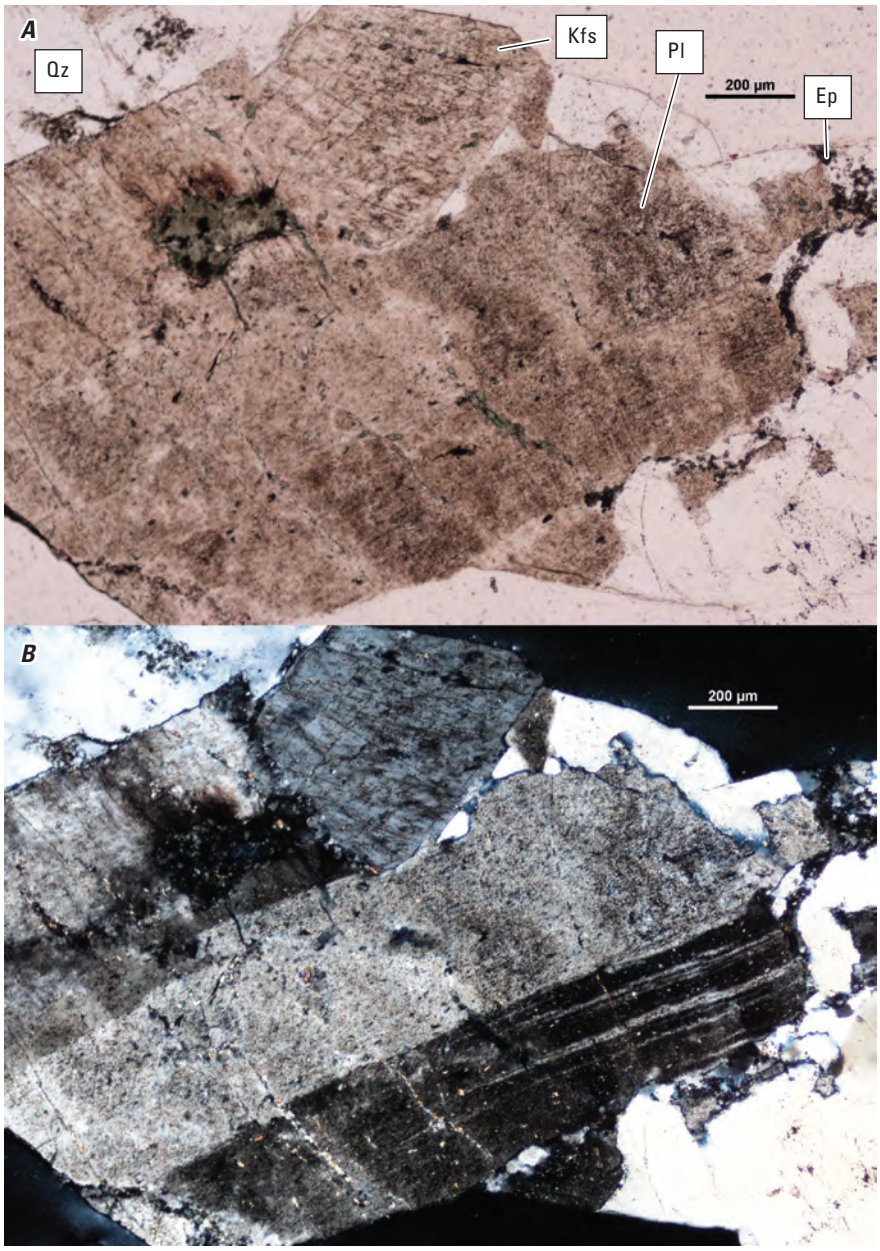

Figure 15. Pair of photomicrographs of a representative granitic cuttings fragment from borehole W12498 from 12,290 to 12,313 feet depth in plane-polarized light (*A*) and cross-polarized light (*B*). Terms: Qz, quartz; Kfs, potassium feldspar; Pl, plagioclase; Ep, epidote; µm, micrometer. Photomicrographs by Ryan Deasy, U.S. Geological Survey.

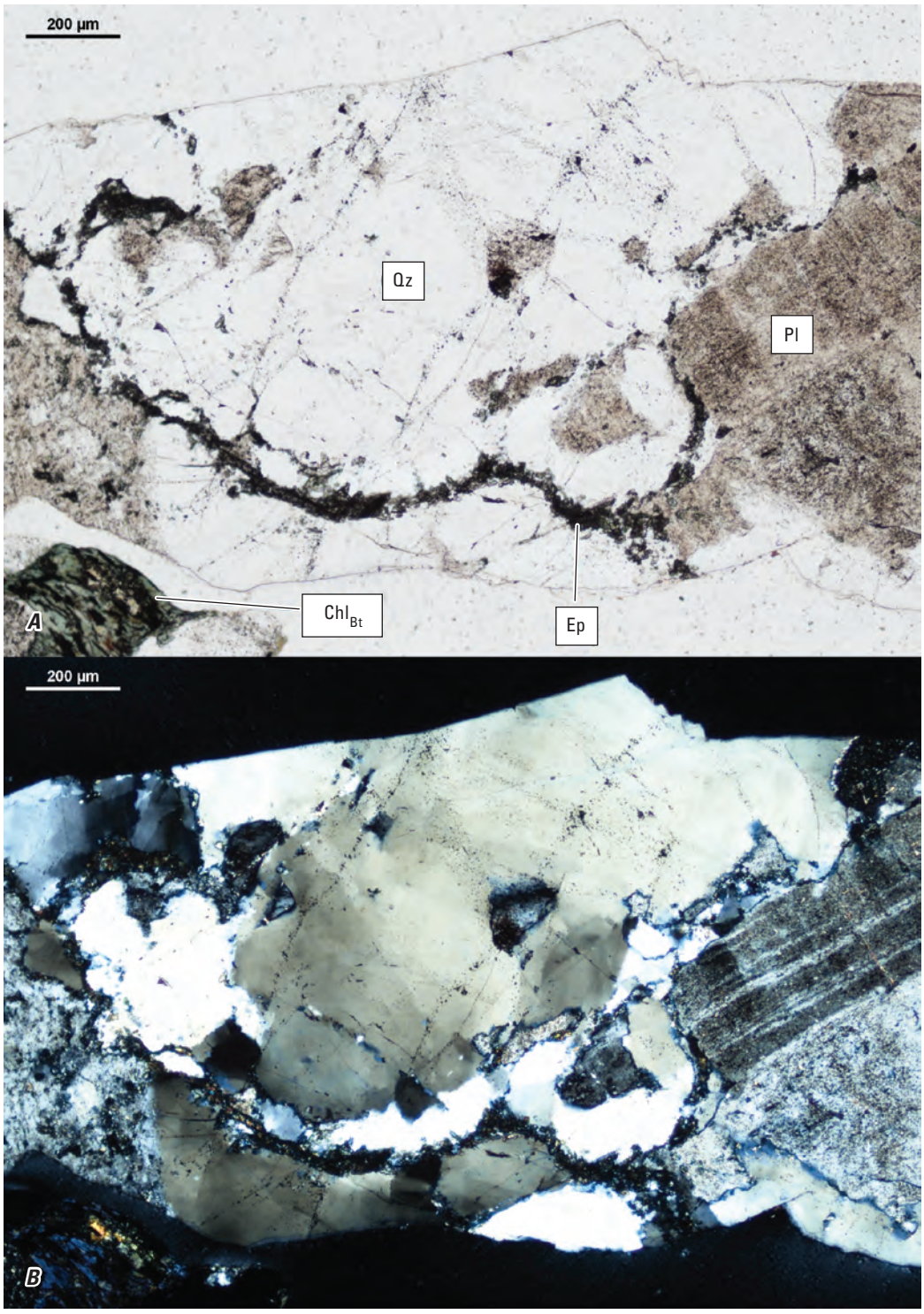

Figure 16. Pair of photomicrographs of a representative granitic cuttings fragment from borehole W12498 from 12,290 to 12,313 feet depth in plane-polarized light (*A*) and cross-polarized light (*B*). Terms: Qz, quartz; Pl, plagioclase; Chl_{Bt}, chlorite (pseudomorph after biotite [Bt]); Ep, epidote; µm, micrometer. Photomicrographs by Ryan Deasy, U.S. Geological Survey.

Borehole W12509

Granitic fragments dominate cuttings from 12,880 to 13,284 ft depth.

Previous Work

This borehole is first mentioned in table 1 of Barnett (1975, p. 136) as "Granodiorite, late Precambrian or early Cambrian?" with no further description or data. A feldspar concentrate from 12,950 to 12,990 ft depth analyzed by the K-Ar method returned an age of 709±25 million years ago (Ma) (Krueger Enterprises, 1981, as first cited in Lloyd [1985, p. 55]); Lloyd (1985) also includes the following note for the age reference: "Unpublished age determination (memo on file at Fla. Bureau of Geology); material submitted by H. Kelley Brooks to Krueger Enterprises, Inc., Geochron Laboratories Division." A Neoproterozoic crystallization age is confirmed by a U-Pb zircon age of 656±38 Ma (Deasy and others, 2023) and a muscovite $^{40}Ar/^{39}Ar$ plateau age of 653.8±3.4 Ma (Deasy and McAleer, 2022).

This is the type borehole and interval (12,880–13,284 ft depth) of the Gaskin intrusive complex of Winston (1992), a name that has been used by some authors to include all granitoids encountered in the Florida panhandle. However, more recent geochronological and thermochronological work (Heatherington and others, 2010; Deasy and McAleer, 2022; Deasy and others, 2023) demonstrates that some granitoids have Permian crystallization ages and that only the undated rocks in boreholes W12309, W12497, and W14644 may potentially be related to the granite in borehole W12509.

Cuttings Log

Summary: Red siltstone and mudstone overlie granitic basement rock and the contact occurs at ~12,880 ft depth. The nonconformable nature of the contact is indicated by the presence of arkosic fragments in the basal sediment, a strong oxidation profile in the uppermost granite, and the absence of any fault-related structures. The granite is coarse grained (~4 mm in maximum dimension), pink to red in color, and contains subequal amounts of quartz, plagioclase, and K-feldspar, with accessory muscovite, magnetite, and apatite. The abundances of magnetite and apatite increase with depth. Magmatic muscovite is a minor accessory throughout but is coarser grained and more abundant in a narrow interval from 13,080 to 13,090 ft depth.

12,800–12,810 ft Red silt to mudstone with minor detrital white mica (<0.5 mm in maximum dimension) in bedding planes.

12,810–12,820 ft As in the interval immediately above (AA).

12,820–12,830 ft AA.

12,830–12,840 ft AA, with the addition of arkosic fragments and arkosic beds within fragments (fig. 17).

12,840–12,850 ft Granitic fragments present, but exceedingly rare: 3 clasts observed in ~50-g bag of cuttings.

12,850–12,860 ft AA.

12,900–12,910 ft Cuttings dominated by fine-grained red silt and mudstone with minor detrital white mica flakes up to 1 mm in diameter. Approximately 5 percent of cuttings are granitic fragments up to 7 mm in diameter, with translucent quartz, pink K-feldspar, and white plagioclase. There is a very weak magnetic response from a few fragments of both granite and sandstone. Quartz composes two-thirds or more of most granitic fragments. Loose K-feldspar cleavage fragments are present among cuttings. No loose plagioclase or other magmatic grains observed.

12,930–12,940 ft Sedimentary fragments dominate. Granitic fragments contain orange-red feldspars, translucent to white quartz, and rare clusters of magnetite and apatite.

12,960–12,970 ft Granite is a deeper red than in lower intervals. Quartz is milky. Rare clusters of intergrown oxide(s) and apatite.

12,970–12,980 ft Magmatic quartz grains are translucent to faintly milky. Magnetite and apatite most commonly occur together. Magnetite rarely occurs without apatite, but apatite is not observed without adjacent magnetite in this interval.

12,980–12,990 ft AA, with some finer grained apatite.

12,990–13,000 ft AA.

13,000–13,010 ft Magmatic quartz grains are translucent to faintly milky. Magnetite and apatite most commonly occur together. Magnetite rarely occurs without apatite, but apatite is not observed without adjacent magnetite in this interval.

13,070–13,080 ft Pink-red granite. Stained with red oxides and slightly chalky from weathering. Apatite occurs as rare, deep green resinous grains ranging from 0.2 to 1.0 mm in diameter without associated magnetite. Magnetite is less common than from 13,160 ft to TD.

13,080–13,090 ft Granite contains abundant euhedral muscovite books up to 1 mm in diameter. Otherwise, AA.

13,100–13,110 ft AA. Muscovite is very rare.

13,120–13,130 ft Apatite grains occur in clusters with magnetite but also occur without magnetite. Apatite tends to be sucrosic and more yellow when with magnetite, and resinous and greener when not with magnetite. Quartz is milky. No muscovite observed.

13,140–13,150 ft Apatite-magnetite clusters are abundant. Quartz is milky. Feldspars are orange-red as in preceding intervals.

13,160–13,170 ft Pink granitic fragments (2–5 mm in maximum dimension) dominate the cuttings, with ~10 percent contamination by red siltstone fragments (2–6 mm in maximum dimension). Grain size of quartz and feldspars (~4 mm in maximum dimension) is similar to that of cuttings, perhaps larger in places; therefore, the maximum grain size is unknown. K-feldspar grains are pink to red to deep red. Quartz is translucent and commonly contains magnetite inclusions ~0.05–0.1-mm in maximum dimension. Plagioclase is pink, paler than K-feldspar, and weakly translucent. Magnetite is common, ranges from 0.05 to 0.5 mm in maximum dimension, and is commonly euhedral. It occurs as inclusions in quartz grains or at quartz-feldspar grain boundaries, where it commonly occurs with apatite. Apatite is yellow to green, brittle, sucrosic to resinous, very fine grained to coarse grained (up to 3 mm in maximum dimension), and intimately associated with magnetite.

13,250–13,260 ft Contains subequal amounts of pink-red granite and red siltstone contaminant. Siltstone fragments are consistently larger than igneous bits. Other contaminants are rare and include limestone and white sandstone. Granite occurs AA.

13,260–13,270 ft AA. Granitic fragments occur with pink-red feldspars and translucent quartz (with abundant red siltstone contaminant). Two granitic fragments contain 1-mm thick, very fine grained chlorite(?) veins and parallel submillimeter fractures filled with calcite. This composition indicates a small, low-grade shear zone. Magnetite-apatite clusters are common. Apatite is sucrosic to resinous. One siltstone fragment (contaminant from above) contains pale yellow mineral grains, which may be detrital apatite.

13,270–13,284 ft (TD) Pink-red granite fragments, AA, compose a slim majority. Larger red mudstone and fine-grained sandstone fragments are abundant and commonly contain conspicuous mica (0.1–0.5 mm in maximum dimension) and rare large (0.5 mm in diameter) quartz grains, which seem to be matrix-supported. Other contaminants are rare and include limestone and white sandstone.

Thin Section Petrography

Thin sections were prepared of cuttings from the following depth intervals:

12,960–12,970 ft

12,970–12,980 ft

12,980–12,990 ft

13,080–13,090 ft

The basement lithology here is a massive, coarse-grained, pink to red-orange granite comprised of subequal amounts of quartz, plagioclase, and K-feldspar with minor muscovite, apatite, and opaque minerals, as well as rare zircon. Plagioclase grains are commonly euhedral with polysynthetic and deformation twins and contain ubiquitous fine-grained inclusions of sericite and hematite (figs. 18–21), which impart the red color to the rock fragments. K-feldspar grains are typically anhedral with crosshatch twinning. Compared to plagioclase, K-feldspar grains are relatively unaltered except for muscovite fillings along cleavages (figs. 19–21), although K-feldspar and plagioclase are similarly altered in the topmost sampled interval (fig. 18). A patchy red oxide staining—a deeper, darker red than the pink-orange hue imbued by the alteration of plagioclase—is common along grain boundaries in fragments from the upper intervals (12,960–12,980 ft depth; for example, fig. 19) but is not present in the lower sample (13,080–13,090 ft depth; for example, fig. 21). Graphic intergrowths of quartz and K-feldspar are rare but present in some fragments. Quartz grains are equant, anhedral to euhedral (fig. 18), and commonly display undulose or patchwork extinction. Muscovite occurs as euhedral to subhedral flakes up to 1 mm across and as anhedral inclusions within plagioclase (figs. 19 and 21). These muscovite populations are strongly associated with Ti oxides (for example, on the right side of fig. 19). Muscovite also occurs as fillings along cleavages of K-feldspar grains (figs. 18, 19, 21). Calcite occurs in rare veins 50–100 micrometers (μm) thick and in micropores within feldspars. Opaque grains commonly retain euhedral outlines (fig. 20), but the primary phases are exsolved to mottled symplectic intergrowths of iron (Fe) and Ti oxides. Apatite and zircon grains are commonly euhedral and are strongly associated with opaque grains, within which they commonly occur as inclusions.

Notes on XRD Methods and Results

Granitic fragments were separated from sedimentary fragments and other contaminating cuttings by hand under a binocular microscope. Five subsamples of granitic cuttings weighing 0.6–0.8 g each were separated from the following depth intervals:

12,960–12,970 ft

12,970–12,980 ft

12,980–12,990 ft

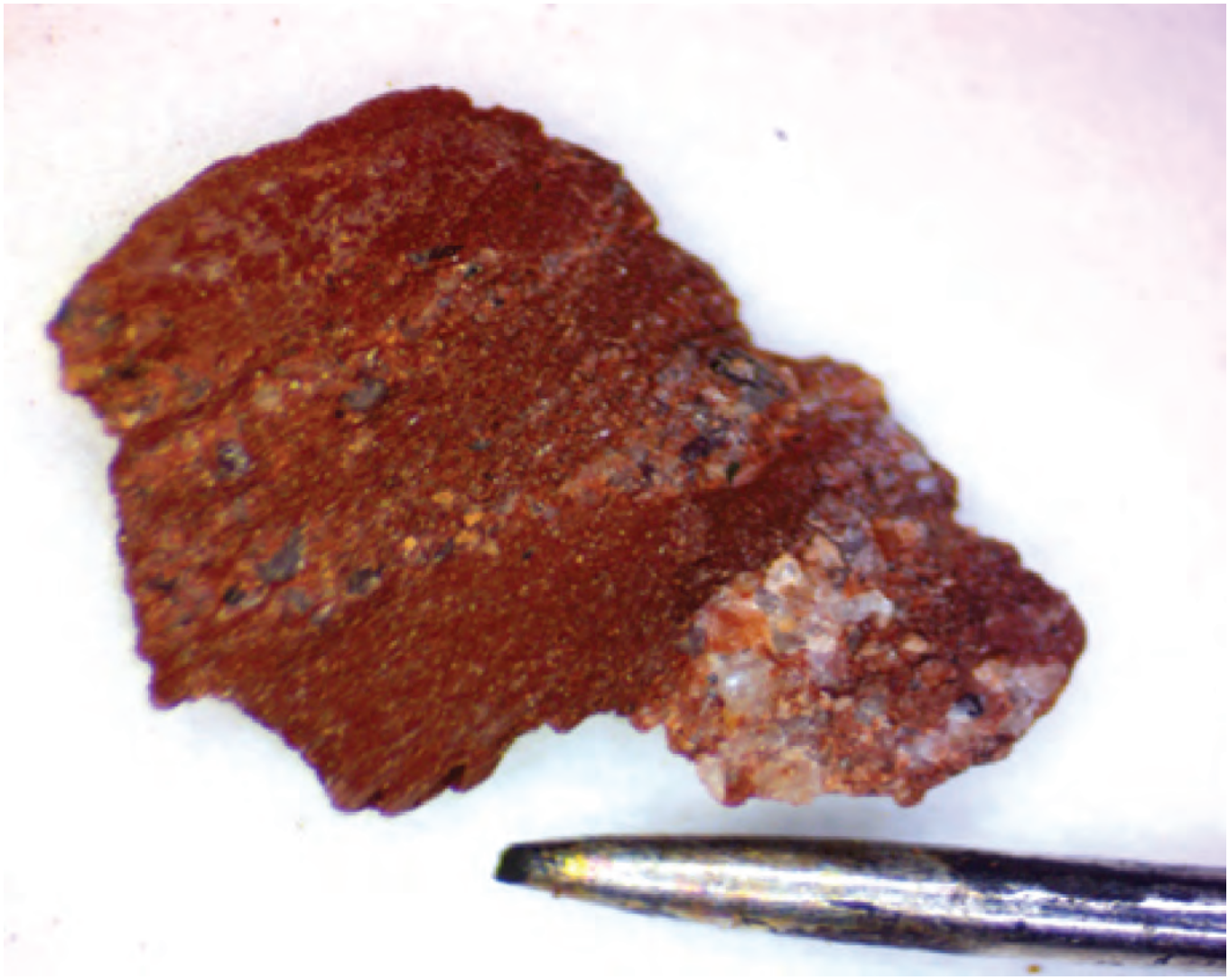

Figure 17. Arkosic fragment from borehole W12509 from 12,830 to 12,840 feet depth. Width of metal pin is approximately 2 millimeters. Photograph by Ryan Deasy, U.S. Geological Survey.

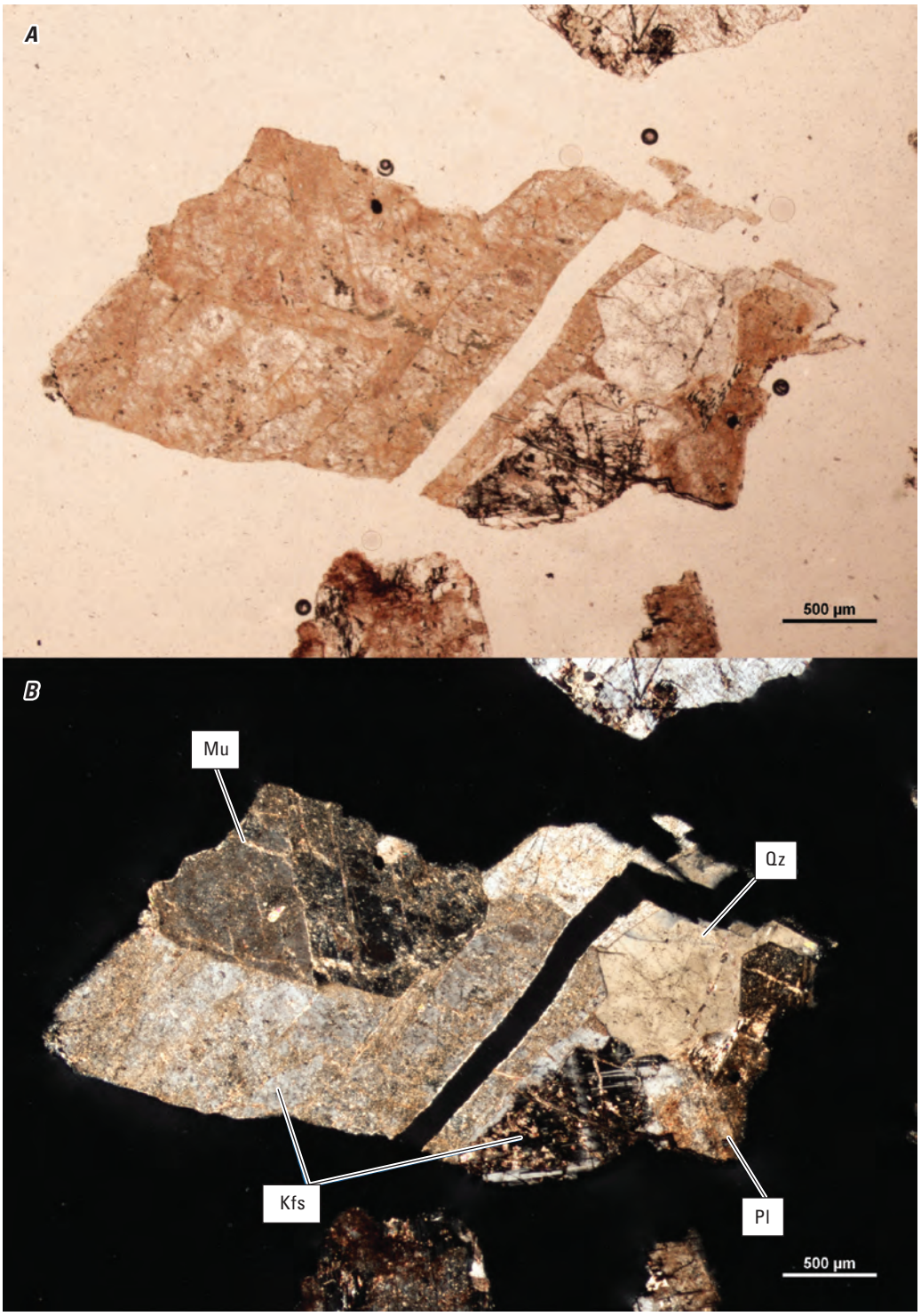

Figure 18. Pair of photomicrographs in plane-polarized light (*A*) and cross-polarized light (*B*) of granitic cuttings fragments from borehole W12509 from 12,970 to 12,980 feet depth. Terms: Kfs, potassium feldspar; Qz, quartz; Mu, muscovite; Pl, plagioclase; µm, micrometer. Photomicrographs by Ryan Deasy, U.S. Geological Survey.

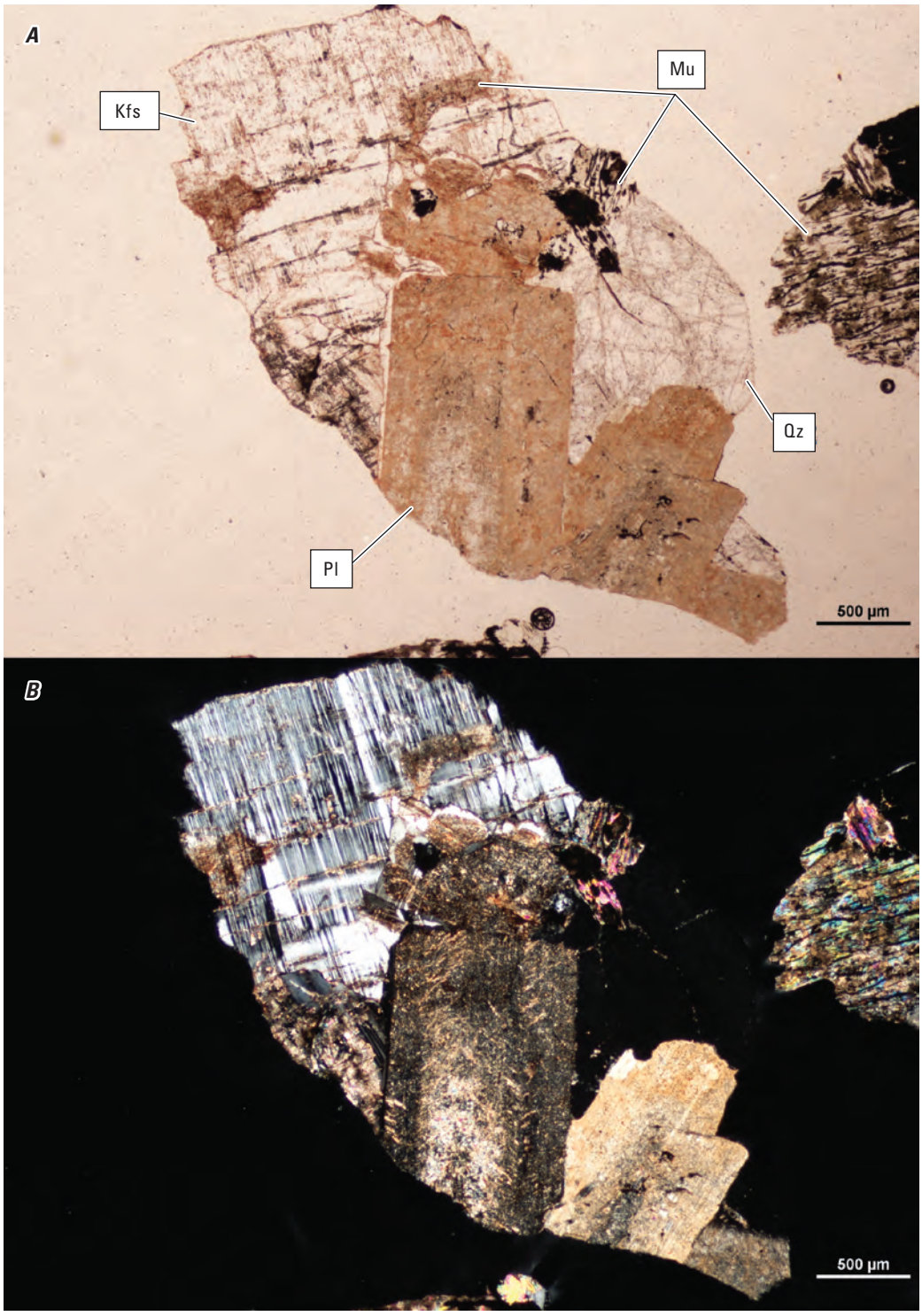

Figure 19. Pair of photomicrographs in plane-polarized light (*A*) and cross-polarized light (*B*) of cuttings fragments from borehole W12509 from 12,980 to 12,990 feet depth. Terms: Kfs, potassium feldspar; Qz, quartz; Mu, muscovite; Pl, plagioclase; µm, micrometer. Photomicrographs by Ryan Deasy, U.S. Geological Survey.

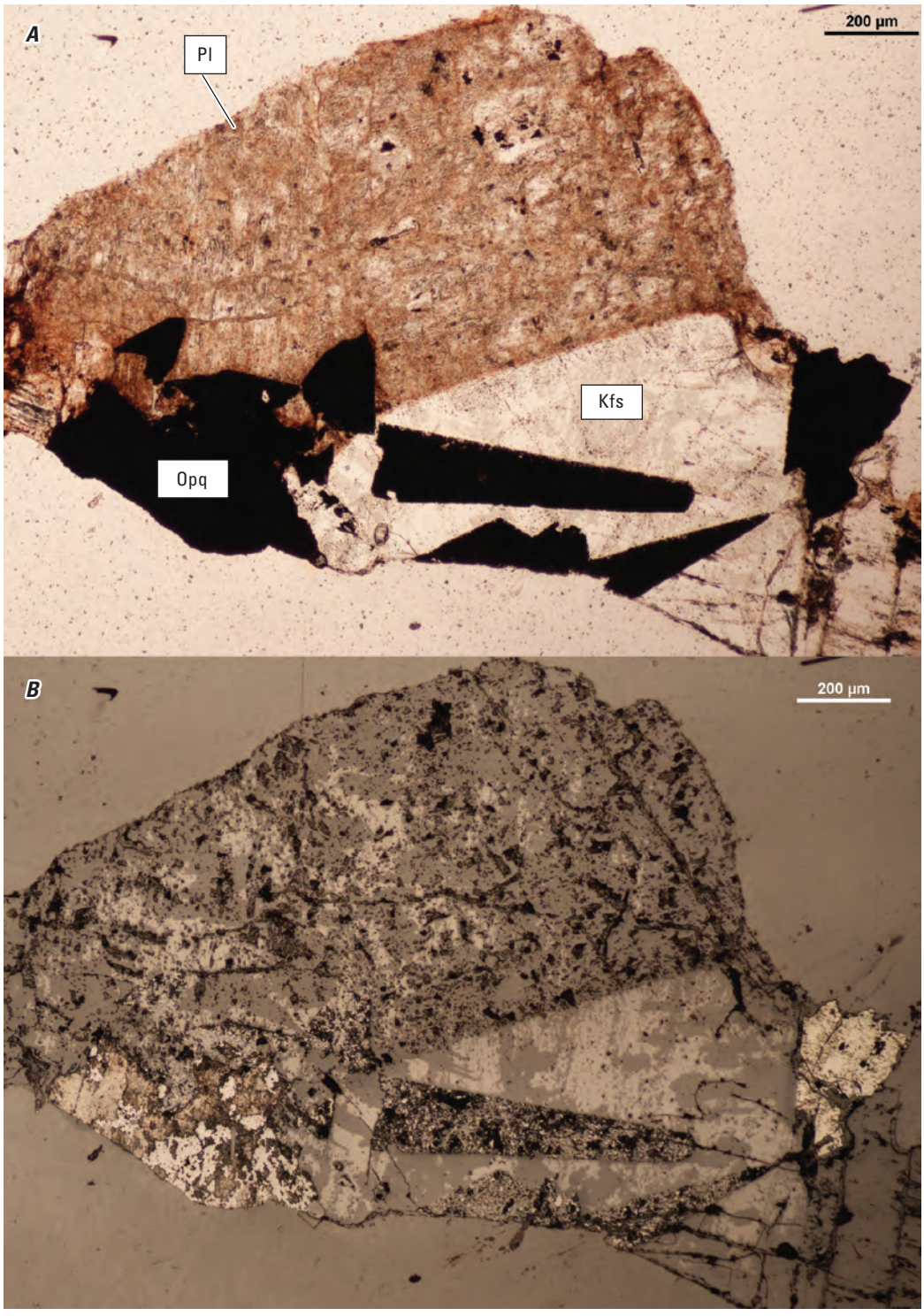

Figure 20. Pair of photomicrographs in plane-polarized light (*A*) and reflected light (*B*) of cuttings fragments from borehole W12509 from 12,970 to 12,980 feet depth. Terms: Kfs, potassium feldspar; Mu, muscovite; Opq, opaque mineral; µm, micrometer. Photomicrographs by Ryan Deasy, U.S. Geological Survey.

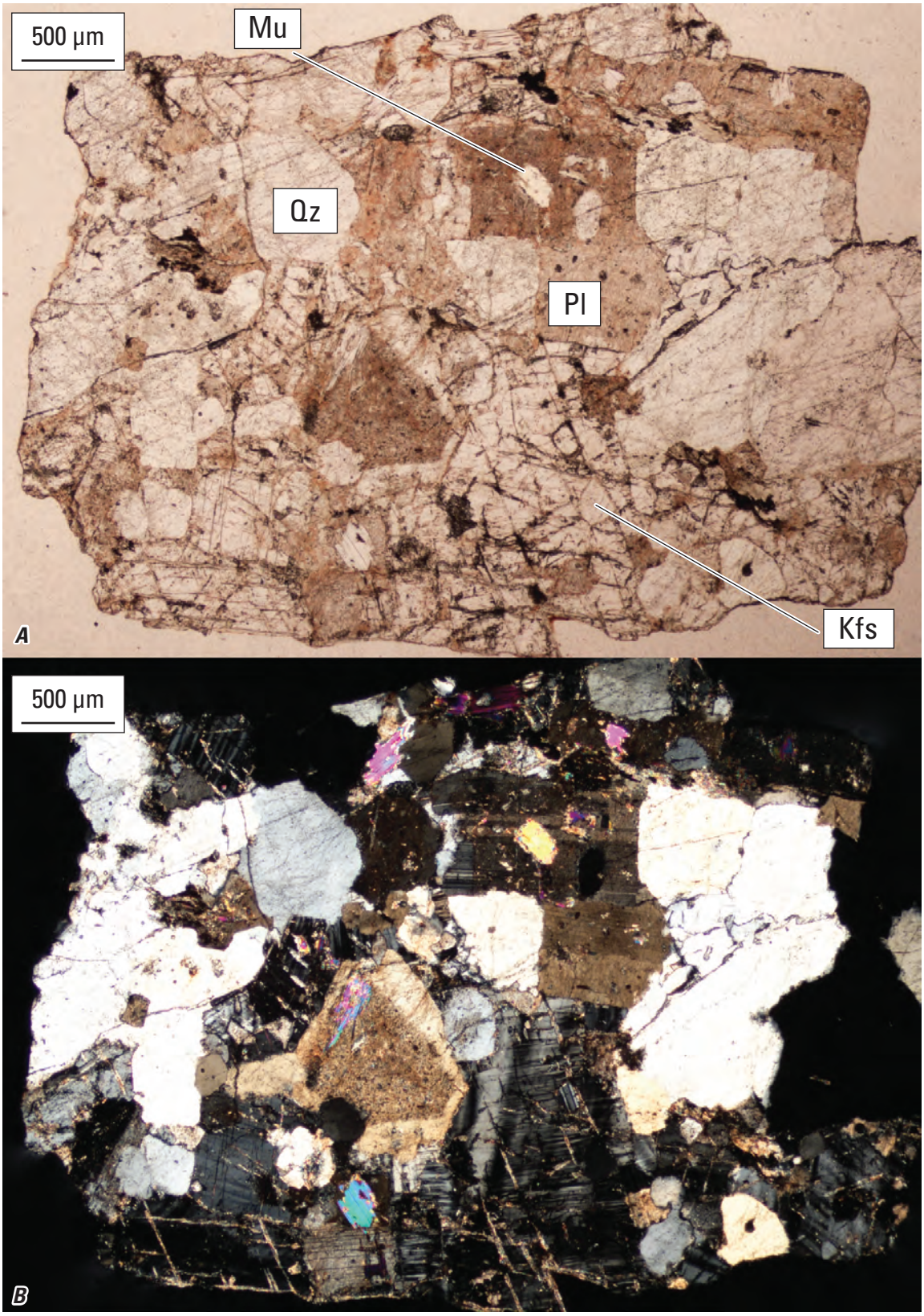

Figure 21. Pair of photomicrographs in plane-polarized light (*A*) and cross-polarized light (*B*) of cuttings fragments from borehole W12509 from 13,080 to 13,090 feet depth. Terms: Kfs, potassium feldspar; Qz, quartz; Mu, muscovite; Pl, plagioclase; µm, micrometer. Photomicrographs by Ryan Deasy, U.S. Geological Survey.

There was sufficient granitic material among the cuttings in each of these intervals to separate and analyze two subsamples from each of the upper two intervals. These subsamples provided an opportunity to test both the effectiveness of the hand-picking method and the representativeness of the sample fractions by revealing compositional variations between small fractions of ostensibly identical coarse-grained rock. The five subsamples were each ground by hand in an agate mortar and pestle while being continuously lubricated with acetone during grinding. The mortar and pestle were thoroughly cleaned between subsamples. The resulting fine powders were allowed to air dry. The powders were placed in 2-cm-wide cavities of circular "back-pack" mounts and scanned in a Panalytical X'Pert diffractometer with a Cu anode from an angular range of 3–90° 2Θ. Semiquantitative mineral abundances (Deasy and others, 2024b) were obtained by Rietveld refinement modeling in HighScore Plus (Malvern Panalytical, 2018).

Additionally, a sample of K-feldspar concentrate (prepared for $^{40}Ar/^{39}Ar$ analysis) from 12,980 to 12,990 ft depth was placed in an automated Brinkman grinder fitted with an agate mortar and pestle. The sample was continuously lubricated with acetone during grinding. The resulting coarse powder was further ground by hand in a corundum mortar and pestle, again lubricated with acetone, and allowed to air dry. The powder was then mounted on a silicon "zero background" smear mount and analyzed on a Bruker D8 diffractometer with a Cu anode and point detector from an angular range of 2–100° 2Θ at a rate of 8 sec/0.02° step. Following this analysis, the still-mounted sample was placed in a chamber with an EG-saturated atmosphere for 24 hours before being removed and immediately reanalyzed on the Bruker instrument from an angular range of 2–30° 2Θ at a rate of 2 sec/0.02° step. No change in the diffraction pattern resulted from EG solvation (fig. 22); therefore, the sample is interpreted not to contain expandable clay minerals. Semiquantitative mineral abundances in each subsample (Deasy and others, 2024b) were determined by Rietveld modeling in TOPAS (Bruker AXS, 2011). Major and trace element geochemical analyses of all powders were thereafter obtained by instrumental neutron activation analysis (INAA)/inductively coupled plasma optical emission spectrometry (ICP-OES)/inductively coupled plasma mass spectrometry (ICP-MS) by Activation Laboratories, Inc. (Deasy and others, 2024a).

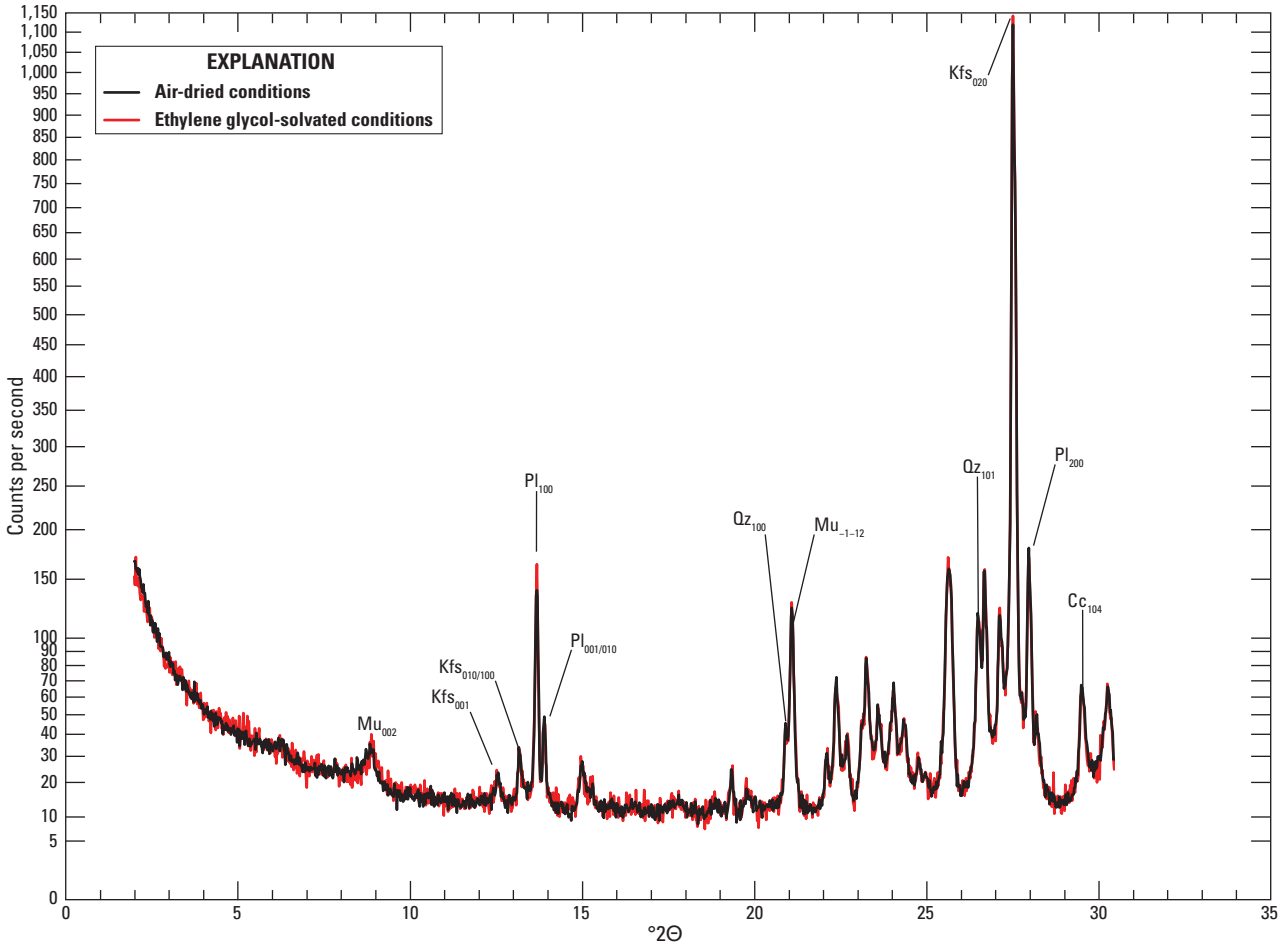

Figure 22. X-ray diffractograms of potassium-feldspar concentrate from borehole W12509 from 12,980 to 12,990 feet depth under air-dried (black line) and ethylene glycol-solvated (red line) conditions. The *y*-axis is in square root scale. Selected peaks are labeled with mineral abbreviations. Numbers in subscript denote Miller indices. Terms: °2Θ, degrees two theta; Kfs, potassium feldspar; Qz, quartz; Mu, muscovite; Pl, plagioclase; Cc, calcite.

Borehole W12497

Two basement lithologies are present in cuttings from this borehole. Olivine gabbro was first encountered at ~12,120 ft depth; granodiorite occurs from 12,280 to 12,400 ft depth.

Previous Work

Barnett (1975, p. 134) reports 360 ft of basement rock penetration from 12,040 to 12,400 ft depth and describes a thin section of cuttings from 12,390 to 12,400 ft depth (TD) as follows:

> Altered granophyric granite to granodiorite. 70% myrmekitic intergrowth of quartz and highly sericitized feldspar, indeterminate. Few corroded and altered phenocrysts feldspar with Carlsbad twinning. 15% anhedral quartz. 10% remains of mafic minerals (augite?) altered to chlorite (penninite) and magnetite. 5% dispersed opaques (magnetite), euhedral. Traces epidote and calcite. Also 2 pieces fresher basic rock-gabbro? 70% plagioclase (labradorite). 30% augite, fractured, edges being replaced with actinolite and chlorite.

Cuttings Log

Summary: Two basement lithologies are penetrated in this borehole: a gabbro and a granodiorite. Red micaceous siltstone and gray micaceous marl overlie gabbroic rock at ~12,120 ft depth. Rounded pebbles of the gabbro are present in the basal sediment, indicating an erosional nonconformable contact. Granodiorite occurs at 12,280–12,400 ft depth. Beyond this basic structural juxtaposition, any relationship between the granodiorite and gabbro is not obvious from the cuttings. Some cuttings of both the gabbro and granodiorite are deeply weathered. Whereas the fresh (partially chloritized but not red from oxide staining) gabbroic fragments are green to gray, the weathered gabbroic fragments are a deep rusty red; sharp contacts between red and gray-green domains are present in rare fragments. Fresh granodioritic fragments are pink and the weathered granodioritic fragments are chalky and white. No contacts between weathered white and fresh pink domains were seen among the cuttings.

12,000–12,010 ft Cuttings are 90 percent gray to purple micaceous siltstone with minor red micaceous siltstone, some with reduction spots. The gray rock reacts weakly with 10 percent hydrochloric acid (HCl). The red rock does not react with HCl. Rare subangular granitic fragments, composed dominantly of quartz and commonly bleached pale, do not contain oxides and may or may not be related to the basement rock from 12,280 ft to TD.

12,040–12,050 ft AA.

12,060–12,070 ft AA, with the addition of ~1 percent rounded, white, calcite-bearing, soft kaolinite(?) pebbles.

12,100–12,110 ft AA, with red siltstone composing a greater fraction of cuttings, and the addition of very fine grained quartz arenite. The arenite has no reaction in HCl. Rounded kaolinite pebbles.

12,110–12,120 ft AA.

12,120–12,130 ft First occurrence of significant igneous fragments. Approximately 3 percent igneous fragments of uncertain composition, which are typically deep red, but rare fragments are mottled green, white, and black. Gray siltstone dominates the cuttings—mostly without conspicuous mica, but some clasts contain abundant mica up to 2 mm in diameter—with minor red-purple siltstone and rare marl. Red and white sandstone also present. Several grains of bladed, radial, white zeolite(?).

12,130–12,140 ft Dominantly gabbroic fragments. Some gabbroic fragments are rusty red, others retain fresh olivine. Gray quartz(?) veins observed in 2 gabbroic fragments and in one gray siltstone fragment. Red sandstone clasts with opaque grains are also present (as contaminant). Mica in siltstone is aligned in bedding plane, with ratty edges.

12,140–12,150 ft Very few igneous fragments; nearly all cuttings are contaminant. Gray siltstone contains minor calcite and reacts weakly with HCl. One rounded sandstone fragment containing potential mafic lithic grains also reacts weakly. White mica in siltstone is commonly coarser here than above. Mica flakes are anhedral and are strongly aligned in bedding planes; that is, the flakes are probably detrital, not authigenic. Texture of siltstone fragments is consistently well bedded and thinly laminated. Marl fragments are layered with tan and dark gray bands, are harder than siltstone, and have a strong reaction with HCl.

12,150–12,157 ft Cuttings contain 5–10 percent orthopyroxene- and olivine-bearing gabbroic rock. Grain sizes are 1–2 mm. Some clasts have fine-grained white matrix and contain red (altered) orthopyroxene grains with green overgrowth rims.

12,160–12,170 ft Greater abundance of gabbroic fragments than above.

12,180–12,190 ft AA.

12,200–12,210 ft A plurality of cuttings is red (oxidized) and green (fresh) gabbro, with the remainder being siltstone contamination and rare, deep-red, K-feldspar-bearing fragments that are dissimilar to the basement rock from 12,280 ft to TD.

12,220–12,230 ft AA.

12,240–12,250 ft Red and green gabbroic fragments dominate cuttings, with siltstone contaminant.

12,260–12,270 ft AA, with the addition of ~1 percent epidote vein(?) fragments.

12,270–12,280 ft AA.

12,280–12,290 ft First appearance of characteristic granodiorite. The fraction of felsic fragments increases with depth from here.

12,320 ft–TD Granodiorite fragments dominate the cuttings.

Thin Section Petrography

Olivine Gabbro

The olivine gabbro is a poikilitic rock comprising clinopyroxene oikocrysts enclosing calcic plagioclase and olivine. Most fragments are massive, with randomly oriented phenocrysts (fig. 23). However, in some fragments, plagioclase grains have a shape-preferred orientation and olivine grains have a weak preferred distribution that, together, are suggestive of magmatic foliation or layering (fig. 24). Accessory magmatic minerals include chromite, biotite, and magnetite (fig. 25). In altered fragments, chlorite, clinoamphibole, talc, serpentine, magnetite, and hematite pseudomorphically replace magmatic minerals, preserving magmatic textures (figs. 26–28). Evidence of deformation is limited to rare veins observed in some fragments. These veins are mineralogically and texturally zoned, indicating episodic opening. For example, the fragment shown in figure 29 contains a ~1-mm-thick vein recording at least three episodes of unitaxial fibrous serpentine growth crosscut by a syntaxial fine-grained epidote core.

Clinopyroxene oikocrysts are optically continuous in nearly all fragments (figs. 23, 24, 26); that is, fragments containing more than one clinopyroxene crystal are rare. The size of clinopyroxene grains must therefore be significantly greater than the size of cuttings fragments (~4 mm). Partial replacement of clinopyroxene by clinoamphibole or chlorite occurs in some fragments, but most clinopyroxene is preserved even in the most highly altered fragments (figs. 26–28). Plagioclase occurs as subhedral to euhedral lath-shaped to tabular grains up to 2 mm in maximum dimension. Plagioclase grains are commonly clustered (figs. 23 and 24). Boundaries between clinopyroxene and plagioclase grains are pristine, and both minerals are unaltered in fresh fragments, whereas the boundaries between plagioclase and olivine are lined with chlorite (figs. 23–25). Partial to complete pseudomorphic replacement of plagioclase by prehnite, chlorite, or epidote-clinozoisite occurs in altered fragments. Olivine grains are euhedral to anhedral subequant grains up to 1 mm across and may be unaltered or partially to completely pseudomorphically replaced by chlorite, serpentine and magnetite, or other Fe oxides. Notably, anhedral olivine is more likely to be unaltered (figs. 23 and 25), whereas euhedral outlines are commonly preserved in pseudomorphic replacements (figs. 26–28). Biotite is rare and is identified only in fresh fragments where it is unaltered and shares irregular edges with plagioclase and ilmenite (fig. 25). Primary magnetite makes up a minor fraction of most fragments, forming subhedral to euhedral grains up to 0.5 mm across (fig. 25). Magnetite is also a common product of the alteration of olivine and orthopyroxene, where it occurs in microfractures with serpentine or chlorite (fig. 27). Chromite grains are anhedral, 0.01–0.05-mm subequant to ellipsoidal blebs that occur most commonly as inclusions within olivine (figs. 25–28). Chromite grains are unaltered even where the enclosing mineral has been completely replaced (fig. 26).

Granodiorite

The more felsic basement lithology in this borehole is a pink, massive granodiorite containing euhedral lath-shaped to blocky plagioclase up to 1 mm in maximum dimension (commonly with albite and Carlsbad twins) and subhedral to euhedral clinopyroxene grains up to 0.6 mm in maximum dimension enclosed in graphically intergrown, coarse-grained K-feldspar+quartz (figs. 30–38). K-feldspar and quartz are both optically continuous in domains comprising a quarter or more of each fragment; therefore, the size of K-feldspar+quartz grains are approximately the size of the cuttings fragments (~1–4 mm). Accessory minerals include subhedral to euhedral, wedge-shaped titanite up to 0.4 mm in maximum dimension (figs. 31, 37–39); anhedral to euhedral, subequant magnetite grains up to 0.3 mm across (figs. 30–33, 37–39); subhedral to euhedral, subequant to acicular zirconolite(?) needles up to 0.1 mm in length (figs. 35–39); and apatite (figs. 37 and 38).

The magmatic assemblage has undergone partial alteration, including the replacement of graphic K-feldspar+quartz by spherules of myrmekitic albite+quartz (0.25–2 mm in diameter), which commonly radiate from plagioclase phenocrysts (figs. 30–34, 36–38). Clinopyroxene is partially replaced by fine-grained amphibole along cleavage planes (fig. 38), and magmatic plagioclase has been partially to completely replaced by albite, chlorite, prehnite, and (or) muscovite (figs. 30–34, 37–39). Some magnetite grains and zirconolite(?) needles are uniform in texture (fig. 35), but most are replaced by symplectic intergrowths of ilmenite, rutile, titanite, and (or) magnetite; titanite overgrowths on magnetite and ilmenite are common (figs. 37–39). Some zirconolite(?) grains also contain exsolved baddeleyite (fig. 35) or, less commonly, zircon. Zircon that is not associated with ilmenite is very rare; it occurs in clusters of anhedral to euhedral grains (1–20 µm in maximum dimension), commonly with similarly sized euhedral thorite (fig. 40).

Sharp contacts between coarse-grained laumontite and granodiorite are common in cuttings at all intervals from 12,280 to 12,400 ft depth (fig. 33) and are interpreted as laumontite veins. Because both vein walls have not been observed to occur in the same cuttings fragment and pink to white bladed zeolite fragments are a minor constituent of cuttings fragments, the aperture of laumontite veins must be greater than 4 mm.

The soft, chalky, altered fragments of granodiorite were not investigated in thin section.

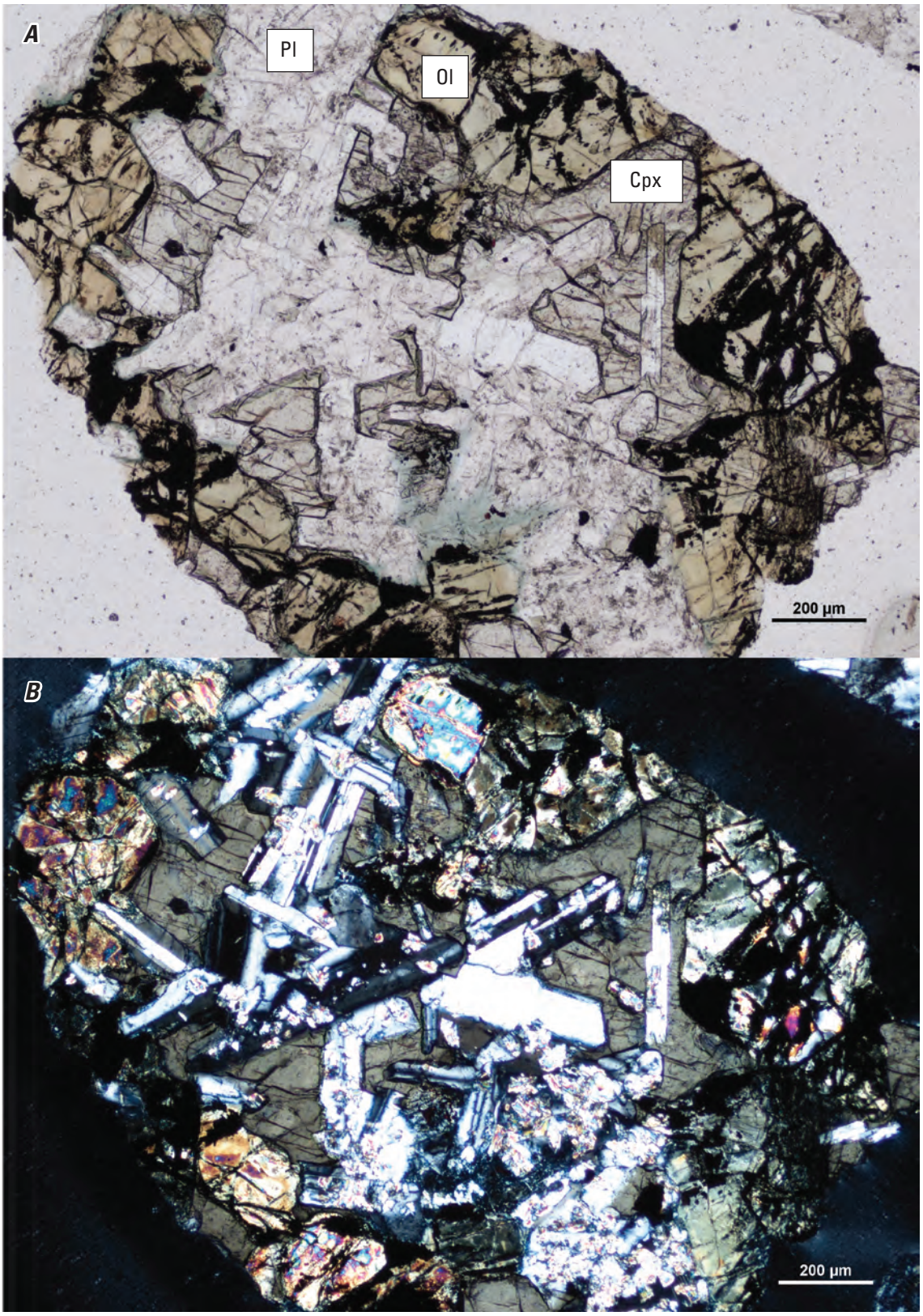

Figure 23. Pair of photomicrographs in plane-polarized light (*A*) and cross-polarized light (*B*) of a gabbroic fragment from borehole W12497 from 12,250 to 12,260 feet depth consisting of an unaltered clinopyroxene oikocryst surrounding partially altered olivine and plagioclase phenocrysts. Terms: Pl, plagioclase; Ol, olivine; Cpx, clinopyroxene; µm, micrometer. Photomicrographs by Ryan Deasy, U.S. Geological Survey.

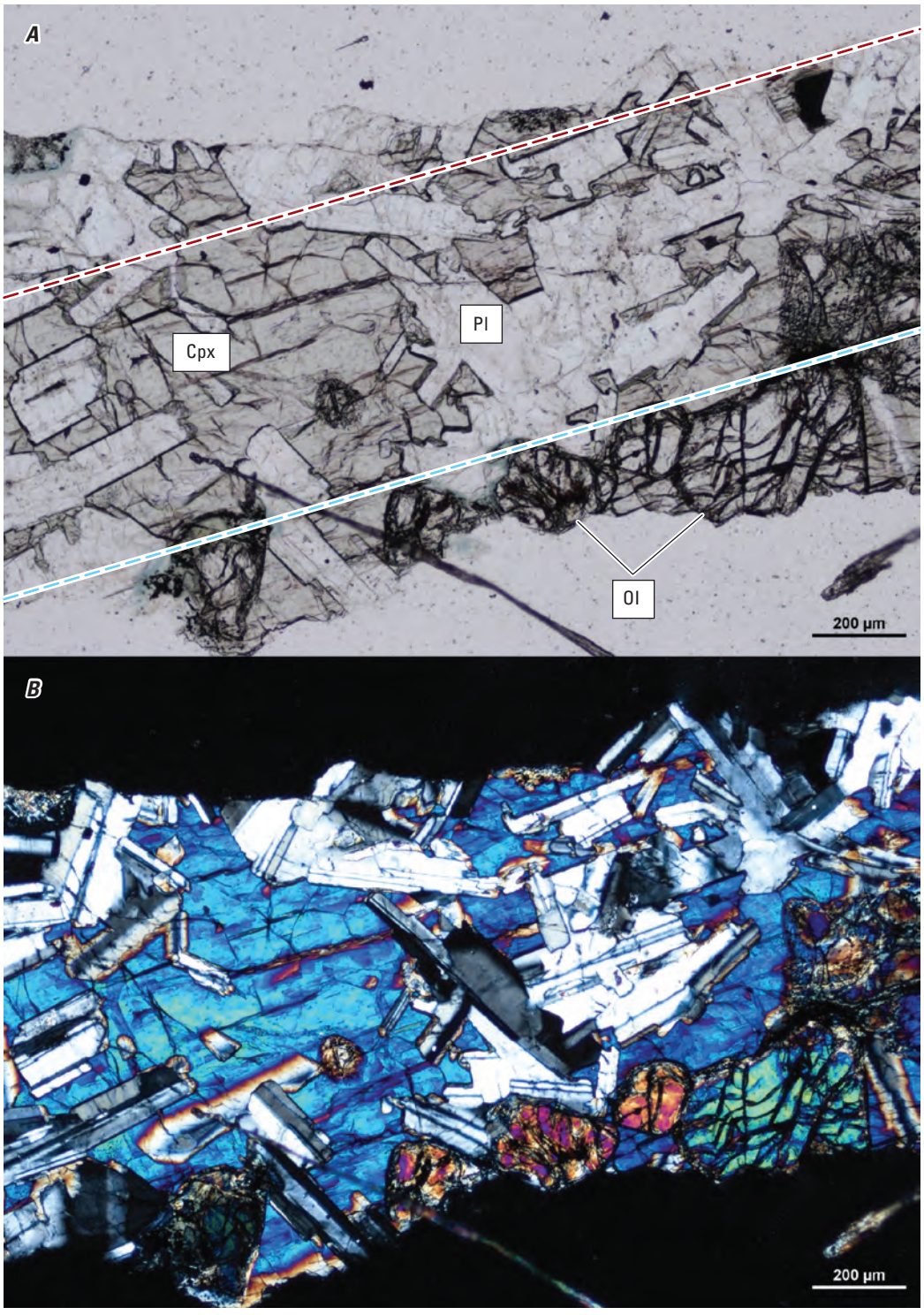

Figure 24. Pair of photomicrographs in plane-polarized light (*A*) and cross-polarized light (*B*) of a gabbroic fragment from borehole W12497 from 12,230 to 12,240 feet depth. The red and blue dashed lines in part *A* indicate the orientations of plagioclase shape-preferred orientation and olivine preferred distribution, respectively. Terms: Cpx, clinopyroxene; Pl, plagioclase; Ol, olivine; µm, micrometer. Photomicrographs by Ryan Deasy, U.S. Geological Survey.

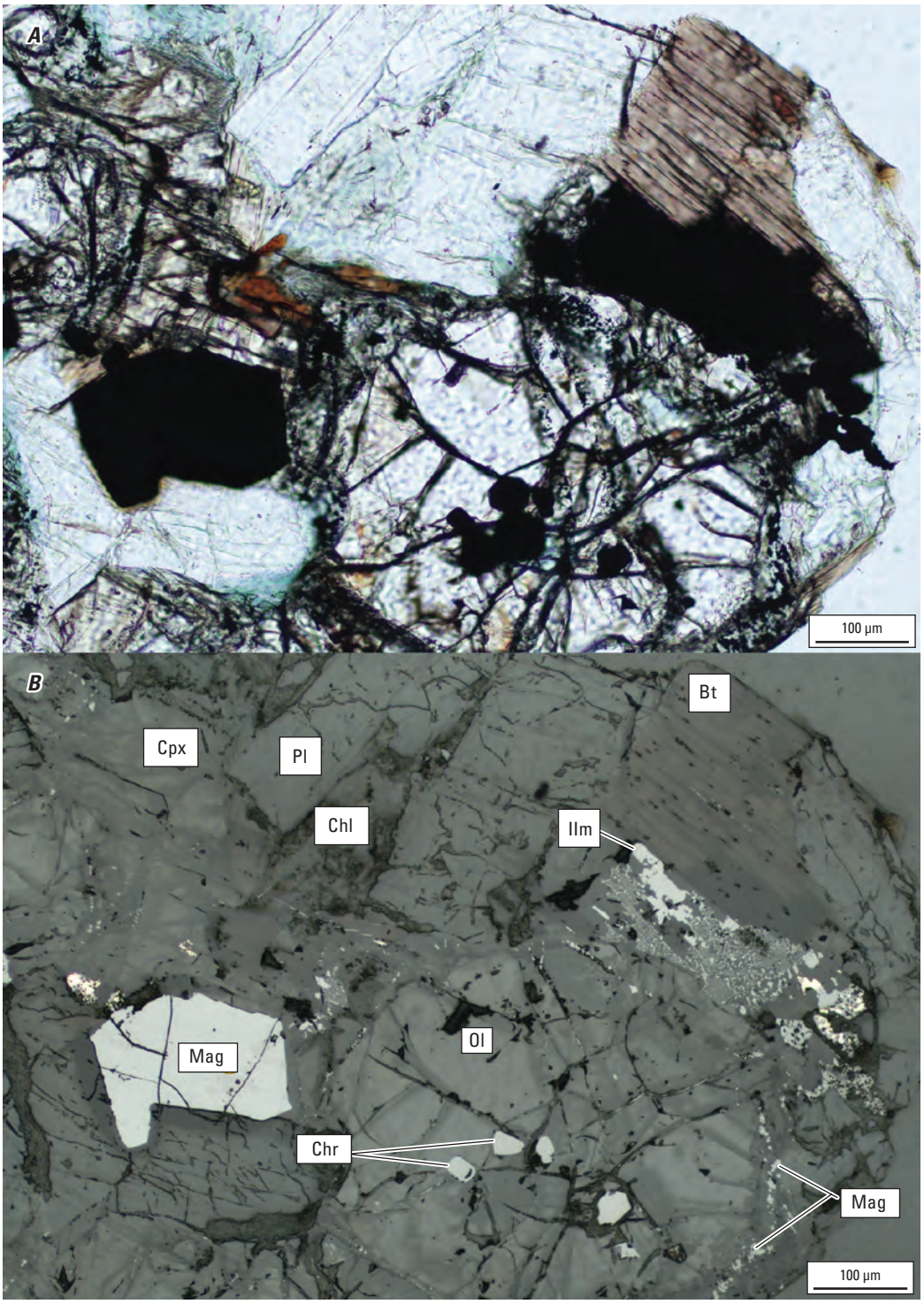

Figure 25. Pair of photomicrographs in plane-polarized light (*A*) and reflected light (*B*) of a gabbroic fragment from borehole W12497 from 12,250 to 12,260 ft depth. Terms: Cpx, clinopyroxene; Pl, plagioclase; Chl, chlorite; Bt, biotite; Ilm, ilmenite; Mag, magnetite; Ol, olivine; Chr, chromite; µm, micrometer. Photomicrographs by Ryan Deasy, U.S. Geological Survey.

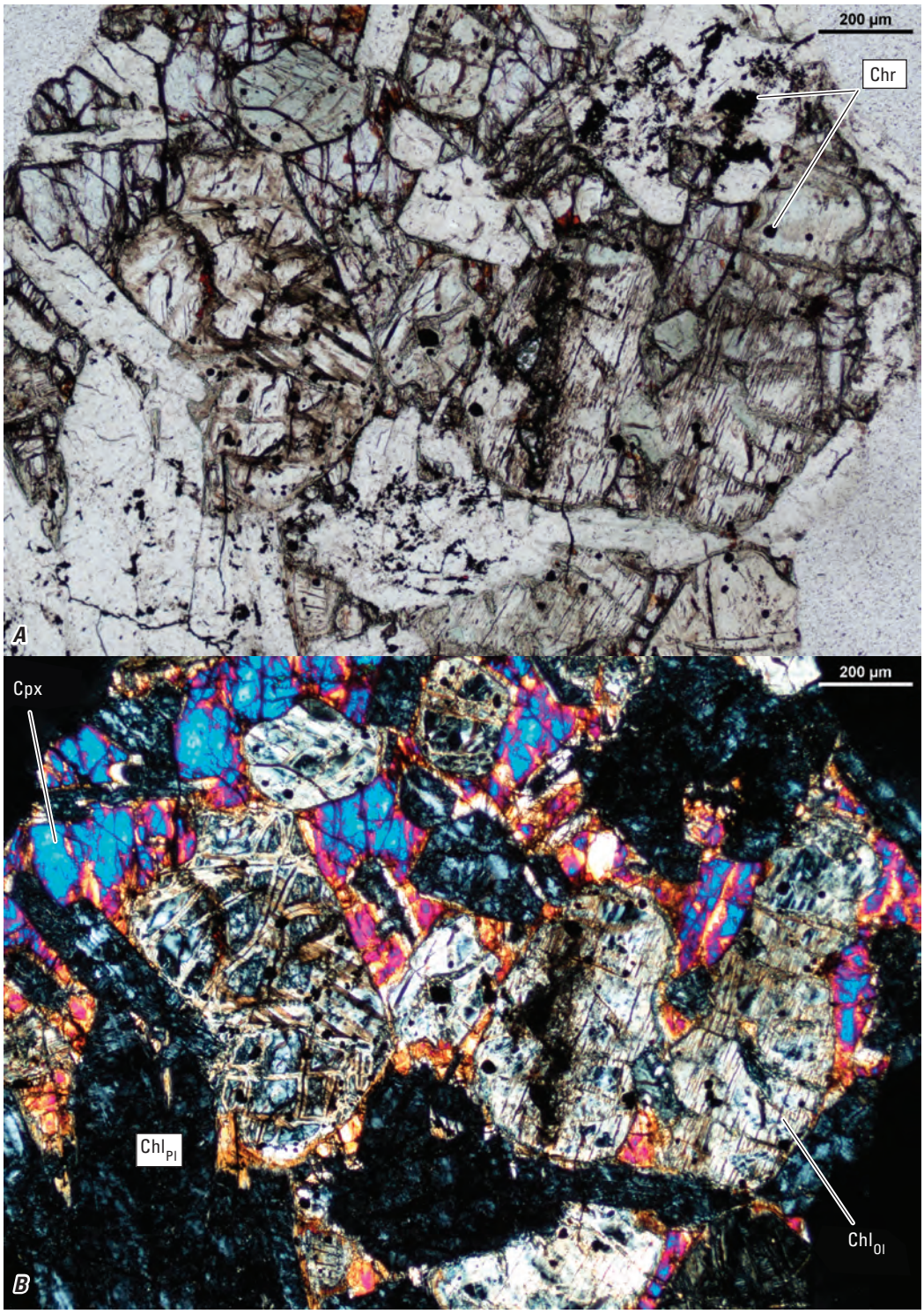

Figure 26. Pair of photomicrographs in plane-polarized light (*A*) and cross-polarized light (*B*) of an altered gabbroic fragment from borehole W12497 from 12,380 to 12,390 feet depth. Mineral abbreviations in subscripts indicate the primary mineral inferred from pseudomorph habit. Terms: Chr, chromite; Cpx, clinopyroxene; Chl, chlorite; Pl, plagioclase; Ol, olivine; µm, micrometer. Photomicrographs by Ryan Deasy, U.S. Geological Survey.

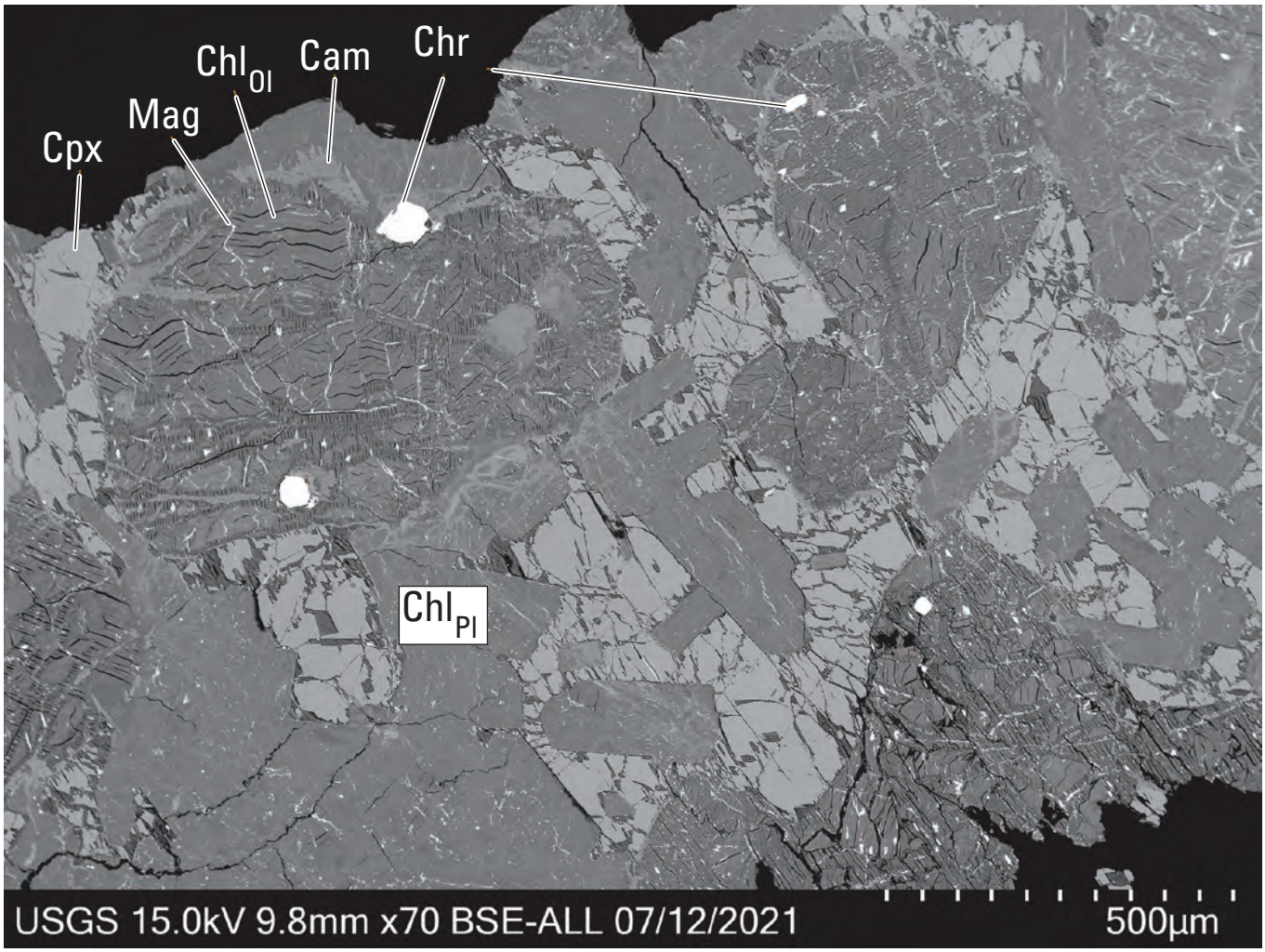

Figure 27. Back-scattered electron (BSE) image of a gabbroic fragment from borehole W12497 from 12,360 to 12,370 feet depth. The same fragment is shown in figure 28. Mineral abbreviations in subscripts indicate the primary mineral inferred from pseudomorph habit. Text in the bottom left identifies data source (USGS); operating conditions including beam potential in kilovolts (15.0 kV), working distance in millimeters (9.8 mm), and image magnification in multiples of actual size (70 times); and date of acquisition (07/12/2021). Terms: Cpx, clinopyroxene; Mag, magnetite; Chl, chlorite; Pl, plagioclase; Ol, olivine; Cam, clinoamphibole; Chr, chromite; µm, micrometer; USGS, U.S. Geological Survey; kV, kilovolt; mm, millimeter; BSE-ALL, back-scattered electron, all energies. Photomicrograph by Ryan Deasy, U.S. Geological Survey.

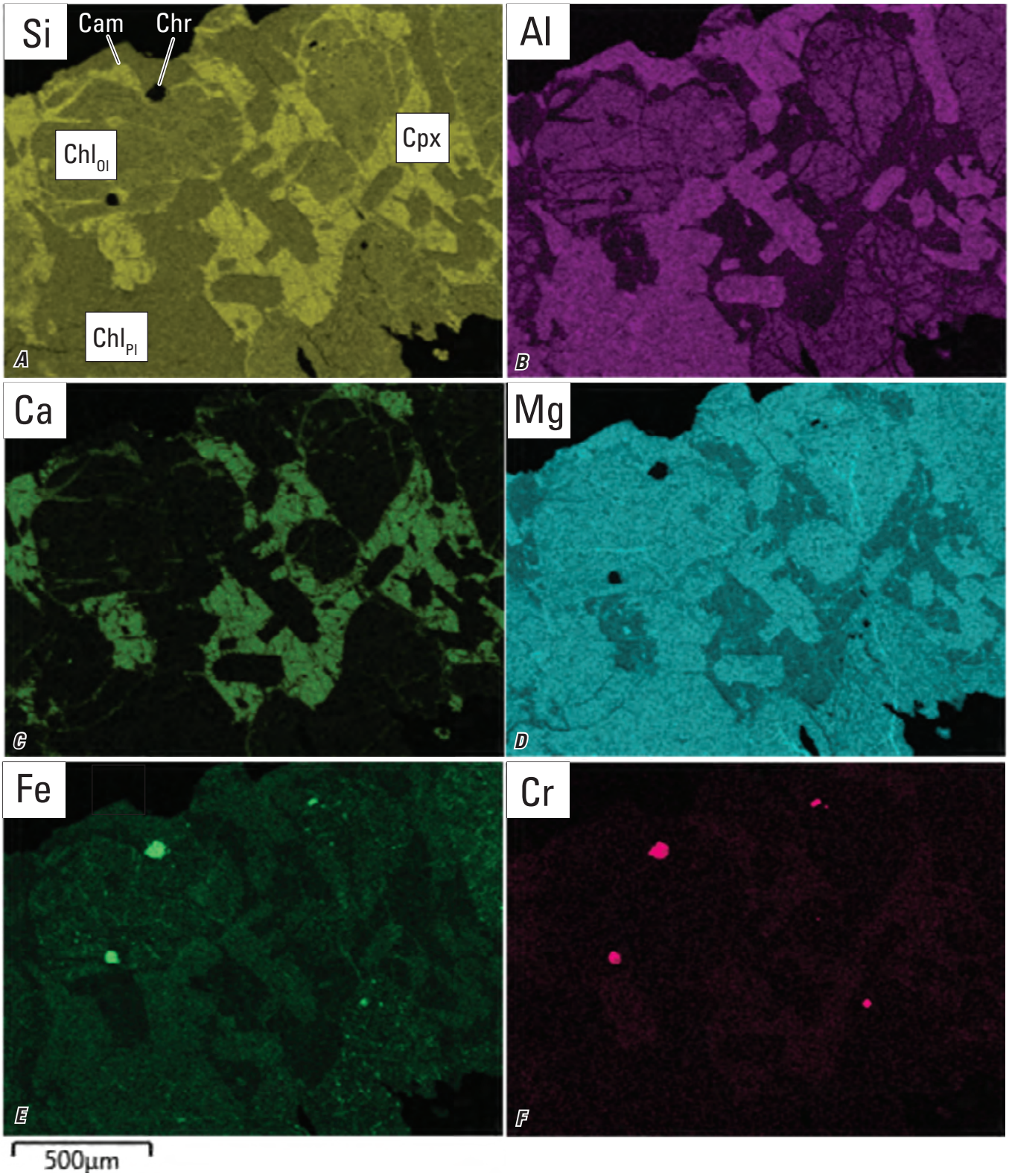

Figure 28. Selected element maps from energy dispersive spectroscopy (*A*–*F*) of a gabbroic fragment from borehole W12497 from 12,360 to 12,370 feet depth. The same fragment is shown in figure 27. Mineral abbreviations in subscripts indicate the primary mineral inferred from pseudomorph habit. Terms: Cam, clinoamphibole; Chr, chromite; Chl, chlorite; Cpx, clinopyroxene; Pl, plagioclase; Ol, olivine; µm, micrometer; Si, silicon; Al, aluminum; Ca, calcium; Mg, magnesium; Fe, iron; Cr, chromium. Photomicrographs by Ryan Deasy, U.S. Geological Survey.

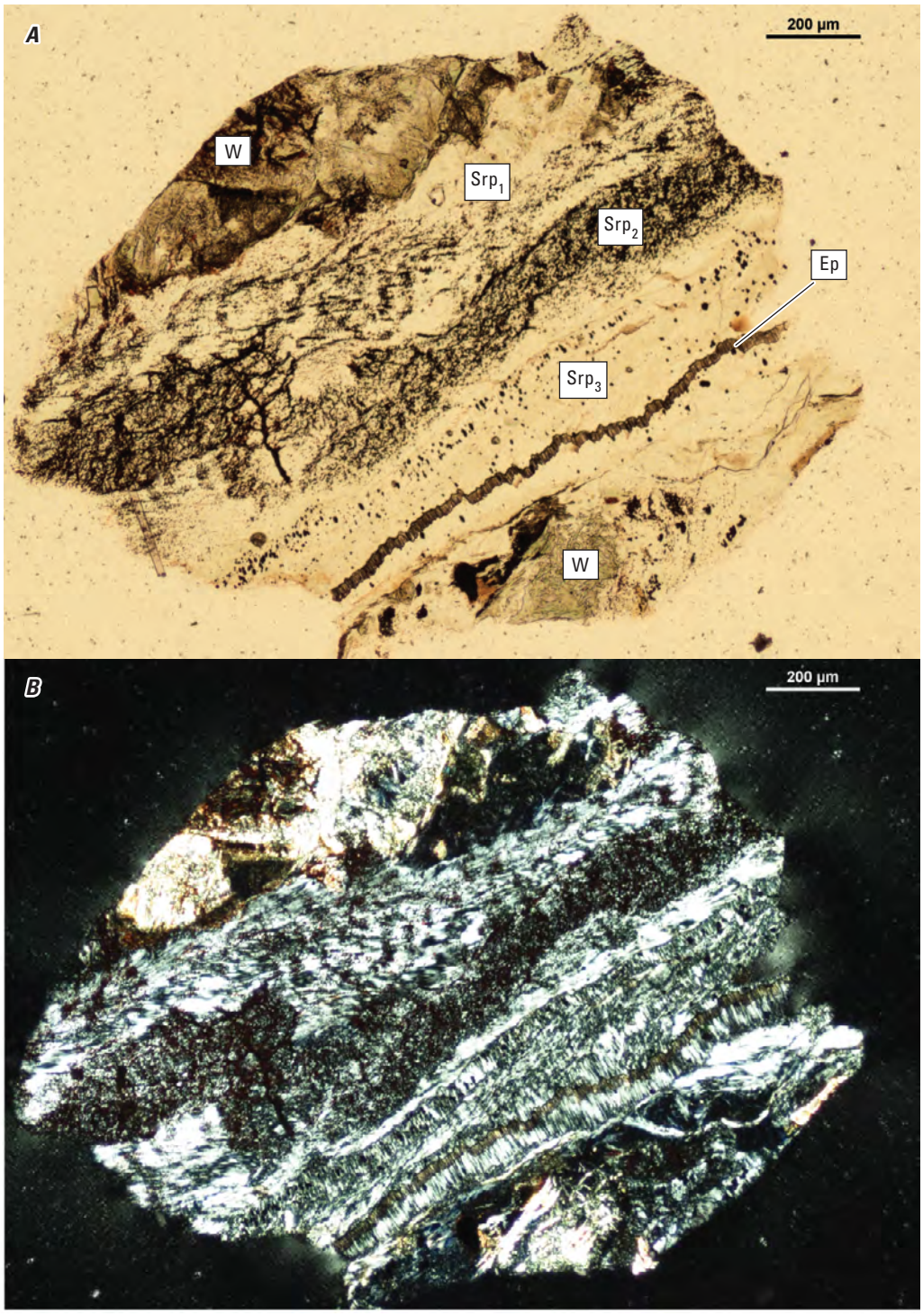

Figure 29. Pair of photomicrographs in plane-polarized light (*A*) and cross-polarized light (*B*) of a vein-bearing fragment from borehole W12497 from 12,230 to 12,240 ft depth. Numbers in subscripts indicate successive generations of serpentine growth in a unitaxial vein. A final pulse of syntaxial opening produced the epidote core. Terms: W, wall rock; Srp, serpentine; Ep, epidote; µm, micrometer. Photomicrographs by Ryan Deasy, U.S. Geological Survey.

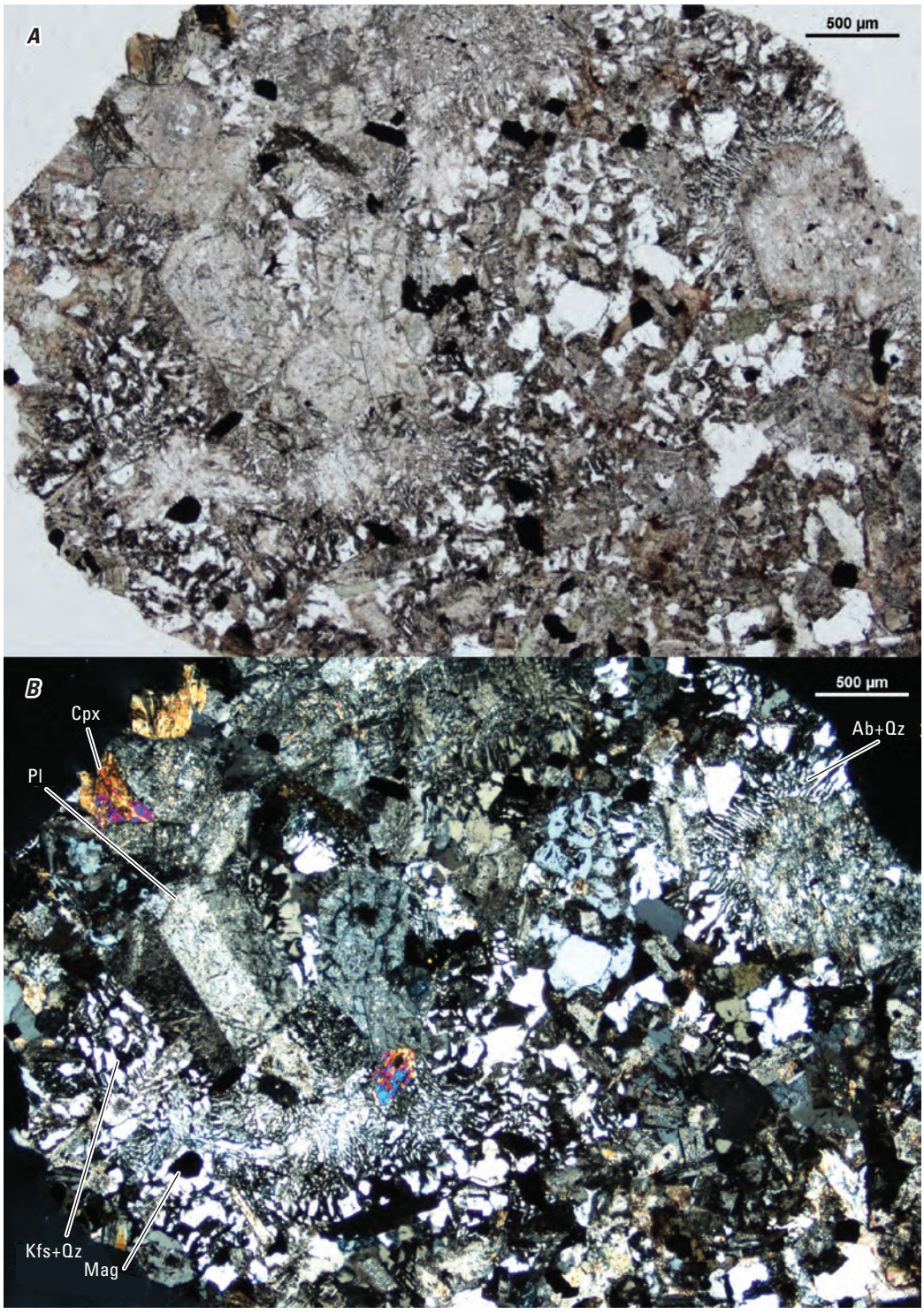

Figure 30. Pair of photomicrographs in plane-polarized light (*A*) and cross-polarized light (*B*) of a granodiorite fragment from borehole W12497 from 12,390 to 12,400 feet depth. Terms: Pl, plagioclase; Cpx, clinopyroxene; Ab, albite; Qz, quartz; Kfs, potassium feldspar; Mag, magnetite; µm, micrometer. Photomicrographs by Ryan Deasy, U.S. Geological Survey.

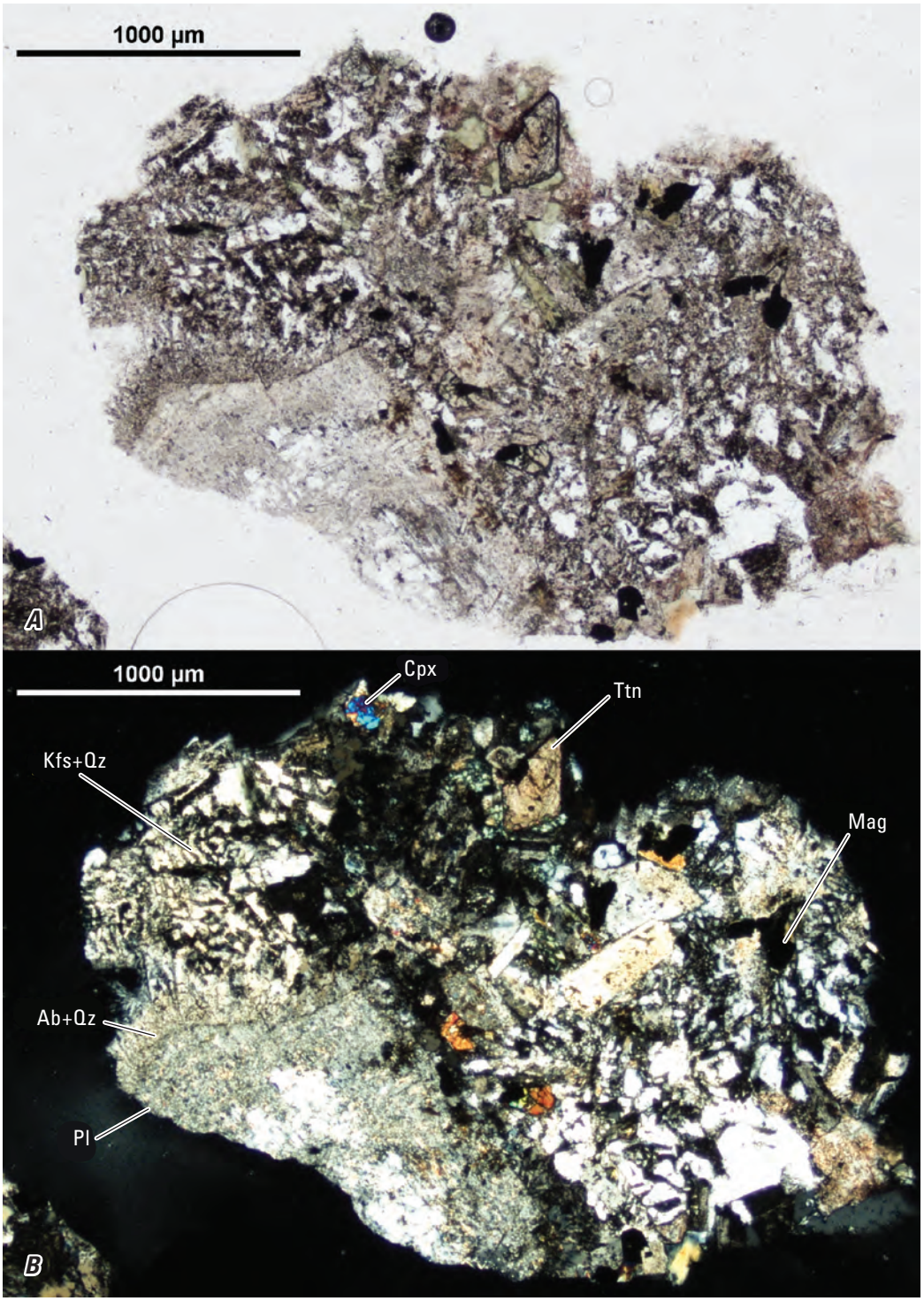

Figure 31. Pair of photomicrographs in plane-polarized light (*A*) and cross-polarized light (*B*) of a granodiorite fragment from borehole W12497 from 12,340 to 12,350 feet depth. Terms: Cpx, clinopyroxene; Qz, quartz; Kfs, potassium feldspar; Mag, magnetite; Ab, albite; Ttn, titanite; Pl, plagioclase; µm, micrometer. Photomicrographs by Ryan Deasy, U.S. Geological Survey.

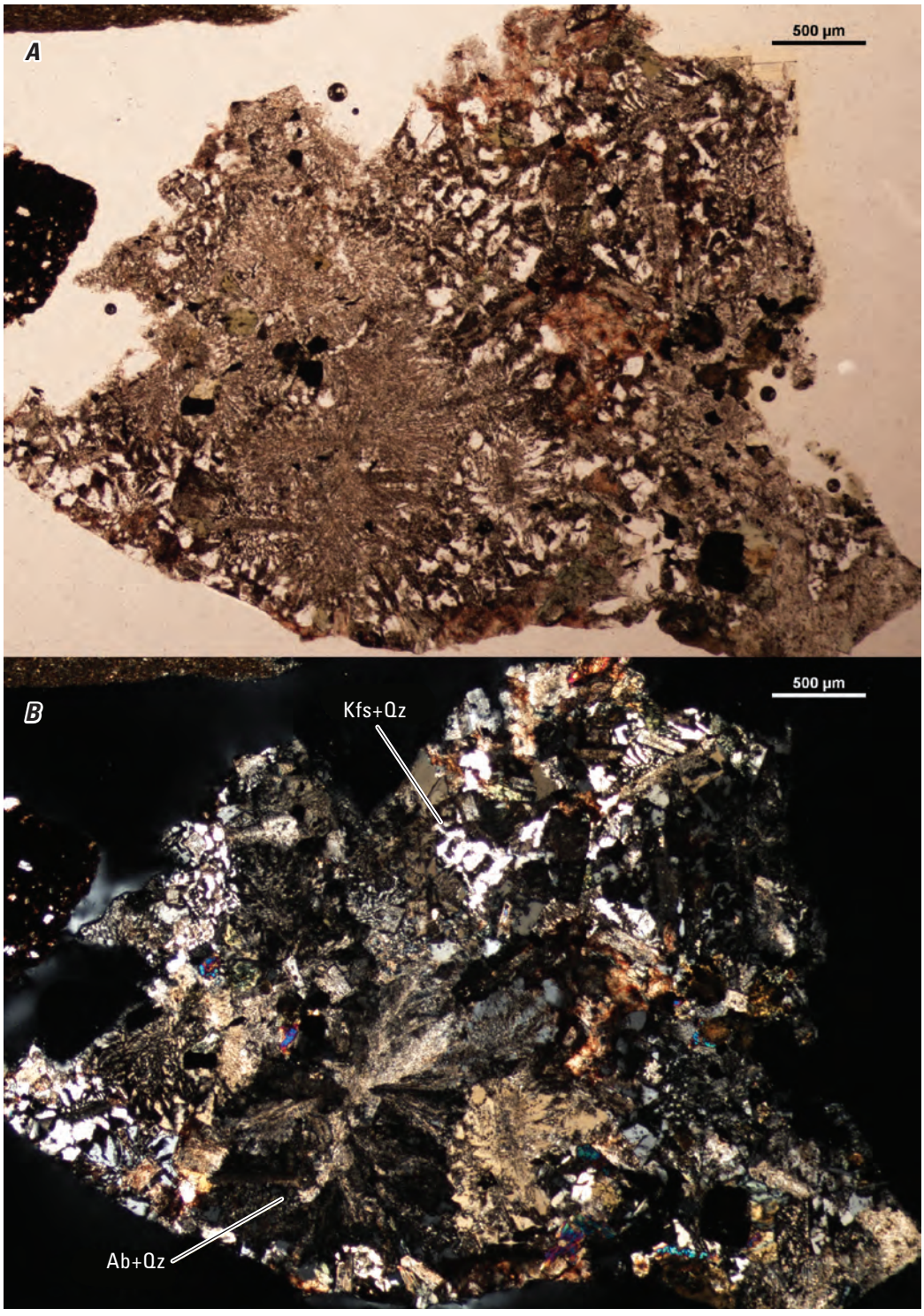

Figure 32. Pair of photomicrographs in plane-polarized light (*A*) and cross-polarized light (*B*) of a granodiorite fragment from borehole W12497 from 12,370 to 12,380 feet depth. Note the radial pattern of albite+quartz (Ab+Qz) myrmekitic intergrowths (left side) overprinting graphic potassium feldspar+quartz (Kfs+Qz) intergrowths. Term: µm, micrometer. Photomicrographs by Ryan Deasy, U.S. Geological Survey.

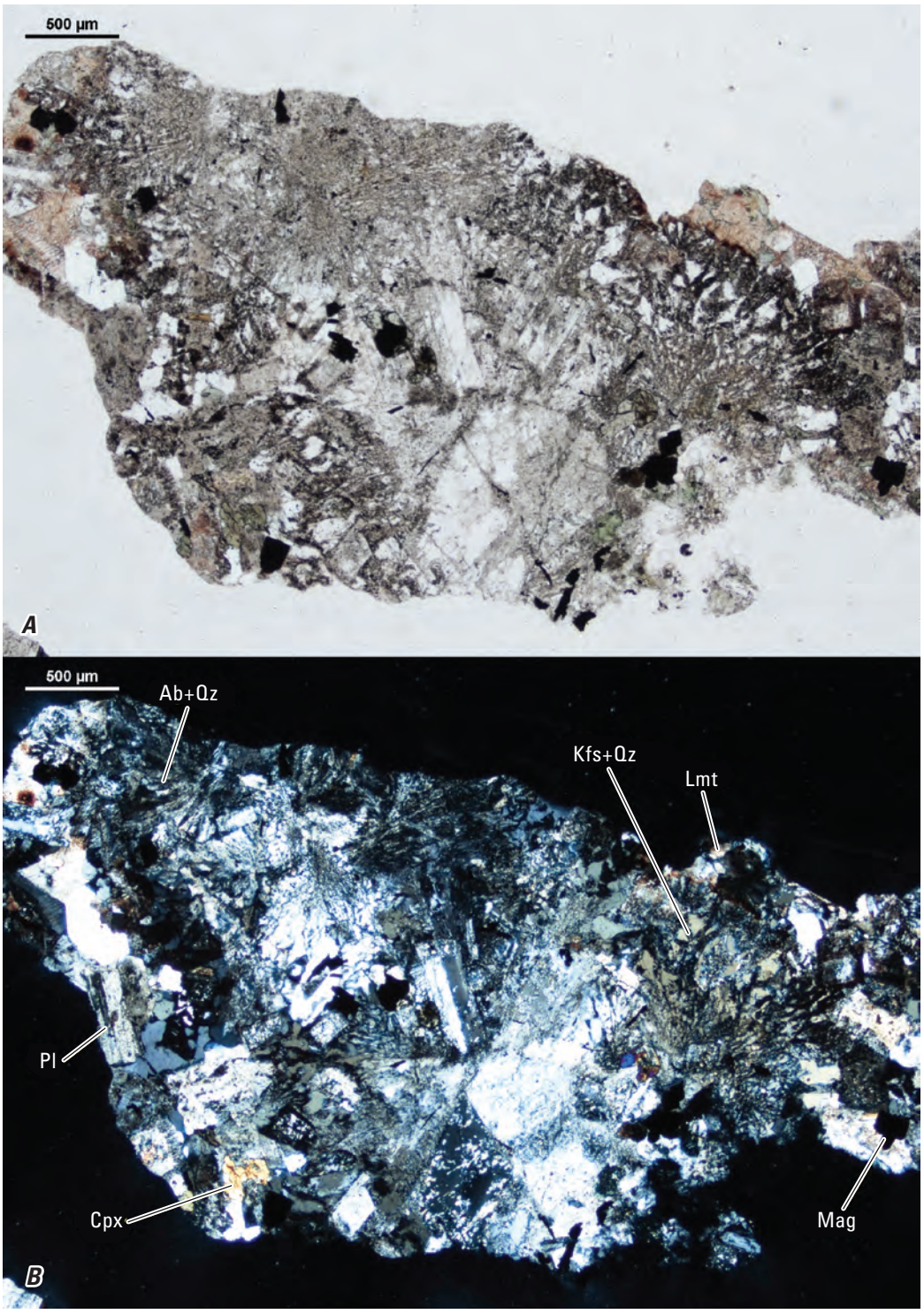

Figure 33. Pair of photomicrographs in plane-polarized light (*A*) and cross-polarized light (*B*) of a granodiorite fragment from borehole W12497 from 12,390 to 12,400 feet depth. Terms: Ab, albite; Qz, quartz; Kfs, potassium feldspar; Lmt, laumontite; Pl, plagioclase; Cpx, clinopyroxene; Mag, magnetite; µm, micrometer. Photomicrographs by Ryan Deasy, U.S. Geological Survey.

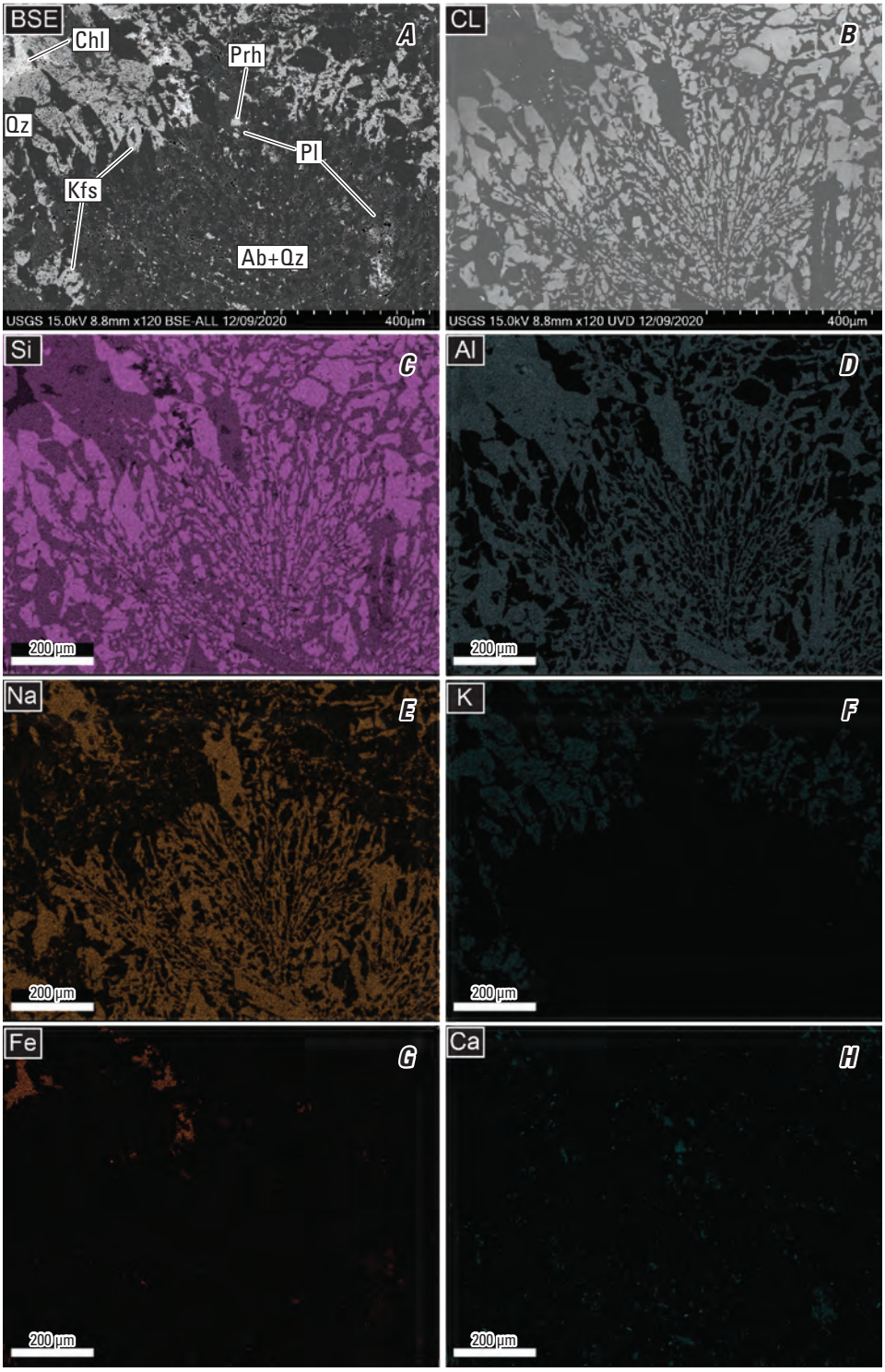

Figure 34. Back-scattered electron (BSE) (*A*), cathodoluminescence (CL) (*B*), and selected element maps from energy dispersive spectroscopy (*C*–*H*) of myrmekite alteration in a granodiorite fragment from borehole W12497 from 12,390 to 12,400 feet depth. Text in the bottom left of parts *A* and *B* identifies data source (USGS); operating conditions including beam potential in kilovolts (15.0 kV), working distance in millimeters (8.8 mm), and image magnification in multiples of actual size (120 times); and date of acquisition (12/09/2020). Terms: Chl, chlorite; Prh, prehnite; Qz, quartz; Kfs, potassium feldspar; Pl, plagioclase; Ab, albite; µm, micrometer; USGS, U.S. Geological Survey; kV, kilovolt; mm, millimeter; BSE-ALL, back-scattered electron, all energies; CL, cathodoluminescence; UVD, ultra variable-pressure detector; Si, silicon; Al, aluminum; Na, sodium; K, potassium; Fe, iron; Ca, calcium. Photomicrographs by Ryan Deasy, U.S. Geological Survey.

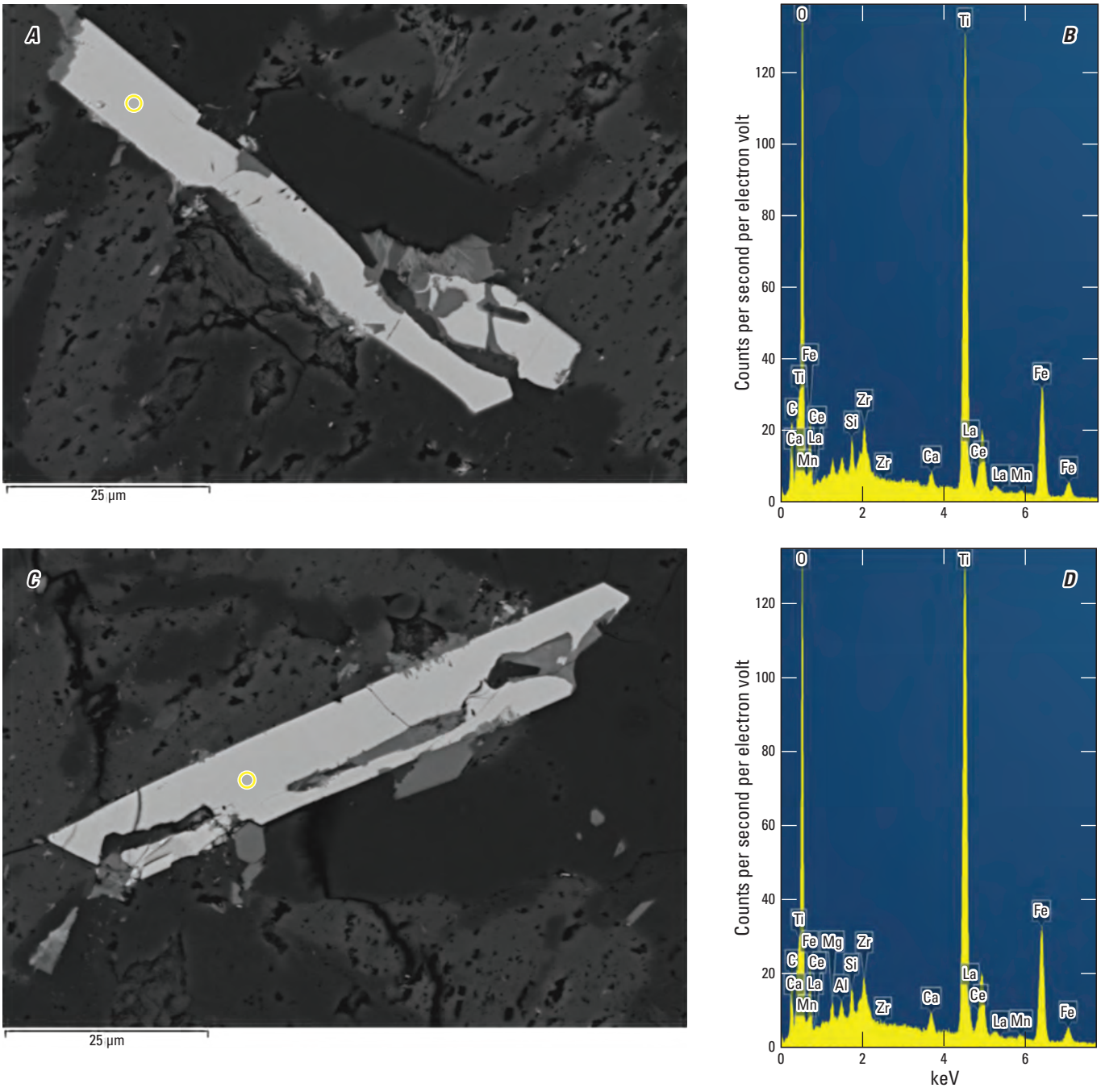

Figure 35. Representative back-scattered electron images (*A* and *C*) and energy dispersive spectroscopy (EDS) spectra (*B* and *D*) for zirconolite(?) needles in granodiorite fragments from borehole W12497 from 12,390 to 12,400 feet depth. Locations of EDS analyses (*B* and *D*) are indicated by yellow circles in their respective back-scattered electron images (*A* and *C*). Terms: µm, micrometer; C, carbon; Ca, calcium; Ti, titanium; O, oxygen; Mn, manganese; Fe, iron; La, lanthanum; Ce, cerium; Si, silicon; Zr, zirconium; keV, kiloelectronvolt. Photomicrographs by Ryan Deasy, U.S. Geological Survey.

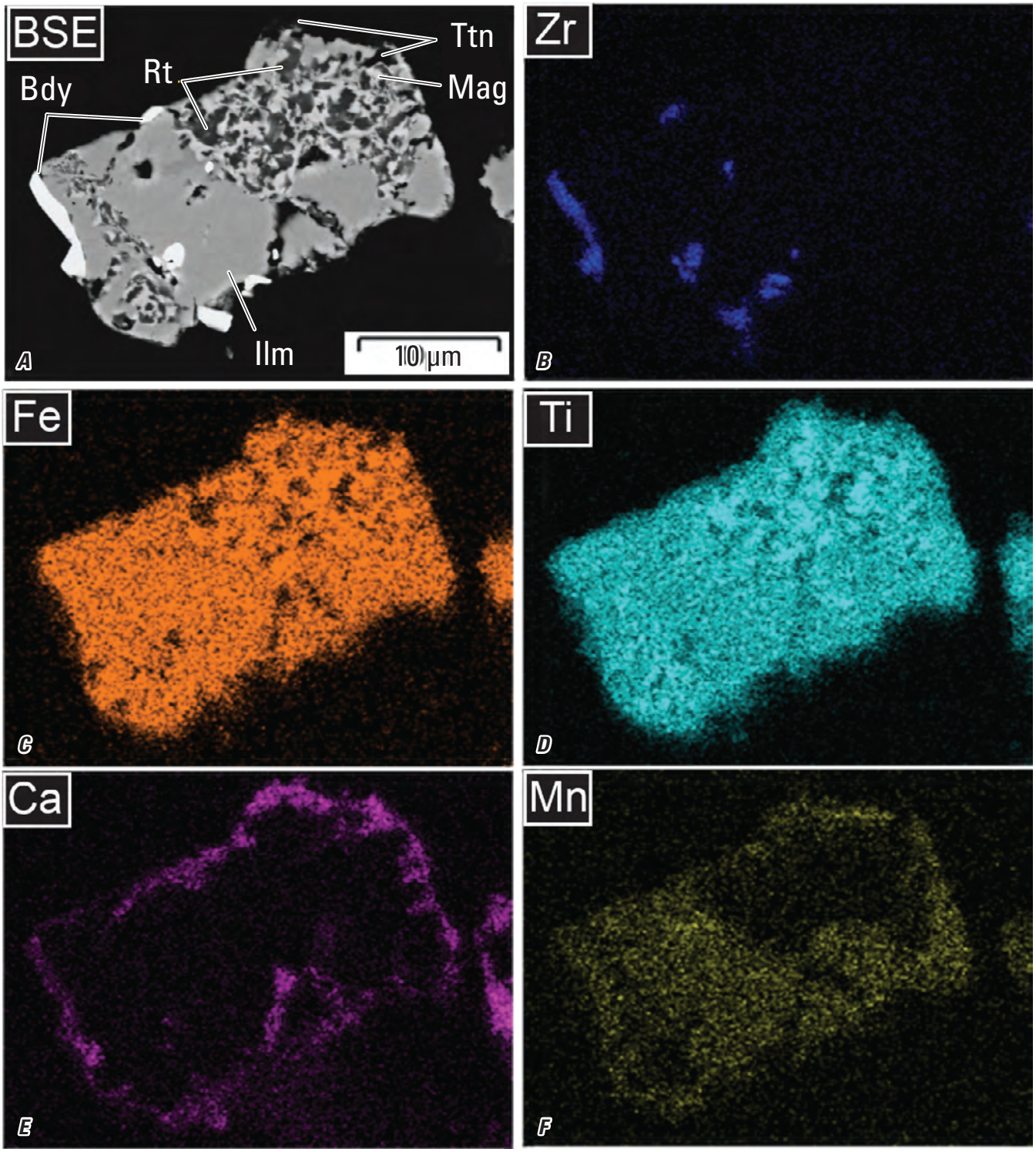

Figure 36. Back-scattered electron (BSE) (*A*) and selected element maps from energy dispersive spectroscopy (*B*–*F*) of an ilmenite grain intergrown with baddeleyite and symplectic titanite+rutile+magnetite in a fragment of granodiorite from borehole W12497 from 12,390 to 12,400 feet depth. Terms: Bdy, baddeleyite; Rt, rutile; Ttn, titanite; Mag, magnetite; Ilm, ilmenite; µm, micrometer; Zr, zirconium; Fe, iron; Ti, titanium; Ca, calcium; Mn, manganese. Photomicrographs by Ryan Deasy, U.S. Geological Survey.

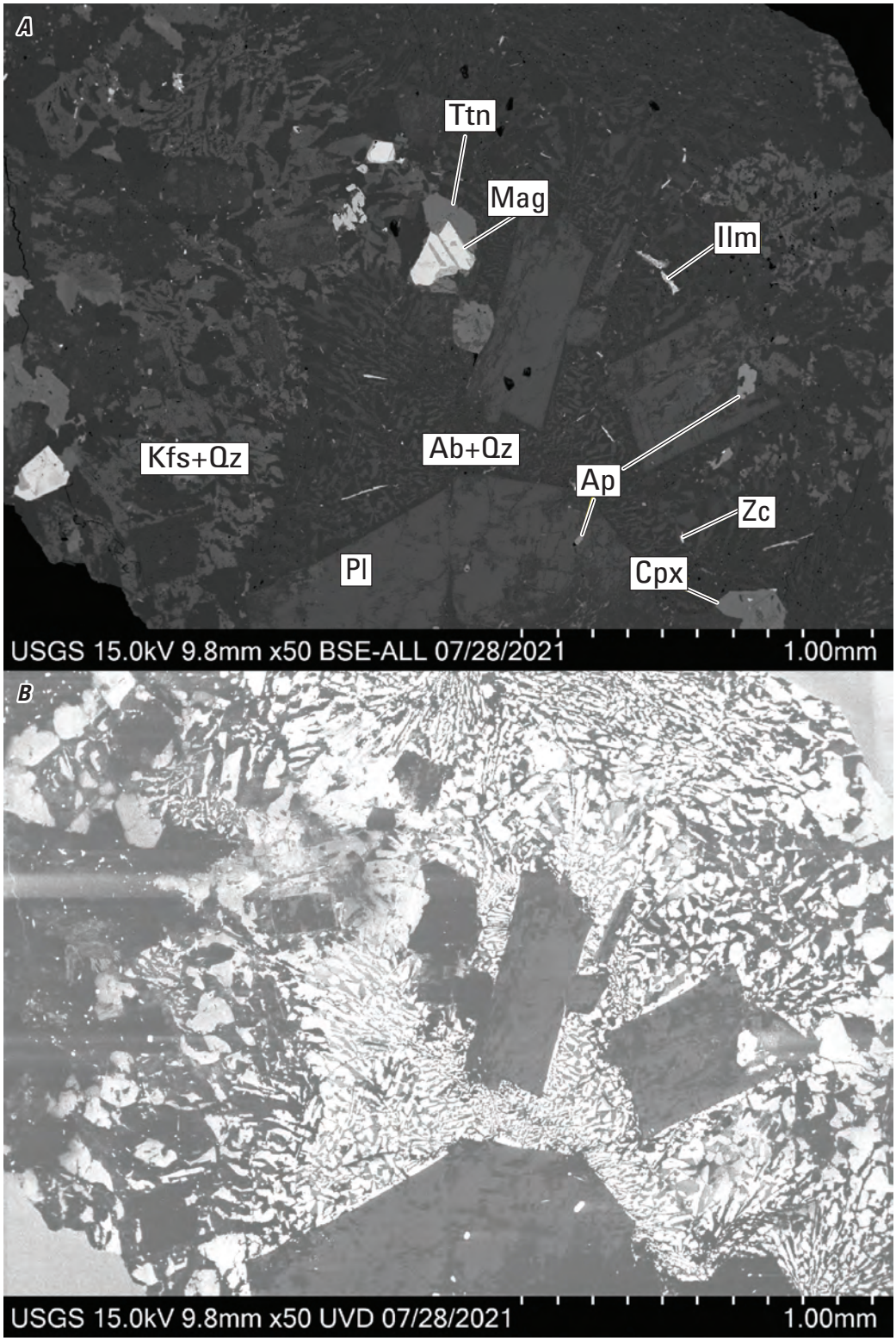

Figure 37. Back-scattered electron (BSE) (*A*) and cathodoluminescence (*B*) images of a granodiorite fragment with myrmekite overprint from borehole W12497 from 12,390 to 12,400 feet depth. The same fragment is shown in figure 33. Text in the bottom left of each image identifies data source (USGS); operating conditions including beam potential in kilovolts (15.0 kV), working distance in millimeters (9.8 mm), and image magnification in multiples of actual size (50 times); and date of acquisition (07/28/2021). Terms: Ttn, titanite; Mag, magnetite; Ilm, ilmenite; Kfs, potassium feldspar; Qz, quartz; Pl, plagioclase; Ab, albite; Ap, apatite; Zc, zirconolite(?); Cpx, clinopyroxene; mm, millimeter; USGS, U.S. Geological Survey; kV, kilovolt; BSE-ALL, back-scattered electron, all energies; UVD, ultra variable-pressure detector. Photomicrographs by Ryan Deasy, U.S. Geological Survey.

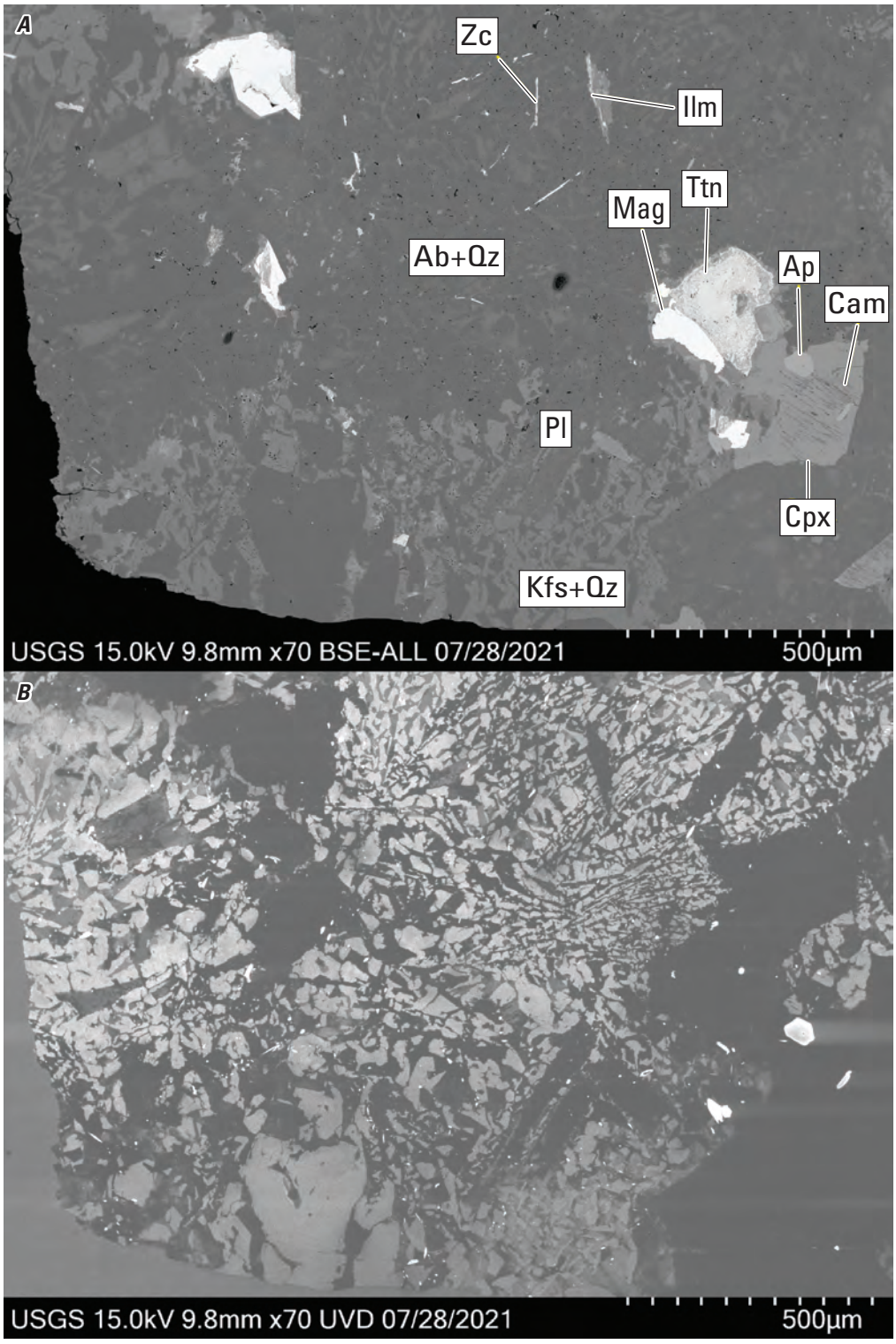

Figure 38. Back-scattered electron (BSE) (*A*) and cathodoluminescence (*B*) images of a granodiorite fragment from borehole W12497 from 12,390 to 12,400 feet depth. Text in the bottom left of each image identifies data source (USGS); operating conditions including beam potential in kilovolts (15.0 kV), working distance in millimeters (9.8 mm), and image magnification in multiples of actual size (70 times); and date of acquisition (07/28/2021). Terms: Zc, zirconolite(?); Ilm, ilmenite; Ttn, titanite; Mag, magnetite; Qz, quartz; Kfs, potassium feldspar; Pl, plagioclase; Ab, albite; Ap, apatite; Cpx, clinopyroxene; Cam, clinoamphibole; µm, micrometer; USGS, U.S. Geological Survey; kV, kilovolt; mm, millimeter; BSE-ALL, back-scattered electron, all energies; UVD, ultra variable-pressure detector. Photomicrographs by Ryan Deasy, U.S. Geological Survey.

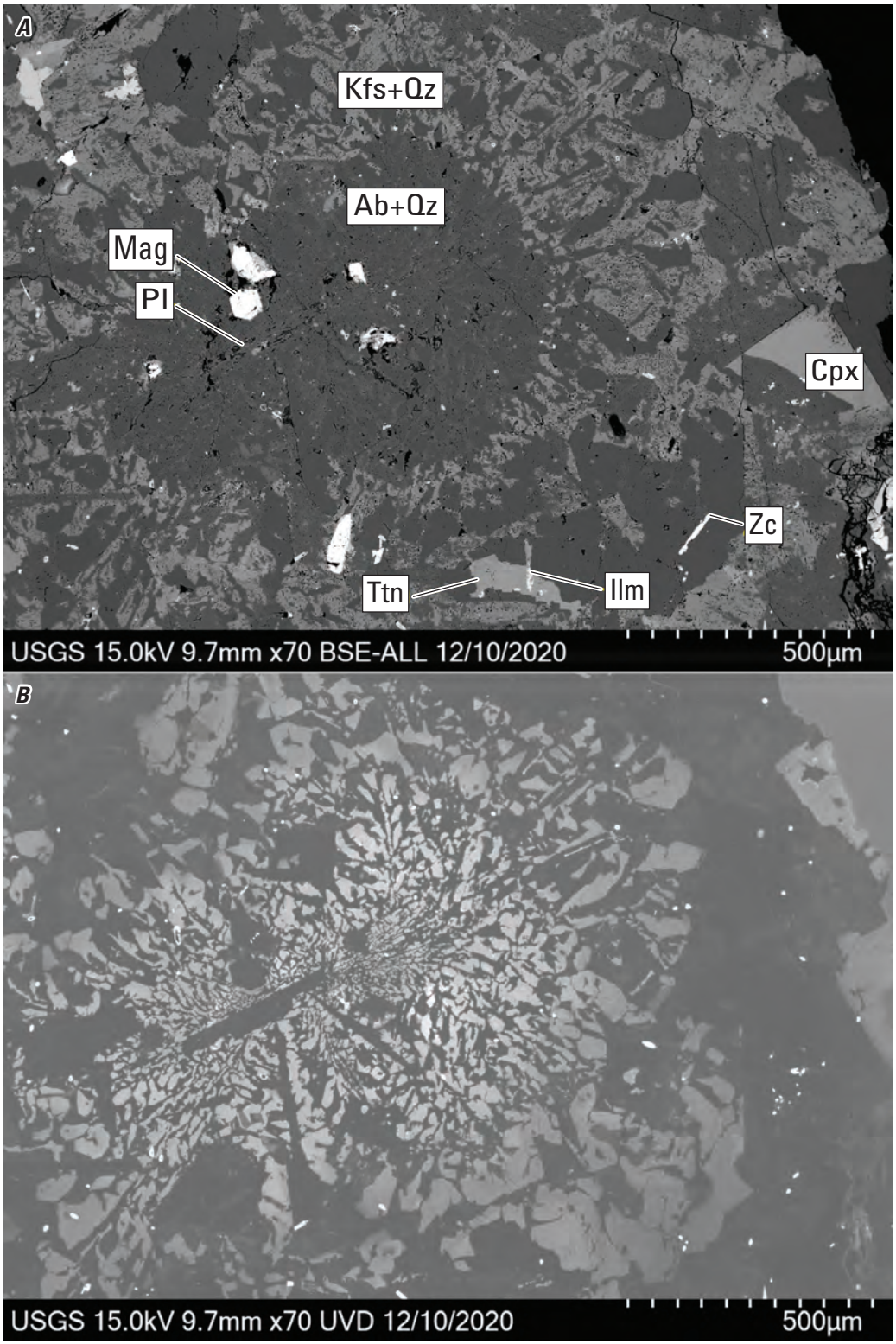

Figure 39. Back-scattered electron (BSE) (*A*) and cathodoluminescence (*B*) images of a granodiorite fragment with spherulitic myrmekite from borehole W12497 from 12,390 to 12,400 feet depth. Text in the bottom left of each image identifies data source (USGS); operating conditions including beam potential in kilovolts (15.0 kV), working distance in millimeters (9.7 mm), and image magnification in multiples of actual size (70 times); and date of acquisition (12/10/2020). Terms: Kfs, potassium feldspar; Qz, quartz; Ab, albite; Mag, magnetite; Pl, plagioclase; Zc, zirconolite(?); Cpx, clinopyroxene; Ttn, titanite; Ilm, ilmenite; µm, micrometer; USGS, U.S. Geological Survey; kV, kilovolt; mm, millimeter; BSE-ALL, back-scattered electron, all energies; UVD, ultra variable-pressure detector. Photomicrographs by Ryan Deasy, U.S. Geological Survey.

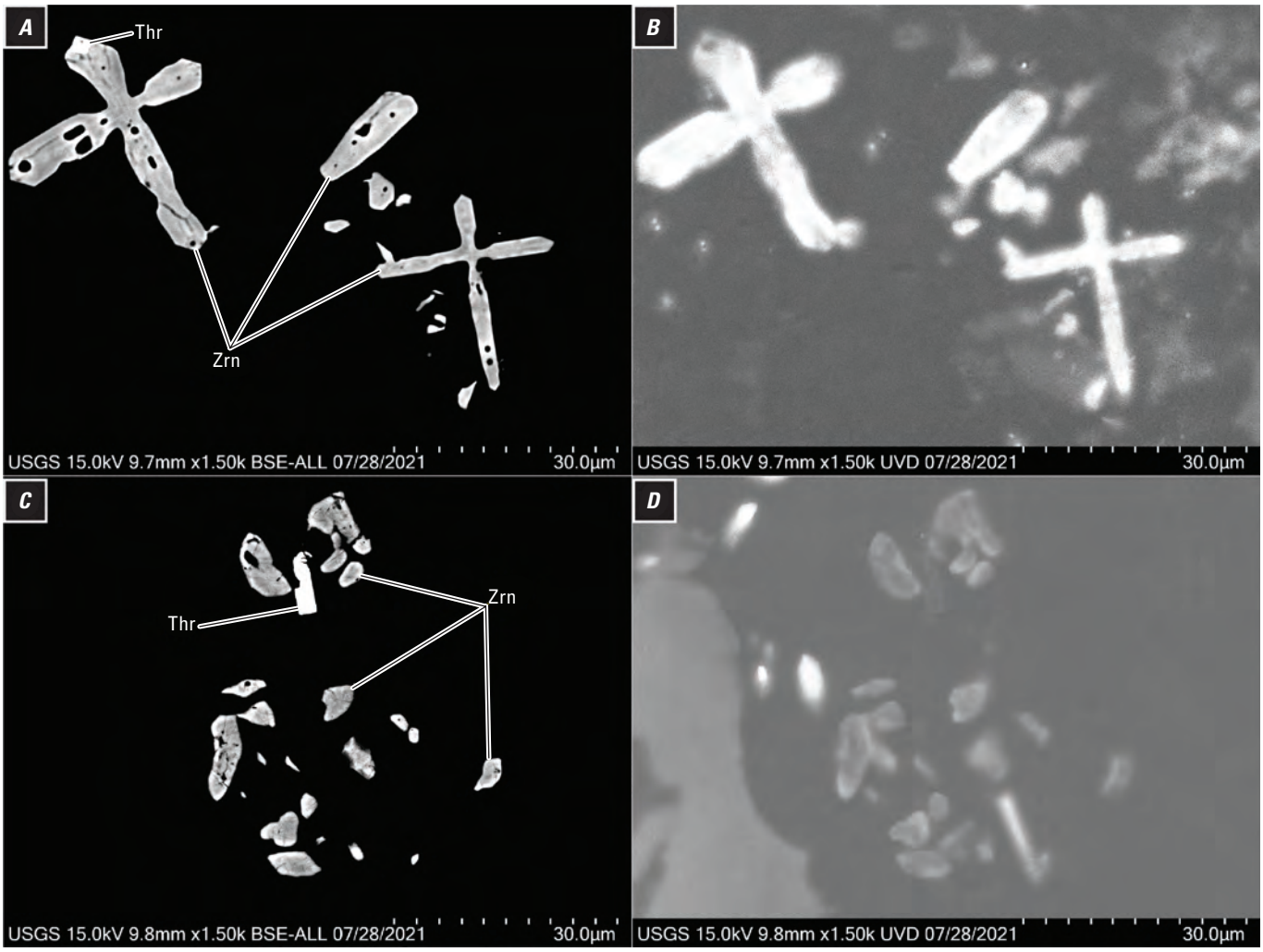

Figure 40. Two pairs of images in back-scattered electron (BSE) (*A* and *C*) and cathodoluminescence (*B* and *D*) of the characteristic occurrences of zircon (Zrn) and thorite (Thr) in granodioritic fragments from borehole W12497 from 12,390 to 12,400 feet depth. Text in the bottom left of each image identifies data source (USGS); operating conditions including beam potential in kilovolts (15.0 kV), working distance in millimeters (9.7 or 9.8 mm), and image magnification in multiples of actual size (1,500 times); and date of acquisition (07/28/2021). Terms: µm, micrometer; USGS, U.S. Geological Survey; kV, kilovolt; mm, millimeter; BSE-ALL, back-scattered electron, all energies; UVD, ultra variable-pressure detector. Photomicrographs by Ryan Deasy, U.S. Geological Survey.

Notes on XRD Methods and Results

Granodioritic and gabbroic fragments were separated by hand from sedimentary fragments and other contaminants under a binocular microscope. A ~10-g composite sample of granodioritic cuttings from 12,350 to 12,390 ft depth was isolated, and additional subsamples of granodioritic cuttings (each weighing 0.9–1.1 g) were separated from the following intervals (the number of subsamples per interval is given in parentheses):

12,340–12,350 ft (3)

12,370–12,380 ft (3)

12,380–12,400 ft (2)

The redundant samples from each depth interval facilitate a test of both the effectiveness of the hand-picking method and the representativeness of the sample fractions by revealing compositional variations between small fractions of ostensibly identical coarse-grained rock.

Separate subsamples of altered and fresh gabbroic fragments (each weighing 0.6–0.7 g) were separated from the following depth intervals:

12,230–12,290 ft

12,340–12,400 ft

The larger composite sample was ground in an automated Brinkmann grinder fitted with an agate mortar and pestle. It was continuously lubricated with acetone during grinding. The resulting powder was further ground by hand in a corundum

mortar and pestle, again lubricated with acetone. An aliquot of sample was placed in the 2×3×0.1-cm cavity of a Ti "front-pack" mount and analyzed in a Bruker D8 diffractometer with a Cu anode and point detector from 2 to 100° 2Θ at a step size of 0.02° and scanning rate of 9 sec/step. Semiquantitative mineral abundances (Deasy and others, 2024b) were determined by Rietveld refinement modeling in TOPAS (Bruker AXS, 2011). The sample was subsequently analyzed for its major and trace element geochemical composition by Activation Laboratories, Inc. (Deasy and others, 2024a).

All subsamples were ground by hand in an agate mortar and pestle and were continuously lubricated with acetone during grinding. The mortar and pestle were thoroughly cleaned between subsamples. The resulting powders were allowed to air dry. The powders were placed in 1.5-cm-wide cavities of circular "back-pack" mounts and scanned in a Panalytical Empyrean diffractometer with a Cu anode and X'Celerator detector from an angular range of 3–90° 2Θ. Semiquantitative mineral abundances (Deasy and others, 2024b) were obtained by Rietveld refinement modeling in HighScore Plus (Malvern Panalytical, 2018). Major and trace element geochemical analyses of four granodioritic subsamples, two altered gabbroic subsample, and two fresh gabbroic subsamples were thereafter obtained by INAA/ICP-OES/ICP-MS by Activation Laboratories, Inc. (Deasy and others, 2024a).

Additionally, to test the variable abundances of alteration minerals within each lithology, we analyzed small amounts of altered and fresh gabbroic and granitic fragments by XRD. Between one and four cuttings fragments were separately ground by hand using the methods described above. Each powder was mounted in a slurry with distilled water on a quartz "zero background" plate, was allowed to air dry, and was then scanned on a Bruker D8 diffractometer from 2 to 90° 2Θ at a minimum of 8 sec/step. The mounted sample was then placed in a chamber saturated with EG for ~24 hours before being scanned again, immediately upon removal from the EG chamber, from 2 to 40° 2Θ at 4 sec/step. Representative diffractograms are given in figures 41–44.

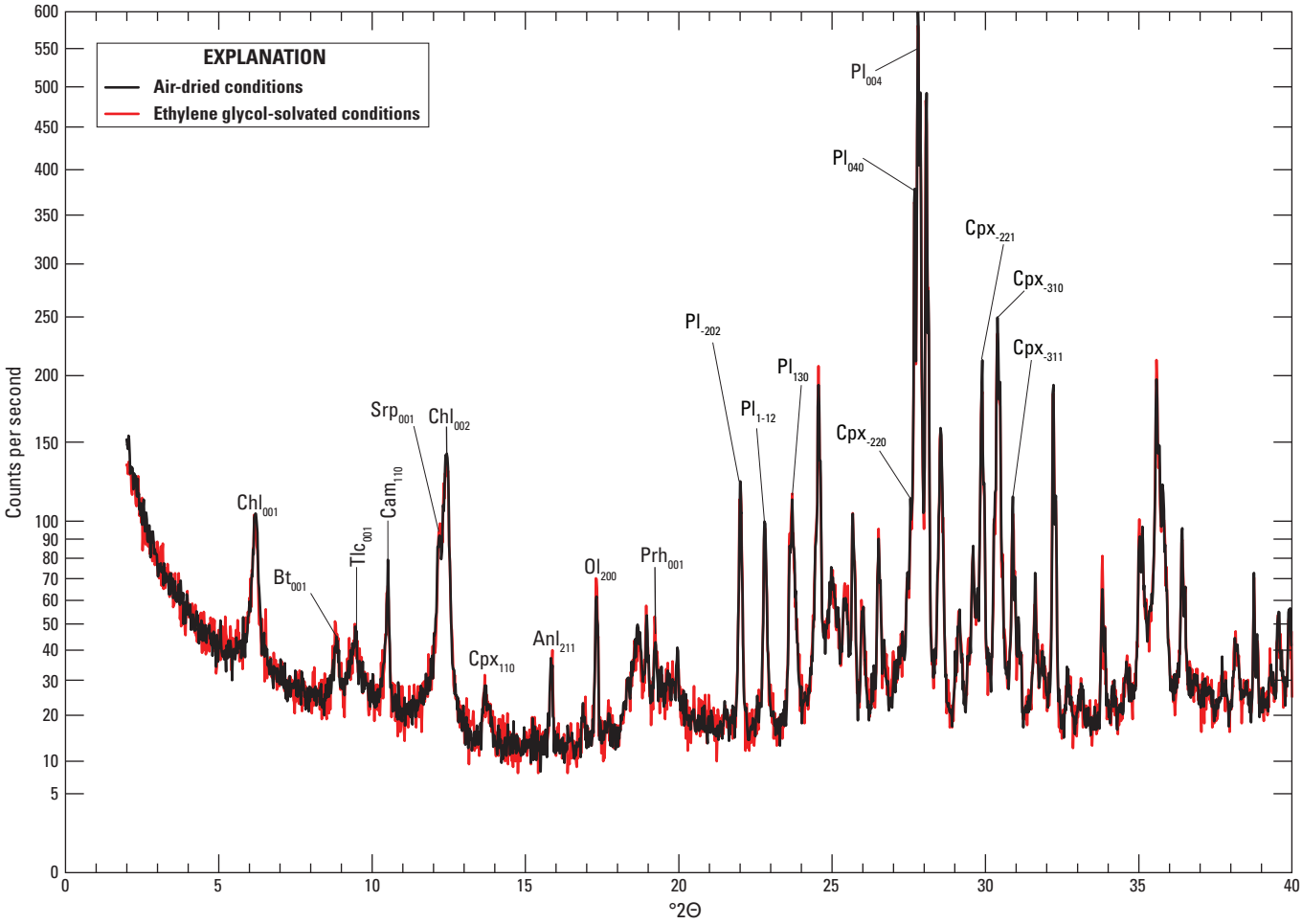

Figure 41. X-ray diffractograms of a fresh gabbroic fragment from borehole W12497 from 12,370 to 12,380 feet depth under air-dried and ethylene glycol-solvated conditions. The *y*-axis is in square root scale. Selected peaks are labeled with mineral abbreviations; numbers in subscript denote Miller indices. Terms: °2Θ, degrees two theta; Chl, chlorite; Bt, biotite; Tlc, Talc; Cam, clinoamphibole; Srp, serpentine; Cpx, clinopyroxene; Anl, analcime; Ol, olivine; Prh, prehnite; Pl, plagioclase.

The XRD patterns of fresh gabbro and of some fragments of red, altered gabbro are unaffected by EG solvation (fig. 41), indicating the absence of expandable clays in these samples. In contrast, some fragments of red, weathered gabbro have patterns that are strongly affected by EG solvation (fig. 42). Specifically, under air-dried conditions, these patterns have high low-angle (2–3° 2Θ) intensity and a ~6° 2Θ (d=1.42 nm) peak with a broad, high-angle shoulder. Upon EG solvation, the 1.42 nm peak loses peak intensity and becomes narrower, the intensity from 2 to 3° 2Θ is diminished, and a broad peak centered at ~5° 2Θ (d=1.62 nm) appears (fig. 42). This behavior is consistent with the presence of chlorite/smectite. Although unquantified, the expandable clay accounts for a significant fraction of the 28.8 weight percent (wt. pct.) chlorite estimated by Rietveld modeling (Deasy and others, 2024b). Other alteration minerals include illite, talc, prehnite, actinolite, serpentine and, in the oxidized samples, hematite.

The XRD patterns of the fresh granodiorite are very weakly affected by EG solvation (figs. 43 and 44), with weak, broad peaks appearing at ~6 and ~12° 2Θ, demonstrating the presence of trace amounts of chlorite/smectite. Other alteration minerals identified by XRD include chlorite, muscovite, prehnite, actinolite, and laumontite. The chalky, altered fragments of granodiorite respond weakly to EG solvation, indicating the presence of small amounts of chlorite/smectite (fig. 43), and contain significantly more illitic clay than the fresh rock. Semi-quantitative mineral abundances from Rietveld modeling of the eight aforementioned splits of fresh granodiorite and of one sample of altered granodiorite are available in Deasy and others (2024b). Several minerals that were identified optically or in electron microscopy did not appear in whole-rock powder XRD analyses and were therefore not included in Rietveld modeling. These minerals include, in decreasing order of abundance, ilmenite, apatite, zirconolite(?), baddeleyite, zircon, and thorite.

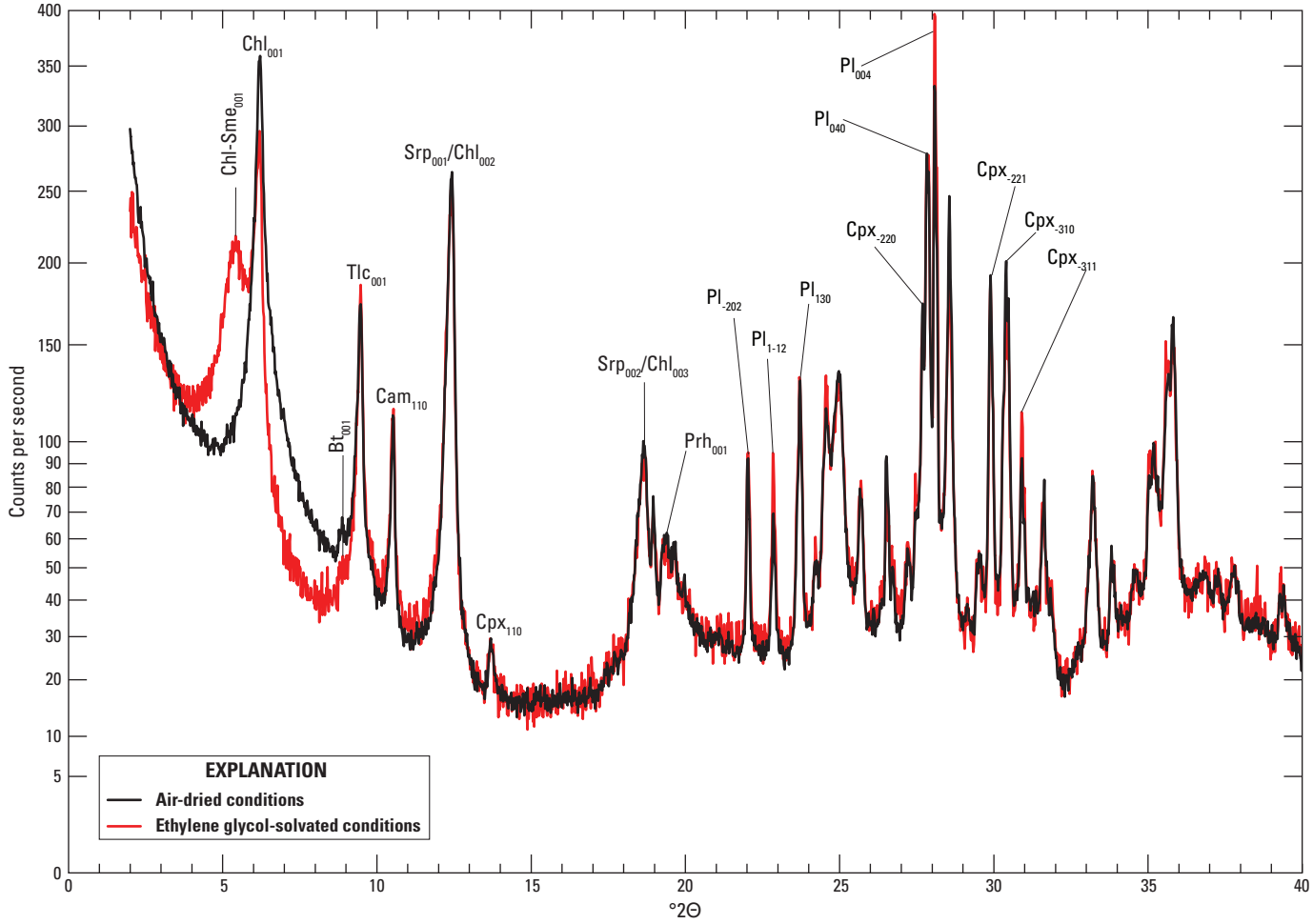

Figure 42. X-ray diffractograms of a red, altered gabbroic fragment from borehole W12497 from 12,340 to 12,350 feet depth under air-dried and ethylene glycol-solvated conditions. The y-axis is in square root scale. Selected peaks are labeled with mineral abbreviations; numbers in subscript denote Miller indices. Terms: °2Θ, degrees two theta; Chl-Sme, chlorite-smectite; Chl, chlorite; Bt, biotite; Tlc, Talc; Cam, clinoamphibole; Srp-Chl, serpentine-chlorite; Cpx, clinopyroxene; Prh, prehnite; Pl, plagioclase.

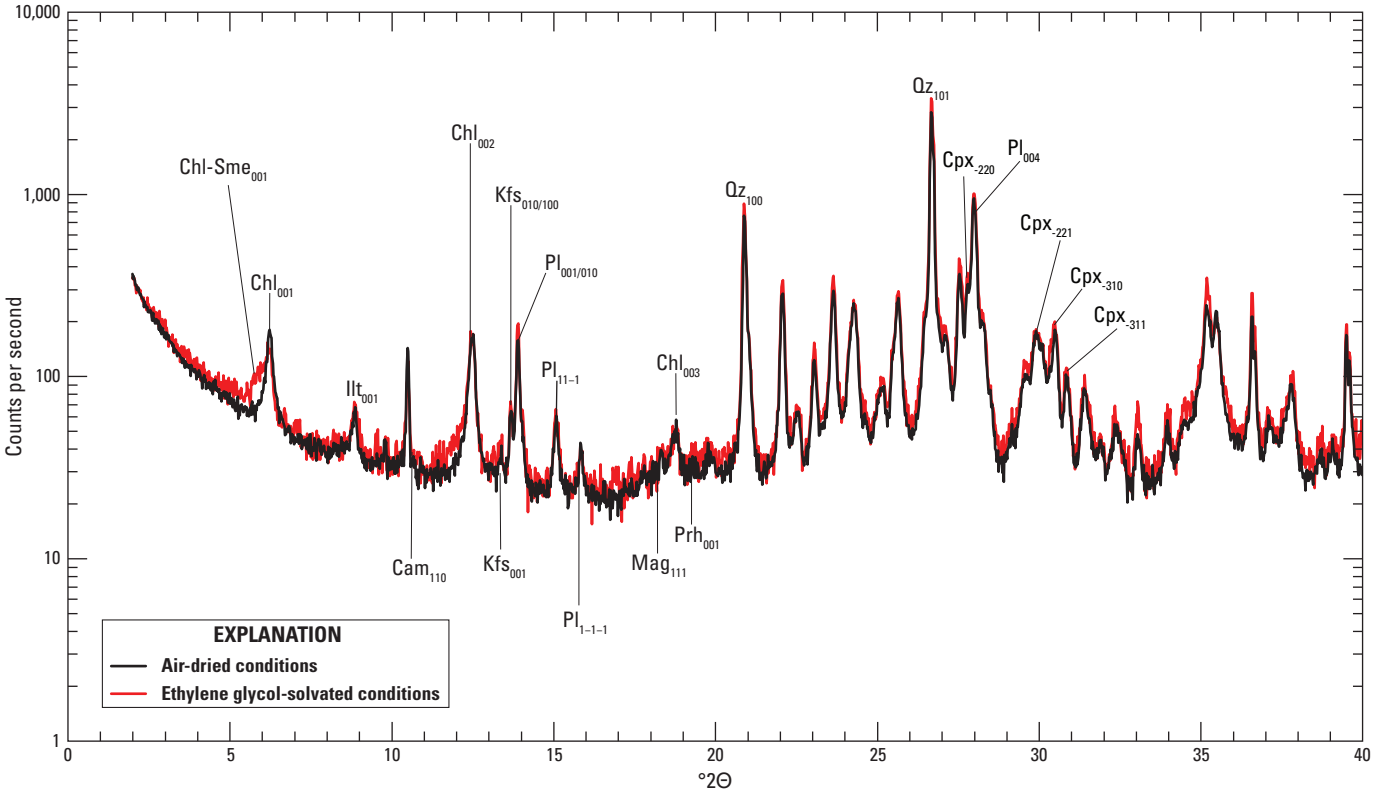

Figure 43. X-ray diffractograms of a fresh granodiorite fragment from borehole W12497 from 12,350 to 12,360 feet depth under air-dried and ethylene glycol-solvated conditions. The *y*-axis is in logarithmic scale. Selected peaks are labeled with mineral abbreviations; numbers in subscript denote Miller indices. Terms: °2Θ, degrees two theta; Chl-Sme, chlorite-smectite; Chl, chlorite; Ilt, illite; Cam, clinoamphibole; Kfs, potassium feldspar; Pl, plagioclase; Mag, magnetite; Cpx, clinopyroxene; Prh, prehnite; Qz, quartz.

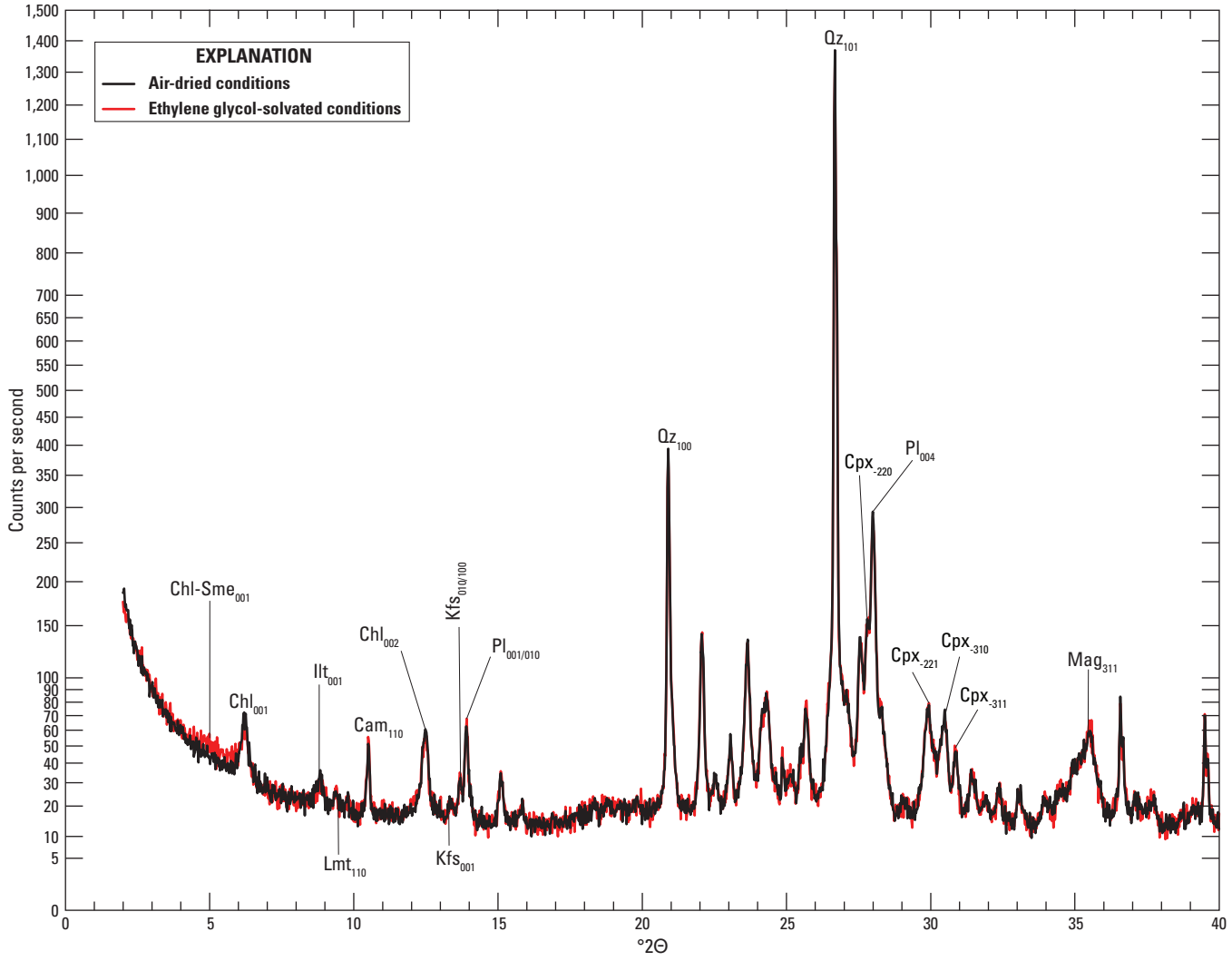

Figure 44. X-ray diffractograms of four white, altered granodiorite fragments from borehole W12497 from 12,370 to 12,380 feet depth under air-dried and ethylene glycol-solvated conditions. The *y*-axis is in square root scale. Selected peaks are labeled with mineral abbreviations; numbers in subscript denote Miller indices. Terms: °2Θ, degrees two theta; Chl-Sme, chlorite-smectite; Chl, chlorite; Ilt, illite; Lmt, laumontite; Cam, clinoamphibole; Kfs, potassium feldspar; Pl, plagioclase; Mag, magnetite; Cpx, clinopyroxene; Qz, quartz.

Borehole W12496

The basement lithologies in this borehole include early Mesozoic sandstone from 11,753 to 12,131 ft depth intruded by diabase sills at 12,060–12,070 ft depth and 12,095–12,131 ft depth. Diabase from 12,090 to 12,124 ft depth was investigated in this study.

Previous Work

Barnett (1975) reports that the Eagle Mills Formation is present at 11,753–12,131 ft depth (TD), with diabase sills at 12,060–12,070 ft depth and 12,095–12,131 ft depth.

Thin Section Petrography

A description of thin sections of diabase from borehole W12496 at 12,090–12,124 ft depth follows. Rock is diabasic with subhedral to euhedral plagioclase laths enclosed in clinopyroxene oikocrysts (fig. 45). Plagioclase grains have penetration twins and aspect ratios of 2:1 to ~5:1, although the upper limit is unknown due to the small size of the cuttings (~2 mm). Grain size of clinopyroxene is unknown but is larger than cuttings fragments. Some fragments contain subhedral to euhedral orthopyroxene(?), completely pseudomorphically replaced by chlorite+talc+actinolite. Plagioclase and clinopyroxene are mostly unaltered, and a massive magmatic texture is preserved in all fragments. Evidence of deformation is limited to intracrystalline veins of prehnite, chlorite, talc, and actinolite.

Notes on XRD Methods and Results

Fragments of diabase were separated from drill cuttings by hand under a binocular microscope. The diabase separate was then placed in an automated Brinkman grinder fitted with an agate mortar and pestle. The sample was continuously lubricated with acetone during grinding. The resulting powder was further ground by hand in a corundum mortar and pestle, again lubricated with acetone, and allowed to air dry. An aliquot of powder was then mounted in the 2-cm-wide cavity of a standard "back-pack" mount and analyzed on a Panalytical Empyrean diffractometer with a Cu anode from an angular range of 3–100° 2Θ. Semiquantitative mineral abundances in this sample (Deasy and others, 2024b) were determined by Rietveld modeling in TOPAS (Bruker AXS, 2011). The major and trace element composition of the powder was thereafter obtained by INAA/ICP-OES/ICP-MS at Activation Laboratories, Inc. (Deasy and others, 2024a).

Borehole W12483

Felsic porphyry occurs in core from 14,261 to 14,297 ft depth. Core chips from 14,270 to 14,288; 14,289; and 14,290 ft depth were investigated in this study.

Previous Work

Barnett (1975, p. 134) reports 36 ft of penetration of felsic porphyry from 14,261 to 14,297 ft depth and includes the following description of thin sections of core:

> *Megascopic description:* massive medium brown, slightly reddish, porphyritic rhyolite, oblique fractures at 14,264 and 14,267 ft., weak subhorizontal layering and streaking, no flow structure, few dark stylotic [sic] seams in upper part; dense felsitic groundmass appears granular rather than crystalline or vitreous.
>
> *Microscopic description:* dacite porphyry with about 60 percent hematite-stained cryptocrystalline groundmass. Phenocrysts 0.3 mm to 3 mm are fractured, strained, corroded. Include plagioclase, quartz, microcline, sanidine. Also, lithic fragments, few shreds muscovite, rounded lumps with brown crust, devitrified interior, occasional vesicular and spherulitic structure. Some signs of matrix molding around phenocrysts.

Thin Section Petrography

Thin sections of porphyritic rhyolite were prepared from core chips recovered from the following depths:

14,270 ft

14,288 ft

14,289 ft

14,290 ft

All samples are quartz and K-feldspar-phyric, welded crystal tuffs with ~50–70 percent cryptocrystalline matrix and variable minor xenolithic content. Whereas the shallowest sample is massive (fig. 46), a foliation defined by the shape-preferred orientations of phenocrysts and lithic clasts becomes stronger with depth (figs. 47–49). Evidence of compaction can be found in fiamme (fig. 48), the slight embayment of fiamme by adjacent quartz grains, and the in situ brecciation of quartz phenocrysts (fig. 48).

K-feldspar phenocrysts are blocky to elongate and up to 0.4 cm in maximum dimension. All feldspar phenocrysts are faintly reddish, have a high turbidity (compared to quartz phenocrysts), and are partially altered to sericite and, locally, to calcite (fig. 50). A patchy, fine-scale (tens of micrometers), weakly developed perthitic texture is pervasive among K-feldspar phenocrysts (figs. 50–52). Many of the more elongate feldspar grains have Carlsbad twins (figs. 51 and 52). Quartz grains are typically either euhedral phenocrysts or angular fragments. Rare round quartz grains (fig. 49) may be sedimentary xenocrysts. Other xenoliths include angular clasts of felsic porphyry up to 0.5 cm across (fig. 46, lower left), quartzitic sandstone (fig. 49, center right), and opaque grains. Some opaque grains, such as those with dendritic edges (fig. 47, center right), may be authigenic or have authigenic overgrowths. The volcanic clasts have finer grained matrices than the host rock, and many have strong foliations suggestive of flow banding (fig. 46, lower left; fig. 49, center right; fig. 52, right) which are absent in the host rock.

Notes on XRD Methods and Results

Four chips from three depth intervals (one each from 14,270 and 14,271 ft depth, and two from 14,288 ft depth) were separated from core with a diamond bandsaw and shattered in a steel percussion mortar. The broken pieces were placed in an automated Brinkman grinder fitted with an agate mortar and pestle. The samples were continuously lubricated with acetone during grinding. The resulting coarse powders were further ground by hand in a corundum mortar and pestle, again lubricated with acetone, and were allowed to air dry. An aliquot of each powder was then mounted in the 2.0×3.0×0.1-cm cavities of Ti "front-pack" mounts and analyzed on a Bruker D8 diffractometer with a Cu anode and point detector from an angular range of 2–70° 2Θ, 2–90° 2Θ, or 2–100° 2Θ at a step size of 0.02° 2Θ and step rate of 4, 5, or 6 sec/step. Semiquantitative mineral abundances in this sample (Deasy and others, 2024b) were determined by Rietveld modeling in TOPAS (Bruker AXS, 2011). The presence of elongate phenocrysts with Carlsbad twins and the pervasiveness of weak perthite development suggests that K-feldspar in these samples may be incompletely ordered and that monoclinic and triclinic domains may be extant among the grains. Therefore, K-feldspar in these samples was modeled in Rietveld refinements with a combination of microcline, orthoclase, and sanidine structures.

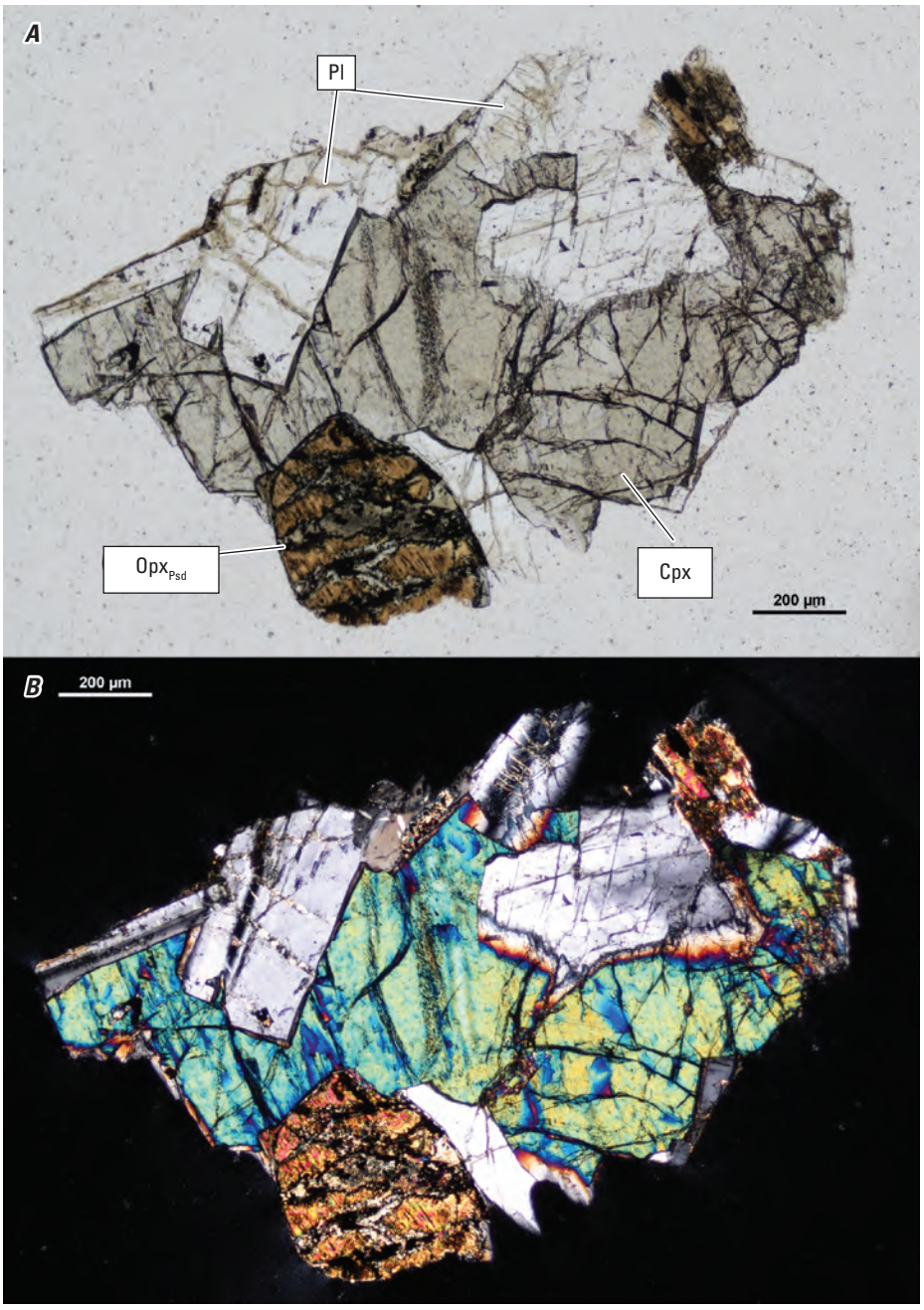

Figure 45. Pair of photomicrographs of a representative fragment of diabasic cuttings in plane-polarized light (*A*) and cross-polarized light (*B*) from borehole W12496 from 12,090 to 12,124 feet depth. A clinopyroxene (Cpx) oikocryst encloses euhedral lath-shaped plagioclase (Pl) crystals and an orthopyroxene(?) grain pseudomorphically replaced by chlorite, actinolite, and talc (Opx_{Psd}). Term: µm, micrometer. Photomicrographs by Ryan Deasy, U.S. Geological Survey.

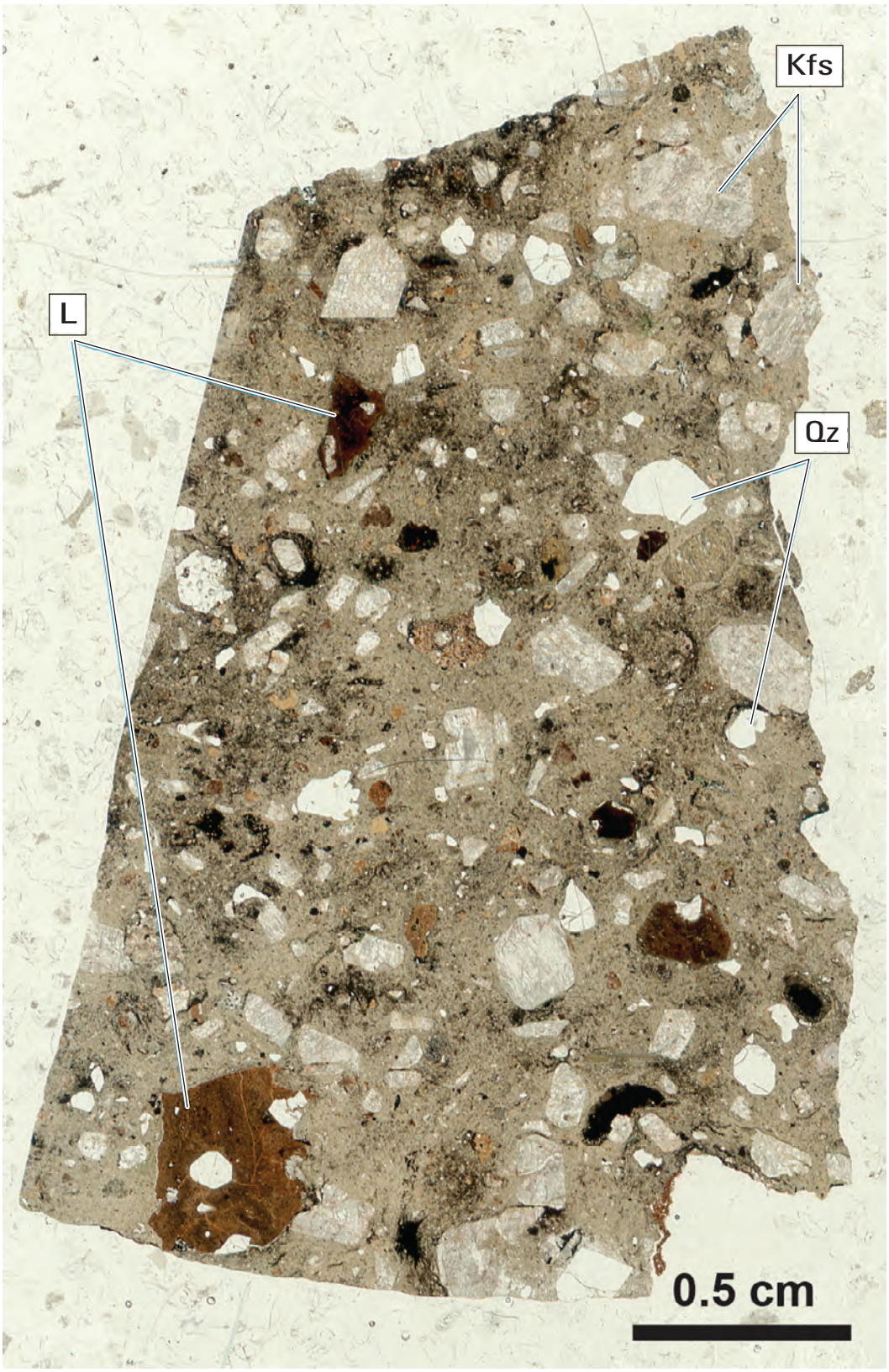

Figure 46. Full thin section scan in plane-polarized light of massive rhyolite porphyry from borehole W12483 at 14,270 feet depth. Terms: L, rhyolitic lithic clasts; Kfs, potassium feldspar; Qz, quartz; cm, centimeter. Photomicrograph by Ryan Deasy, U.S. Geological Survey.

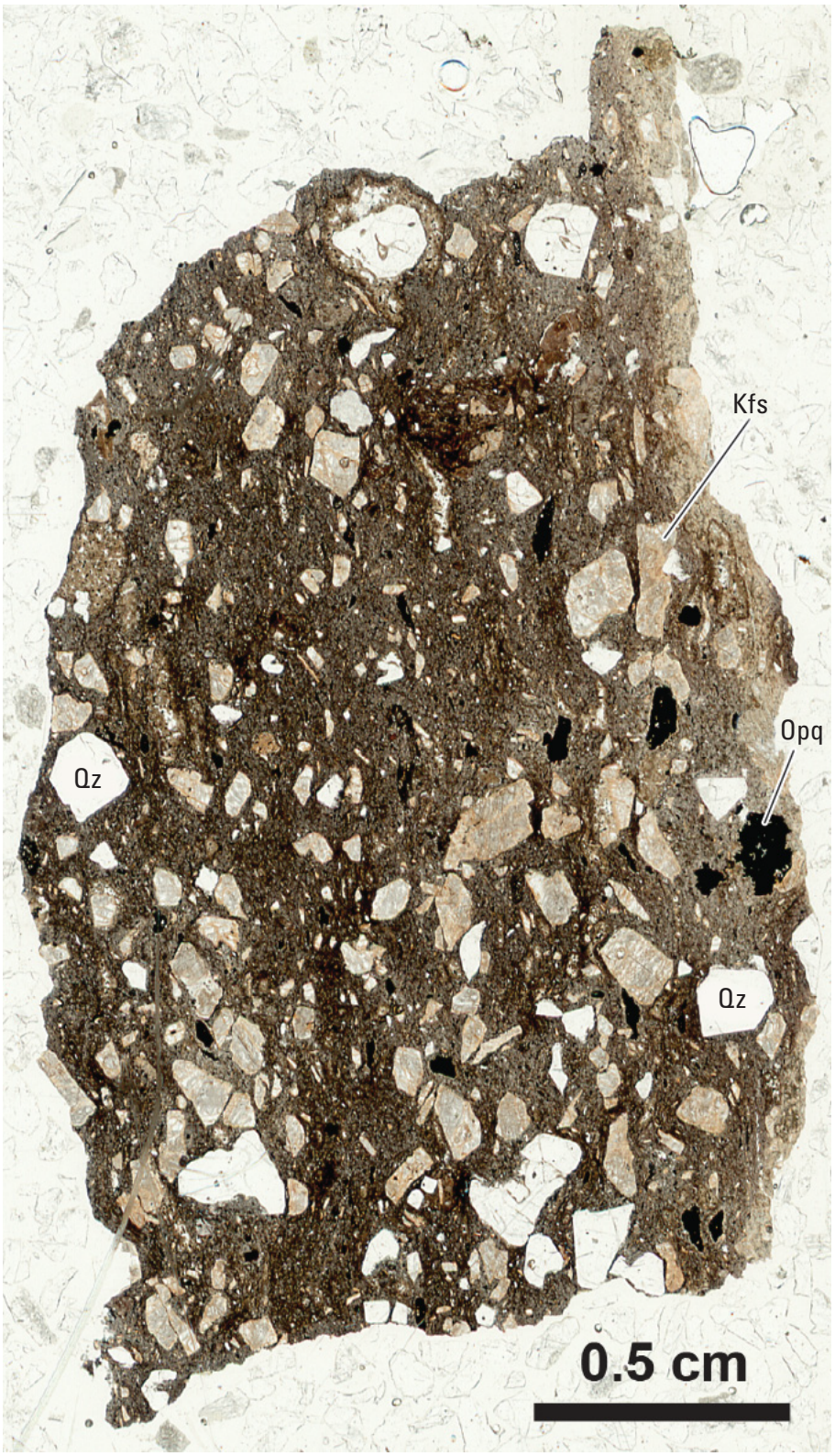

Figure 47. Full thin section scan in plane-polarized light of rhyolite porphyry from borehole W12483 at 14,288 feet depth. A weak foliation, vertical in this view, is interpreted as primary layering. Quartz (Qz) and potassium feldspar (Kfs) phenocrysts have euhedral and broken faces. Opaque minerals (Opq) are common and some have authigenic, dendritic overgrowths (center right). Term: cm, centimeter. Photomicrograph by Ryan Deasy, U.S. Geological Survey.

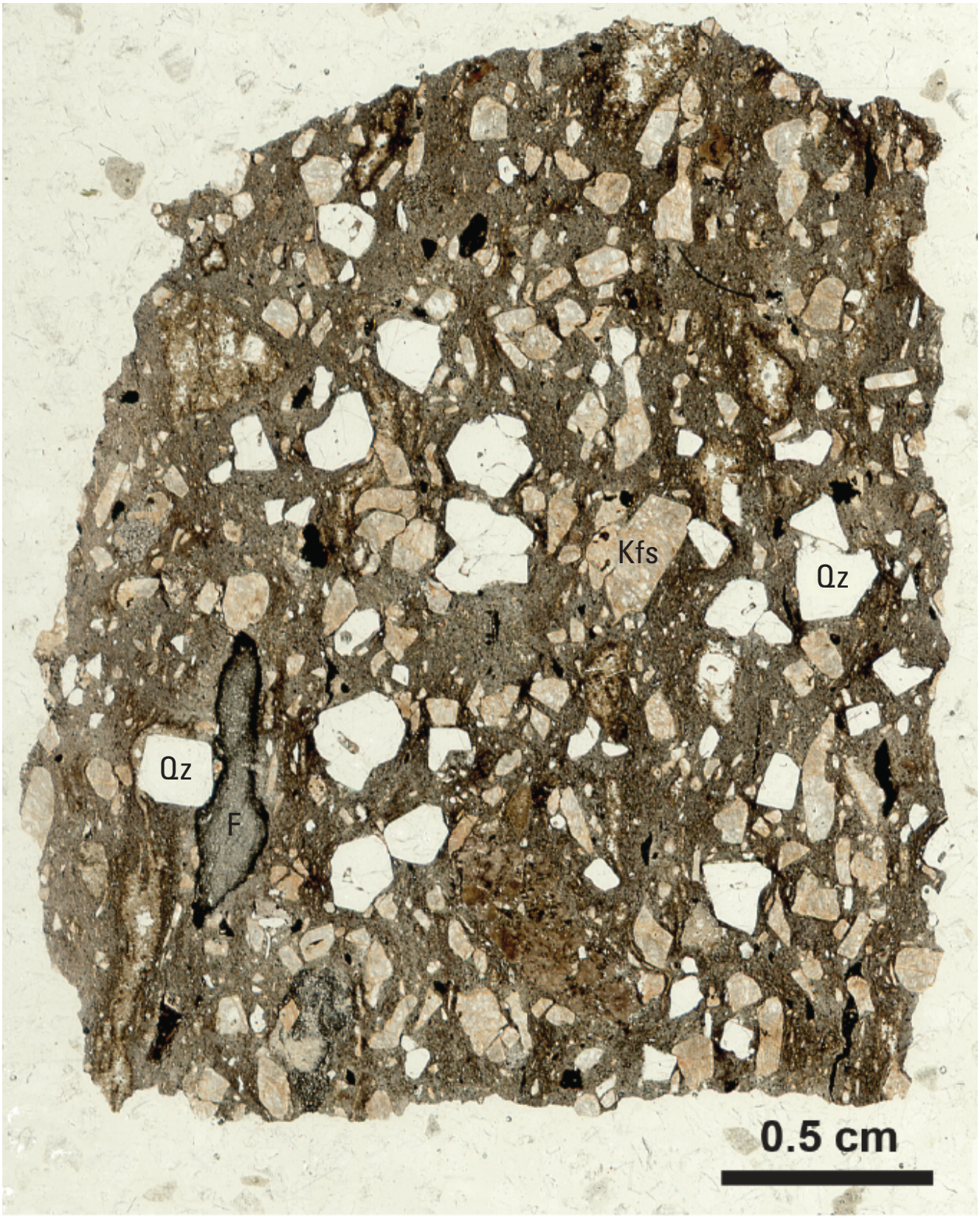

Figure 48. Full thin section scan in plane-polarized light of rhyolite porphyry from borehole W12483 at 14,289 feet depth. Quartz (Qz) grains are mostly euhedral, but some are brecciated (center right). Fiamme (F) are elongate in a moderately well-developed primary (flow or bedding) foliation and may be embayed by other grains or clasts, which is evidence of compaction. Terms: Kfs, potassium feldspar; cm, centimeter. Photomicrograph by Ryan Deasy, U.S. Geological Survey.

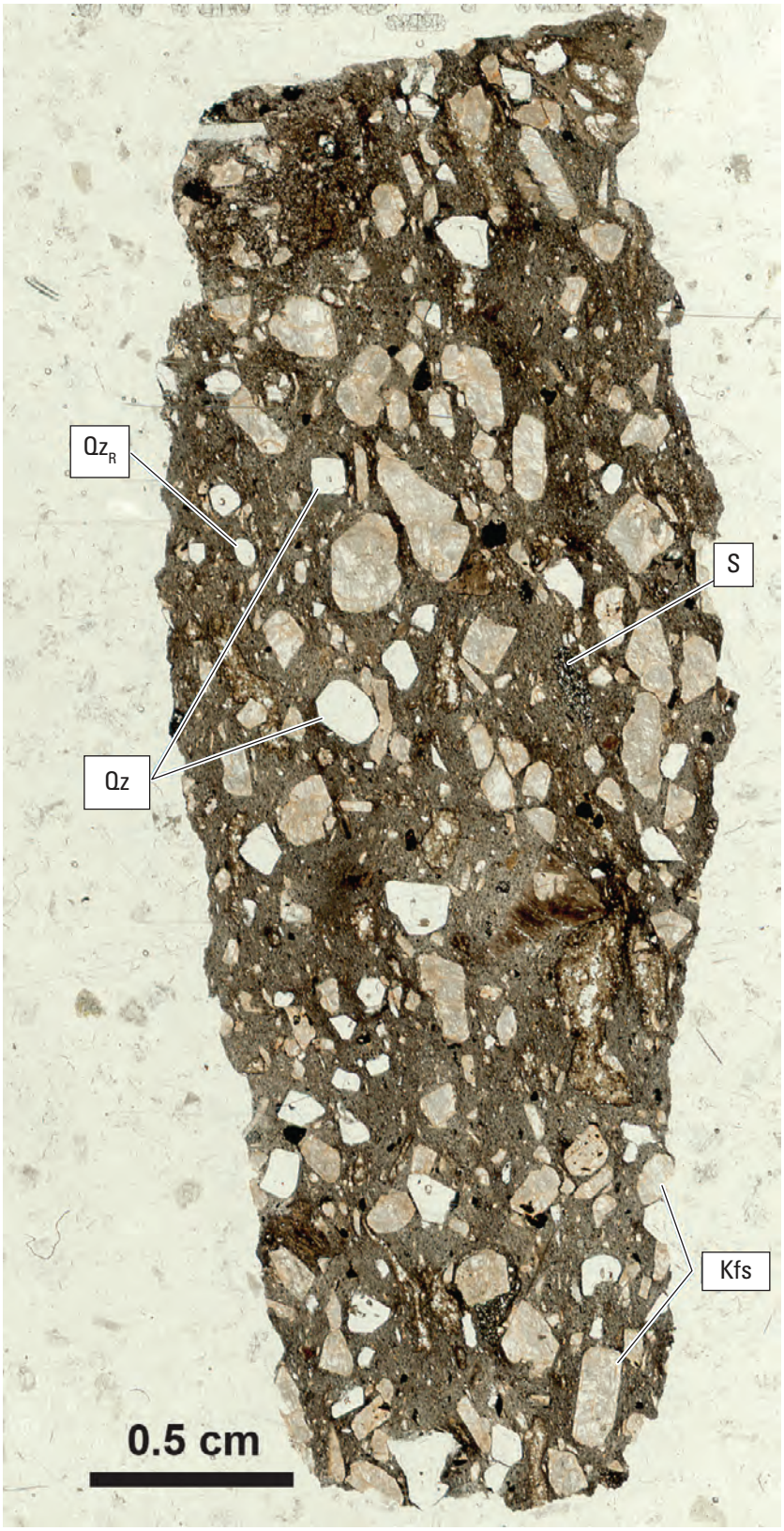

Figure 49. Full thin section scan in plane-polarized light of rhyolite porphyry from borehole W12483 at 14,290 feet depth. Terms: S, sandstone clast; Qz, quartz phenocryst; Qz_R, rounded quartz grain; Kfs, potassium feldspar; cm, centimeter. Photomicrograph by Ryan Deasy, U.S. Geological Survey.

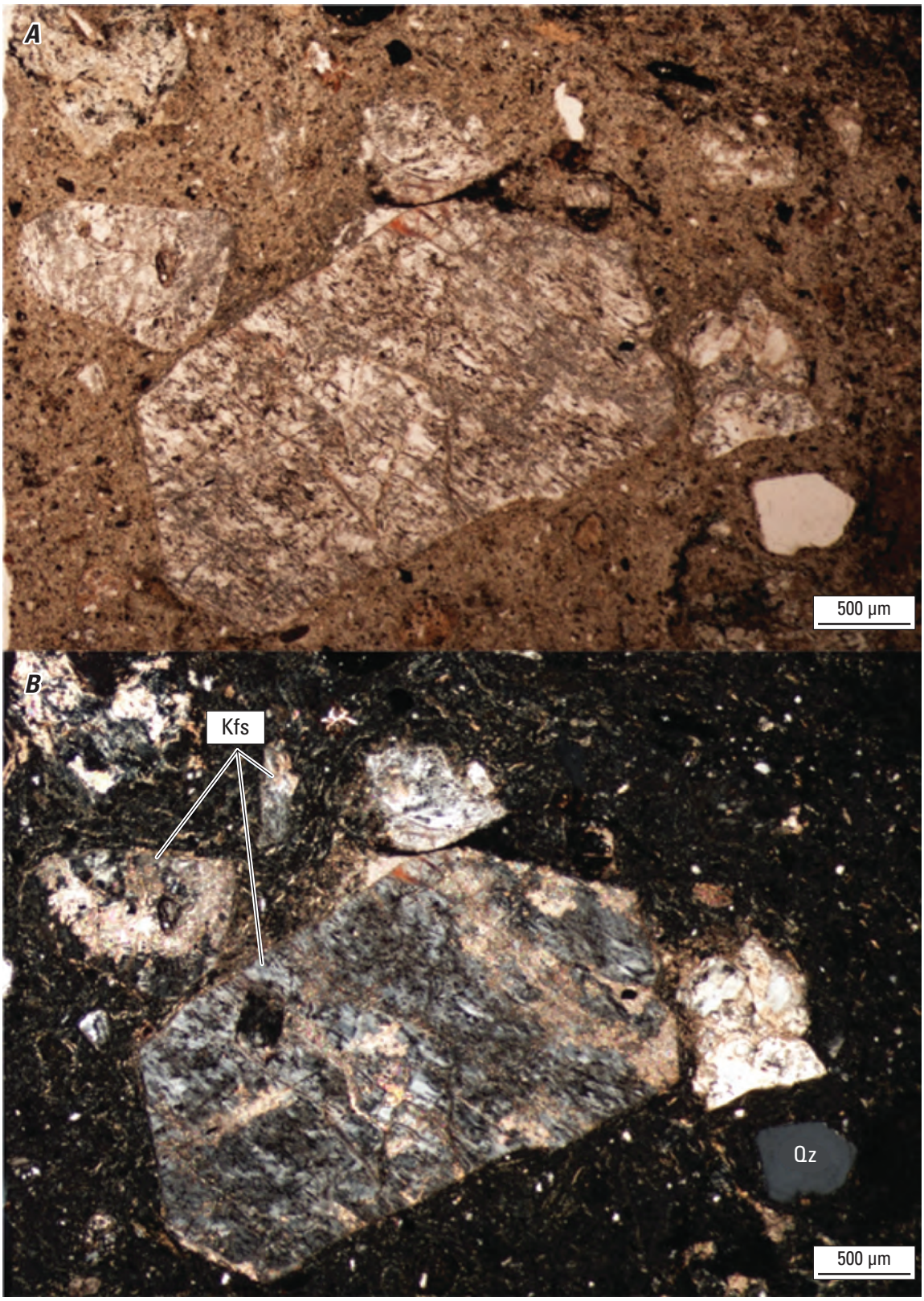

Figure 50. Pair of photomicrographs of rhyolite porphyry from borehole W12483 at 14,270 feet depth in plane-polarized light (*A*) and cross-polarized light (*B*). Terms: Kfs, potassium feldspar; Qz, quartz; µm, micrometer. Photomicrographs by Ryan Deasy, U.S. Geological Survey.

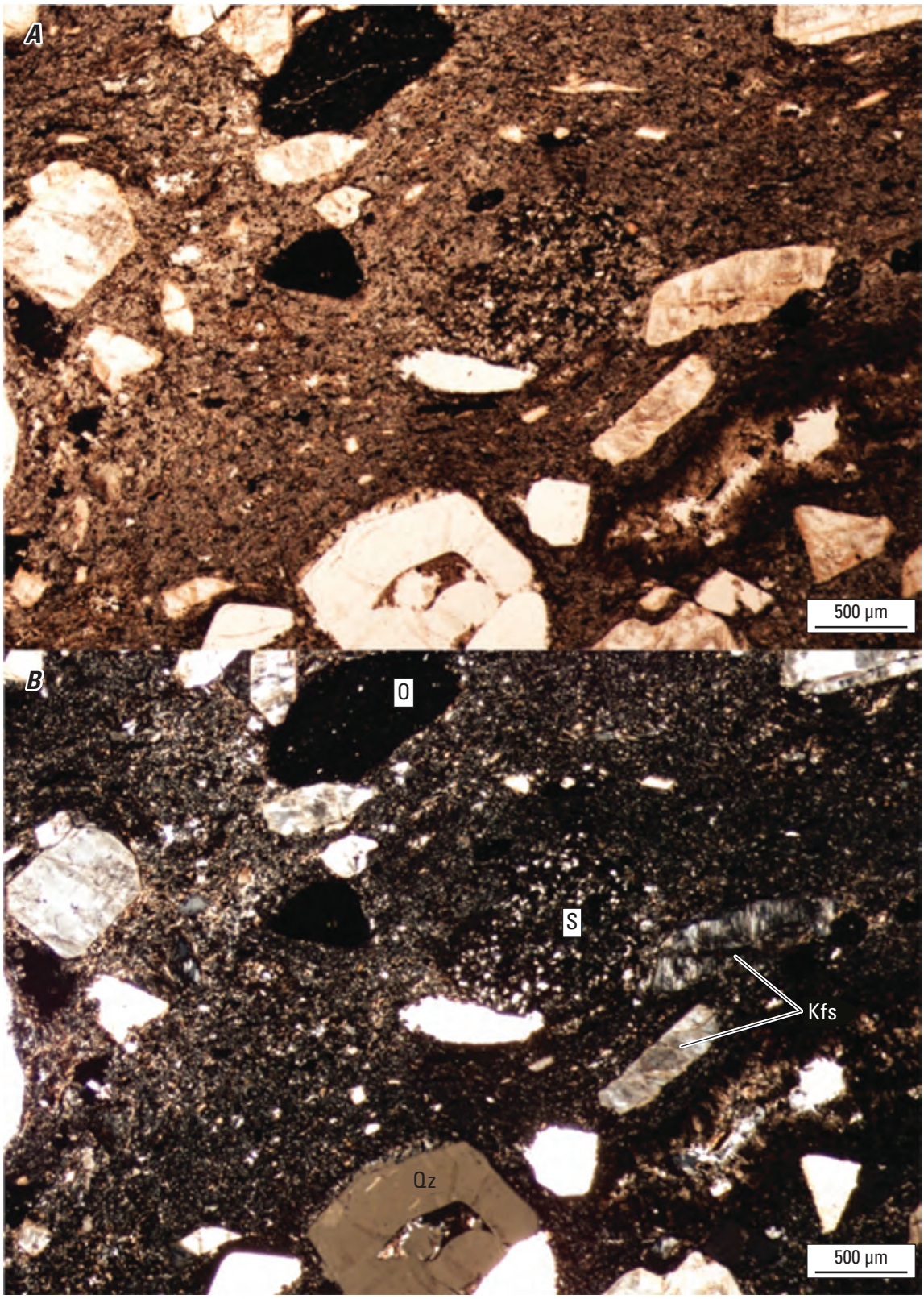

Figure 51. Pair of photomicrographs of rhyolite porphyry from borehole W12483 at 14,289 feet depth in plane-polarized light (*A*) and cross-polarized light (*B*). Note the Carlsbad twins in potassium feldspar (Kfs) phenocrysts. Terms: Qz, quartz; O, opaque mineral; S, sandstone clast; µm, micrometer. Photomicrographs by Ryan Deasy, U.S. Geological Survey.

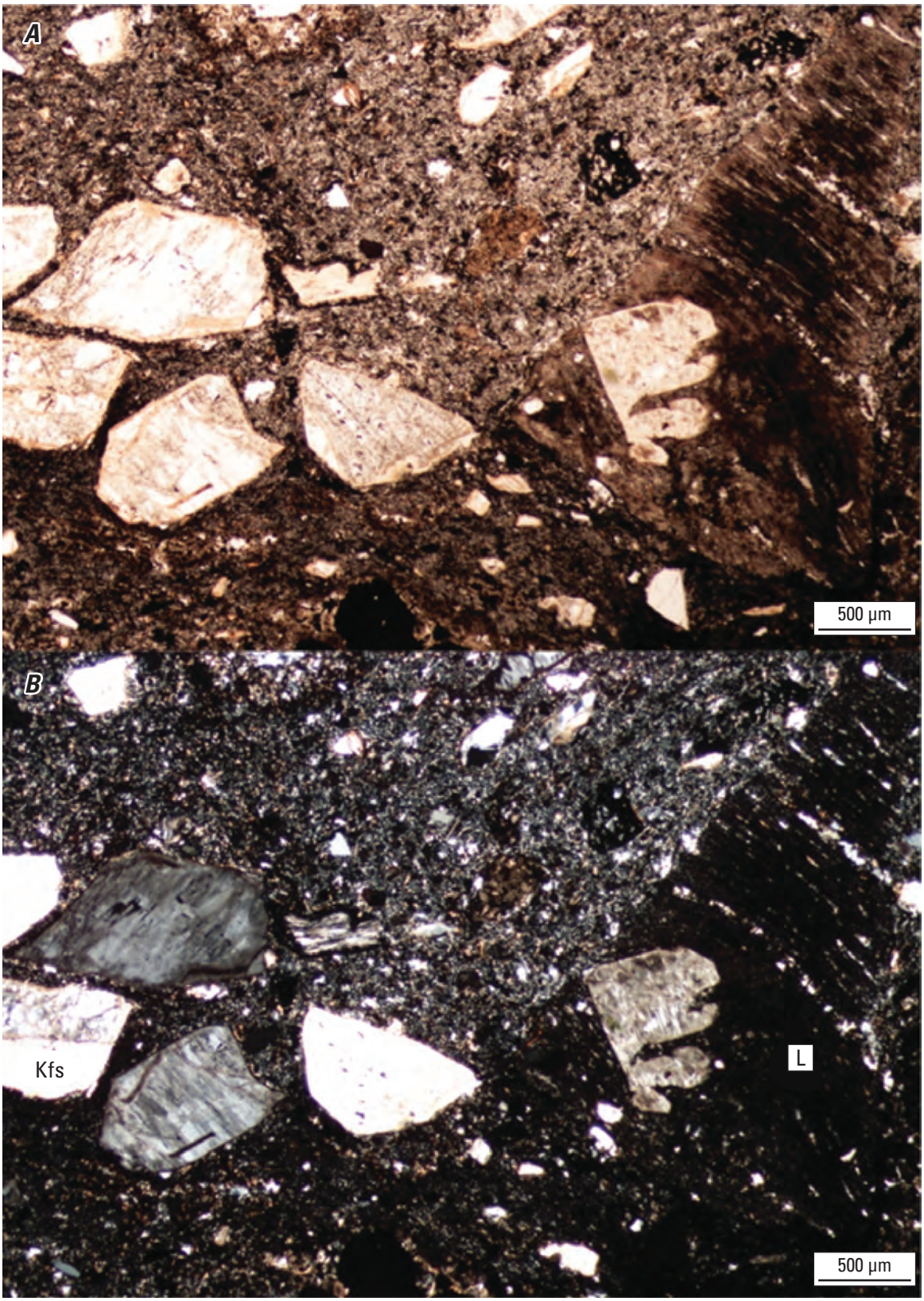

Figure 52. Pair of photomicrographs of rhyolite porphyry from borehole W12483 at 14,290 feet depth in plane-polarized light (*A*) and cross-polarized light (*B*). Note the Carlsbad twin in potassium feldspar phenocryst (Kfs) and flow banding in rhyolitic lithic clast (L). Term: µm, micrometer. Photomicrographs by Ryan Deasy, U.S. Geological Survey.

Borehole W15078

Basement rocks observed in this borehole include Paleozoic sedimentary strata from 4,620 to 9,960 ft depth overlying mafic to intermediate porphyritic volcanic rock from 9,960 to 10,078 ft depth.

Previous Work

Duncan (1998) contributes a comprehensive description of cuttings from 4,610 to 10,078 ft depth (TD) and defines major units and depths to important boundaries in Suwannee basin strata, including depth to volcanic rock at 9,960 ft depth.

Cuttings Log

Summary: Undifferentiated Mesozoic red sandstone overlies Paleozoic Suwannee basin rocks at 4,620 ft depth. Suwannee basin units, all informally named by Duncan (1998), include the Cherry Lake formation (4,620–6,030 ft depth), a transitional stratum (6,030–6,460 ft depth), the Cooks Hammock formation (6,460–9,417 ft depth), and the basal Pumpkin Swamp formation (9,417–9,960 ft depth). Mafic to intermediate porphyritic volcanic rock was encountered from 9,960 to 10,078 ft depth (TD).

4,590–4,620 ft Fine-grained red sandstone. Some fragments are mottled with white "reduction" spots or have sharp contacts between red and white domains, which are larger than the cuttings fragments. Some fragments are coarser grained (0.2–0.4 mm) white quartz arenite. Minor fraction of large, angular to subrounded, red, feldspar-phyric rhyolite fragments, some of which have quartz veins; it is unclear if these fragments are a contaminant or if they belong to this stratum. Contaminants include minor gray limestone and white, coarse-grained, rounded fragments of quartz arenite.

4,620–4,640 ft Missing. Per Duncan (1998), the contact between undifferentiated Mesozoic sandstone above and Ordovician Cherry Lake formation below is at ~4,620 ft.

4,640–4,660 ft Muscovite-rich quartz sandstone. Muscovite grains up to 0.4 mm in diameter are commonly euhedral. In some fragments, the euhedral mica grains are randomly oriented and, in others, white mica defines a weak, discontinuous foliation.

4,660–4,680 ft Missing.

4,680–4,690 ft AA. Rare fragments of the muscovite-rich sandstone contain pink (zeolite?) veins. Rare fragments contain submillimeter-sized pyrite cubes.

4,690–4,700 ft AA, with significant red sandstone contaminant.

4,800–4,810 ft Medium-grained, well-cemented quartz sandstone. Many fragments contain randomly oriented muscovite porphyroblasts up to 0.4 mm in diameter. There is, however, a higher abundance of muscovite-free fragments than in 4,640–4,660 ft and 4,680–4,700 ft. Sharp contacts between muscovite-rich and muscovite-free domains in some fragments are probably bedding contacts. Muscovite-poor to muscovite-free (that is, pure quartz arenite) layers are as thin as 0.3 mm. The minimum upper limit is only constrained by the largest quartzite cuttings at greater than (>)3 mm. Quartz arenite is well sorted and comprised of distinct, well-rounded grains 0.1–0.2 mm in diameter. The HCl test was very weakly positive on one of two quartz arenite clasts and negative on one muscovite-rich clast. A slight sulfuric smell emitted from the muscovite-rich fragment, however.

4,900–4,910 ft AA. Gray muscovite-rich, granofelsic fragments are slightly dominant over quartz arenite. A 0.5-mm-thick quartz vein seen in one muscovite-rich clast. "Granofels" is used here as a descriptive term to denote a coarse-grained, massive metamorphic rock of unspecified protolith.

5,000–5,010 ft AA.

5,100–5,110 ft Missing.

5,110–5,120 ft AA.

5,180–5,190 ft Most cuttings are AA. New here are fine-grained, marl(y), poorly sorted (contains floating 0.2-mm quartz grains) quartz wacke or dirty limestone fragments. Strong positive HCl test.

5,240–5,250 ft Muscovite-rich sandstone dominates over quartz arenite. Contains less marl than in 5,180–5,190 ft but extant fragments are larger and probably contaminant from above.

5,290–5,300 ft AA. Fragments contain muscovite porphyroblasts up to 0.4 mm. Flakes <0.05 mm are most common. Sharp contact between coarse muscovite and fine-grained muscovite-bearing domains in one fragment.

5,340–5,350 ft AA. Higher proportion of quartz arenite relative to muscovite-bearing rock.

5,370–5,750 ft Missing.

5,750–5,760 ft Cuttings similar to 5,340–5,350 ft in proportion of quartz arenite and muscovite-bearing fragments.

5,800–5,810 ft AA.

5,900–5,910 ft AA.

6,010–6,120 ft AA, but muscovite-bearing fragments are more abundant than quartz arenite.

[Note: Duncan (1998) interprets the interval from 6,030–6,460 ft as transitional between Cherry Lake formation and Cooks Hammock formation.]

6,050–6,060 ft AA, including fragments bearing euhedral, authigenic muscovite (fig. 53).

6,100–6,110 ft AA, some quartz arenite fragments have a green hue.

6,210–6,220 ft AA, quartz arenite more abundant than muscovite rich.

6,300–6,310 ft AA, more green quartz arenite.

6,400–6,410 ft AA.

6,450–6,460 ft Quartz arenite is much more abundant than muscovite-bearing rock.

6,700–6,710 ft AA, including granofels with euhedral muscovite porphyroblasts, white to pale green quartz arenite with visible detrital grains 0.2–0.4 mm in diameter, and lots of loose quartz sand and limestone contaminant.

6,800–6,810 ft AA, but quartz arenite is progressively greener and granofelsic fragments are becoming purplish rather than gray.

6,900–6,910 ft Very little gray muscovite-bearing rock. Mostly white to pale green quartz arenite. New here is reddish, fine-grained quartz sandstone with black lithic(?) grains (not magnetic).

6,950–6,960 ft AA.

7,000–7,010 ft Detrital grains in quartz arenite are more homogeneous. Muscovite-rich fragments are rare, but muscovite-bearing fragments are common.

7,030–7,140 ft Missing. One bag labeled "7130-40" has "1" crossed out in pencil, and "2" written above; it was not investigated.

7,140–7,150 ft Clean white quartz arenite. Detrital grains readily visible. Very weakly positive reaction with HCl indicates some interstitial or cementing calcite. Muscovite-rich clasts are very rare and may be a contaminant in this interval.

7,200–7,210 ft AA, but with even fewer muscovite-rich granofelsic fragments. Muscovite porphyroblasts are also rare in quartz arenite fragments.

7,220–7,230 ft Quartz arenite. Little to no muscovite.

7,230–7,490 ft Missing.

7,490–7,500 ft Quartz arenite with minor muscovite-rich metasandstone. Euhedral muscovite porphyroblasts are present in quartz arenite.

7,530–7,540 ft AA.

7,540–7,660 ft Missing.

7,660–7,690 ft Empty bags marked "NO RECOVERY."

7,690–7,700 ft White and pale quartz arenite is slightly dominant over muscovite granofels. Muscovite porphyroblasts are up to 0.4 mm in diameter. Well-rounded quartz grains are as large as ~1 mm.

7,750–7,760 ft White and light gray quartz arenite dominate. Some fragments have faint pink or green hues. Muscovite porphyroblasts in sandstone are up to 0.2 mm in diameter. Muscovite granofels are rare.

7,850–7,860 ft White, pink, and green sandstone with muscovite porphyroblasts and minor muscovite granofels.

7,950–7,960 ft Pink and green sandstone with minor muscovite granofels. Granofels might be contaminant.

7,960–8,110 ft Missing.

8,110–8,120 ft Light gray to green or pink sandstone and arkose with muscovite porphyroblasts and dark gray muscovite granofels. Feldspar cleavage seen in the grains in some fragments.

8,200–8,210 ft AA.

8,320–8,330 ft Light gray to green or pink sandstone with muscovite porphyroblasts and dark gray muscovite granofels.

8,380–8,390 ft Light gray sandstone and dark gray muscovite granofels. Pink, green, and black grains are common in sand. No feldspar cleavage was seen among detrital grains. Most opaque grains are not magnetite; the fragments gave a very weak magnetic response.

8,390–8,700 ft Missing.

8,720–8,730 ft Preponderance of white, pink, and green sandstone fragments. Fragments of muscovite-porphyroblastic granofels are minor and are probably contaminant.

9,050–9,060 ft Pink to green quartz, feldspar, and lithic pebble sandstone. Grains are well rounded, 0.05–>1 mm in diameter, translucent to white to yellow to green to orange to red to black, and often display this color variation within a single cuttings fragment. Grains are free of oxide staining. Very weak magnetic response.

[Note: Per Duncan (1998), the contact between the Cambrian–Ordovician Cooks Hammock formation (above) and Cambrian–Ordovician Pumpkin Swamp formation (below) is at 9,417 ft depth, or 9,357 feet below sea level.]

9,500–9,510 ft Multicolored lithic pebble metasandstone. Grains are well rounded, 0.05–>1 mm in diameter, with the same color variation and distribution as in 9,050–9,060 ft. Sharp contact between phyllite and multicolored sandstone occurs in one large fragment; here, the quartz-rich side contains euhedral authigenic muscovite 0.1–0.2 mm. Magnetite is rare. Strong red (hematite?) staining on many fragments from in situ oxidation of detrital grains, whereas others are white. Rare muscovite granofels fragments are AA.

9,790–9,800 ft Red, coarse-grained (0.2–>1 mm) quartz sandstone comprises well-rounded, multicolored grains. Rare fragments are green. Very weakly magnetic.

9,810–9,820 ft AA. Very rare granitic clasts are comprised of quartz, K-feldspar, magnetite, and muscovite.

9,900–9,910 ft Dominantly coarse-grained red sandstone with well-rounded grains. Not much magnetite but appreciably more than in overlying muscovite granofels and multicolored sandstone. Minor red to purplish, fine-grained, well-indurated sandstone.

9,950–9,960 ft Mostly AA, with higher proportion of multicolored sandstone and muscovite granofels (contaminant).

9,960–9,970 ft Red to purple, coarse-grained sandstone to mudstone. Well indurated. Minor muscovite granofels. Minor multicolored and green quartzite.

9,970–9,980 ft First appearance of green to black volcanic fragments that compose ~50 percent of cuttings.

10,000–10,010 ft Pale-green to green to green-black volcanic fragments and mottled green and white weathered volcanic fragments. Darkest grains are sulfide bearing. Vein fragments of epidote and epidote+quartz are present; zoned where both minerals are present, but zoning direction is not clear.

10,060–10,070 ft Volcanic fragments are highly altered. Those with preserved magmatic textures (distinct plagioclase shapes) are chalky and fragile. Abundance of vein fragments comprise epidote, epidote+quartz, or calcite.

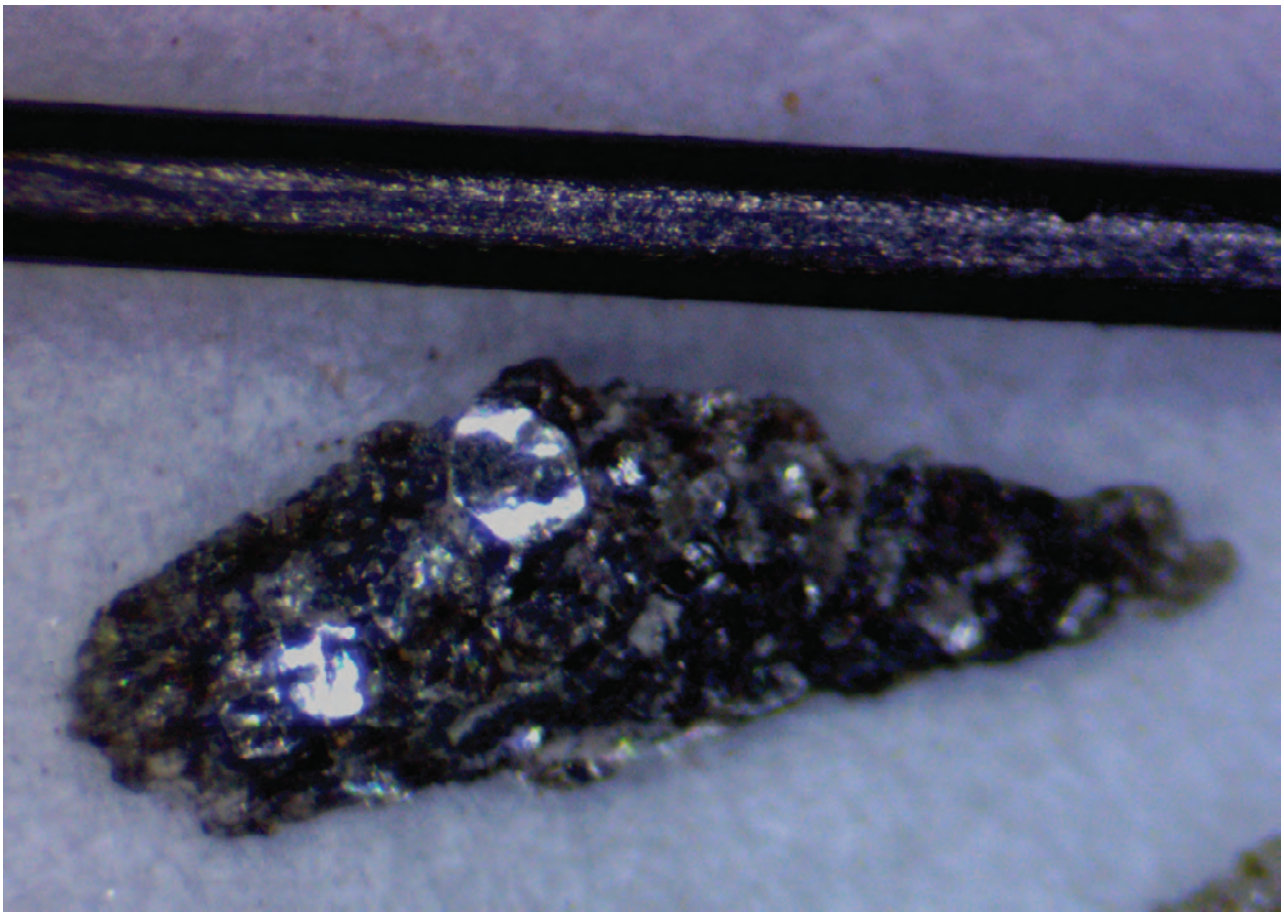

Figure 53. Photograph of representative fragments from borehole W15078 from 7,000 to 7,010 feet depth containing euhedral muscovite. The width of the pin is 5 millimeters. Photograph by Ryan Deasy, U.S. Geological Survey.

Thin Section Petrography

4,640–4,650 ft Cherry Lake formation (Duncan, 1998). Muscovite-rich quartz sandstone. Muscovite flakes are euhedral and up to 4 mm in diameter (fig. 54).

8,970–8,980 ft Pumpkin Swamp formation (Duncan, 1998). Arkose and conglomerate. Clasts are angular to rounded quartz, feldspar, epidote, opaques, and lithics (fig. 55). Lithic clasts include porphyritic volcanics identical to those in the underlying basement rock (fig. 56).

10,010–10,050 ft North Florida volcanic series (informal name of Heatherington and others, 1996). Volcanic fragments are plagioclase- and clinopyroxene-phyric mafic to intermediate porphyry. Most are massive, with randomly oriented phenocrysts and static replacement textures (figs. 57–59). Euhedral to amoeboidal oxide grains with exsolved magnetite-titanite and magnetite-rutile lamellae ~5 µm thick are common (fig. 59). Alteration is pervasive, and metamorphic minerals include euhedral epidote (fig. 60) and andradite (fig. 61) porphyroblasts. Although widely distributed, these minerals are more abundant in and near cataclastic zones, where they are commonly brecciated. Some fragments are faulted, with sharp boundaries filled with chlorite or calcite (fig. 62). Additionally, several fragments contain cataclastic fabrics (figs. 59 and 60). Many fragments contain veins or are entirely vein material. Vein minerals include calcite, chlorite, quartz, and epidote. Where zoned, veins have quartz cores and epidote rims.

Notes on XRD Methods and Results

Individual cuttings fragments from 4,640 to 4,650 ft were independently powdered by hand in a corundum mortar and pestle. Each sample was continuously lubricated with acetone during grinding. The grinding equipment was cleaned thoroughly between samples. Resulting powders were mounted on quartz “zero background” plates in a slurry with deionized water and analyzed on a Bruker D8 diffractometer from an angular range of 2–70° 2Θ at a rate of 15 sec/0.02° step. Then, the mounted samples were placed in a chamber with an atmosphere saturated in EG for 24 hours. Immediately upon removal from the chamber, the samples were analyzed again from 2 to 40° 2Θ at 4 sec/step. Representative diffractograms under air-dried and EG-solvated conditions for a single cuttings fragment from 4,640 to 4,650 ft are shown in figure 63.

Additionally, volcanic fragments were handpicked under a binocular microscope and separated into subsamples for mineralogical and geochemical analyses. A ~5-g subsample from 10,010 to 10,050 ft was separated for X-ray fluorescence (XRF)/ICP-MS and, to test for variability and control for potential contamination, three ~0.6-g subsamples of pale green and dark gray volcanic rock were separated from 10,020 to 10,040 ft; from 10,040 to 10,050 ft (green); and from 10,010 to 10,050 ft (gray). The larger subsample was ground in an automated Brinkman grinder fitted with an agate mortar and pestle while being continuously lubricated with acetone. This subsample was then ground further by hand in a corundum mortar and pestle. An aliquot of the subsample was placed in the 2×3×0.1-cm cavity of a Ti “front-pack” mount and analyzed on a Bruker D8 diffractometer from 2 to 70° 2Θ at a rate of 8 sec/0.02° step. Semiquantitative mineral abundances (Deasy and others, 2024b) were determined by Rietveld modeling in TOPAS (Bruker AXS, 2011), and the geochemistry of the subsample was determined by XRF/ICP-MS (Deasy and others, 2024a). The three smaller subsamples were each ground by hand in an agate mortar and pestle while being continuously lubricated with acetone and were allowed to air dry. They were mounted in the 2-cm-wide round cavities of standard “back-pack” mounts and analyzed on a Panalytical X’Pert diffractometer from 3 to 90° 2Θ. Mineral abundances were determined with HighScore Plus (Malvern Panalytical, 2018) and the Rietveld method (Deasy and others, 2024b). Alteration minerals identified by XRD include disseminated calcite, chlorite, prehnite, actinolite, as well as minor illite and talc. Major and trace element geochemical analyses were thereafter obtained by INAA/ICP-OES (Deasy and others, 2024a).

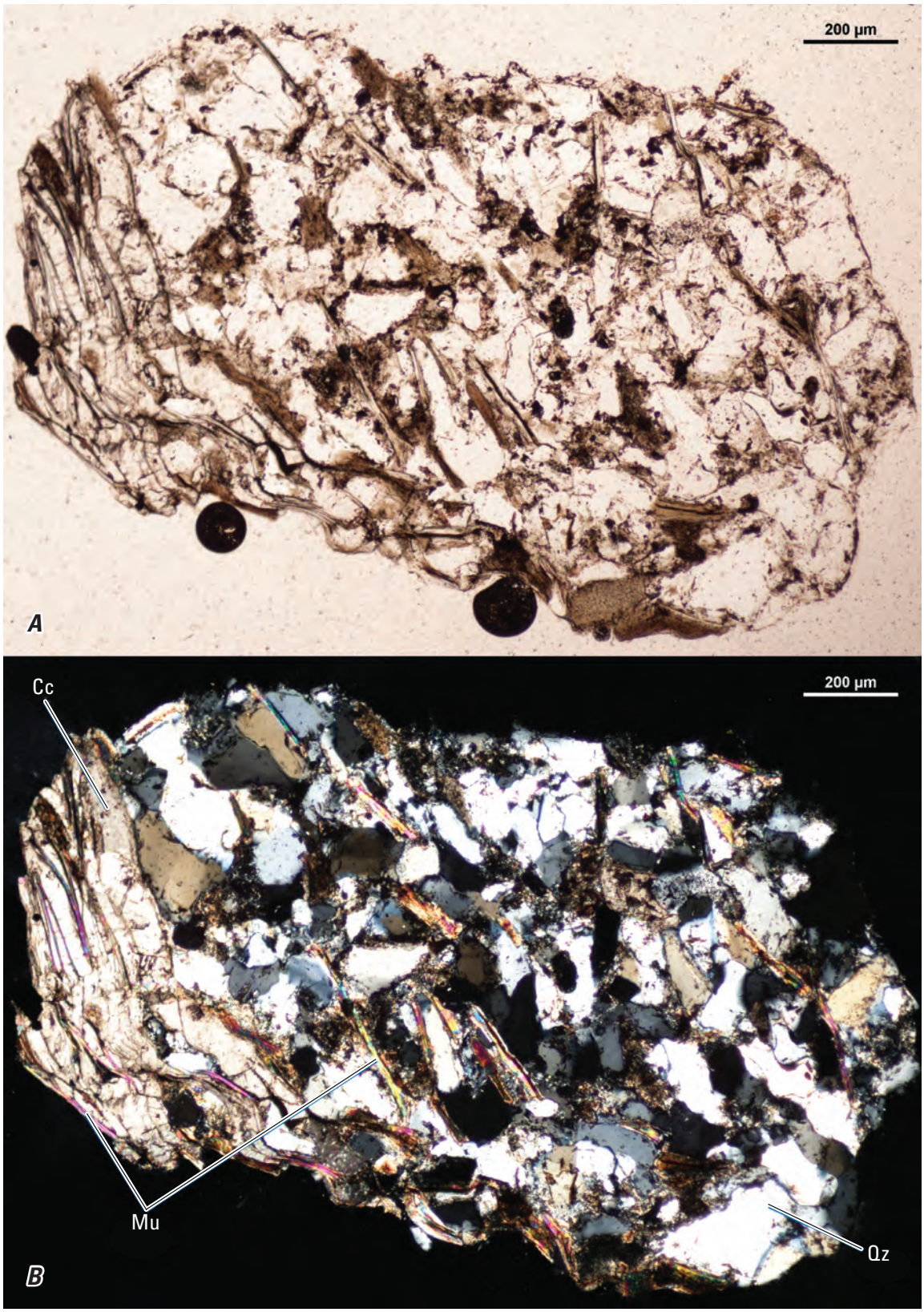

Figure 54. Pair of photomicrographs of a representative fragment of the Cherry Lake formation from borehole W15078 from 4,640 to 4,650 feet depth in plane-polarized light (*A*) and cross-polarized light (*B*). Terms: Cc, calcite; Mu, muscovite; Qz, quartz; µm, micrometer. Photomicrographs by Ryan Deasy, U.S. Geological Survey.

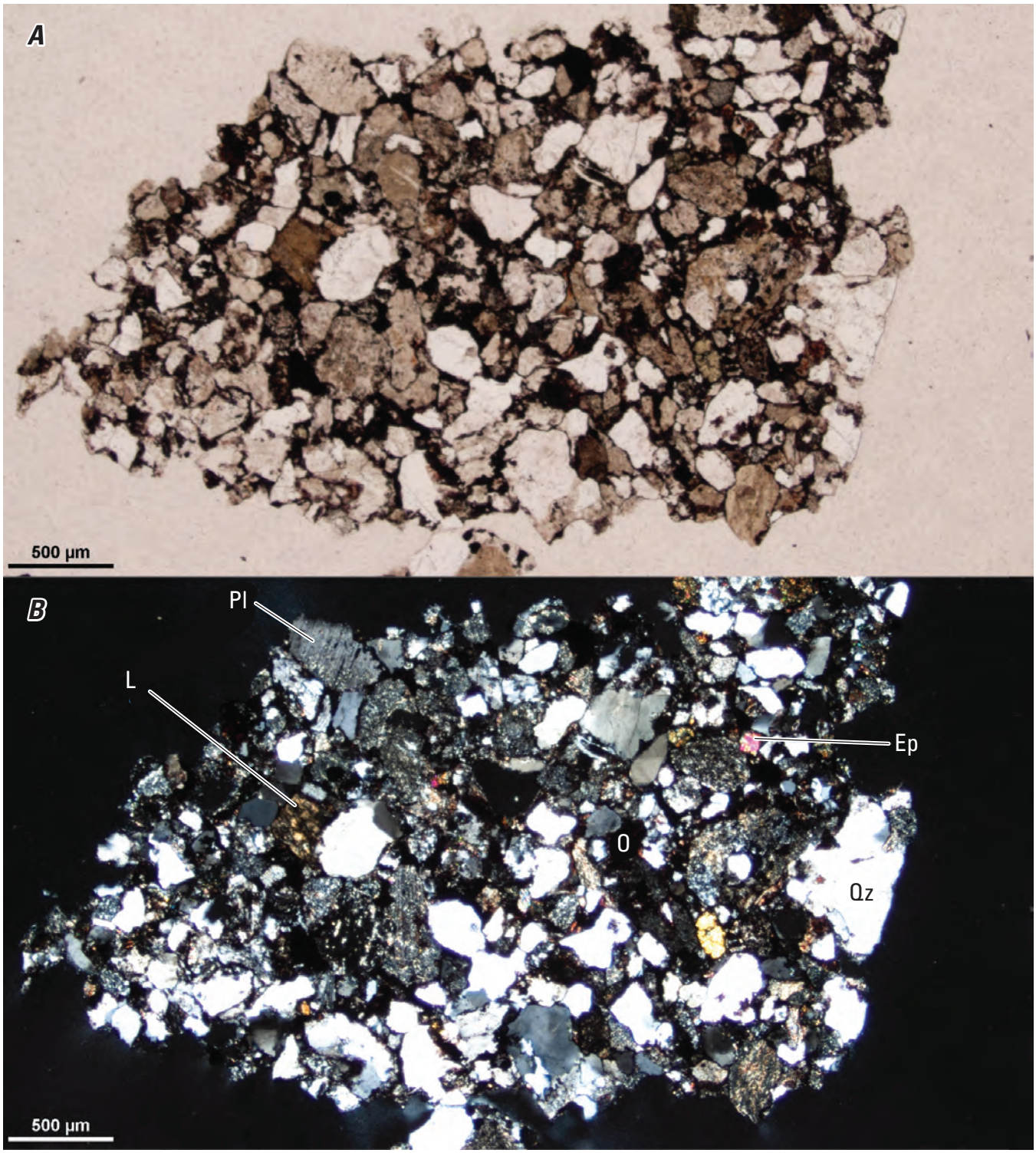

Figure 55. Pair of photomicrographs of a representative sandstone fragment of the Pumpkin Swamp formation from borehole W15078 from 8,970 to 8,980 feet depth in plane-polarized light (*A*) and cross-polarized light (*B*). Terms: Pl, plagioclase; L, lithic clast; Ep, epidote; O, opaque mineral; Qz, quartz; µm, micrometer. Photomicrographs by Ryan Deasy, U.S. Geological Survey.

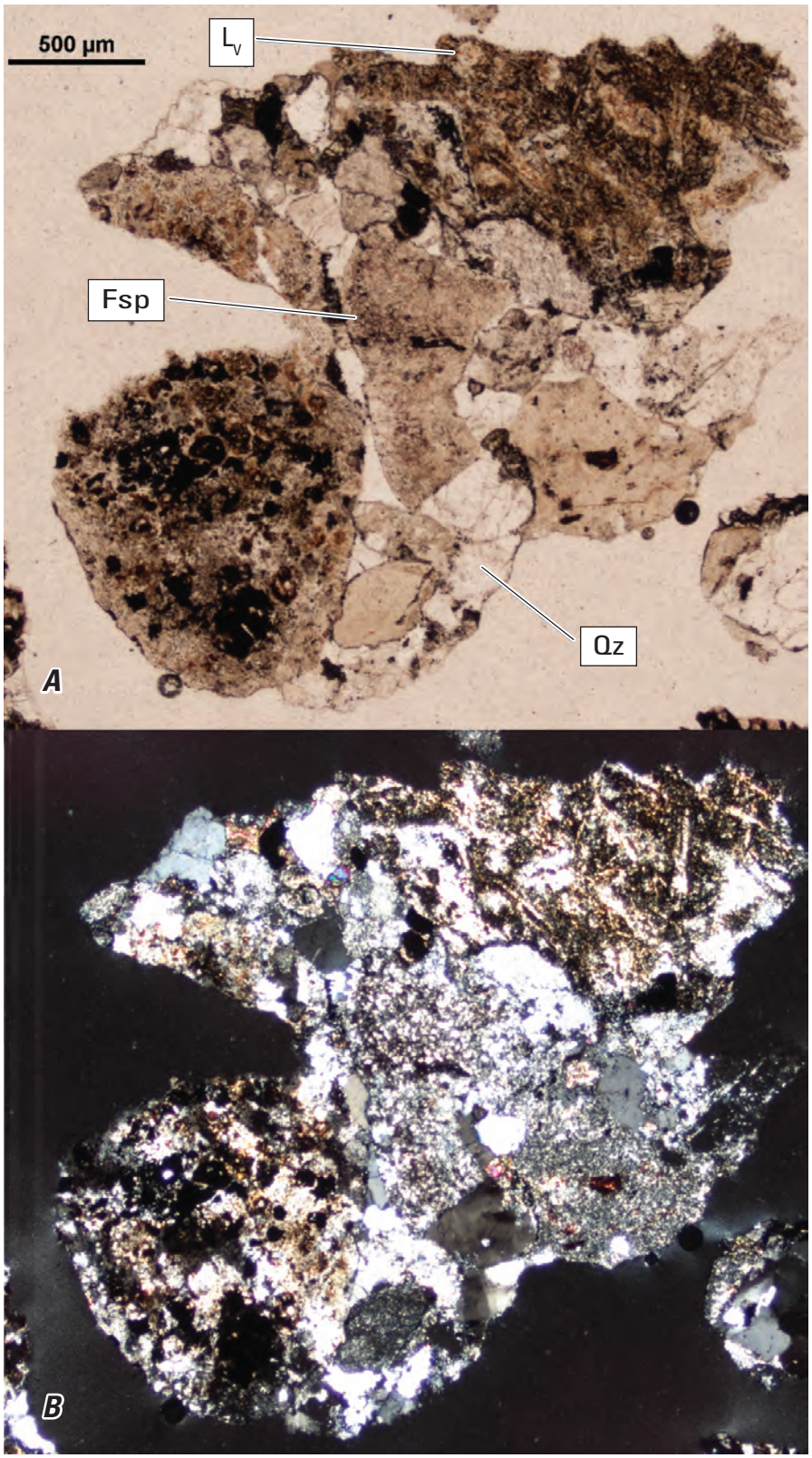

Figure 56. Pair of photomicrographs of a representative fragment of sandstone from the Pumpkin Swamp formation containing volcanic lithic clasts (L_V) from borehole W15078 from 9,790 to 9,800 feet depth in plane-polarized light (*A*) and cross-polarized light (*B*). Terms: Fsp, feldspar; Qz, quartz; µm, micrometer. Photomicrographs by Ryan Deasy, U.S. Geological Survey.

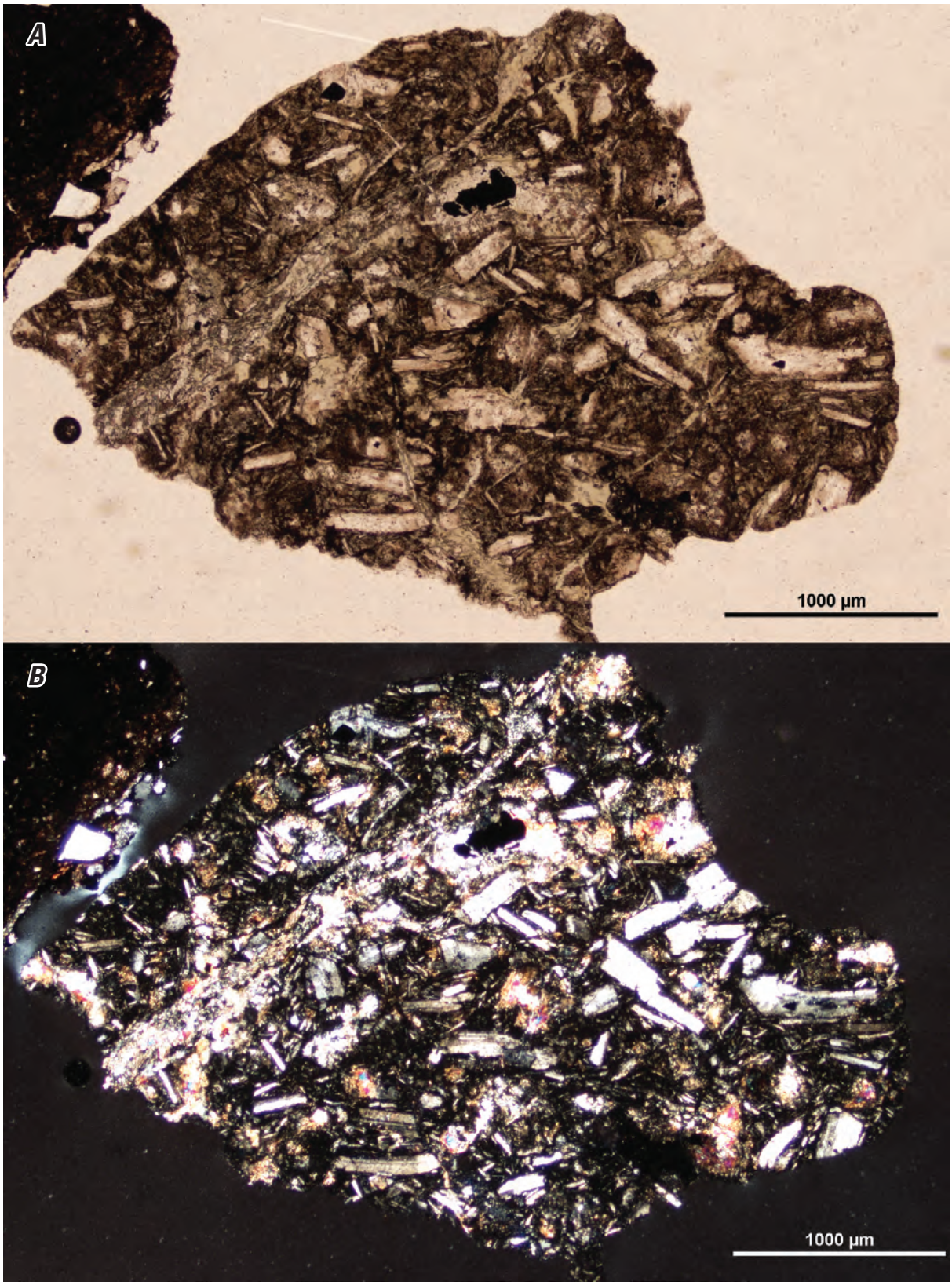

Figure 57. Pair of photomicrographs of a representative fragment of mafic porphyry from borehole W15078 from 10,010 to 10,030 feet depth in plane-polarized light (*A*) and cross-polarized light (*B*). Term: µm, micrometer. Photomicrographs by Ryan Deasy, U.S. Geological Survey.

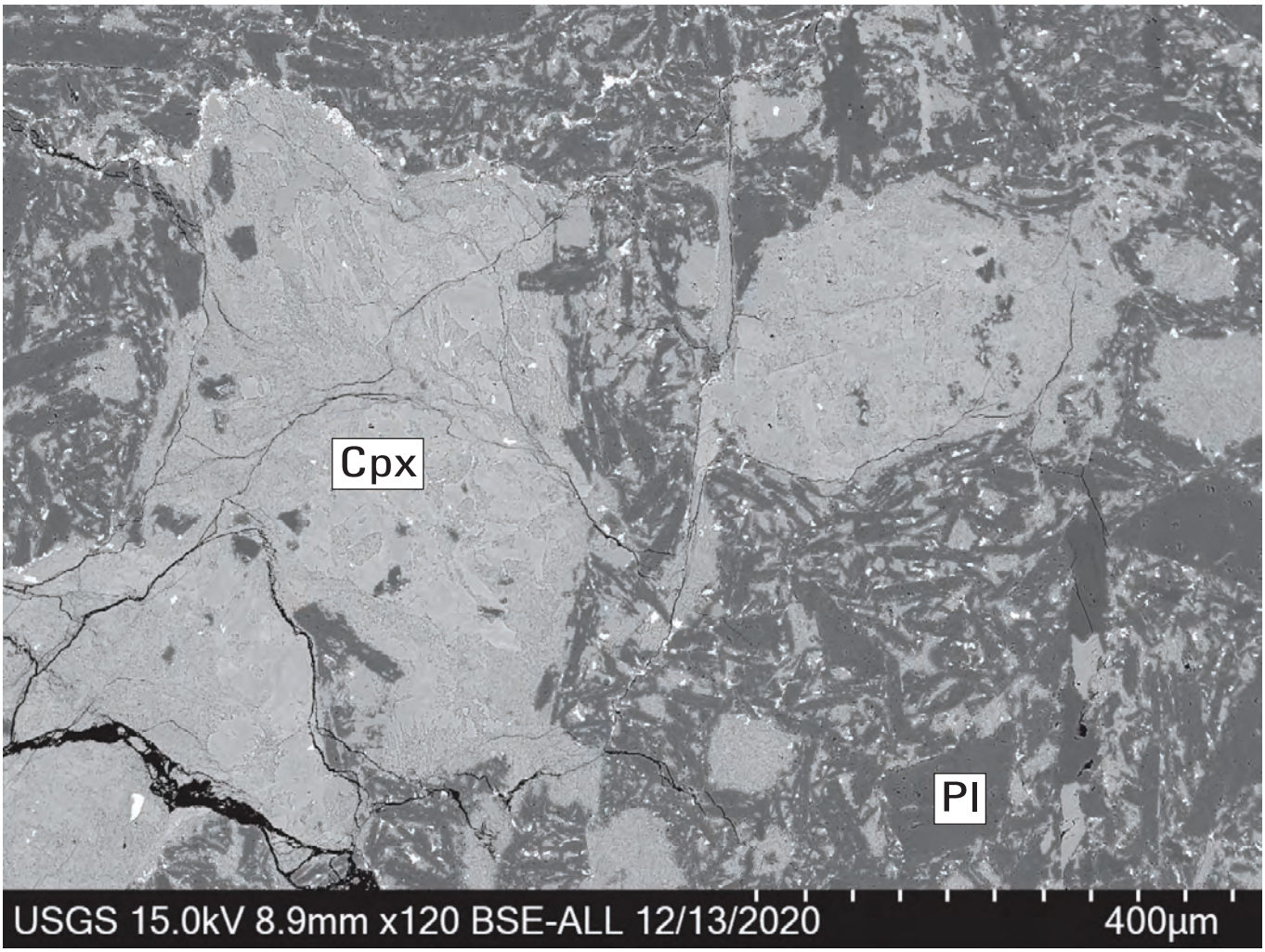

Figure 58. Back-scattered electron (BSE) image of massive plagioclase- and clinopyroxene-phyric porphyry from borehole W15078 from 10,040 to 10,050 feet depth. Text in the bottom left identifies data source (USGS); operating conditions including beam potential in kilovolts (15.0 kV), working distance in millimeters (8.9 mm), and image magnification in multiples of actual size (120 times); and date of acquisition (12/13/2020). Terms: Cpx, clinopyroxene; Pl, plagioclase; USGS, U.S. Geological Survey; kV, kilovolt; mm, millimeter; BSE-ALL, back-scattered electron, all energies; µm, micrometer. Photomicrograph by Ryan Deasy, U.S. Geological Survey.

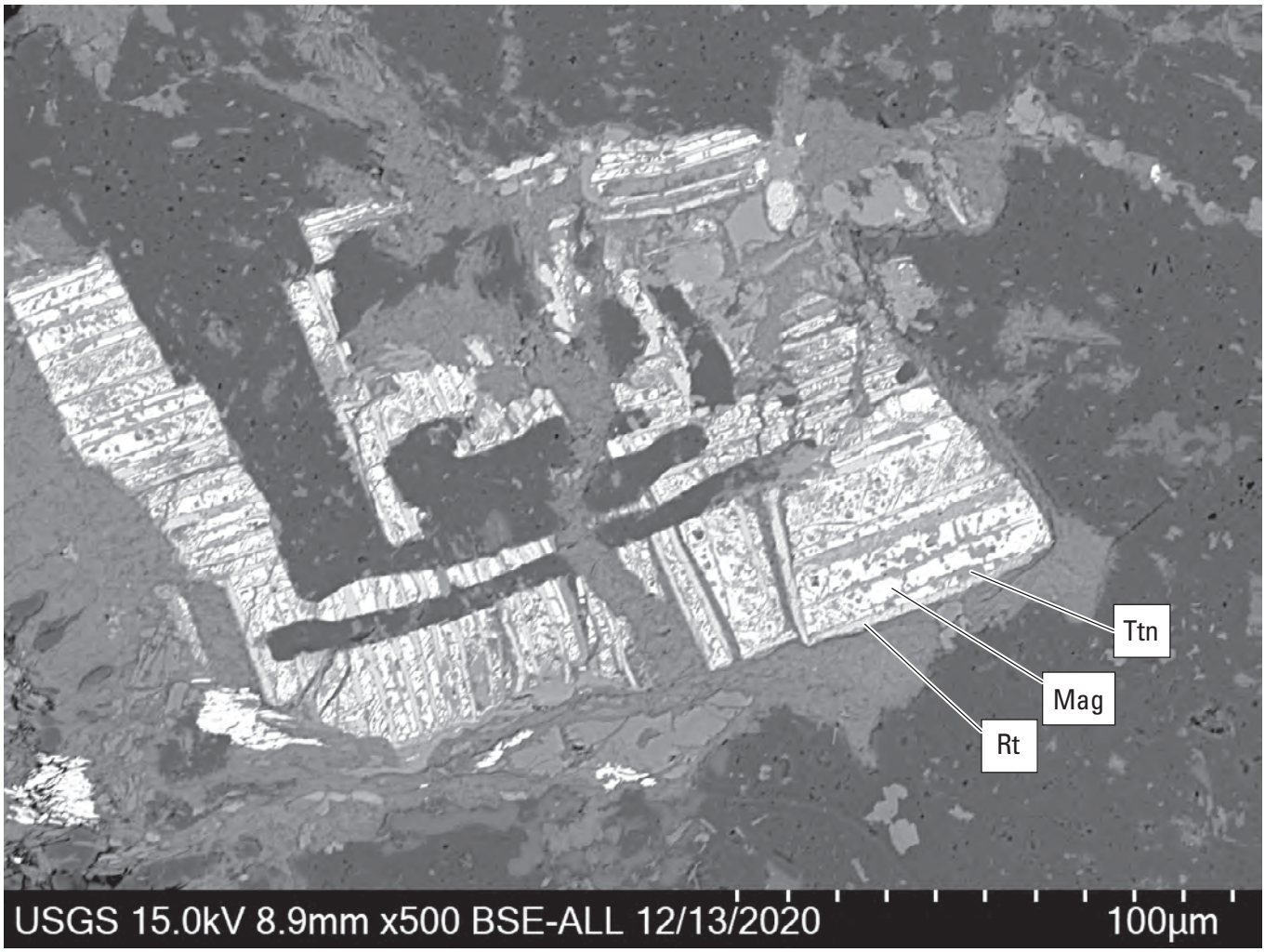

Figure 59. Back-scattered electron (BSE) image of representative magnetite-titanite-rutile symplectite from borehole W15078 from 10,030 to 10,040 feet depth. Text in the bottom left identifies data source (USGS); operating conditions including beam potential in kilovolts (15.0 kV), working distance in millimeters (8.9 mm), and image magnification in multiples of actual size (500 times); and date of acquisition (12/13/2020). Terms: Ttn, titanite; Mag, magnetite; Rt, rutile; USGS, U.S. Geological Survey; kV, kilovolt; mm, millimeter; BSE-ALL, back-scattered electron, all energies; µm, micrometer. Photomicrograph by Ryan Deasy, U.S. Geological Survey.

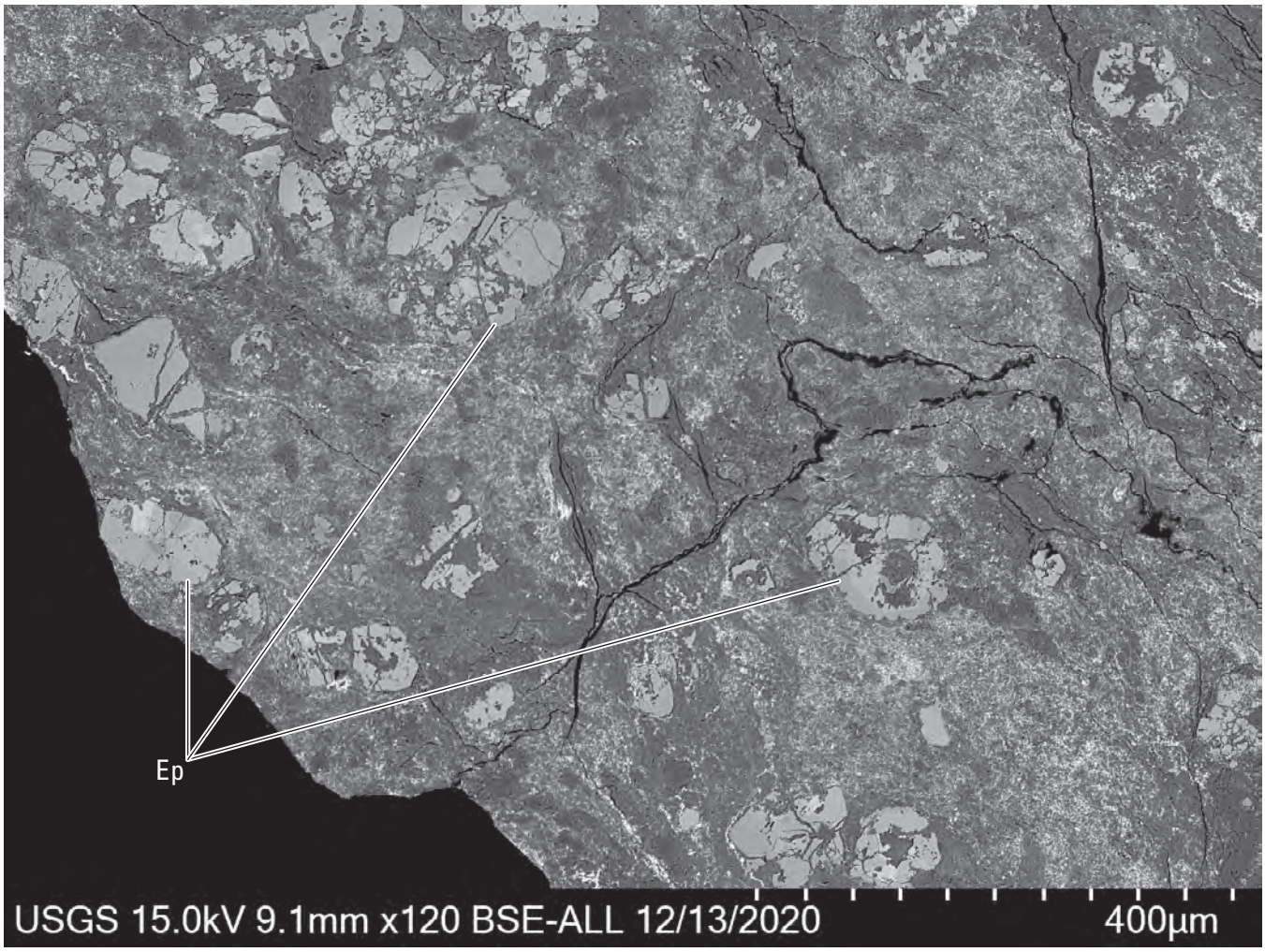

Figure 60. Back-scattered electron (BSE) image of cataclastic texture in a fragment from borehole W15078 from 10,030 to 10,040 feet depth. Text in the bottom left identifies data source (USGS); operating conditions including beam potential in kilovolts (15.0 kV), working distance in millimeters (9.1 mm), and image magnification in multiples of actual size (120 times); and date of acquisition (12/13/2020). Terms: Ep, epidote; USGS, U.S. Geological Survey; kV, kilovolt; mm, millimeter; BSE-ALL, back-scattered electron, all energies; µm, micrometer. Photomicrograph by Ryan Deasy, U.S. Geological Survey.

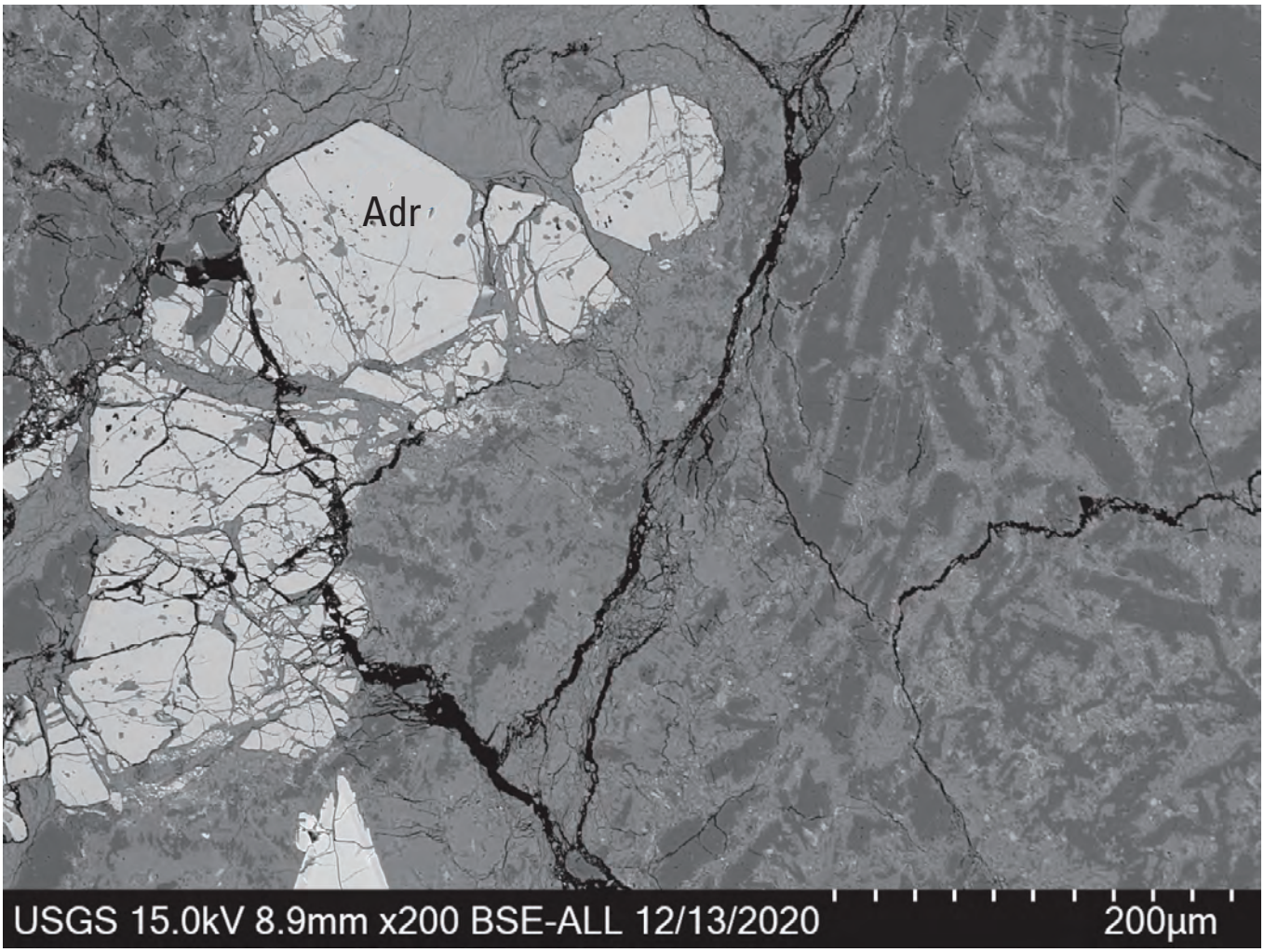

Figure 61. Back-scattered electron (BSE) image of a cataclastic zone with brecciated euhedral andradite (Adr) cutting massive plagioclase porphyry in a fragment from borehole W15078 from 10,030 to 10,040 feet depth. Text in the bottom left identifies data source (USGS); operating conditions including beam potential in kilovolts (15.0 kV), working distance in millimeters (8.9 mm), and image magnification in multiples of actual size (200 times); and date of acquisition (12/13/2020). Terms: Adr, andradite; USGS, U.S. Geological Survey; kV, kilovolt; mm, millimeter; BSE-ALL, back-scattered electron, all energies; µm, micrometer. Photomicrograph by Ryan Deasy, U.S. Geological Survey.

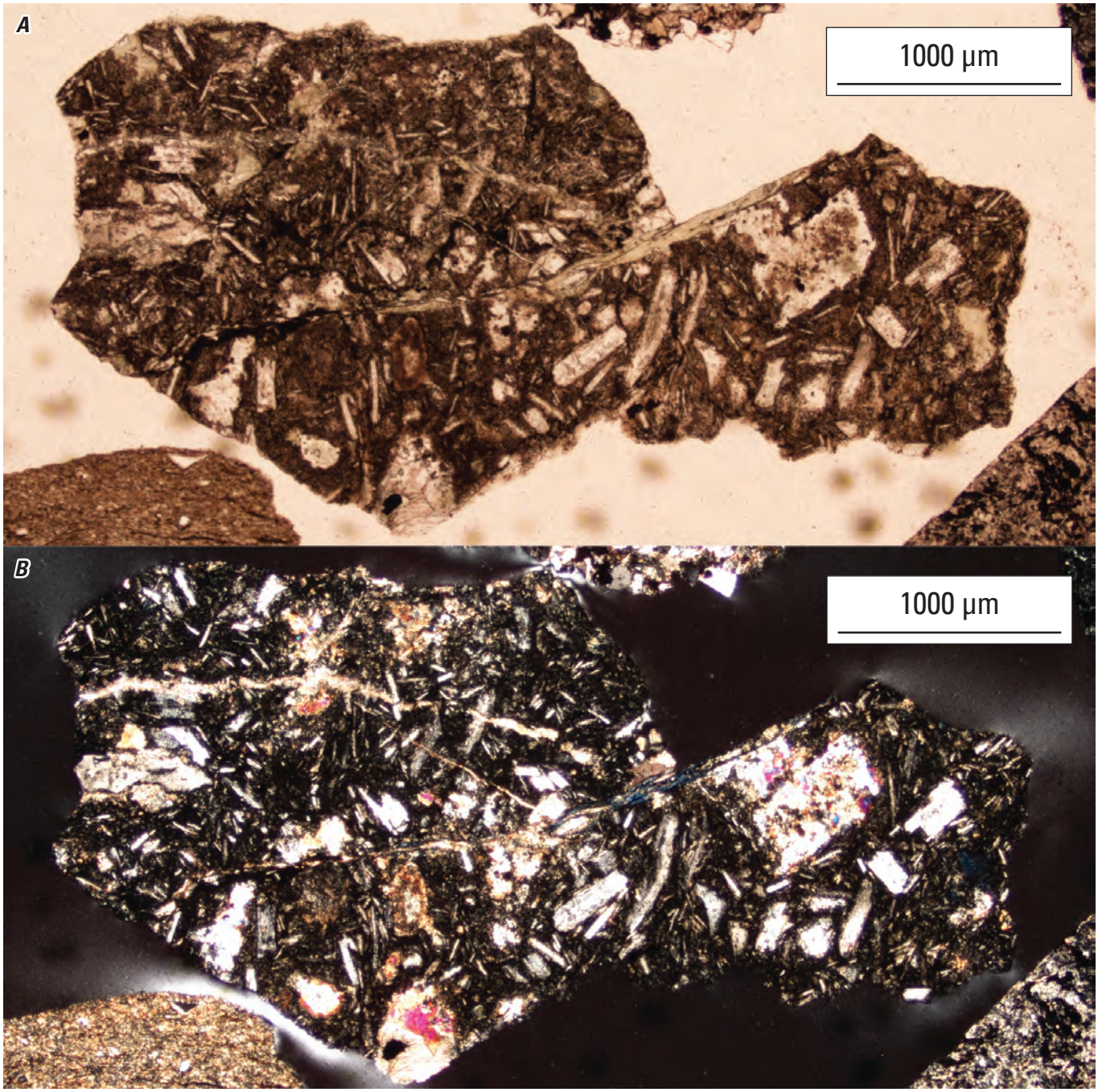

Figure 62. Example of a faulted volcanic fragment from borehole W15078 from 10,030 to 10,040 feet depth in plane-polarized light (*A*) and cross-polarized light (*B*). Term: µm, micrometer. Photomicrographs by Ryan Deasy, U.S. Geological Survey.

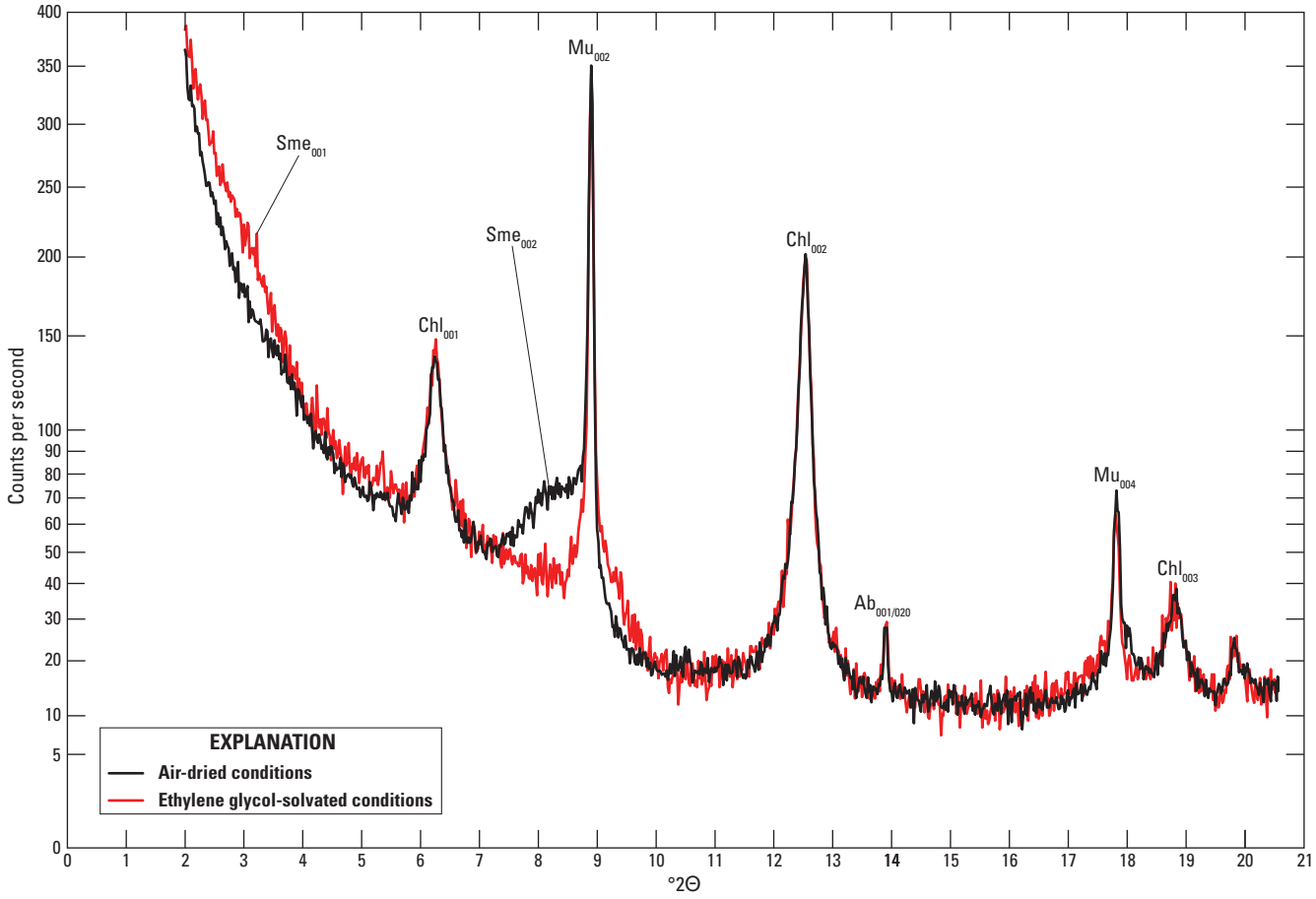

Figure 63. X-ray diffractograms of a single cuttings fragment from borehole W15078 from 4,640 to 4,650 feet depth under air-dried and ethylene glycol-solvated conditions. The *y*-axis is in square root scale. Selected peaks are labeled with corresponding mineral abbreviations; numbers in subscript denote Miller indices. Terms: °2Θ, degrees two theta; Sme, smectite; Chl, chlorite; Mu, muscovite; Ab, albite.

Borehole W15489

Paleozoic sedimentary strata occur from 4,940 to 7,660 ft depth and overlie mafic to intermediate porphyritic volcanic rock from 7,660 to 9,073 ft depth.

Previous Work

Duncan (1998) defines major units and important boundaries in Suwannee basin strata, identifies a nonconformable contact with volcanic basement rock at 7,660 ft depth, and contributes a description of cuttings from 4,840 to 9,073 ft depth (TD). A whole-rock K-Ar age of 552±21 Ma is reported for volcanic rock from 9,073 ft depth (Amoco Corporation unpublished data, as cited in Duncan [1998]).

Cuttings Log

Summary: Undifferentiated Mesozoic(?) red beds overlie Paleozoic Suwannee basin sedimentary rocks at 4,940 ft depth. Suwannee basin units, per Duncan (1998), include the Cambrian–Ordovician Cooks Hammock formation (4,940–7,510 ft depth) and the Cambrian–Ordovician Pumpkin Swamp formation (7,510–7,660 ft depth). Below this, nearly 1,400 ft of volcanic rock of the North Florida volcanic series were penetrated before a total depth of 9,073 ft was reached. The volcanic rock is interbedded with siliceous, fossiliferous carbonate rock from 8,080 to 8,240 ft (Duncan, 1998; not seen in this study). The volcanic rock contains green to dark aphanitic rock, weakly plagioclase-phyric mafic to intermediate porphyry, and welded lapilli tuff.

Mesozoic Sandstone

4,450–4,480 ft Red sandstone to siltstone and poorly consolidated white quartz arenite.

4,750–4,780 ft Loose quartz sand. Well-rounded grains, translucent to white to yellow, 0.25–1.5 mm in diameter. Minor red fine-grained sandstone fragments and coarser grained white to pink sandstone fragments are both free of conspicuous muscovite flakes.

4,900–4,930 ft Pink to orange to red fine-grained sandstone. Loose quartz grains, limestone, and other contaminants compose ~50 percent of cuttings.

Cooks Hammock Formation

4,930–4,940 ft This interval is the first appearance of muscovite-rich gray granofels and white quartzite with or without muscovite. Similar to cuttings from 4,640 to 6,120 ft in borehole W15078, although Duncan (1998) identifies those cuttings as Cherry Lake formation and these as Cooks Hammock formation. Roughly equal proportions of muscovite-bearing rocks and contaminating red sandstone.

4,960–4,970 ft AA, with a greater fraction of muscovite-bearing fragments.

5,000–5,010 ft White quartzite with euhedral muscovite. Red sandstone contaminant ~30 percent.

7,180–7,190 ft White to pale green or pink sandstone mixed with muscovite-rich sandstone. Similar to cuttings from 6,100 to 9,060 ft in borehole W15078.

7,390–7,400 ft AA.

7,500–7,510 ft Unwashed. Quartz arenite, translucent to white to light gray. Some fragments are speckled with pink (feldspar?) and black (lithic?) grains. Minor muscovite-rich sandstone. Other cuttings types, interpreted as contaminants, are loose rounded quartz grains, chalky white clay-rich sandstone (negative HCl test). Observed one loose K-feldspar cleavage fragment, 1 mm in diameter.

Pumpkin Swamp Formation

7,600–7,610 ft Coarse-grained quartz and feldspar sandstone. Large, rounded detrital grains >1 mm in diameter are identifiable within some fragments. Many fragments are single, rounded, broken quartz grains. Many fragments have a glassy appearance. Muscovite grains within cuttings fragments are rare but present.

7,650–7,660 ft Loose quartz grains, green, pink, and multicolored sandstone fragments, with minor muscovite-bearing sandstone.

North Florida Volcanic Series

7,660–7,670 ft First appearance of green and purplish volcanic fragments as minor component of cuttings dominated by coarse-grained sandstone.

7,670–7,680 ft Cuttings are ~33 percent purple-red, very fine grained, altered volcanic fragments. The remainder are mostly quartz arenite with minor muscovite-bearing sandstone.

7,680–7,690 ft AA, >80 percent purple-red altered volcanic fragments.

7,690–7,700 ft Green and purple altered volcanic fragments.

7,700–7,710 ft AA.

7,750–7,760 ft Green, mottled green-and-white, and green-purple volcanic fragments. White and green grains appear to preserve massive igneous texture (that is, the outlines of plagioclase phenocrysts in fine-grained matrix).

7,790–7,800 ft Green to purple massive aphanitic volcanic fragments. No structures identified. No veins or obvious local vein material. Cuttings are unusually small at <1.5 mm in diameter.

7,900–7,910 ft Massive, fine-grained, green, green-and-white, and purple altered volcanic fragments. Rare calcite veins. Matrix calcite in both green and purple clasts (positive HCl test).

8,000–8,010 ft AA.

8,100–8,110 ft AA. Very fine grained cuttings fragments 0.2–1.5 mm in diameter. Dominated by calcareous aphanitic volcanic fragments. Calcite fragments are also abundant.

8,190–8,200 ft Volcanic fragments are dominantly white, pale green to green, or mottled white and green. Relatively few purple fragments. Volcanic fragments contain abundant matrix calcite.

8,280–8,290 ft Purple fragments are present in abundance and tend to be thinly laminated (that is, phyllitic) unlike green fragments, which are massive. Abundance of white and faintly pink vein material here (calcite: positive HCl test). Very little calcite in clast matrices.

8,310–8,320 ft AA. Lots of calcite vein material.

8,400–8,410 ft AA.

8,500–8,510 ft AA.

8,600–8,610 ft AA.

8,700–8,710 ft AA. Very fine grained cuttings, ~0.2–1 mm.

8,800–8,810 ft AA. Some green fragments are composed of round lapilli.

8,900–8,910 ft AA.

9,000–9,010 ft AA.

9,050–9,060 ft AA.

9,060–9,073 ft Missing.

Thin Section Petrography

7,570–7,580 ft Sandstone of the Pumpkin Swamp formation. This is a coarse-grained arkosic sandstone dominated by angular to well-rounded quartz and feldspar clasts, with minor detrital white mica, epidote, opaques, and chert (figs. 64 and 65). The rock is poorly to moderately well cemented with quartz. Grain size is 0.1–4 mm. Bedding structures were not observed among the cuttings fragments, which are not much larger than the grain size of the rock. Microcline clasts are largely unaltered. Conversely, plagioclase clasts are nearly completely altered to sericite, chlorite, or epidote (fig. 65). Deformation twins are common in plagioclase. Whereas most quartz grains have uniform extinction, a minority of grains have undulose or patchwork extinction or show subgrain development (fig. 65).

9,010–9,020 ft Volcaniclastic rock of the North Florida volcanic series. This is an altered mafic to intermediate volcaniclastic rock containing lath-shaped euhedral plagioclase phenocrysts and volcanic lithic clasts (which are themselves also plagioclase-phyric) in a fine-grained matrix of chlorite and calcite (fig. 66). Some fragments are overprinted with an orange to red, iron oxy-hydroxide staining. Calcite veins are common, wherein crystal size and vein aperture range in size from a few hundred micrometers to larger than the cuttings (~6 mm). Chlorite veins are rare and are much smaller, with apertures of only a few tens of micrometers (fig. 67).

Notes on XRD Methods and Results

Fragments of volcanic rock were separated by hand from sedimentary fragments and other contaminants by hand under a binocular microscope. A sample of volcanic rock from 9,010 to 9,040 feet depth was obtained by combining subsamples from the interceding intervals. The sample was ground in an automated Brinkmann grinder fitted with an agate mortar and pestle. It was continuously lubricated with acetone during grinding. The resulting powder was further ground by hand in a corundum mortar and pestle, again while lubricated with acetone. The final powder was allowed to air dry before it was placed in the 1.5-cm-wide cavity of a circular “back-pack” mount and scanned in a Panalytical Empyrean diffractometer with a Cu anode and X’Celerator detector from an angular range of 3–90° 2Θ at 0.02° steps and a scan rate of 50 sec/step. Semiquantitative mineral abundances (Deasy and others, 2024b) were obtained by Rietveld refinement modeling in HighScore Plus (Malvern Panalytical, 2018). A major and trace element geochemical analysis was thereafter obtained by INAA/ICP-OES/ICP-MS by Activation Laboratories, Inc. (Deasy and others, 2024a).

To evaluate the sample for its expandable clay content, an aliquot of powder was mounted in a slurry with distilled water on a quartz “zero background” plate, was allowed to air dry, and was then scanned on the Bruker D8 diffractometer from 2 to 90° 2Θ at 8 sec/step. The mounted sample was then placed in a chamber saturated with EG for ~24 hours before being scanned again, immediately upon removal from the EG chamber, from 2 to 40° 2Θ at 4 sec/step. There was no change in the diffraction pattern of the sample upon EG solvation (fig. 68), demonstrating the absence of expandable clays in this rock.

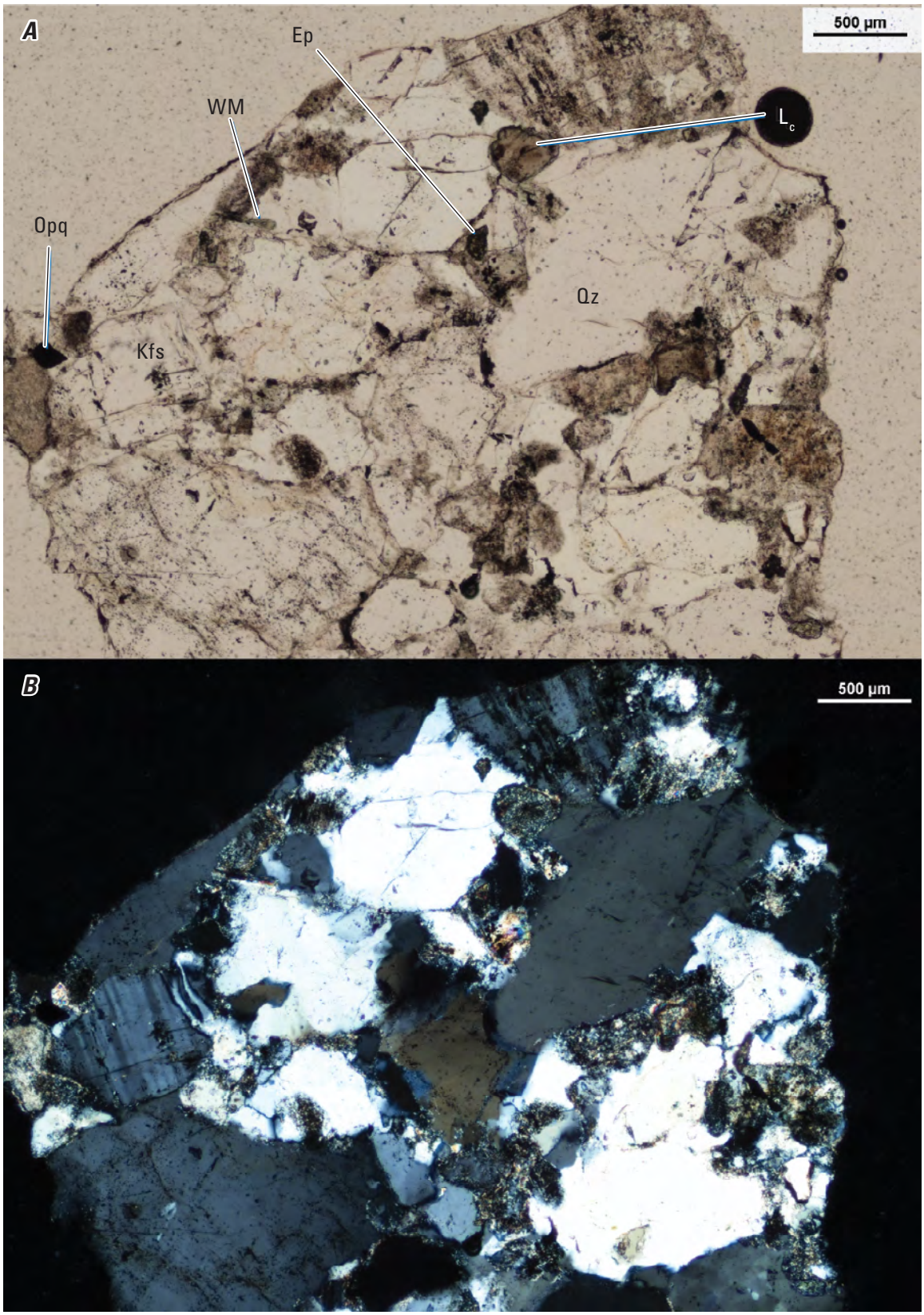

Figure 64. Pair of photomicrographs in plane-polarized light (*A*) and cross-polarized light (*B*) of a representative fragment of sandstone from the Pumpkin Swamp formation from borehole W15489 from 7,570 to 7,580 feet depth. Terms: Ep, epidote; WM, white mica; L_C, lithic clast of chert; Opq, opaque mineral; Kfs, potassium feldspar; Qz, quartz; µm, micrometer. Photomicrographs by Ryan Deasy, U.S. Geological Survey.

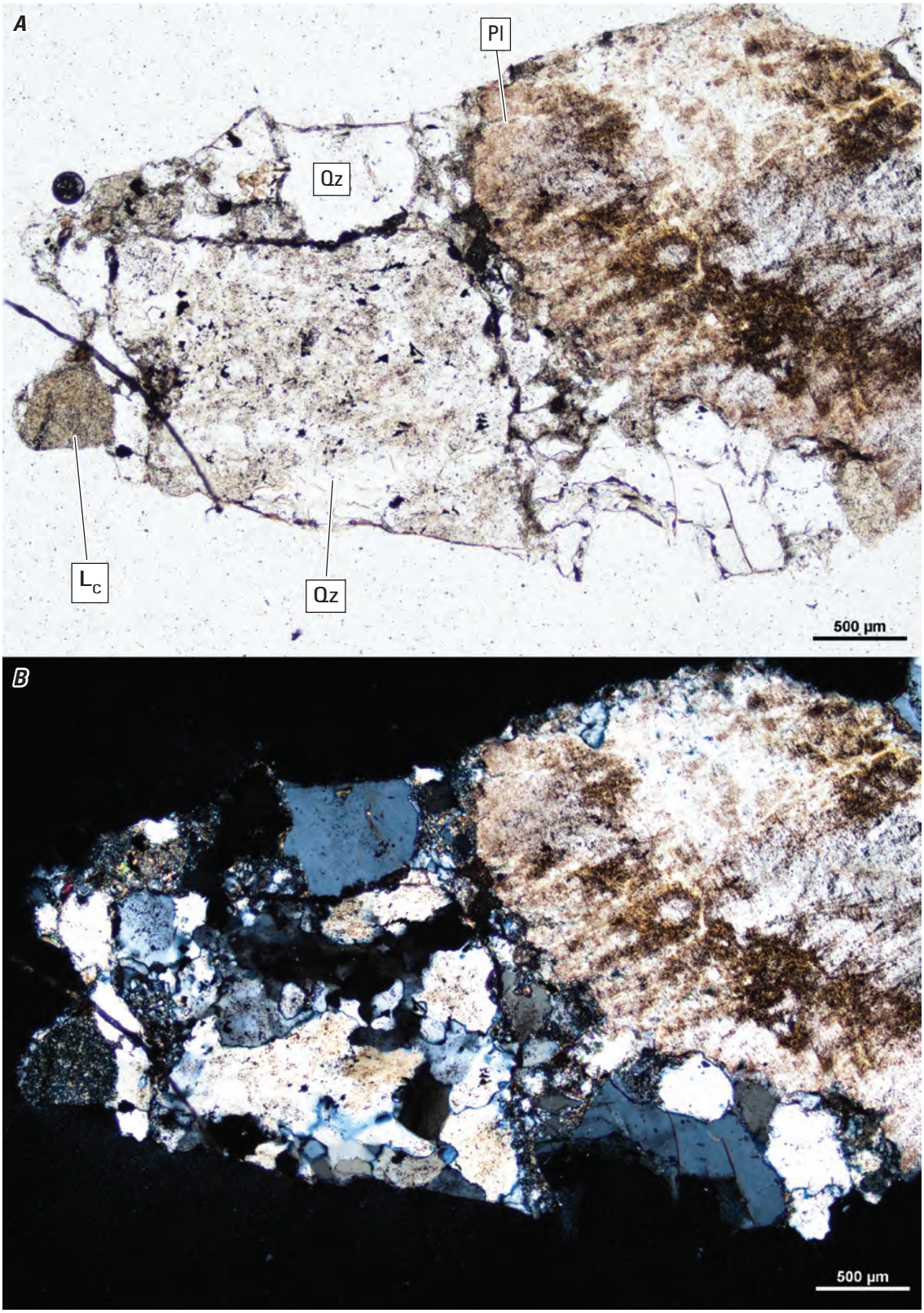

Figure 65. Pair of photomicrographs in plane-polarized light (*A*) and cross-polarized light (*B*) of a representative arkosic fragment of the Pumpkin Swamp formation from borehole W15489 from 7,570 to 7,580 feet depth. Note the strong alteration of plagioclase (Pl). Quartz (Qz) grains may have uniform or extinction (top) or have subgrains (bottom). Chert clasts (L_c) are well rounded. Term: µm, micrometer. Photomicrographs by Ryan Deasy, U.S. Geological Survey.

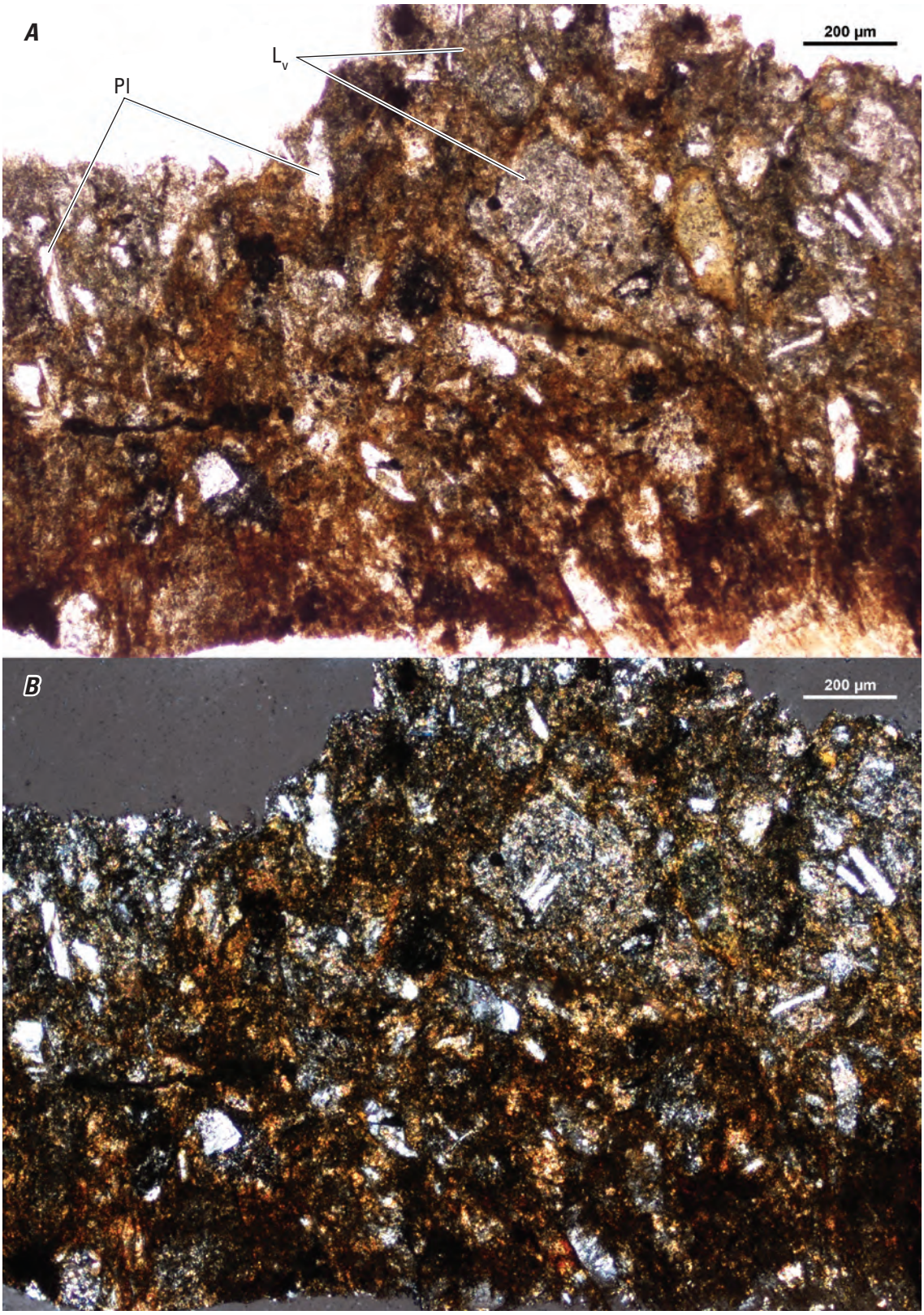

Figure 66. Pair of photomicrographs in plane-polarized light (*A*) and cross-polarized light (*B*) of a representative fragment of mafic to intermediate porphyry of the North Florida volcanic series from borehole W15489 from 9,010 to 9,040 feet depth. Plagioclase (Pl) phenocrysts are lath shaped and enclosed in a strongly altered and iron-oxide-stained matrix. Lithic clasts (L_v) are Pl-phyric volcanic bits. Term: µm, micrometer. Photomicrographs by Ryan Deasy, U.S. Geological Survey.

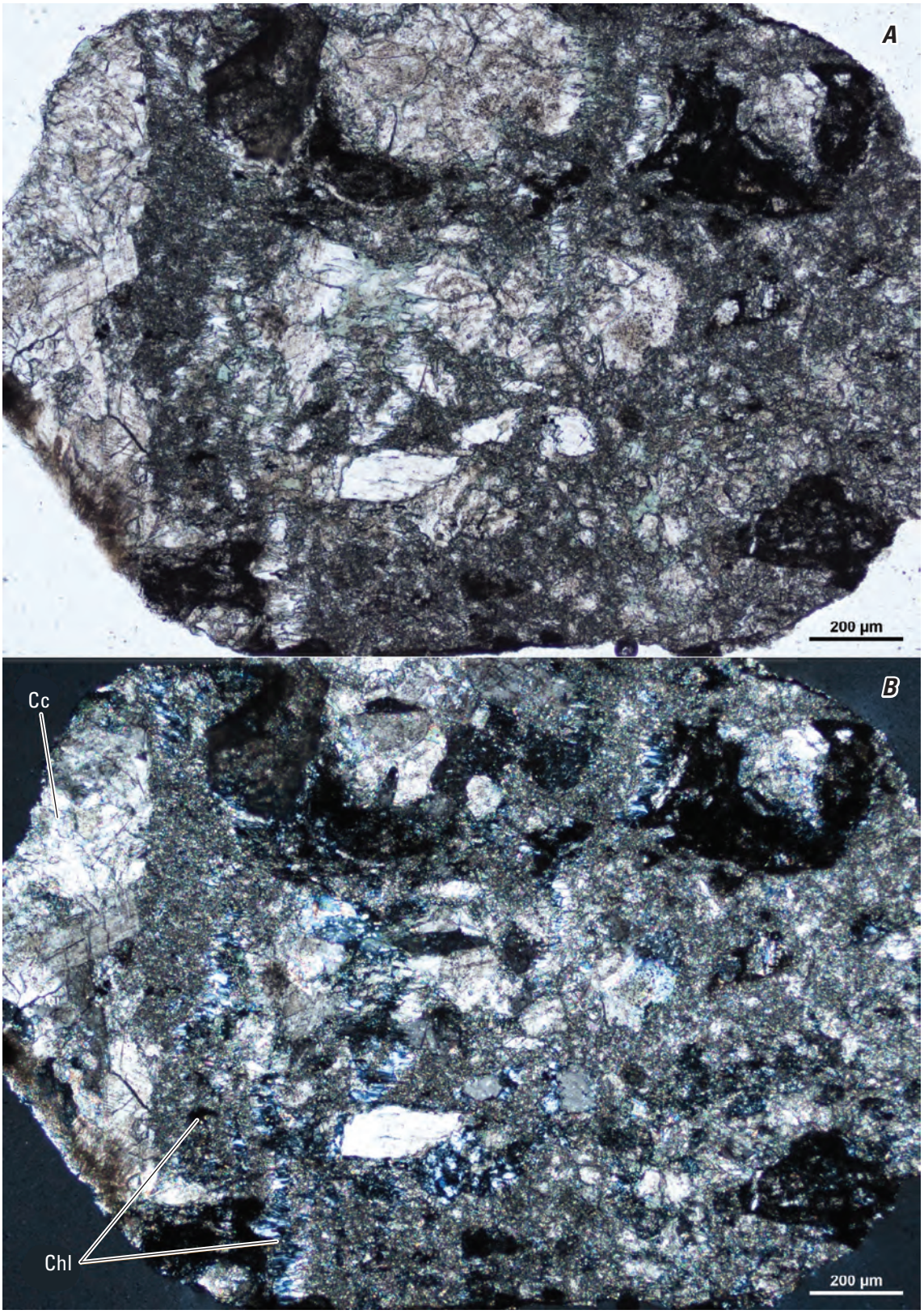

Figure 67. Pair of photomicrographs in plane-polarized light (*A*) and cross-polarized light (*B*) of a carbonate rock fragment of the North Florida volcanic series from borehole W15489 from 9,010 to 9,040 feet depth. Terms: Cc, calcite; Chl, chlorite; µm, micrometer. Photomicrographs by Ryan Deasy, U.S. Geological Survey.

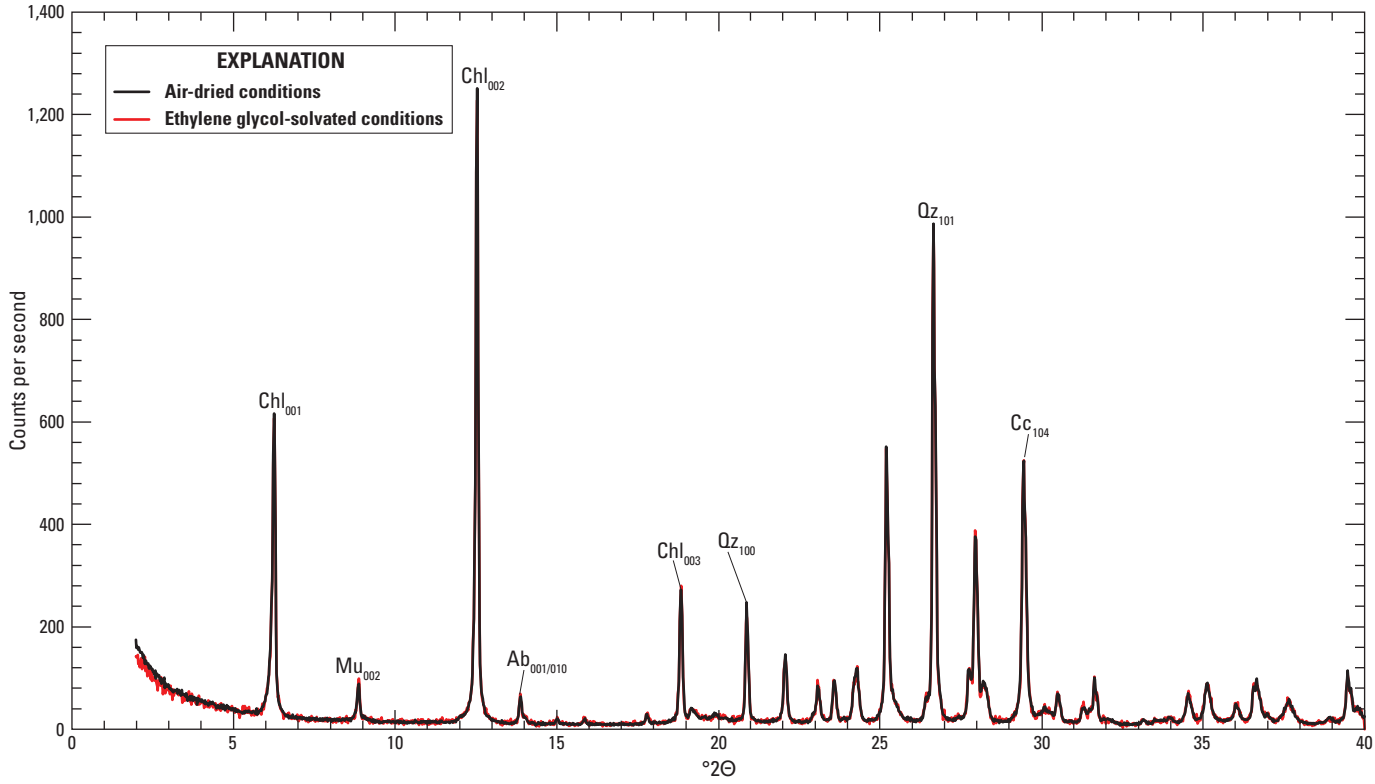

Figure 68. X-ray diffractograms of volcanic cuttings from borehole W15489 from 9,010 to 9,040 feet depth under air-dried and ethylene glycol-solvated conditions. The *y*-axis is in linear scale. Selected peaks are labeled with corresponding mineral abbreviations; numbers in subscript denote Miller indices. Terms: °2Θ, degrees two theta; Chl, chlorite; Mu, muscovite; Ab, albite; Qz, quartz; Cc, calcite.

Borehole W1838

Porphyritic rhyolite occurs in core from 3,873 to 3,892 ft depth (TD). A core chip from 3,879 to 3,885 ft depth was investigated in this study.

Previous Work

Applin (1951, p. 21) reports 19 ft of basement rock penetration of "volcanic ash and tuff" from 3,873 to 3,892 ft depth (TD). A whole-rock major element geochemical analysis of core from 3,881 ft depth returns a rhyolitic composition (Milton and Grasty, 1969). Bass (1969) presents a petrographic report of cuttings from 3,766 to 3,892 ft depth, wherein the identification of minerals and mineral compositions is supported by XRD analysis. Milton (1972) summarizes Bass (1969) and adds several photomicrographs. Two samples from 3,889 to 3,890 ft depth and from 3,890 to 3,892 ft depth are also rhyolitic (Mueller and Porch, 1983). Heatherington and others (1996) report additional whole-rock geochemical and isotopic data of samples from 3,885 to 3,892 ft depth.

Thin Section Petrography

A thin section of a core chip from 3,883 to 3,885 ft depth shows tan-gray porphyritic rhyolite tuff (fig. 69). The tuff contains dispersed subhedral to euhedral quartz and plagioclase phenocrysts up to 100 µm long and round ash lapilli up to 1 mm in diameter in a massive, fine-grained matrix. This texture is overprinted by red-orange Liesegang banding and dendritic Mn(?)-oxide stylolites(?).

Notes on XRD Methods and Results

Core chips of rhyolitic rock from 3,879 to 3,883 ft depth were prepared for XRD and geochemical analysis as follows. Contaminants were first removed by hand with tweezers under a binocular microscope. The chips were then placed in an automated Brinkman grinder fitted with an agate mortar and pestle. The sample was continuously lubricated with acetone during grinding. The sample was then further ground by hand in a corundom mortar and pestle, again lubricated with acetone, and allowed to air dry. An aliquot of the resulting fine powder was placed in the 2×2×0.1-cm cavity of a Ti "front-pack" mount and analyzed on a Bruker D8 diffractometer from 2 to 90° 2Θ at a rate of 5 sec/0.02° step. Mineral abundances (Deasy and others, 2024b) were

then determined by the Rietveld method using TOPAS (Bruker AXS, 2011). Major and trace element concentrations in the same powder were thereafter determined by XRF/ICP-MS analysis (Deasy and others, 2024a).

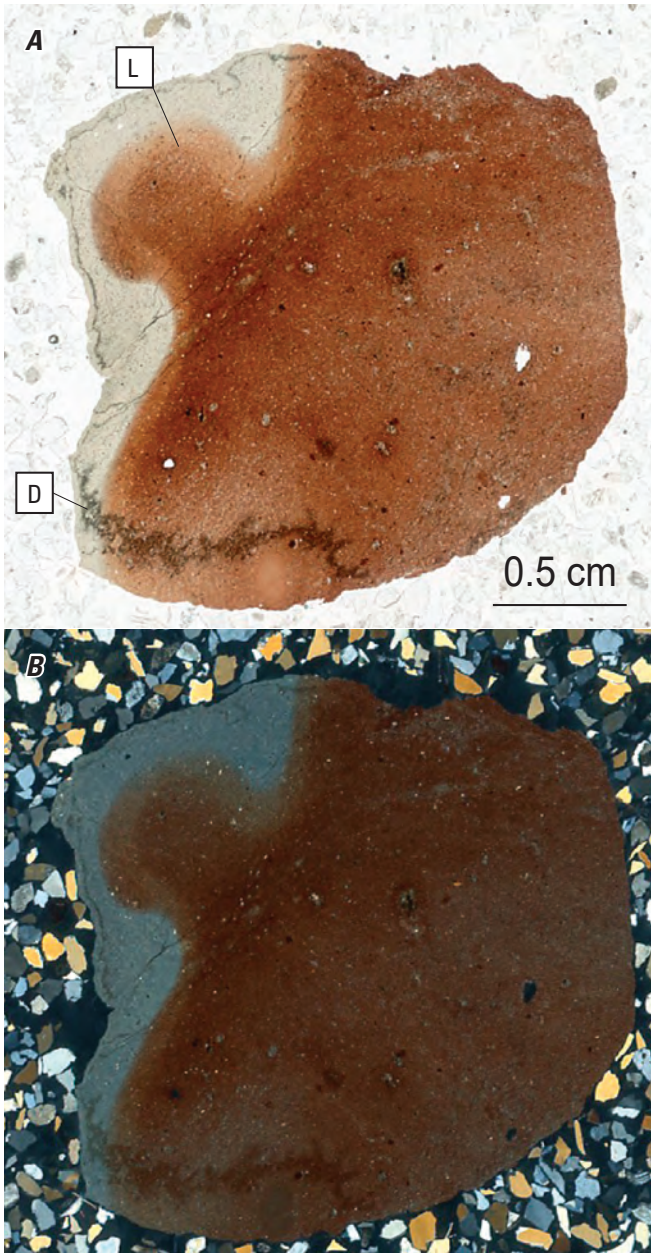

Figure 69. Pair of scanned images of a core chip from borehole W1838 from 3,883 to 3,885 feet depth in plane-polarized light (*A*) and cross-polarized light (*B*). Note dendritic manganese(?)-oxide stylolite(?) in the lower part of the fragment (D) and banded Liesegang alteration (L). Term: cm, centimeter. Photomicrographs by Ryan Deasy, U.S. Geological Survey.

Borehole W11530

Cuttings of felsic volcanic rock occur from ~4,420 to 5,050 ft depth, with intermediate volcanic rock at 5,050–5,572 ft depth. Cuttings of intermediate volcanic rock from 5,100 to 5,130; from 5,300 to 5,330; and from 5,555 to 5,570 ft depth were investigated in detail in this study.

Previous Work

Barnett (1975) mentions penetration of volcanic rock from 4,426 to 5,572 ft depth. In the ~1,150 ft of basement rock penetration, Winston (1992) distinguishes 630 ft of an upper rhyolitic lithology, including shaley beds at 4,500 and 4,570 ft depth, from an underlying 490 ft of andesite.

Cuttings Log

Summary: The contact between Cretaceous(?) limestone and basement rhyolite occurs between 4,420 and 4,440 ft depth. The first appearance of intermediate (andesitic) volcanic fragments occurs at 4,700 ft depth, and the first appearance of intermediate volcanics dominate cuttings occurs from 4,800 to 5,572 ft depth (TD). The contact between the volcanic rocks may be interleaved or reworked. Of the two basement lithologies, only the lower, andesitic unit was sampled in this study.

4,350 ft Dominantly gray micritic limestone. A plurality of white, sandy limestone with rounded quartz grains <0.5 mm in diameter. Other cuttings include very fine grained quartz arenite with calcite cement, locally stained with red-orange limonite; subangular to well-rounded, clear, white, pink, or orange quartz grains 0.5–2 mm in diameter; and muscovite flakes 0.5–3 mm across. Metal drilling fragments are a common contaminant.

4,360–4,370 ft Missing.

4,380 ft AA, with a greater proportion of angular to rounded clear to rosy quartz grains 1–3 mm in diameter.

4,390–4,410 ft Missing.

4,420 ft Subangular to well-rounded quartz sand with 1–2-mm grains more abundant here than in gray limestone.

4,430 ft AA.

4,440 ft Rhyolite. Sucrosic, white, gray, yellow-green to green, and pinkish-purplish very fine grained rhyolite. Negative HCl test. Opaque grains <0.2 mm in diameter are present within rhyolite fragments. Well-rounded, clear to yellow-orange, loose quartz grains present (as contaminant).

4,450 ft AA.

4,460 ft AA.

4,470 ft AA.

4,480 ft Rhyolite is consistently a deep red-purple hue.

4,490 ft Rhyolite is more variable in color again and varies in color within clasts. Fine-grained pyrite grains (0.1–0.2 mm) are disseminated in rhyolite.

4,500 ft AA.

4,510 ft AA.

4,540–4,550 ft AA.

4,550–4,560 ft Rhyolite is mostly a pale gray with finely disseminated opaques (magnetite, maybe others). Negative HCl test.

4,560–4,570 ft AA. First appearance of rare red rhyolite fragments.

4,570–4,580 ft Rhyolite is pale to dark gray, yellow, or pinkish. Some fragments contain rounded black mafic(?) grains 0.5–1 mm in maximum dimension, similar to those in rhyolite below.

4,580–4,590 ft Deep red rhyolite appears in abundance. Rhyolite fragments contain dark, rounded grains, rare pink to orange feldspar, and quartz. No muscovite seen. Many sucrosic quartzite clasts are apple green.

4,590–4,600 ft AA.

4,610–4,620 ft Red rhyolite. Rounded black grains (xenoliths?), 0.5–1 mm in diameter, are common within rhyolite fragments.

4,670–4,680 ft Rhyolite fragments similar to above, with greater fraction of large gray limestone (contaminant).

4,700–4,710 ft Cuttings contain rhyolitic and andesitic(?) fragments. First appearance of intermediate volcanic fragments.

4,750–4,760 ft Multicolored quartzite and red rhyolitic fragments are the most common cuttings, with minor gray and green-gray mafic/intermediate volcanic fragments.

4,800–4,810 ft Gray and gray-green mafic/intermediate volcanic fragments dominate cuttings. Cuttings are 1–2 mm in diameter. Euhedral pyrite grains <0.5 mm in diameter are common within volcanic fragments. No veins or contacts within cuttings fragments. Visible structures are limited to apple green (prehnite?) splotches in gray clasts. Contacts between green and gray areas are non-planar.

4,850–4,860 ft Unwashed. Mix of quartzite, rhyolite, and intermediate volcanic cuttings.

4,950–4,960 ft Unwashed. Dominantly green-gray andesitic fragments. Some clasts have pink splotches that may be laumontite or wairakite veins.

5,000–5,010 ft Gray andesite with apple-green (prehnite and [or] epidote?) and pink (zeolite?) splotches. Some fragments comprise small, rounded, welded tephra. Some fragments are chalky and soft (weathered to clay?); an HCl test on these fragments is negative. Minor contaminants include loose, rounded quartz grains; multicolored chert; gray limestone; and a few deep red rhyolitic fragments.

5,100–5,110 ft Unwashed. Gray andesite with epidote veins and pink zeolite(?). A few clasts are welded tephra.

5,110–5,120 ft Unwashed.

5,150–5,160 ft Intermediate volcanic fragments including welded tephra, chalky white altered bits, and gray fragments with pink and apple-green splotches. Rare fragments contain a banding of lighter and darker gray layers ~0.1 mm thick, although it is unclear what defines the layering.

5,200–5,210 ft Unwashed (or incompletely washed; the cuttings are very dusty). Higher proportion of rounded quartz, limestone, and other contaminants than 5,000–5,010 ft or 5,100–5,160 ft. Andesitic fragments are as found in 5,000–5,010 ft, with less pink and green alteration and more chalky white alteration.

Washed. Volcanic fragments (1–2 mm in maximum dimension) come in a variety of textures. Welded tuff fragments have lapilli 0.1–0.2 mm in diameter; lapilli are round, spherical to ellipsoidal (flattened?), translucent to green to gray to black. These grains are mostly free of carbonate; some grains react weakly with HCl. Many fragments are massive, aphanitic, and sucrosic; these may be pieces of larger lapilli. Chalky white fragments tend to be platy, contain green and translucent grains (epidote and quartz, respectively?) in a very fine grained, soft white matrix (kaolinite?), are commonly stained with dendritic oxides, and contain minor calcite (weakly positive HCl test). The least common volcanic fragments are banded with lighter and darker green-gray layers.

Uncommon chalky white calcitic fragments with euhedral yellow fluorite 0.05–0.1-mm in diameter in this interval may be alteration seams or may be contaminants. These calcitic fragments are not to be confused with the chalky, weathered volcanic fragments, which are not very calcitic, have no fluorite, and contain abundant quartz and epidote.

5,260–5,270 ft Cuttings are mostly welded lapilli and massive andesitic fragments. Relatively few chalky, weathered fragments relative above. A vein with euhedral pyrite is observed in one fragment. Epidote and epidote-quartz vein fragments are more abundant than in 5,200–5,210 ft.

5,300–5,310 ft Unwashed (or incompletely washed; the cuttings are dusty). Relatively uniformly gray andesite with few smaller pink domains. Very few green fragments relative to above interval.

5,310–5,320 ft Washed. AA. Welded tuff is less common than massive sucrosic fragments. Veins, where identifiable, are zoned with translucent quartz cores and epidote walls. Some contain pink cores (zeolite?).

5,360–5,370 ft AA. Most fragments are massive and uniformly green-gray in color. Lapilli are not distinguishable in most fragments; lapilli may simply be larger than cuttings. Sharp contacts between light and dark gray domains are present in some fragments.

5,400–5,410 ft AA.

5,450–5,460 ft AA.

5,490–5,500 ft Fragments of lapilli tuff are more common than above. Chalky, weathered fragments tend to be rounded and smaller than the other volcanic grains. Sucrosic fragments are paler than welded fragments and commonly contain euhedral pyrite. Some fragments are from veins, with sharp contacts between pink zeolite(?), white-to-gray quartz, and green epidote domains. The smallest veins have submillimeter thicknesses; many cuttings are completely composed of vein material, so the upper limit of vein aperture is unconstrained. Where zoned from core to rim, veins are pink, then white, then green.

5,525–5,530 ft AA.

5,555–5,560 ft There is an abundance of polycrystalline epidote fragments and other vein material here. There is the same variety of volcanic textures AA, with the addition of granofelsic actinolite-rich fragments. Epidote+pyrite vein fragments are present.

5,565–5,570 ft AA, with a lower abundance of vein fragments.

Thin Section Petrography

5,100–5,130 ft Most volcanic fragments comprise diverse angular to well-rounded tephra, 0.1–1 mm in maximum dimension, including porphyritic clasts; massive and foliated ash lapilli; round symplectic oxides; and monocrystalline grains of quartz, epidote, and feldspar (figs. 70 and 71). Vugs are filled with chlorite and opaque minerals. Some fragments are finer grained and more uniform in texture, with a weak to strong foliation defined by the shape-preferred orientation of inequant quartz and feldspar grains (fig. 72); discontinuous lenses of fine-grained, secondary opaque minerals commonly decorate the foliation. Coarser grained (tens of micrometers) euhedral opaque minerals (mostly pyrite) follow crosscutting epidote veins (fig. 72). Sharp contacts with respect to tephra size (fig. 73) may be interpreted as bedding contacts in a reworked volcanoclastic sediment. The frequency of subangular to rounded detrital quartz grains among mafic to intermediate (and frequently cryptocrystalline) tephra also supports a partially sedimentary origin of the rock. Additionally, given the small size of cuttings fragments, the possibility for gradational contacts at scales >5 mm cannot be excluded. However, there is no evidence in the cuttings or geophysical log for shaley layers in the andesite as are found in the rhyolite (Winston, 1992), and the presence of fine-grained, foliated lapilli within other fragments (figs. 70 and 71) allows that the fine-grained fragments may simply be pieces of larger tephra, that is, that fine-grained strata are absent in the andesite.

5,300–5,330 ft Fragments are similar to those from 5,100 to 5,130 ft, with a greater proportion of vein material. Volcanic fragments contain diverse tephra, AA, including porphyritic clasts, ash lapilli, and broken quartz grains in a chloritic cement (figs. 74–76). Some fragments preserve sharp contacts between coarse- and fine-grained layers (figs. 75 and 76). A small porphyritic intrusion occurs in one fragment (fig. 77). Veins may be as thin as a few micrometers. Some cuttings are entirely composed of vein material; the upper limit of vein aperture is thus unconstrained. Vein minerals include zeolite, quartz, chlorite, epidote, calcite, and pyrite. Many of the larger vein fragments are mineralogically zoned (fig. 78), whereas others are not (fig. 79).

The occurrences of minerals in the intervals 5,100–5,130 ft and 5,300–5,330 ft are the same. Plagioclase occurs as euhedral laths within porphyritic lapilli and also as detrital grains (figs. 70, 71, 73). Quartz is common as detrital clasts and within tephra, for example, intergrown with plagioclase (fig. 71). Detrital quartz clasts are commonly rounded

with broken edges, and many are brecciated in situ (fig. 70). Chlorite is a common cement, filling interstices between lapilli (figs. 70, 72, 73), where it is green and pleochroic in PPL and has anomalous blue interference colors in XPL. Chlorite is also present as round, fine-grained knots interpreted as authigenic replacement of mafic detritus (figs. 70 and 73) and as vermicular growths in veins (fig. 80). Epidote occurs as fine-grained alteration of plagioclase (possibly authigenic); as cement with chlorite; and in veins with or without quartz, chlorite, calcite, pyrite, and fluorite (figs. 70 and 71). Some epidote may be detrital. Apatite is common, forming subhedral to euhedral crystals up to 0.1 mm in length, and is commonly brecciated (fig. 81). Clusters of ~10-µm euhedral allanite grains are present in some fragments. Chalcopyrite occurs in most fragments as <10-µm grains, but 50-µm grains are present in one fragment. Chromite is rare but found in several fragments as anhedral to subhedral detrital grains ~10 µm in maximum dimension. Pyrite is uncommon, euhedral, and strongly associated with epidote veins (fig. 71) and alteration seams. Titanite and rutile are commonly intergrown in round, symplectic grains (fig. 81). Zeolite in veins is commonly turbid and reddish to brown (figs. 79 and 80). Trace amounts of the following minerals were identified by EDS, in decreasing order of abundance: ilmenite, rare-earth-element (REE)-fluor-carbonate (bastnaesite?), zircon, molybdenite, and Pb-telluride (altaite?).

5,555–5,570 ft Textures of fragments are similar to those above, with an even greater abundance of vein fragments, especially epidote- and K-feldspar-bearing veins, and the addition of diabase fragments (fig. 82). The latter may represent late intrusions similar to the smaller one observed above (fig. 77). Overprint by chlorite and epidote, and the presence of quartz-epidote-chlorite and chlorite-tremolite veins (fig. 83), show that the diabase and surrounding volcanic/volcaniclastic rock were metamorphosed together. In addition to the many vein fragments, brittle deformation is demonstrated by faulting in some fragments (fig. 84).

Notes on XRD Methods and Results

Petrographic evidence shows complex textures, mixed tephra, and detrital quartz grains at the millimeter scale (that is, within individual cuttings fragments) such that each fragment potentially contains multiple unrelated magmatic and sedimentary provenances. Moreover, cuttings from any interval are susceptible to contamination from overlying rocks and anthropogenic sources. Therefore, no combination of cuttings fragments can be said unequivocally to belong to a single stratum, let alone a single eruption. These factors complicate efforts to obtain a representative sampling of the volcanic rock(s) present in this borehole. Therefore, redundant fractions of basement rock from multiple depths were separated for geochemical and mineralogical analyses to test for compositional variability and control for possible contamination.

Volcanic fragments were separated from sedimentary fragments and other contaminating cuttings by hand under a binocular microscope. Subsamples of volcanic cuttings weighing 0.6–1.0 g each were separated from each of the following depth intervals:

5,100–5,110 ft

5,110–5,120 ft

5,120–5,130 ft

5,300–5,310 ft

5,310–5,320 ft

5,320–5,330 ft

5,555–5,560 ft

5,560–5,565 ft

5,565–5,570 ft

Each subsample was ground by hand in an agate mortar and pestle while being continuously lubricated with acetone during grinding. The mortar and pestle were thoroughly cleaned between subsamples. The resulting fine powders were allowed to air dry. The powders were placed in the 2-cm-wide cavities of circular “back-pack” mounts and scanned in a Panalytical X’Pert diffractometer with a Cu anode from an angular range of 3–90° 2Θ. Semiquantitative mineral abundances (Deasy and others, 2024b) were obtained by Rietveld refinement modeling in HighScore Plus (Malvern Panalytical, 2018). Major and trace element geochemical analyses of six of these powders were obtained by INAA/ICP-OES/ICP-MS by Activation Laboratories, Inc. (Deasy and others, 2024a).

Additionally, larger, ~5-g fractions of volcanic rock for XRF/ICP-MS analyses were attained from the following intervals by combining hand-picked cuttings from the interceding 10-ft intervals:

5,100–5,130 ft

5,300–5,330 ft

5,555–5,570 ft

These fractions were placed in an automated Brinkman grinder fitted with an agate mortar and pestle. The samples were continuously lubricated with acetone during grinding. The resulting coarse powders were further ground by hand in a corundum mortar and pestle, again lubricated with acetone, and allowed to air dry. Aliquots of powder were mounted in Ti “front-pack” mounts and analyzed on a Bruker D8 diffractometer from an angular range of 2–100° 2Θ with a Cu anode and point detector. Semiquantitative mineral abundances (Deasy and others, 2024b) were determined by Rietveld modeling in TOPAS (Bruker AXS, 2011). The major and trace element geochemistry of these powders was then determined by XRF/ICP-MS by Activation Laboratories, Inc. (Deasy and others, 2024a).

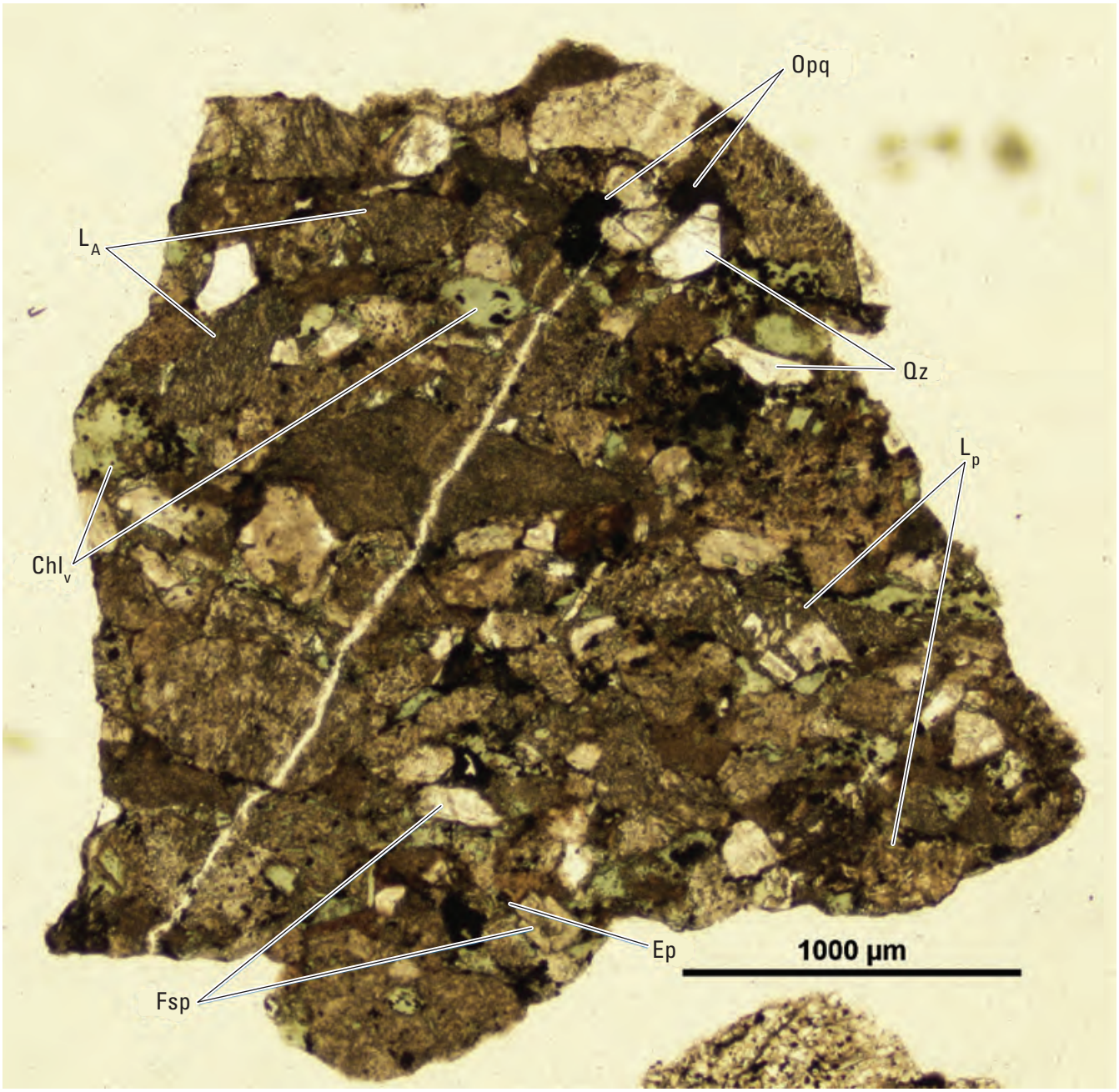

Figure 70. Photomicrograph in plane-polarized light of a representative fragment of welded tuff from borehole W11530 from 5,110 to 5,120 feet depth. The thin vein that cuts across the fragment is filled with quartz. Terms: Opq, opaque mineral; Qz, quartz; L_A, ash lapilli; L_P, porphyritic lithic clast; Chl_V, chlorite-filled vug; Fsp, feldspar; Ep, epidote; µm, micrometer. Photomicrograph by Ryan Deasy, U.S. Geological Survey.

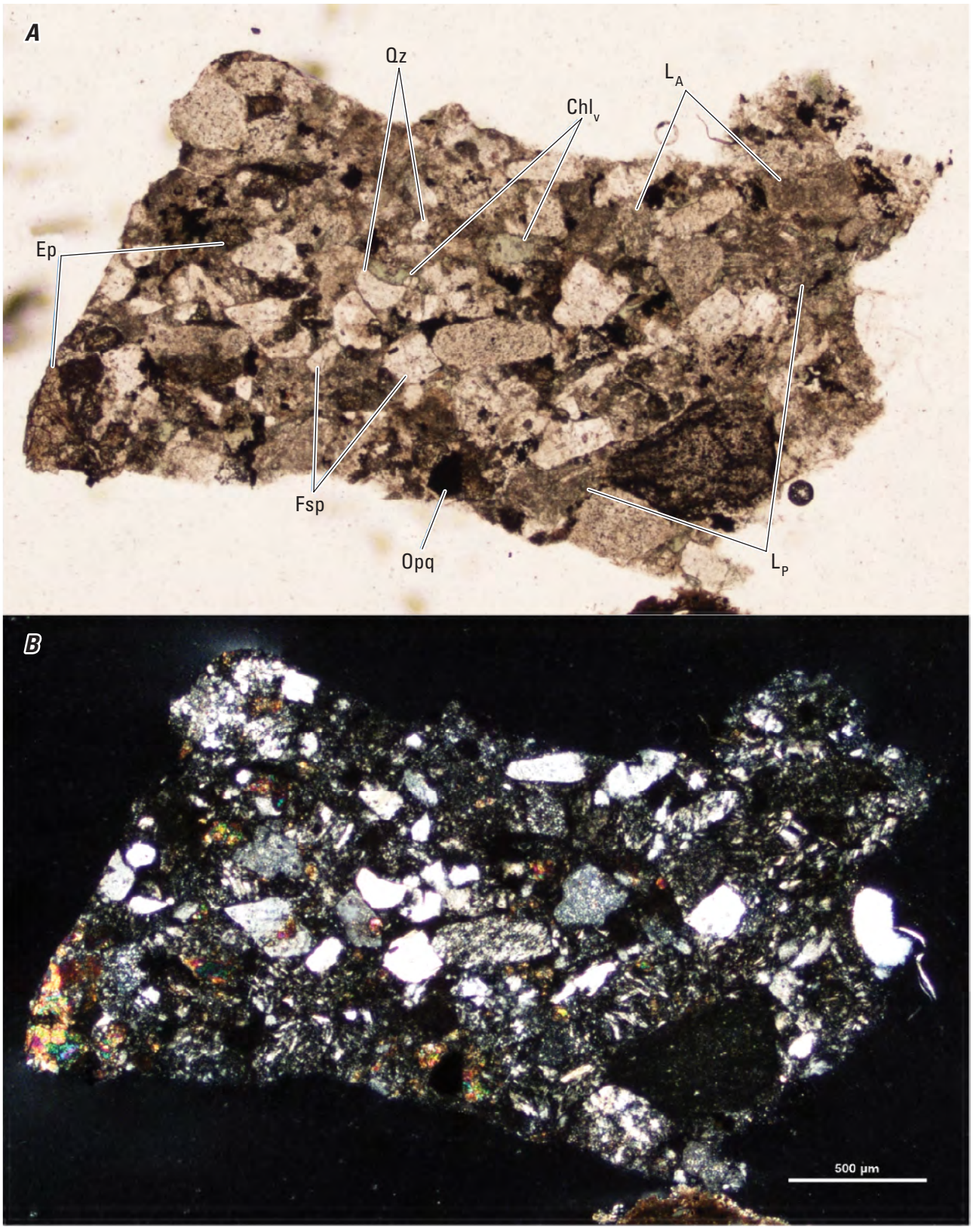

Figure 71. Pair of photomicrographs of a representative fragment of volcanic or volcaniclastic rock from borehole W11530 from 5,120 to 5,130 feet depth in plane-polarized light (*A*) and cross-polarized light (*B*). Terms: Qz, quartz; Chl_V, chlorite-filled vug; L_A, ash lapilli; Ep, epidote; Fsp, feldspar; Opq, opaque mineral; L_P, porphyritic lithic clast; µm, micrometer. Photomicrographs by Ryan Deasy, U.S. Geological Survey.

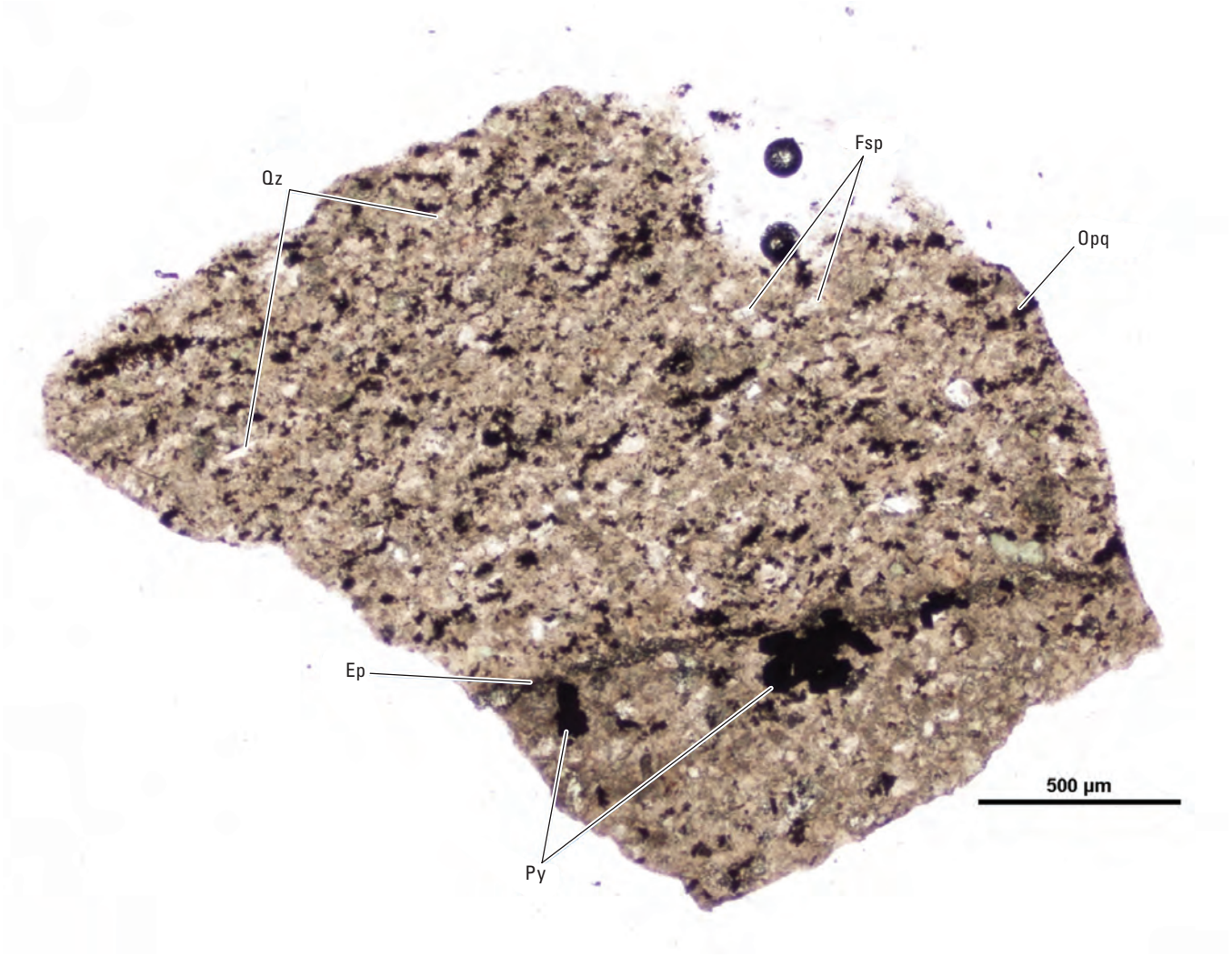

Figure 72. Photomicrograph in plane-polarized light of a representative fragment of volcanic rock from borehole W11530 from 5,110 to 5,120 feet depth. Terms: Qz, quartz; Fsp, feldspar; Opq, opaque mineral; Ep, epidote (vein); Py, pyrite; µm, micrometer. Photomicrograph by Ryan Deasy, U.S. Geological Survey.

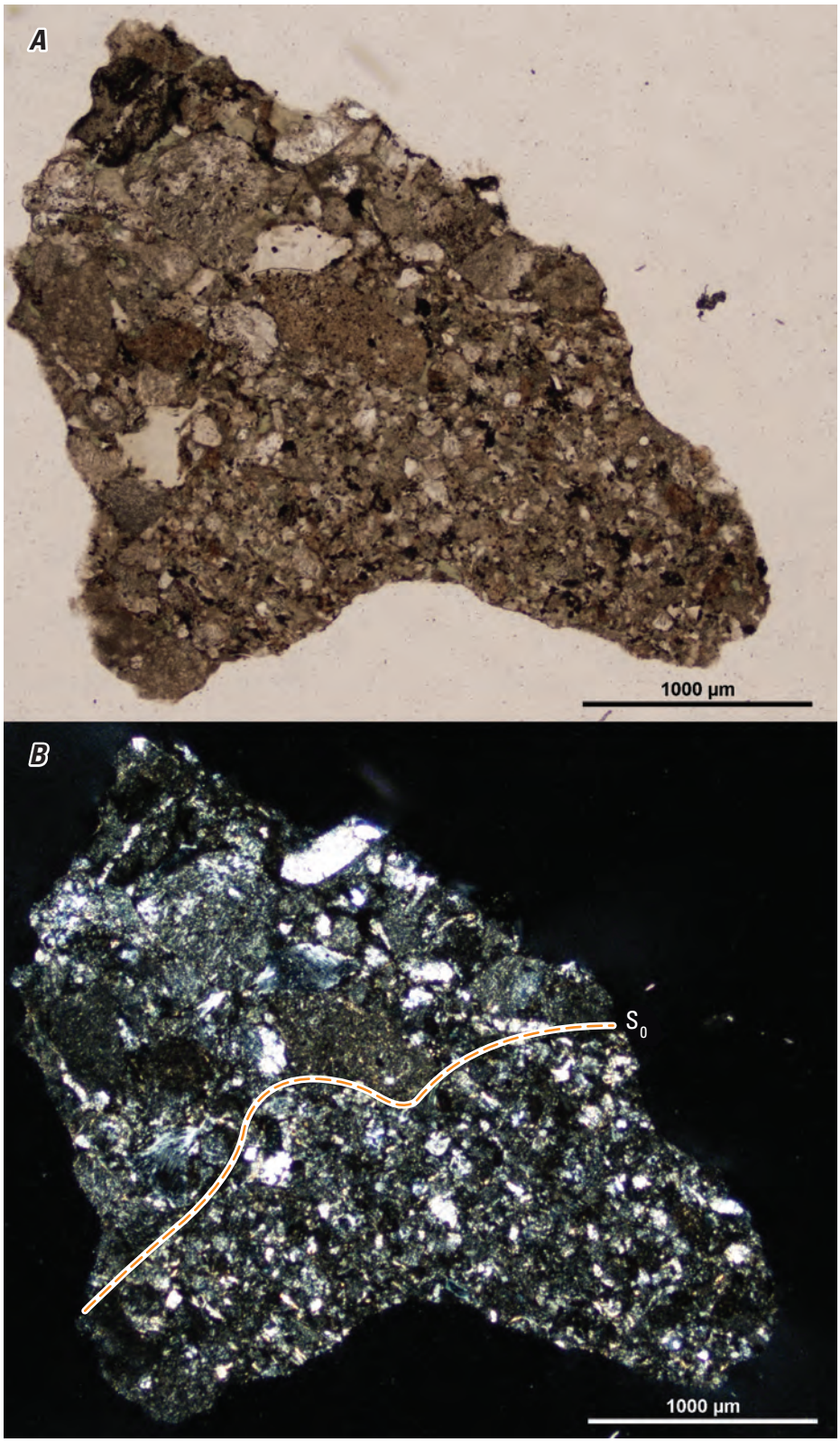

Figure 73. Pair of photomicrographs of a representative fragment from borehole W11530 from 5,120 to 5,130 feet depth in plane-polarized light (*A*) and cross-polarized light (*B*). A sharp contact with respect to tephra size (coarser above, finer below) is interpreted as a bedding contact (S_0, dashed orange line) in a reworked volcaniclastic deposit. Term: µm, micrometer. Photomicrographs by Ryan Deasy, U.S. Geological Survey.

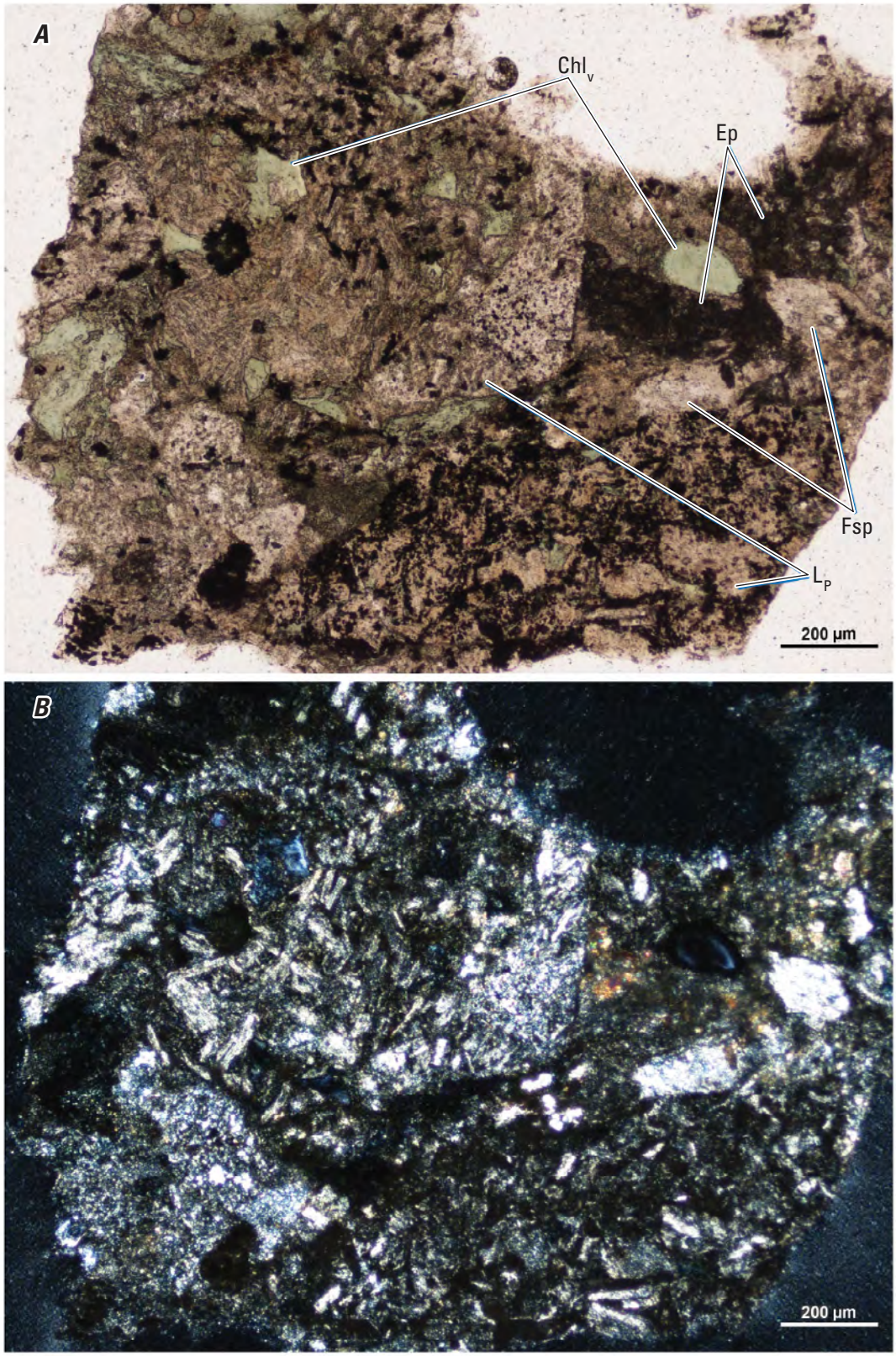

Figure 74. Pair of photomicrographs of a representative fragment from borehole W11530 from 5,310 to 5,320 feet depth in plane-polarized light (*A*) and cross-polarized light (*B*). Terms: Chl_V, chlorite-filled vug; Ep, epidote; L_P, porphyritic lithic clast; Fsp, feldspar; µm, micrometer. Photomicrographs by Ryan Deasy, U.S. Geological Survey.

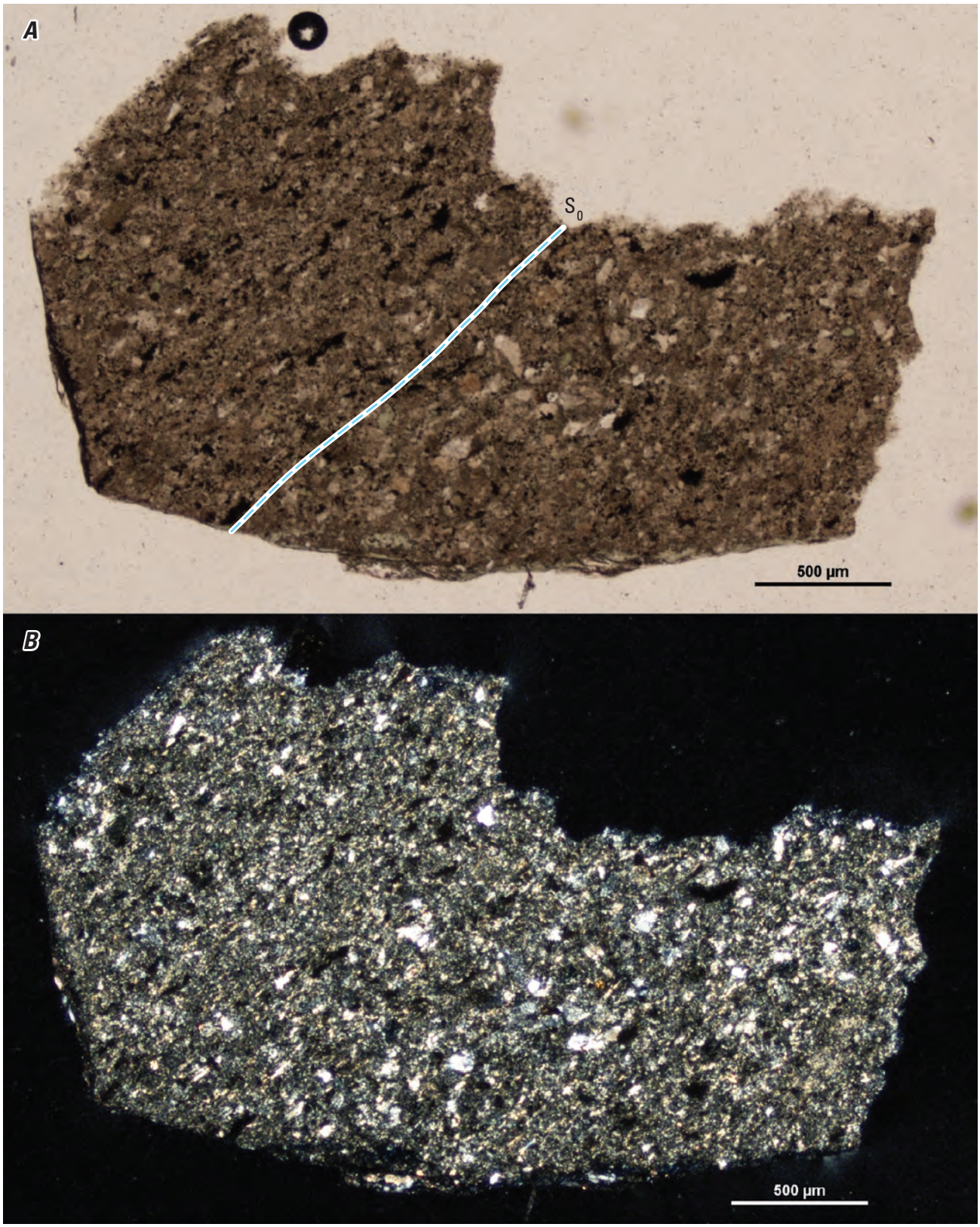

Figure 75. Pair of photomicrographs of a volcanic fragment from borehole W11530 from 5,300 to 5,310 feet depth in plane-polarized light (*A*) and cross-polarized light (*B*). A sharp contact with respect to tephra size (S_0, dashed blue line) is interpreted as a bedding contact. Term: µm, micrometer. Photomicrographs by Ryan Deasy, U.S. Geological Survey.

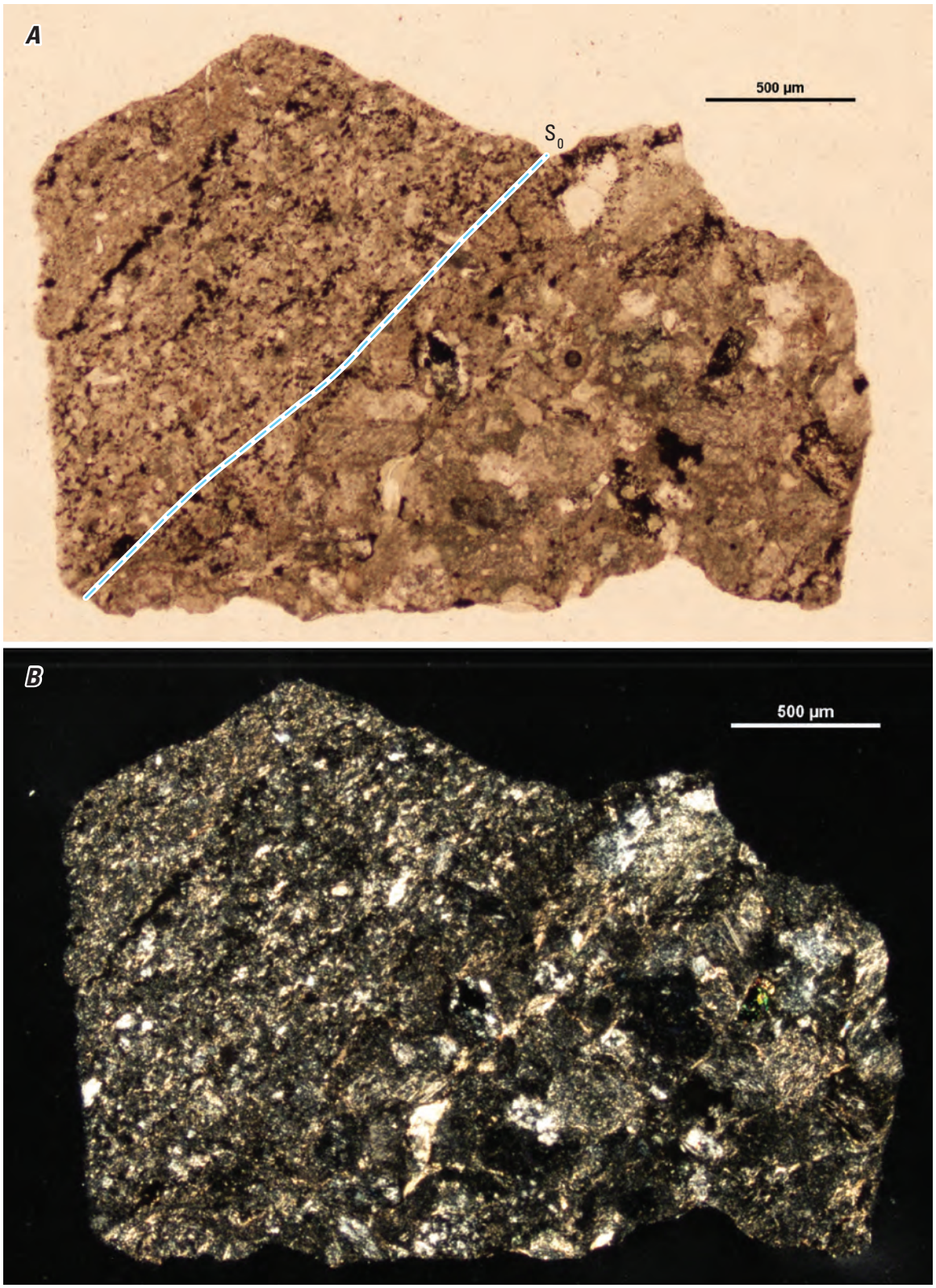

Figure 76. Pair of photomicrographs of a volcanic fragment from borehole W11530 from 5,310 to 5,320 feet depth in plane-polarized light (*A*) and cross-polarized light (*B*). A sharp contact with respect to tephra size (S_0, dashed blue line) is interpreted as a bedding contact. Term: µm, micrometer. Photomicrographs by Ryan Deasy, U.S. Geological Survey.

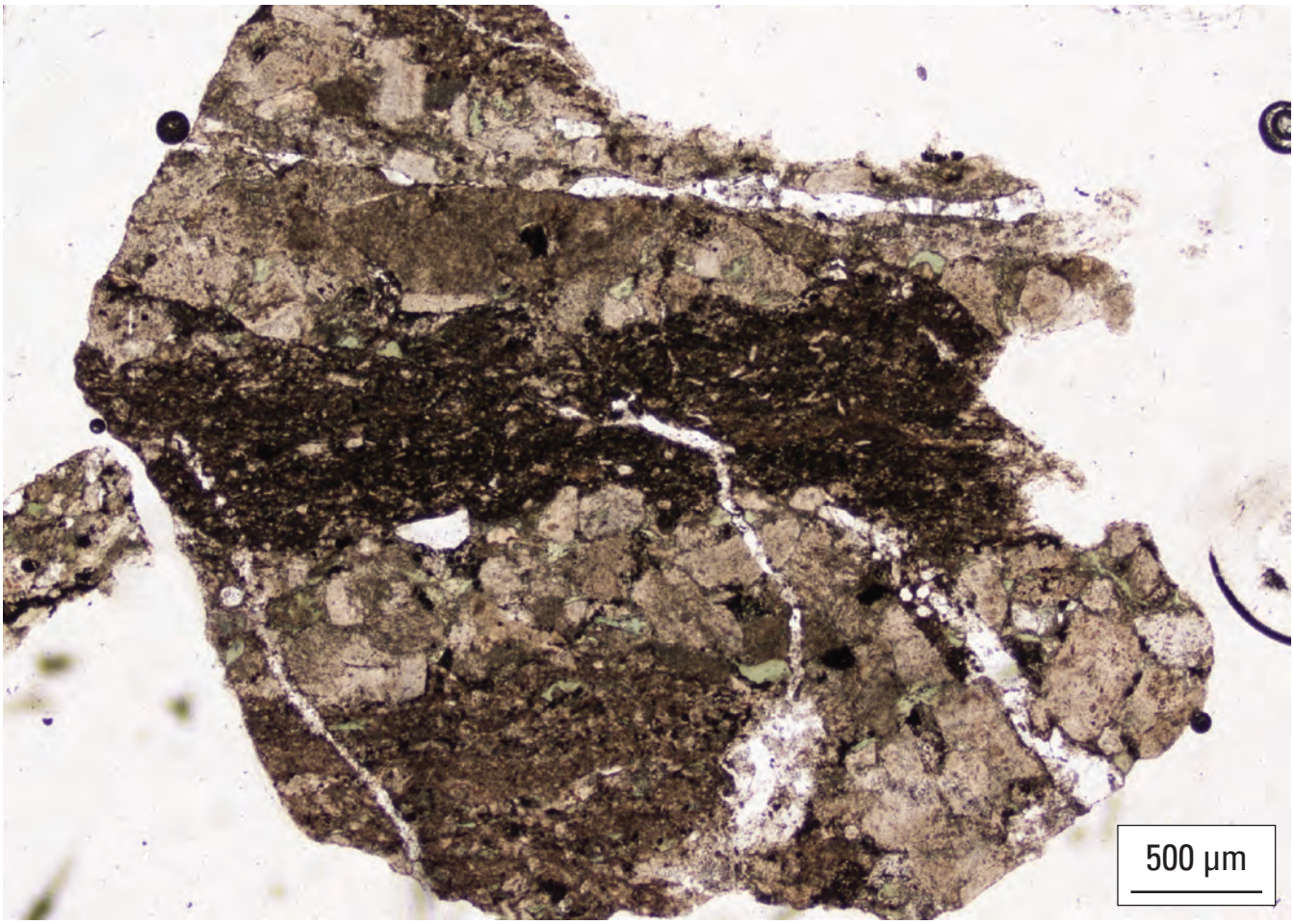

Figure 77. Photomicrograph in plane-polarized light of a volcanic fragment from borehole W11530 from 5,310 to 5,320 feet depth. A small porphyritic dike that crosscuts the fragment is approximately horizontal in this view. Term: µm, micrometer. Photomicrograph by Ryan Deasy, U.S. Geological Survey.

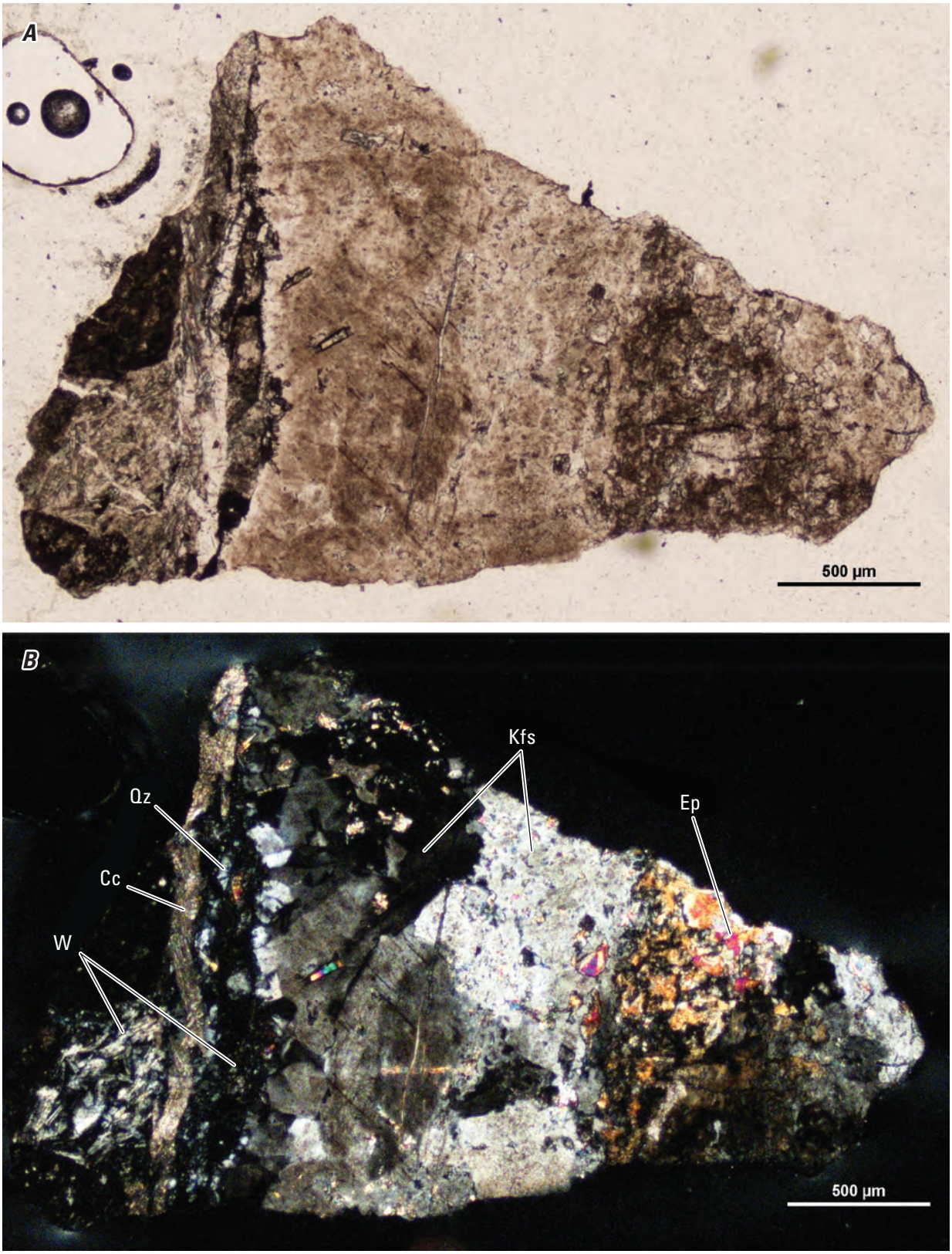

Figure 78. Pair of photomicrographs of a vein fragment from borehole W11530 from 5,310 to 5,320 feet depth in plane-polarized light (*A*) and cross-polarized light (*B*). Terms: W, wall rock; Cc, calcite; Qz, quartz; Kfs, potassium feldspar; Ep, epidote; µm, micrometer. Photomicrographs by Ryan Deasy, U.S. Geological Survey.

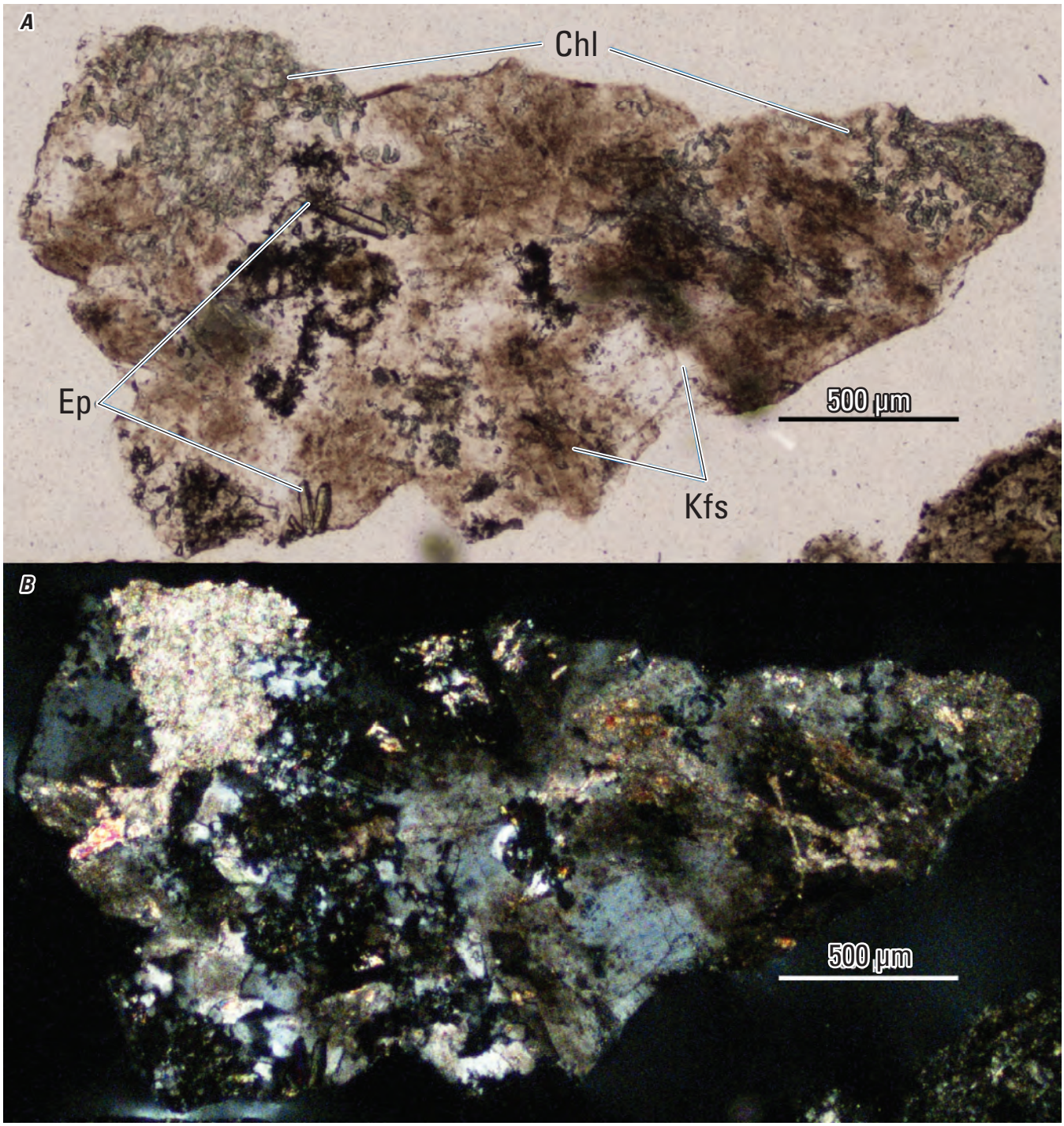

Figure 79. Pair of photomicrographs of a vein fragment from borehole W11530 from 5,300 to 5,310 feet depth in plane-polarized light (*A*) and cross-polarized light (*B*). Terms: Chl, chlorite; Ep, epidote; Kfs, potassium feldspar; µm, micrometer. Photomicrographs by Ryan Deasy, U.S. Geological Survey.

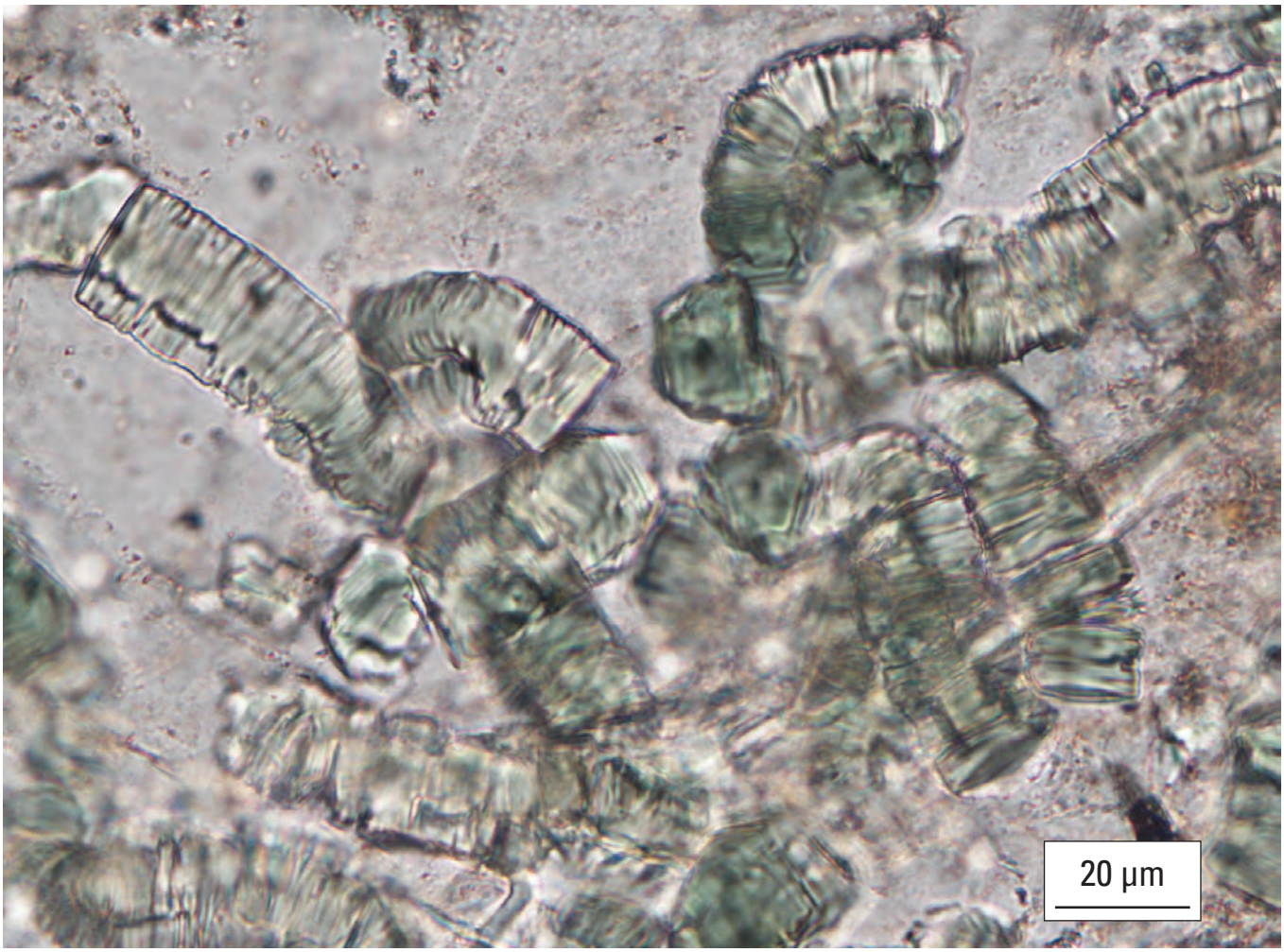

Figure 80. Photomicrograph in plane-polarized light of a vein fragment from borehole W11530 from 5,300 to 5,310 feet depth containing vermicular chlorite within potassium feldspar. Term: µm, micrometer. Photomicrograph by Ryan Deasy, U.S. Geological Survey.

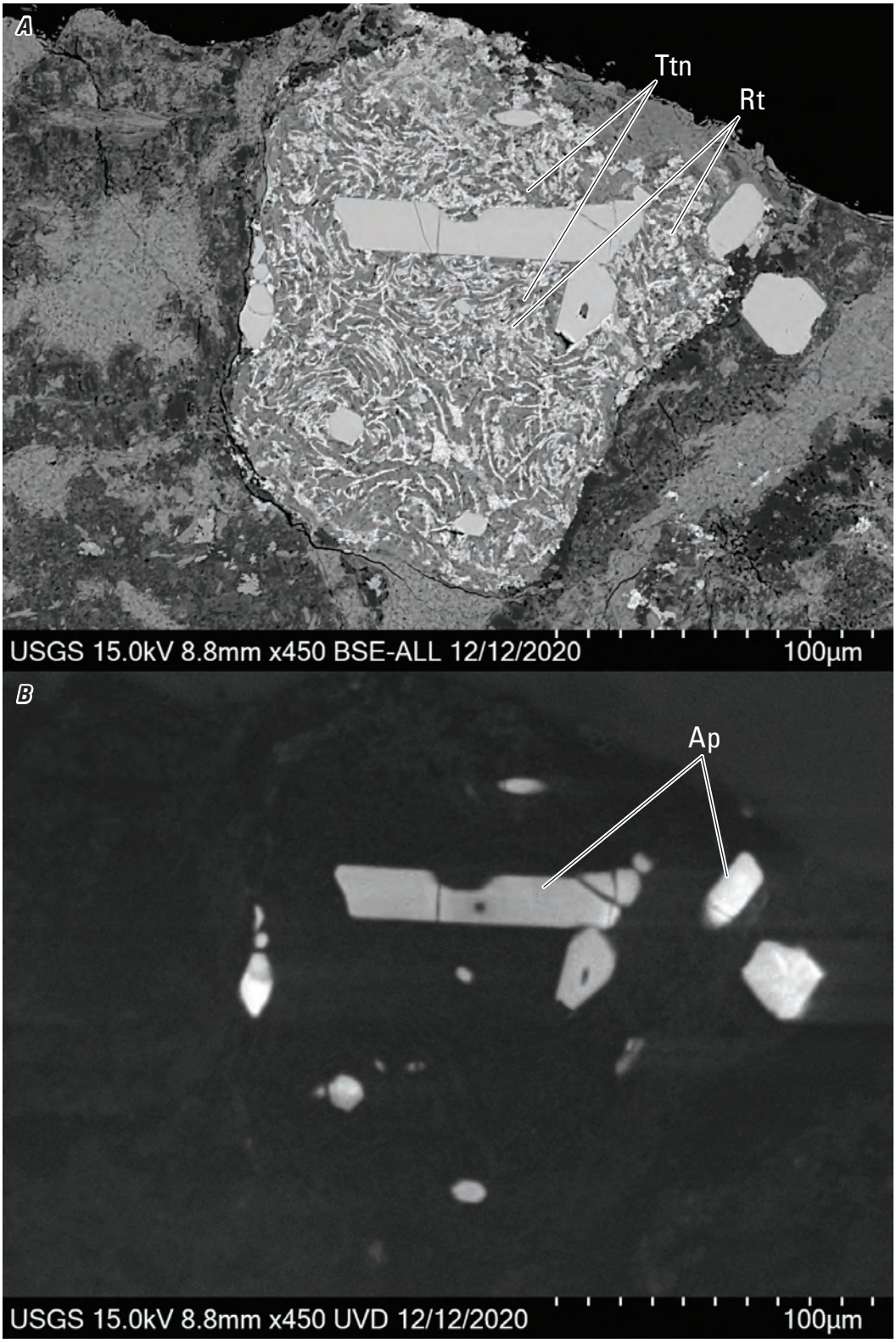

Figure 81. Pair of images in back-scattered electron (BSE) (*A*) and cathodoluminescence (*B*) of apatite (Ap) with intergrowths of titanite (Ttn, dark) and rutile (Rt, bright) in a volcanic fragment from borehole W11530 from 5,300 to 5,310 feet depth. Text in the bottom left of each image identifies data source (USGS); operating conditions including beam potential in kilovolts (15.0 kV), working distance in millimeters (8.8 mm), and image magnification in multiples of actual size (450 times); and date of acquisition (12/12/2020). Terms: Ttn, titanite; Rt, rutile; USGS, U.S. Geological Survey; kV, kilovolt; mm, millimeter; BSE-ALL, back-scattered electron, all energies; µm, micrometer; UVD; ultra variable-pressure detector. Photomicrographs by Ryan Deasy, U.S. Geological Survey.

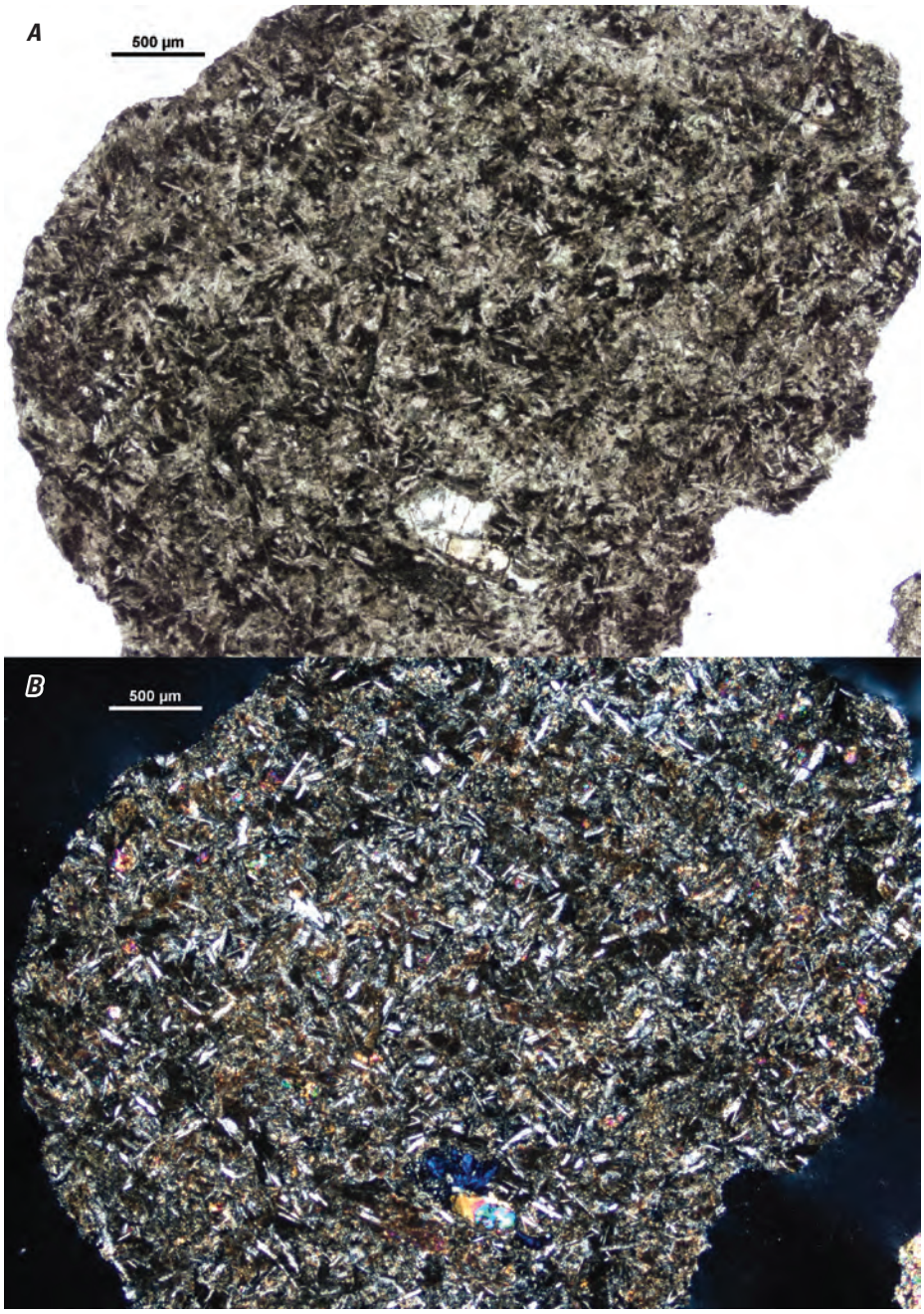

Figure 82. Pair of photomicrographs in plane-polarized light (*A*) and cross-polarized light (*B*) of a diabase fragment from borehole W11530 from 5,555 to 5,570 feet depth. Term: µm, micrometer. Photomicrographs by Ryan Deasy, U.S. Geological Survey.

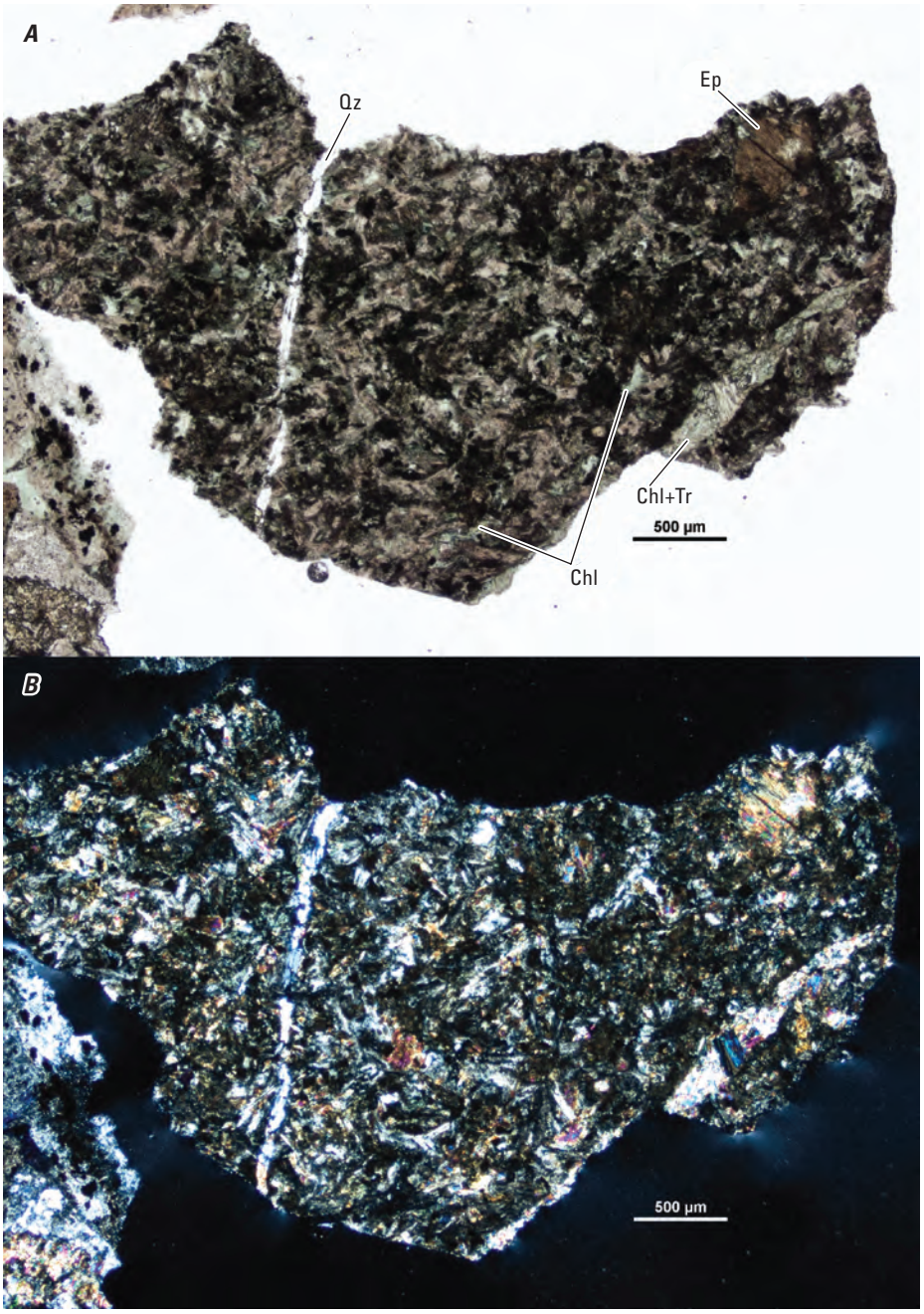

Figure 83. Pair of photomicrographs in plane-polarized light (*A*) and cross-polarized light (*B*) of a volcanic fragment from borehole W11530 from 5,555 to 5,570 feet depth.
Terms: Qz, quartz; Ep, epidote; Chl, chlorite; Tr, tremolite; µm, micrometer.
Photomicrographs by Ryan Deasy, U.S. Geological Survey.

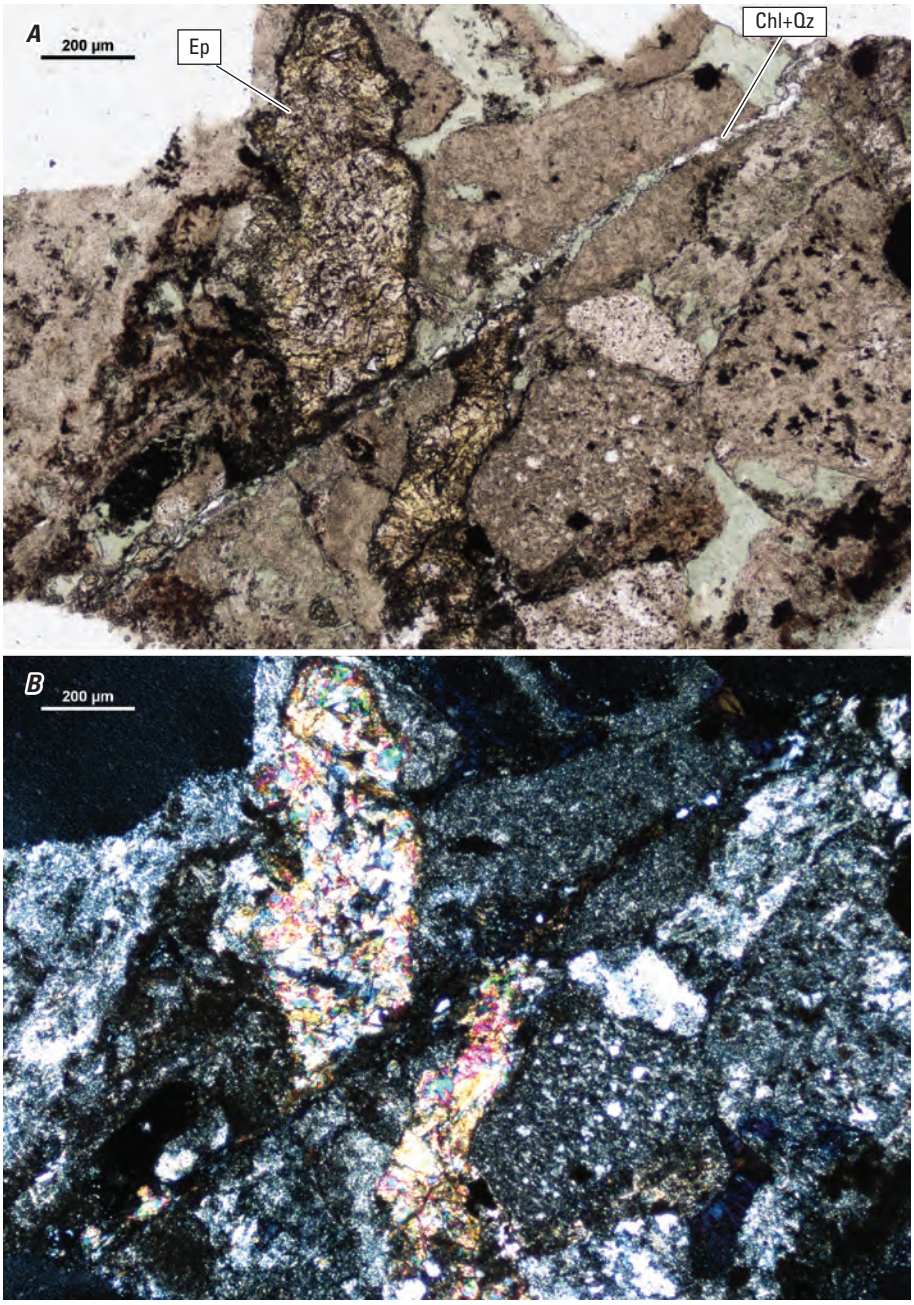

Figure 84. Pair of photomicrographs of a volcanic fragment from borehole W11530 from 5,555 to 5,570 feet depth in plane-polarized light (*A*) and cross-polarized light (*B*). An epidote (Ep) vein is sinistrally displaced across a fault marked by chlorite and quartz (Chl+Qz). Term: µm, micrometer. Photomicrographs by Ryan Deasy, U.S. Geological Survey.

Borehole W1473

Basement rock encountered in this borehole is a volcanic agglomerate of rhyolitic and mafic clasts from 4,588 to 4,644 ft depth.

Previous Work

Applin (1951, p. 21) reports 44 ft of penetration of "tuff and volcanic agglomerate of rhyolitic composition" beginning at 4,588 ft depth and quotes F.F. Grout's remarks, "Mixed tuff derived from an igneous complex. Origin, sedimentary or explosive igneous action." Milton (1972) contributes downhole core descriptions from 4,560 to 4,575 ft depth of white to buff to red, friable to indurated sandstone and from 4,601 to 4,632 ft depth of metamorphosed volcanic agglomerate containing rhyolitic and basaltic clasts, as well as detrital quartz and devitrified glass. Alteration products include epidote, chlorite, and amphibole; veins are filled with zeolite(s) and calcite. Heatherington and others (1996) provide whole-rock geochemical analyses and isotopic data for "rhyolitic breccia" (n=1) and "epidotized mafic volcanic" (n=3) from 4,618 to 4,624 and from 4,624 to 4,639 ft depth, respectively.

Core and Cuttings Log

Recovered materials are core chips and cuttings, where indicated.

Summary: Loosely consolidated, mature quartz arenite overlies bimodal volcanic basement rock. Basement rock recovery includes an upper rhyolitic unit and lower crystal/lapilli tuff of mafic to intermediate composition.

4,404–4,414 ft Poorly consolidated quartz sandstone, with yellow to red limonite+clay(?) cement. Negative HCl test. Quartz grains are subangular to well rounded and ~0.5 mm in diameter.

4,530–4,540 ft Massive quartz arenite, 0.1–1.0-mm grains.

4,570–4,575 ft Clast-supported quartz arenite with yellow-orange and red-purple oxidation staining. Fine-grained cement is white and soft (kaolinite?).

4,575–4,575 ft Quartz arenite, fine-grained soft white cement, negative HCl test.

4,600–4,620 ft (cuttings) Dominantly well-rounded, clear to yellow to pink quartz sand grains ~0.5–6 mm in diameter. 5–10 percent angular to rounded red rhyolite fragments. No dark porphyry observed. Minor gray limestone contaminant.

4,618–4,624 ft Maroon rhyolite porphyry with quartz and feldspar phenocrysts. Fragments contain submillimeter chlorite(?) veins cut at high angle by ~0.5-mm thick quartz vein.

4,620–4,640 ft (cuttings) Mix of maroon rhyolite and a dark gray porphyry. Xenolith of the gray rock found within one maroon fragment. Minor contaminants (<10 percent) include rounded quartz grains, quartz arenite fragments, and rare limestone.

4,630–4,631 ft Dark gray porphyry with epidote veins 0.5–1-mm in aperture oriented roughly 90° from drilling direction. Contains a few volume percent dark, conchoidal, ~0.2-mm quartz crystals.

4,635–4,636 ft Dark, nearly aphanitic volcanic with 0.1–0.2-mm black (quartz?) crystals. Quartz veins are 0.1–0.5 mm thick.

4,638–4,639 ft Very hard, dark porphyritic rock with equant quartz, pink-orange feldspar, and black amphibole (~3:1 aspect ratio, strong cleavage, epidote replacement in microfractures) phenocrysts (~0.2 mm) in aphanitic dark gray matrix. Highly magnetic. One epidote vein is 0.6 mm wide. Sub-millimeter fractures filled with white to orange zeolite(?).

4,639–4,640 ft AA.

4,641–4,642 ft AA. Epidote vein has quartz core. Orange sub-millimeter veins are calcite (positive HCl test).

4,642–4,643 ft AA. The 1–2-cm thick core chip contains 7 fine-grained chloritized shear bands, <0.1 mm thick, spaced 0.5–3 mm apart. Chlorite slickenlines are visible on one surface. Shear planes cut epidote vein at high angle and displace vein ~0.2 mm across each boundary.

4,643–4,644 ft Well-indurated, dark volcanic with submillimeter orange veins. No shear bands.

Thin Section Petrography

Volcanic rock from 4,639 to 4,640 ft depth is a massive, green to black, intermediate to mafic welded tuff with angular to well-rounded tephra 0.1–1.5 mm in diameter (fig. 85). Clastic components include amphibole grains, epidote grains, opaque mineral grains, polycrystalline quartz clasts, subhedral to euhedral epidotized plagioclase crystals, micrographic K-feldspar grains, and porphyritic tephra (figs. 86 and 87). The porphyritic bits are plagioclase-phyric in a dark, massive, fine-grained matrix. The sample contains several submillimeter quartz veins and one chlorite vein with a maximum aperture of ~0.5 mm.

Notes on XRD Methods and Results

A large core chip from 4,639 to 4,640 ft depth was shattered to pea-sized and smaller fragments in a steel percussion mortar. These were ground by hand with an agate mortar and pestle. The sample was continuously lubricated with acetone during grinding. The resulting fine powder was allowed to air dry. An aliquot of the powder was placed in the 2-cm-wide cavity of a circular "back-pack" mount and scanned in a Panalytical X'Pert diffractometer with a Cu anode from an angular range of 3–90° 2Θ. Semiquantitative mineral abundances (Deasy and others, 2024b) were obtained by Rietveld refinement modeling in HighScore Plus (Malvern Panalytical, 2018). Major and trace element geochemical analysis powder was thereafter obtained by INAA/ICP-OES/ICP-MS by Activation Laboratories, Inc. (Deasy and others, 2024a).

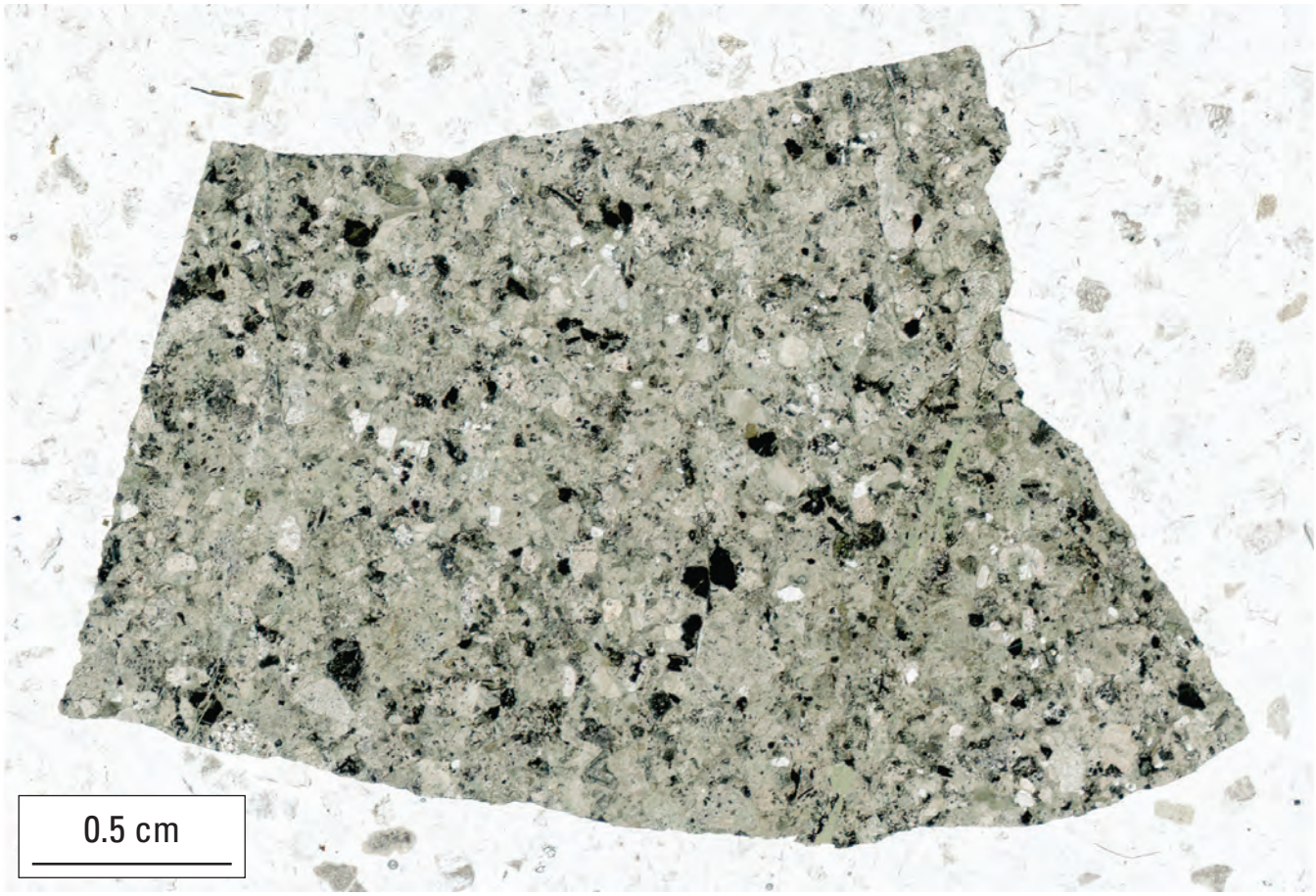

Figure 85. Scan in plane-polarized light of a thin section of welded lapilli tuff from borehole W1473 from 4,638 to 4,639 feet depth. Term: cm, centimeter. Photomicrograph by Ryan Deasy, U.S. Geological Survey.

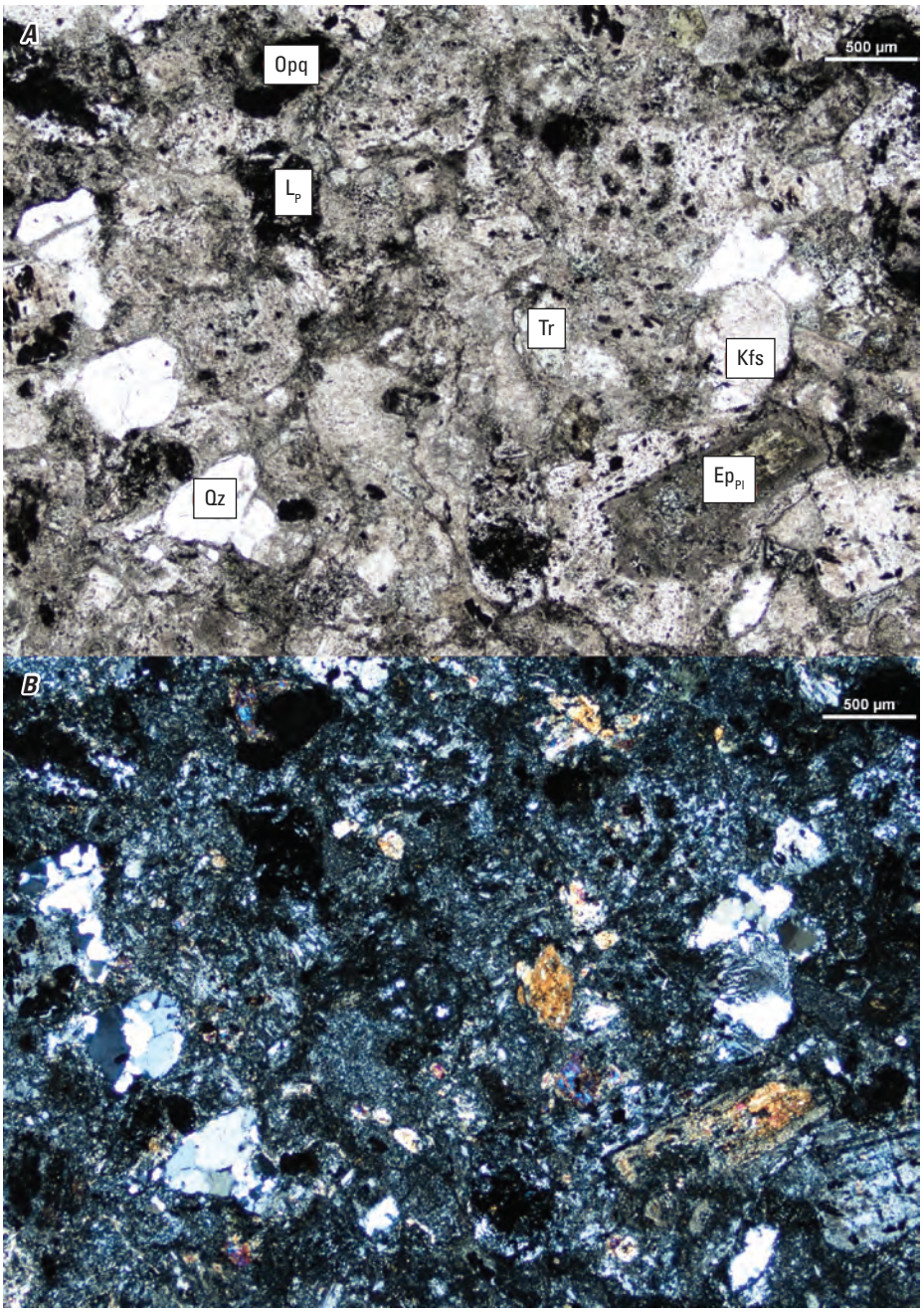

Figure 86. Pair of photomicrographs of a sample from borehole W1473 from 4,638 to 4,639 feet depth in plane-polarized light (*A*) and cross-polarized light (*B*). Terms: Opq, opaque mineral; L_P, porphyritic lithic clast; Tr, tremolite; Kfs, potassium feldspar; Ep_{Pl}, epidote (pseudomorph after plagioclase); Qz, quartz; µm, micrometer. Photomicrographs by Ryan Deasy, U.S. Geological Survey.

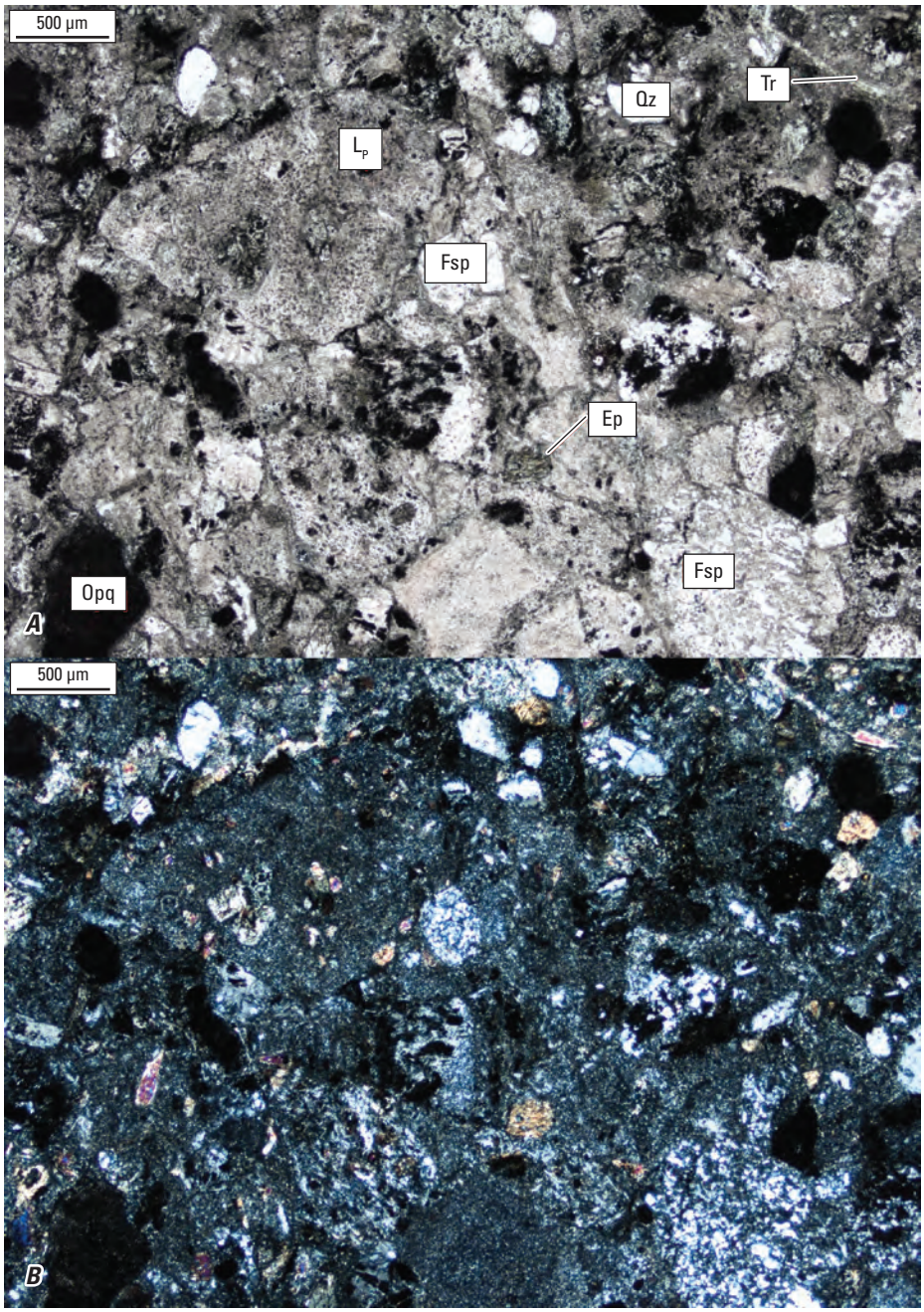

Figure 87. Pair of photomicrographs of a sample from borehole W1473 from 4,638 to 4,369 feet depth in plane-polarized light (*A*) and cross-polarized light (*B*). Terms: L_P, porphyritic lithic clast; Qz, quartz; Tr, tremolite; Fsp, feldspar; Opq, opaque mineral; Ep, epidote; µm, micrometer. Photomicrographs by Ryan Deasy, U.S. Geological Survey.

Borehole W1482

Basement rock encountered in this borehole from 4,615 to 4,624 ft depth is a felsic porphyry.

Previous Work

Applin (1951, p. 21) notes 22 ft of "volcanic agglomerate or tuff of rhyolitic composition" beginning at a depth of 4,615 ft. Carroll (1963) contributes a petrographic report on the overlying Paleozoic sandstone (coarse-grained quartzite and feldspathic quartzite), including some photomicrographs. Bass (1969) presents a petrographic analysis of core and cuttings and notes the presence of small amount of volcanic material in the basal conglomeritic sandstone. Milton (1972) summarized work to date and notes that available samples seem incompatible, suggesting some may be mislabeled. Milton also notes that nearby wells of similar depth penetrated Ordovician(?) sandstones but not volcanic rock. Mueller and Porch (1983) present two major element whole-rock geochemical analyses for dacite at 4,618–4,623.5 ft depth. Heatherington and others (1996) present a U-Pb SHRIMP age for zircon of 552±8 Ma from this sample, as well as two trace element whole-rock geochemical analyses on powders also analyzed by Mueller and Porch (1983).

Thin Section Petrography

A thin section of a core chip from 4,618 to 4,624 ft shows an altered felsic porphyry (fig. 88) in which the gray matrix is thoroughly sericitized. A moderately well-developed preferred orientation of sericite grains is approximately parallel to primary layering. Subhedral to euhedral feldspar phenocrysts are also completely sericitized (fig. 89). Angular to subrounded quartz grains have uniform or sweeping extinction, suggesting multiple sources. Opaque-rich lithic clasts up to ~0.5 cm across are feldspar-phyric tephra (figs. 90 and 91). Several thin quartz veins cut across the sample.

Notes on XRD Methods and Results

A single large (~2×~5 cm) core chip recovered from depth interval 4,618–4,623.5 ft was first broken into smaller pieces. The largest remaining piece was retained for thin section preparation, and the smaller pieces were collected and ground to a powder in an automated Brinkman grinder fitted with an agate mortar and pestle. The sample was continuously lubricated with acetone during grinding. The resulting powder was further ground by hand in a corundum mortar and pestle, again lubricated with acetone, and allowed to air dry. An aliquot of the powder was placed in the 3×2×0.1-cm cavity of a Ti "front-pack" mount and scanned in a Bruker D8 diffractometer from an angular range of 2–100° 2Θ with a Cu anode and point detector at 0.02° steps and a rate of 13 sec/step. Semiquantitative mineral abundances (Deasy and others, 2024b) were obtained by Rietveld refinement modeling in TOPAS (Bruker AXS, 2011).

The strongly asymmetrical shape of the 8.8° 2Θ (d=1.0 nm) peak in diffraction results (fig. 92) prompted re-analysis to characterize clay minerals, as follows. A small amount of the sample was mixed in a slurry with distilled water on a quartz "zero background" plate, was allowed to air dry, and was then scanned on the Bruker D8 from 2 to 56° 2Θ at 5 sec/step. The mounted sample was then placed in a chamber saturated with EG for ~24 hours before being scanned again, immediately upon removal from the EG chamber, from 2 to 40° 2Θ at 2 sec/step.

The asymmetrical ~9° 2Θ (d=~1.0 nm) peak becomes more symmetrical upon EG solvation by both a decrease in lower angle intensity and an increase in higher angle intensity, and a small peak at ~17° 2Θ (d=~0.515 nm) grows slightly more intense (fig. 92). These effects are attributed to the presence of a small amount of illite/smectite. The position of the Ilt-Sme$_{002}$ reflection at ~17° 2Θ indicates that the smectitic component composes 10–20 percent of the illite/smectite (see Moore and Reynolds 1997, table 8.3), although strong interference from other phyllosilicate peaks limits the precision of this estimate.

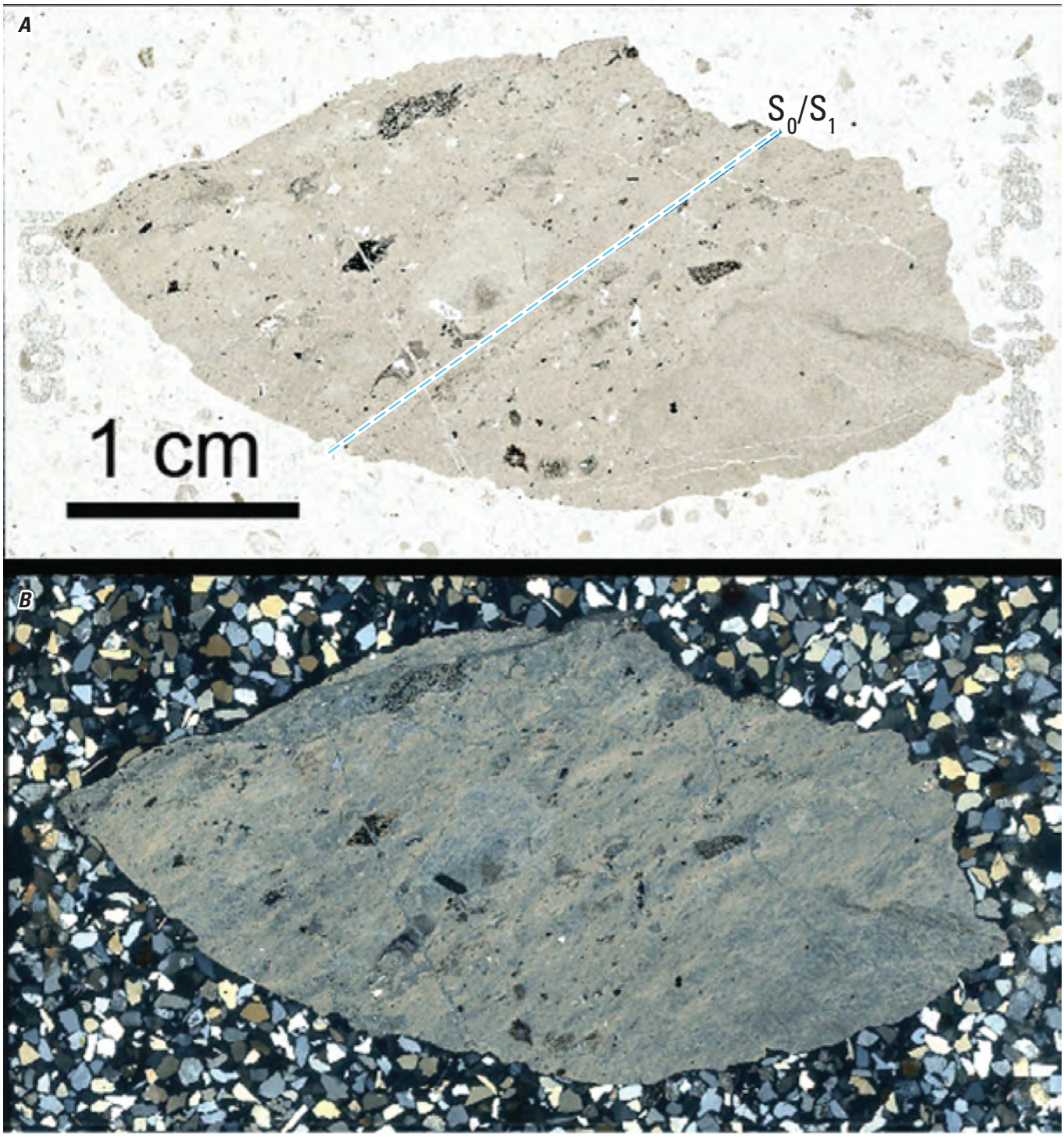

Figure 88. Full thin section scans of sericitized volcanic rock from borehole W1482 from 4,618 to 4,623.5 feet depth in plane-polarized light (*A*) and cross-polarized light (*B*). A fabric defined by the preferred orientation of metamorphic illite and muscovite is parallel to the alignment of inequant clasts (S_0/S_1, dashed blue line). Term: cm, centimeter. Photomicrographs by Ryan Deasy, U.S. Geological Survey.

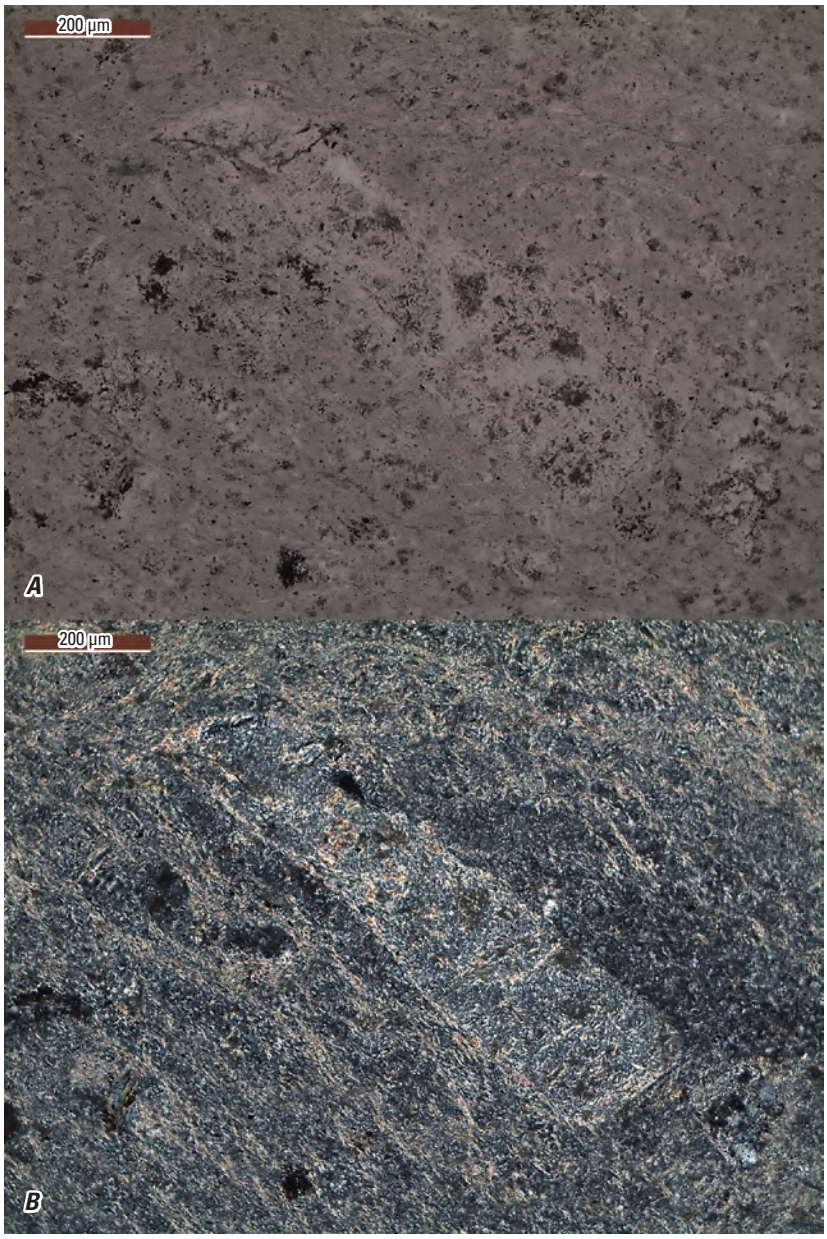

Figure 89. Pair of photomicrographs in plane-polarized light (*A*) and cross-polarized light (*B*) of a sericitized feldspar phenocryst (center) in sericitized volcanic rock in a core chip from borehole W1482 from 4,618 to 4,623.5 feet depth. Term: µm, micrometer. Photomicrographs by Ryan Deasy, U.S. Geological Survey.

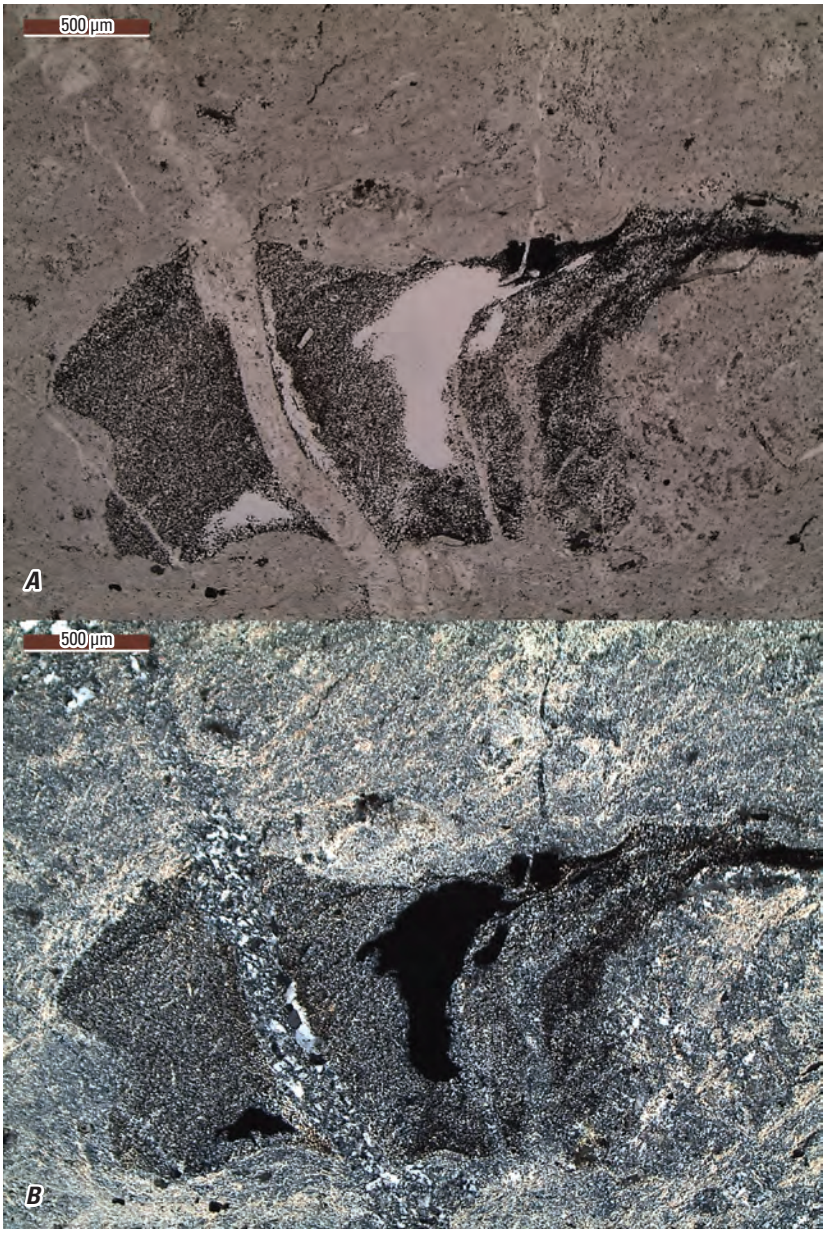

Figure 90. Pair of photomicrographs in plane-polarized light (*A*) and cross-polarized light (*B*) of a sericitized volcanic lithic clast in sericitized dacite in a core chip from borehole W1482 from 4,618 to 4,623.5 feet depth. A quartz vein crosscuts the field of view from upper left to bottom center. The extinct areas in the lithic are holes in the thin section. Term: µm, micrometer. Photomicrographs by Ryan Deasy, U.S. Geological Survey.

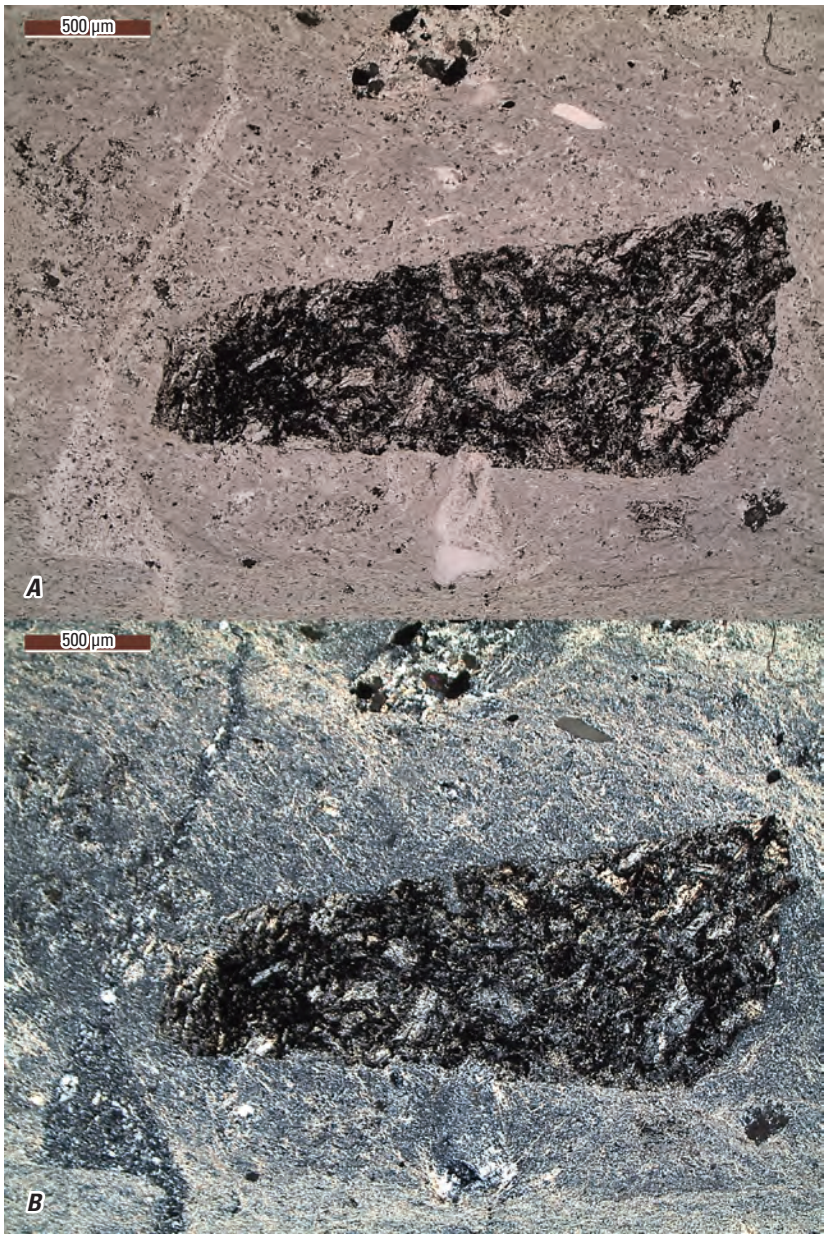

Figure 91. Pair of photomicrographs in plane-polarized light (*A*) and cross-polarized light (*B*) of a sericitized, subrounded porphyritic clast in sericitized dacite in a core chip from borehole W1482 from 4,618 to 4,623.5 feet depth. A quartz vein crosscuts the left side of the field of view from top to bottom. Term: µm, micrometer. Photomicrographs by Ryan Deasy, U.S. Geological Survey.

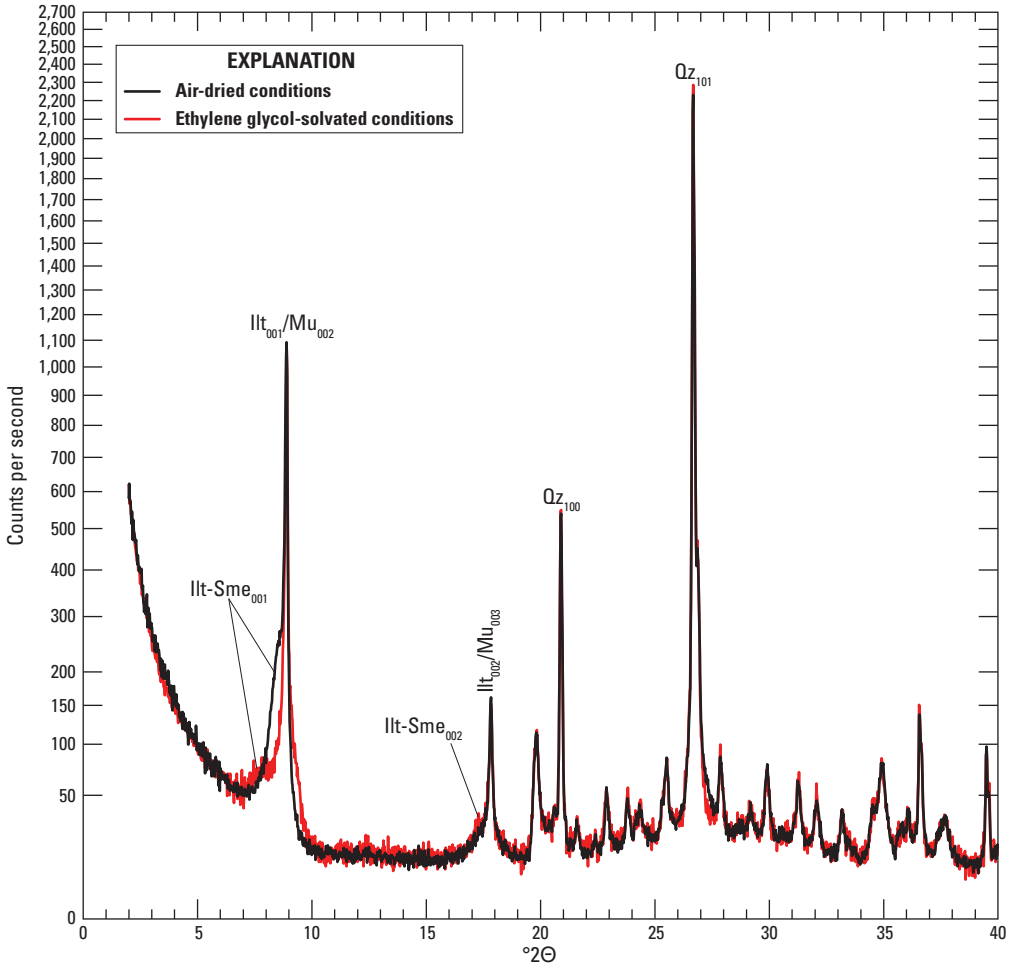

Figure 92. X-ray diffractograms of a sample from borehole W1482 from 4,618 to 4,623.5 feet depth under air-dried and ethylene glycol-solvated conditions. The *y*-axis is in square root scale. Selected peaks are labeled with mineral abbreviations; the numbers in subscripts denote Miller indices. Terms: °2Θ, degrees two theta; Ilt, illite; Sme, smectite; Mu, muscovite; Qz, quartz.

Borehole W1746A

Basement rock encountered in this borehole from ~5,400 to 5,424.5 ft depth is a felsic porphyry with large and abundant plagioclase phenocrysts.

Previous Work

Applin (1951, p. 9) first documented this basement rock as "Rhyolitic(?) volcanic rock." Milton (1972) includes a brief description of cuttings at 5,424.5 ft depth (TD) and an ordinary light thin-section photomicrograph.

Cuttings Log

Summary: The contact between rhyolitic basement rock and sandstone occurs between 5,400 and 5,410 ft depth. The basal sedimentary unit is nearly pure quartz arenite with a minor regolith component. Rhyolite is porphyritic with conspicuous cleavage faces up to 1 mm of plagioclase feldspar, deeply colored in reds and purples. Rhyolite fragments are weakly magnetic and lack conspicuous veining.

5,390–5,400 ft Cuttings dominated by subrounded to well-rounded, 0.5–2-mm white, yellow, orange, and pink quartz sand grains, with minor (<5 percent) 0.5–1-mm pink to red rhyolite fragments. A fraction (~15 percent) of larger (up to 8 mm) limestone clasts are interpreted as contamination from overlying layers.

5,400–5,410 ft AA. Rhyolitic component is minor compared to large limestone clasts and contains subangular to well-rounded quartz grains.

5,410–5,420 ft Dominantly (~90 percent) pink to purple to red, 0.1–5-mm rhyolitic fragments (fig. 93). Rhyolitic fragments are porphyritic with plagioclase cleavage faces up to ~1 mm. No apparent vein material in or on rhyolitic fragments. Minor limestone fragments (contamination) and rare anthropogenic contamination (plastic and metal).

5,424–5,424.5 ft Unwashed. Cuttings are ~90 percent pink-purple-red, 0.1–5-mm (most between 0.5 and 1 mm) rhyolitic fragments. Some plant matter and slivers of metal and plastic comprise contaminant fraction (~10 percent) along with some rounded quartz grains and limestone clasts.

Figure 93. Photograph of cuttings from borehole W1746A from 5,410 to 5,420 feet depth. The ruler scale is in centimeters. Photograph by Ryan Deasy, U.S. Geological Survey.

Thin Section Petrography

A polished thin section of rhyolitic cuttings fragments 1–6 mm in diameter from 5,410 to 5,420 ft depth was prepared (fig. 94). Clasts are red-orange in ordinary light and PPL and are optically dense with a fine-grained, finely disseminated red oxide alteration overprint (figs. 94 and 95). Although pervasive, the red oxide is concentrated in the K-feldspar domains, as is a moderate sericite overprint (fig. 95).

This rock is porphyritic with randomly oriented, euhedral albitic plagioclase phenocrysts in a K-feldspar+quartz matrix, with minor magnetite (fig. 96). Plagioclase phenocrysts range in size from 0.05 to 1 mm and have aspect ratios ranging from 1:1 to 8:1. Plagioclase grains commonly have deformation twins, and the crystals are commonly bent. Zoning profiles are not apparent in EDS spectra of plagioclase grains. Interstices are mostly intergrowths of quartz and K-feldspar.

Accessory phases include, in decreasing order of abundance, magnetite, apatite, rutile, monazite, titanite, chlorite, and xenotime. Magnetite occurs in grains up to 500 µm in diameter, commonly with apatite or rutile inclusions; brecciated magnetite grains have fractures filled with K-feldspar. Apatite is mostly free of inclusions and is commonly euhedral. Rutile grains contain many inclusions including quartz, K-feldspar, and zircon; amoeboidal rutile is closely associated with sericite at magmatic grain boundaries. Fine-grained monazite (5–10 µm) is disseminated throughout, with one large (~1 mm) amoeboidal aggregate grain filling a fracture with titanite and xenotime. Additionally, some clasts are cut by thin, sinuous alteration seams filled with chlorite, titanite, xenotime (fig. 97), and REE-carbonates.

Notes on XRD Methods and Results

Rhyolitic cuttings fragments from the interval between 5,410 and 5,420 ft depth were handpicked under a binocular microscope. The purified rhyolite fragments were placed in an automated Brinkman grinder fitted with an agate mortar and pestle for initial grinding. The sample was continuously lubricated with acetone during grinding. The resulting coarse powder was further ground by hand in a corundum mortar and pestle, again lubricated with acetone, and allowed to air dry. An aliquot of the powder was placed in the 3×2×0.1-cm cavity of a Ti "front-pack" mount and scanned in a Bruker D8 diffractometer from an angular range of 2–80° 2Θ with a Cu anode and point detector. Semiquantitative mineral abundances (Deasy and others, 2024b) were obtained by Rietveld refinement modeling in TOPAS (Bruker AXS, 2011). The major and trace element geochemistry of the powder was then determined by XRF/ICP-MS (Deasy and others, 2024a).

The strong alteration overprint evident in thin section prompted further analysis to characterize the nature and abundances of clay minerals, as follows. A small amount of the powdered sample was mixed in a slurry with distilled water on a quartz "zero background" plate, was allowed to air dry, and was then scanned on the Bruker D8 from 2 to 90° 2Θ at 6 sec/step. The mounted sample was then placed in an EG-saturated chamber for a minimum of 24 hours before being scanned again, immediately upon removal from the EG chamber, from 2 to 40° 2Θ at 4 sec/step. Solvation in EG effected no change in the diffraction pattern (fig. 98), indicating the absence of expandable clays in this sample. A relatively weak 0.307 nm white mica (Ilt_{112}/Mu_{114}) peak suggests a higher abundance of 2M1-type muscovite than 1M-type, illitic mica. Other alteration minerals identified by XRD include small amounts of calcite, dolomite, and kaolinite.

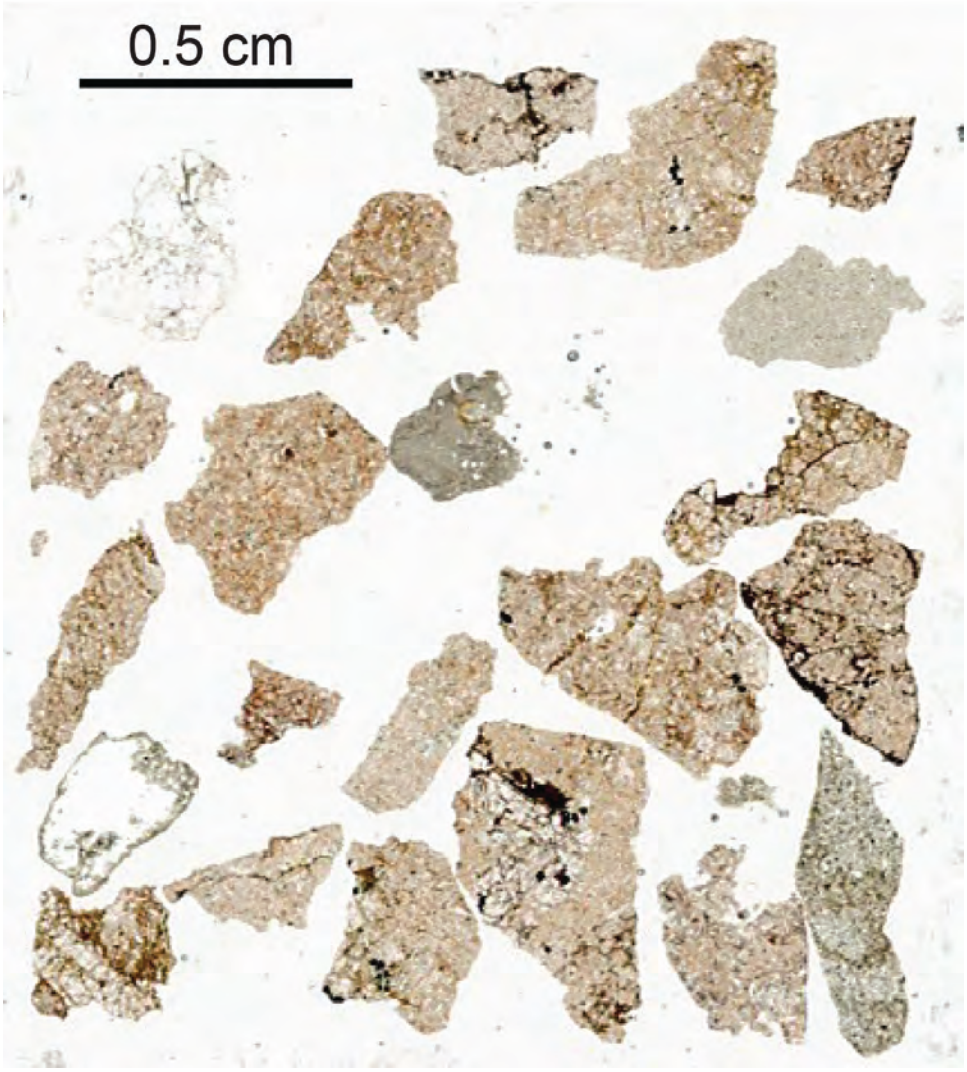

Figure 94. Scan in plane-polarized light of a thin section of cuttings from borehole W1746A from 5,410 to 5,420 feet depth. Term: cm, centimeter. Photomicrograph by Ryan Deasy, U.S. Geological Survey.

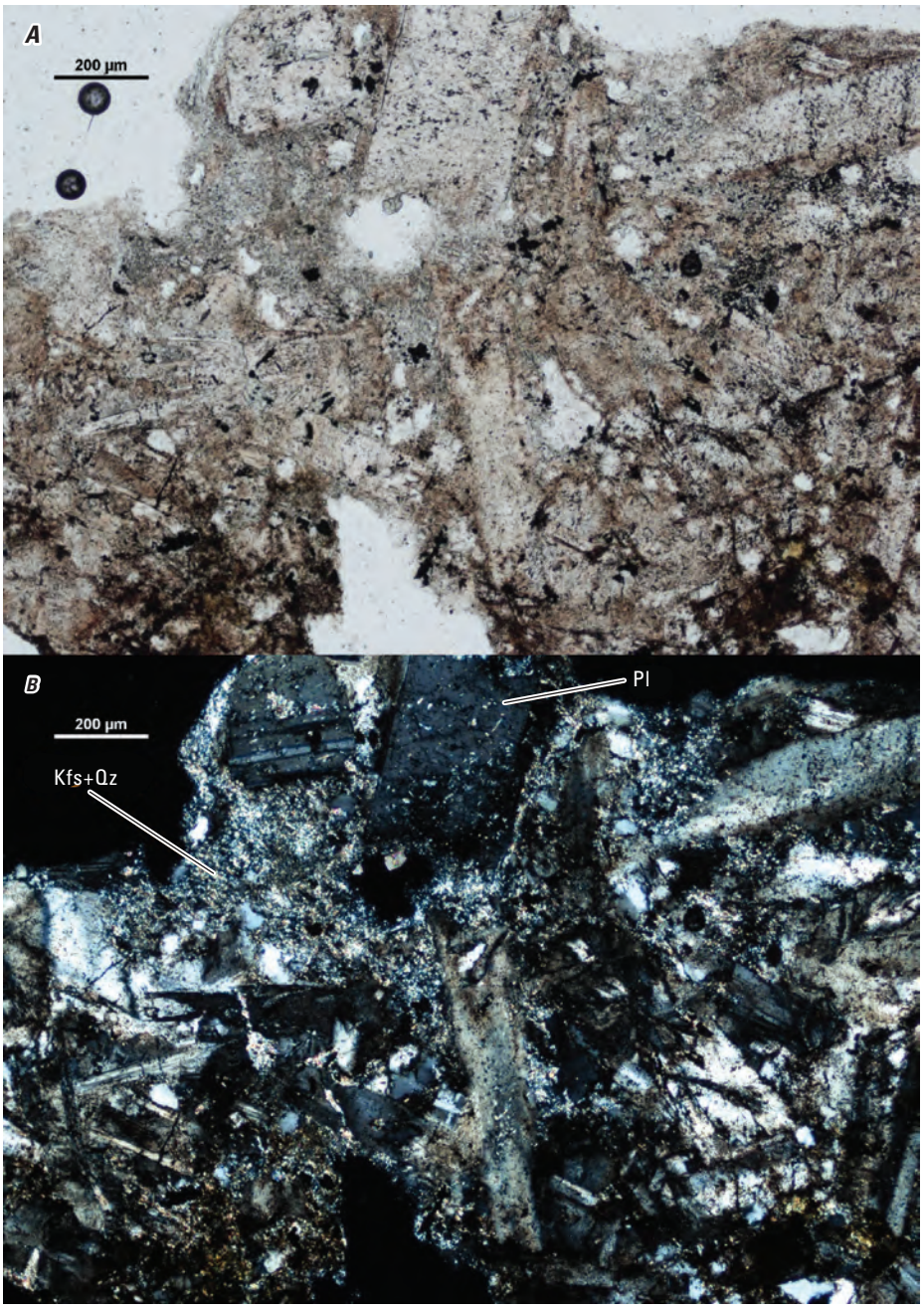

Figure 95. Photomicrographs of a sample from borehole W1746A from 5,410 to 5,420 feet depth in plane-polarized light (*A*) and cross-polarized light (*B*). Terms: Kfs, potassium feldspar; Qz, quartz; Pl, plagioclase; µm, micrometer. Photomicrographs by Ryan Deasy, U.S. Geological Survey.

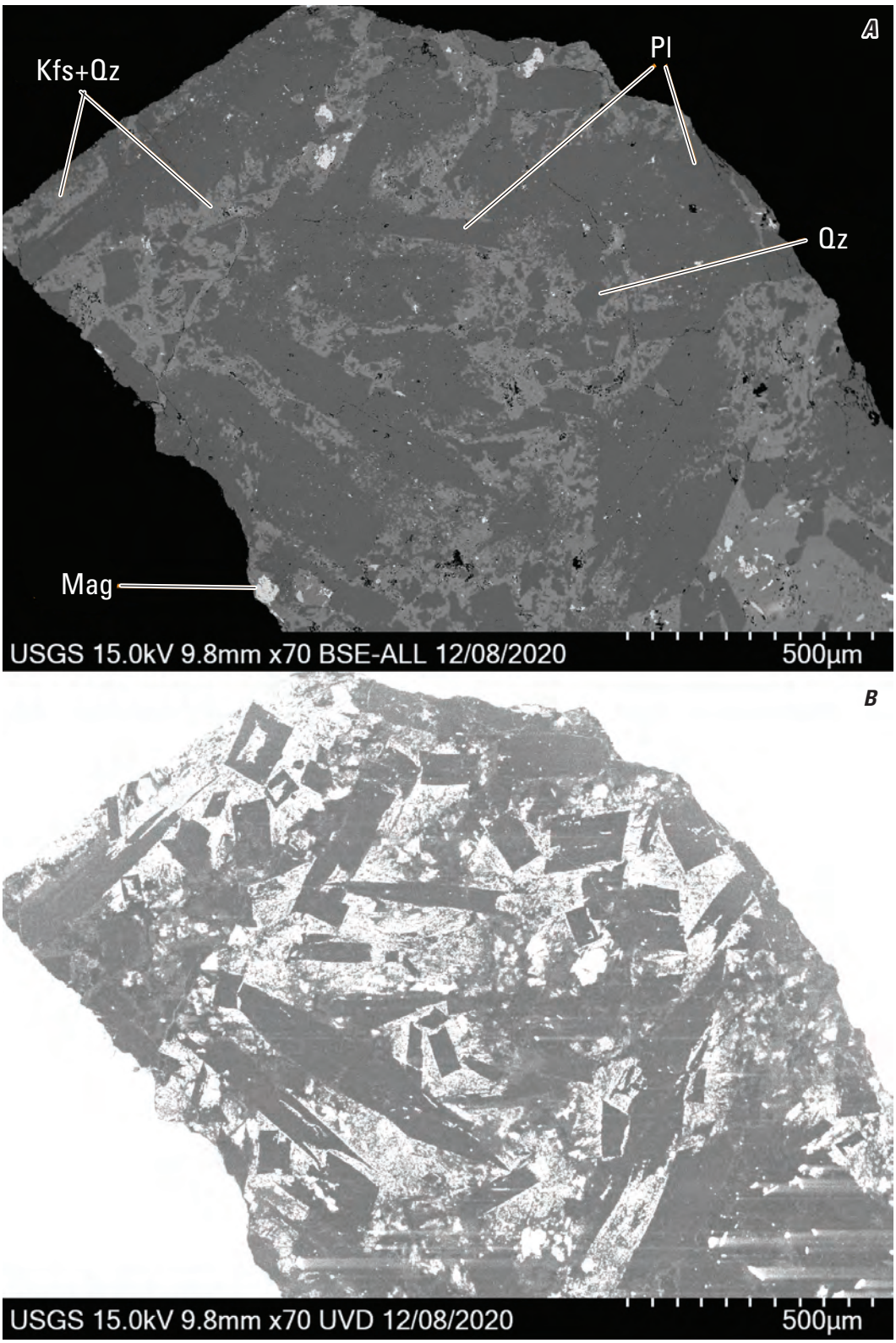

Figure 96. Scanning electron microscope images of a sample from borehole W1746A from 5,410 to 5,420 feet depth in back-scattered electron (BSE) (*A*) and cathodoluminescence (*B*). Text in the bottom left of each image identifies data source (USGS); operating conditions including beam potential in kilovolts (15.0 kV), working distance in millimeters (9.8 mm), and image magnification in multiples of actual size (70 times); and date of acquisition (12/08/2020). Terms: Kfs, potassium feldspar; Qz, quartz; Pl, plagioclase; Mag, magnetite; USGS, U.S. Geological Survey; kV, kilovolt; mm, millimeter; BSE-ALL, back-scattered electron, all energies; UVD; ultra variable-pressure detector; µm, micrometer. Photomicrographs by Ryan Deasy, U.S. Geological Survey.

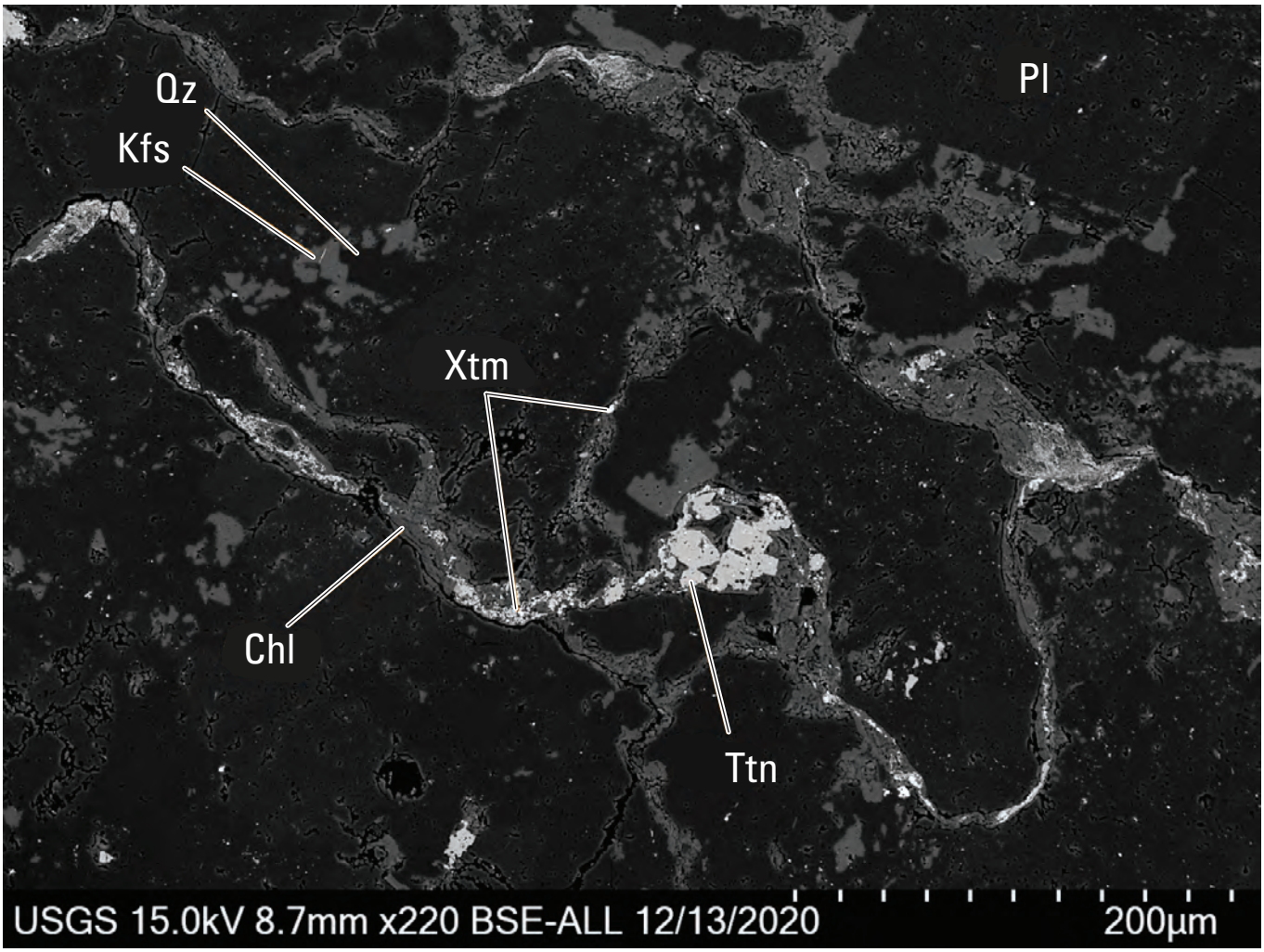

Figure 97. Back-scattered electron (BSE) image of a sample from borehole W1746A from 5,410 to 5,420 feet depth showing a sinuous mineralized seam. Text in the bottom left identifies data source (USGS); operating conditions including beam potential in kilovolts (15.0 kV), working distance in millimeters (8.7 mm), and image magnification in multiples of actual size (220 times); and date of acquisition (12/13/2020). Terms: Kfs, potassium feldspar; Qz, quartz; Pl, plagioclase; Xtm, xenotime; Chl, chlorite; Ttn, titanite; USGS, U.S. Geological Survey; kV, kilovolt; mm, millimeter; BSE-ALL, back-scattered electron, all energies; µm, micrometer. Photomicrograph by Ryan Deasy, U.S. Geological Survey.

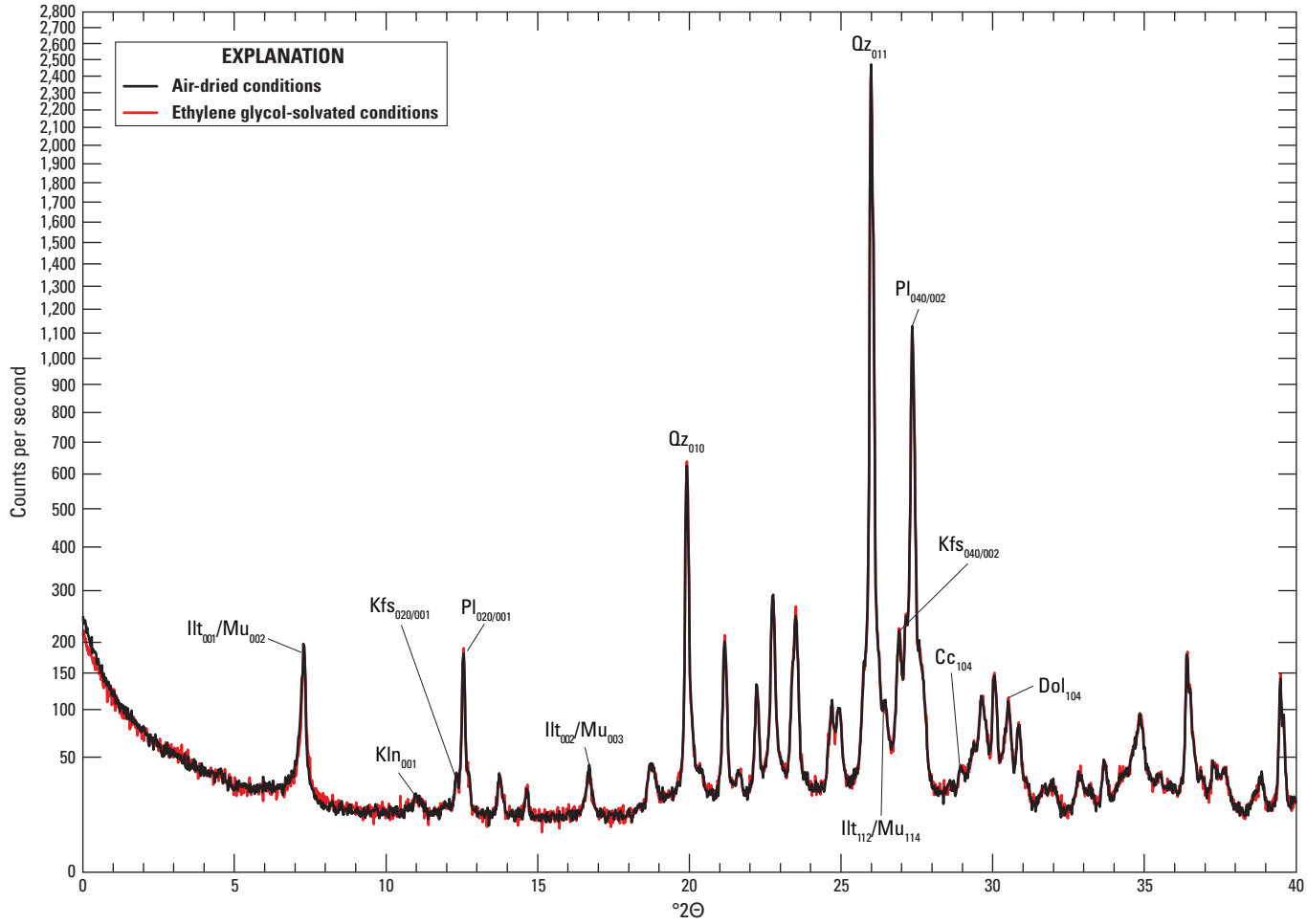

Figure 98. X-ray diffractograms of a powdered sample of rhyolite from borehole W1746A from 5,410 to 5,420 feet depth under air-dried and ethylene glycol-solvated conditions. The *y*-axis is in square root scale. Terms: °2Θ, degrees two theta; Ilt, illite; Mu, muscovite; Kln, kaolinite; Kfs, potassium feldspar; Pl, plagioclase; Qz, quartz; Cc, calcite; Dol, dolomite.

Borehole W11499

Mafic to intermediate volcanic rock composes the basement from 5,195 to 5,397 ft depth in this borehole.

Previous Work

Barnett (1975, p. 136) reports 202 ft of penetration of "deeply weathered basic igneous?" rock from 5,195 to 5,397 ft depth. This information can also be found in Arthur (1988).

Cuttings Log

Summary: Weathered metavolcanic rock of mafic to intermediate composition is overlain by limestone.

5,180–5,190 ft Gray limestone.

5,190–5,200 ft Mottled gray and white igneous rock. Some fragments contain green (epidote?) veins. One cluster of volcanic cuttings fragments is cemented with calcite. The weakly positive reaction with HCl on volcanic fragments may be from dust or a small amount of interstitial calcite.

5,240–5,250 ft Mix of volcanic fragments including gritty, salt-and-pepper fragments with elongate dark grains in white matrices and dark, massive fragments. Vein material is rare; these fragments contain zeolite(?), quartz, and epidote.

5,250–5,260 ft Volcanic fragments include the salt-and-pepper and massive fragments from above, as well as deeply weathered chalky bits and welded tuff comprising submillimeter lapilli. Vein material is rare.

5,270–5,280 ft Mix of dark gray and gritty, pale, salt-and-pepper-textured volcanic fragments.

5,300–5,310 ft A greater proportion of pale, salt-and-pepper-textured bits than above. Epidote and quartz vein material are present but rare, most commonly as loose fragments; that is, the aperture of most veins is probably greater than the size of cuttings. Some 1–2-mm cuttings fragments include 0.5–1-mm dark lapilli.

5,350–5,360 ft Paler, grittier, and more epidote-rich than above. Epidote porphyroblasts are visible in some fragments. Minor pink zeolite(?) veins. Large gray limestone fragments are abundant (as contaminant).

5,370–5,380 ft (TD) AA.

Thin Section Petrography

Volcanic fragments are porphyritic with acicular to lath-shaped plagioclase phenocrysts in a glassy to fine-grained matrix (figs. 99–105). Phenocryst density ranges from sparse to very dense. Plagioclase phenocrysts define a magmatic foliation that ranges from weak (fig. 99) to strong (fig. 100). Contacts between the porphyritic rock and sedimentary country rock are preserved in some fragments (figs. 101–103). Rare miarolitic cavities are lined with quartz and euhedral chlorite and filled with randomly oriented quartz and chlorite (fig. 104). Although magmatic textures are well preserved, the magmatic assemblage has been pervasively replaced by albite, chlorite, epidote, titanite, prehnite, magnetite, and apatite, with rare clinoamphibole. Magnetite grains are euhedral to amoeboidal and contain exsolved lamellae of ilmenite/rutile(?) and hematite(?) (fig. 105).

Notes on XRD Methods and Results

Volcanic fragments were separated from sedimentary fragments and other contaminating cuttings by hand under a binocular microscope. Subsamples of volcanic cuttings weighing 0.6–1.0 g each were separated from each of the following depth intervals:

5,290–5,320 ft

5,320–5,330 ft

5,330–5,350 ft

Each subsample was ground by hand in an agate mortar and pestle while being continuously lubricated with acetone during grinding. The mortar and pestle were thoroughly cleaned between subsamples. The resulting fine powders were allowed to air dry. The powders were placed in 2-cm-wide cavities of circular “back-pack” mounts and scanned in a Panalytical X’Pert diffractometer with a Cu anode from an angular range of 3–90° 2Θ. Semiquantitative mineral abundances (Deasy and others, 2024b) were obtained by Rietveld refinement modeling in HighScore Plus (Malvern Panalytical, 2018). Major and trace element geochemical analyses of these powders were obtained by INAA/ICP-OES/ICP-MS by Activation Laboratories, Inc. (Deasy and others, 2024a).

Additionally, a larger ~5-g fraction of volcanic rock for XRF/ICP-MS analysis was obtained from 5,290 to 5,350 ft depth by combining picked cuttings from the interceding intervals. The hand-picked fragments were placed in an automated Brinkman grinder fitted with an agate mortar and pestle. The sample was continuously lubricated with acetone during grinding. The resulting coarse powder was further ground by hand in a corundum mortar and pestle, again lubricated with acetone, and allowed to air dry. An aliquot of the powder was placed in the 3×2×0.1-cm cavity of a Ti “front-pack” mount and scanned in a Bruker D8 diffractometer from an angular range of 2–80° 2Θ with a Cu anode and point detector. Semiquantitative mineral abundances (Deasy and others, 2024b) were obtained by Rietveld refinement modeling in TOPAS (Bruker AXS, 2011). The major and trace element geochemistry of the powder was then determined by XRF/ICP-MS by Activation Laboratories, Inc. (Deasy and others, 2024a).

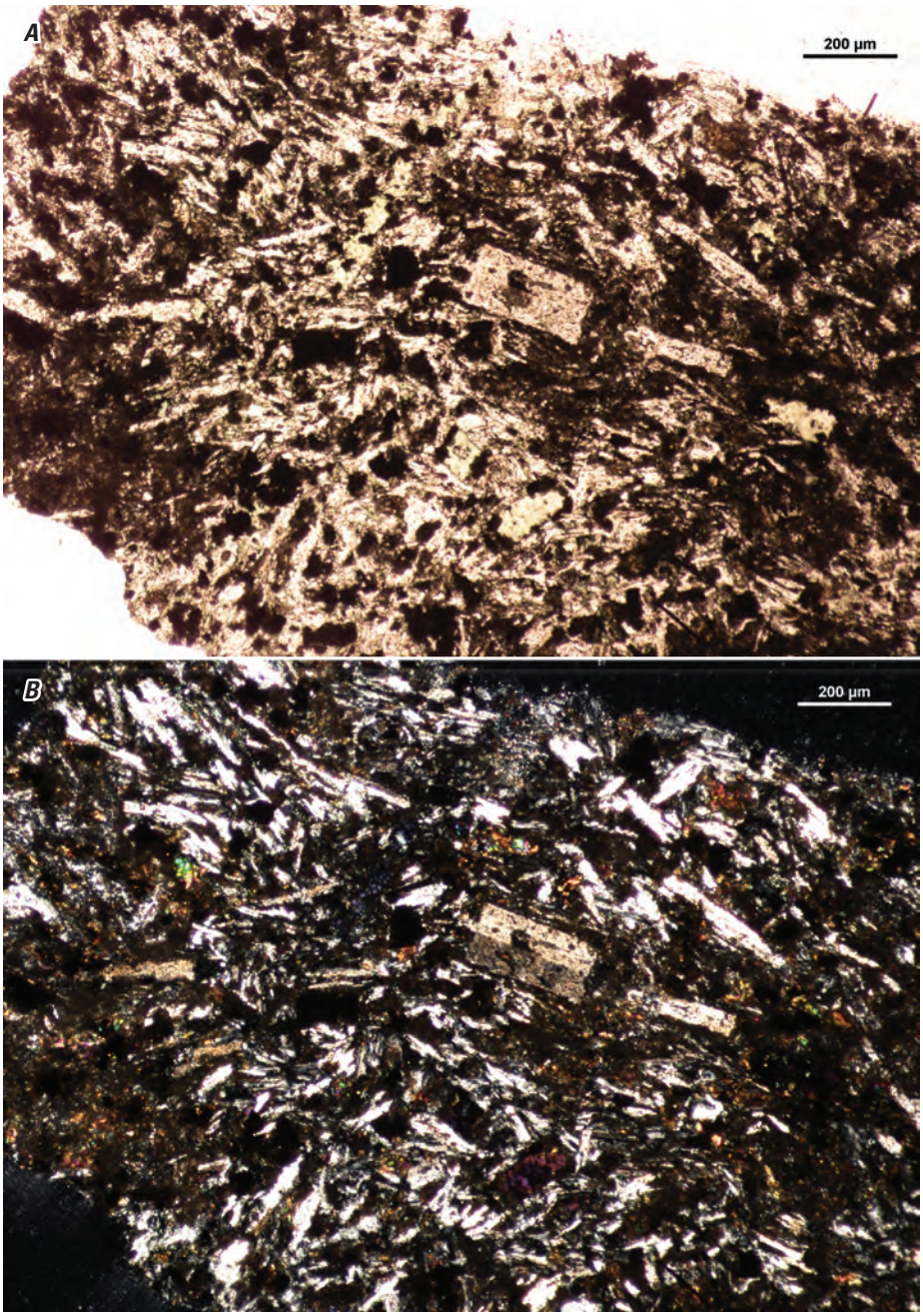

Figure 99. Pair of photomicrographs of volcanic rock from borehole W11499 from 5,300 to 5,310 feet depth in plane-polarized light (*A*) and cross-polarized light (*B*). Term: µm, micrometer. Photomicrographs by Ryan Deasy, U.S. Geological Survey.

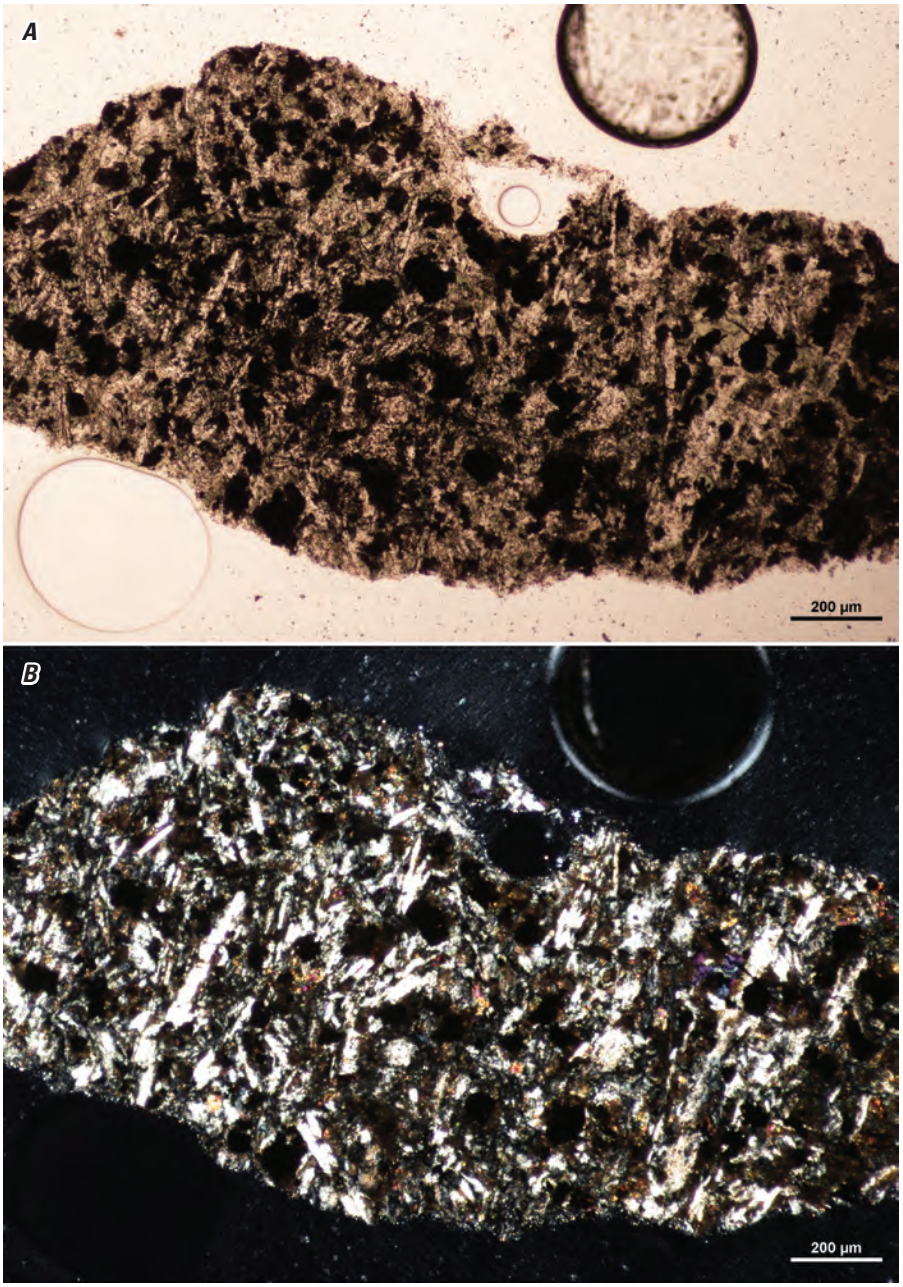

Figure 100. Pair of photomicrographs of volcanic rock from borehole W11499 from 5,310 to 5,320 feet depth in plane-polarized light (*A*) and cross-polarized light (*B*). Term: µm, micrometer. Photomicrographs by Ryan Deasy, U.S. Geological Survey.

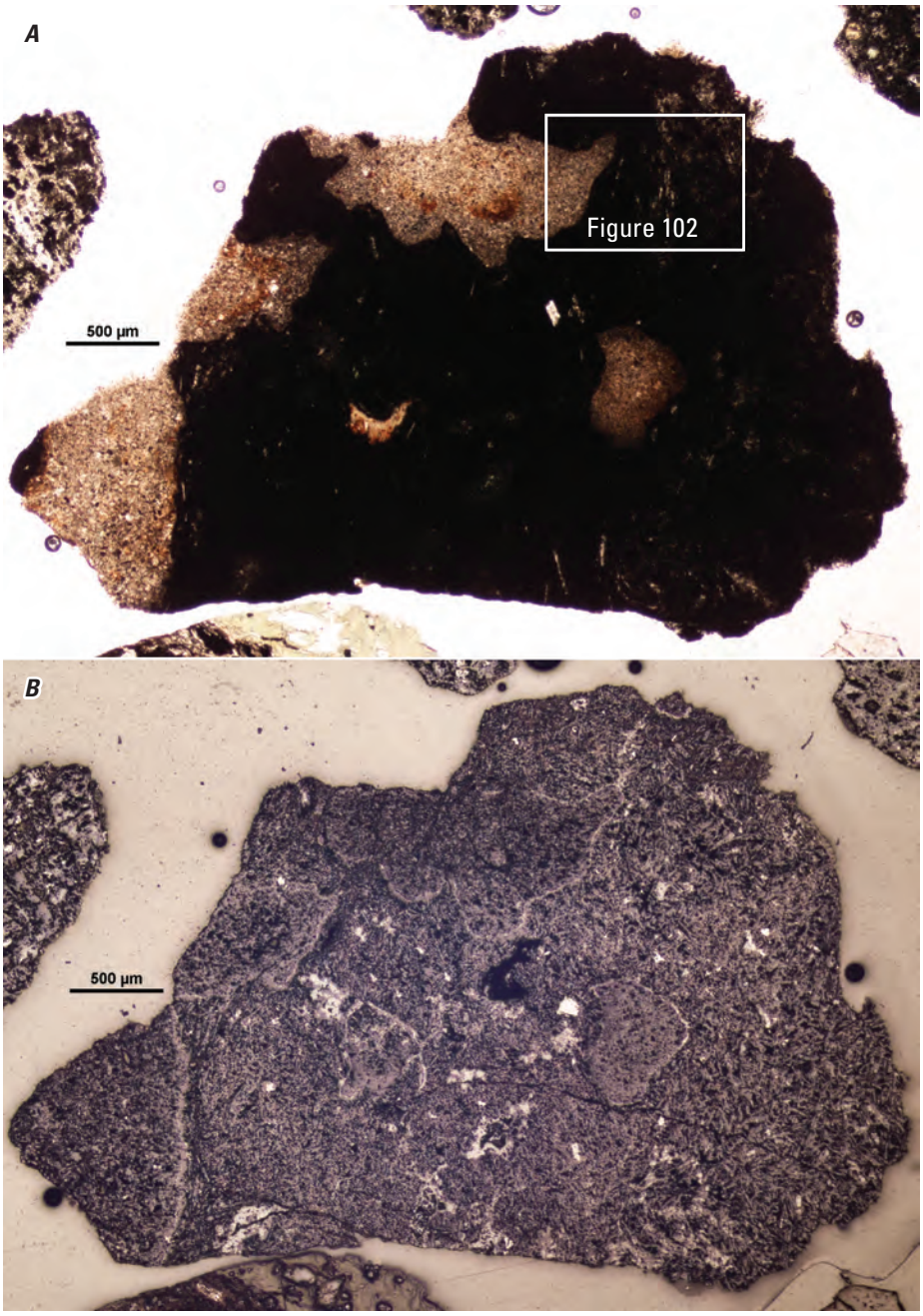

Figure 101. Pair of photomicrographs of a fragment from borehole W11499 from 5,310 to 5,320 feet depth showing the chilled contact between porphyry and sandstone country rock in plane-polarized light (*A*) and reflected light (*B*). The white box in part *A* outlines the area of figure 102. Term: µm, micrometer. Photomicrographs by Ryan Deasy, U.S. Geological Survey.

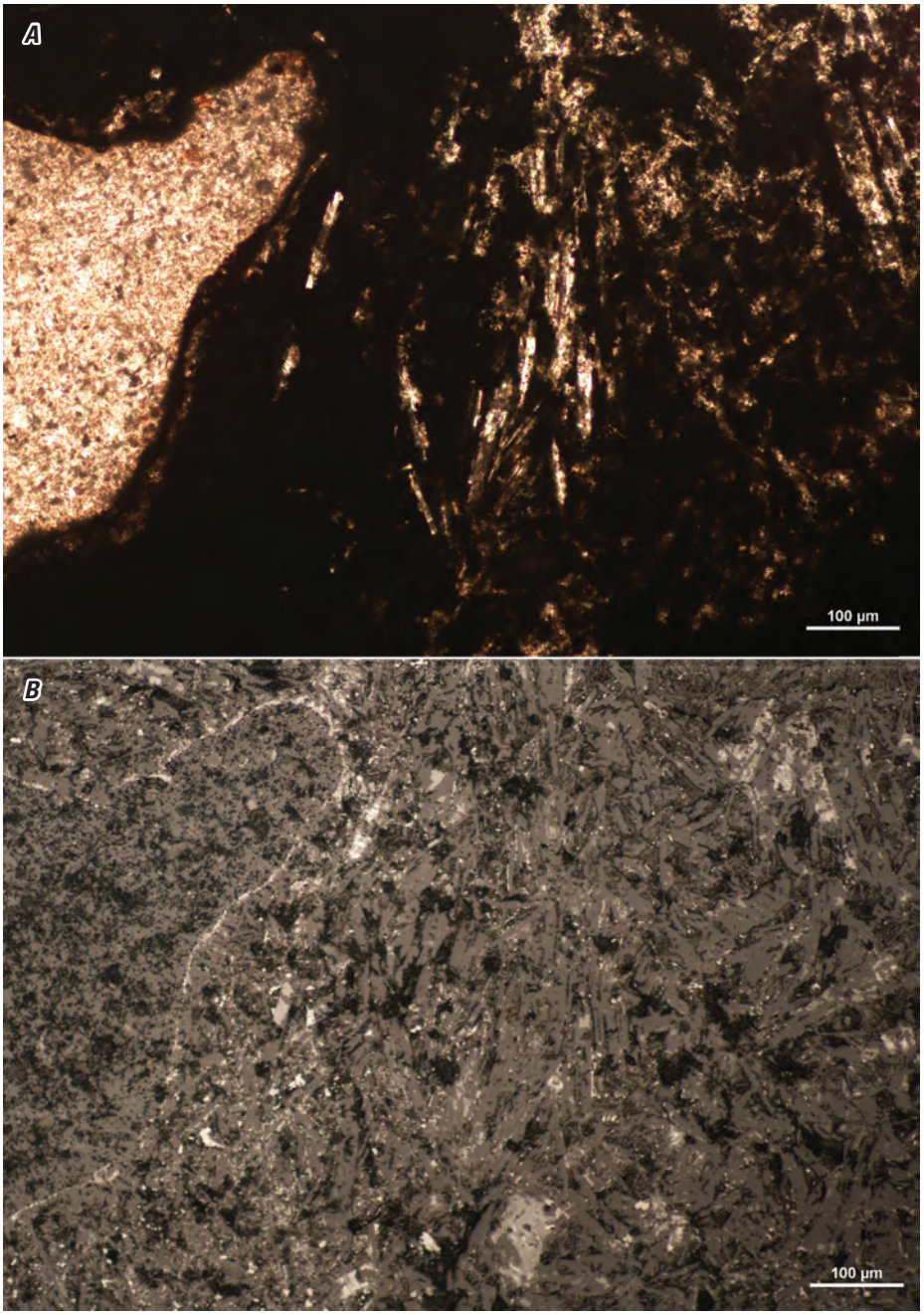

Figure 102. Pair of photomicrographs of a fragment from borehole W11499 from 5,310 to 5,320 feet depth showing the chilled contact between porphyry and sandstone country rock in plane-polarized light (*A*) and reflected light (*B*). The area depicted corresponds to the white inset box in figure 101. Term: µm, micrometer. Photomicrographs by Ryan Deasy, U.S. Geological Survey.

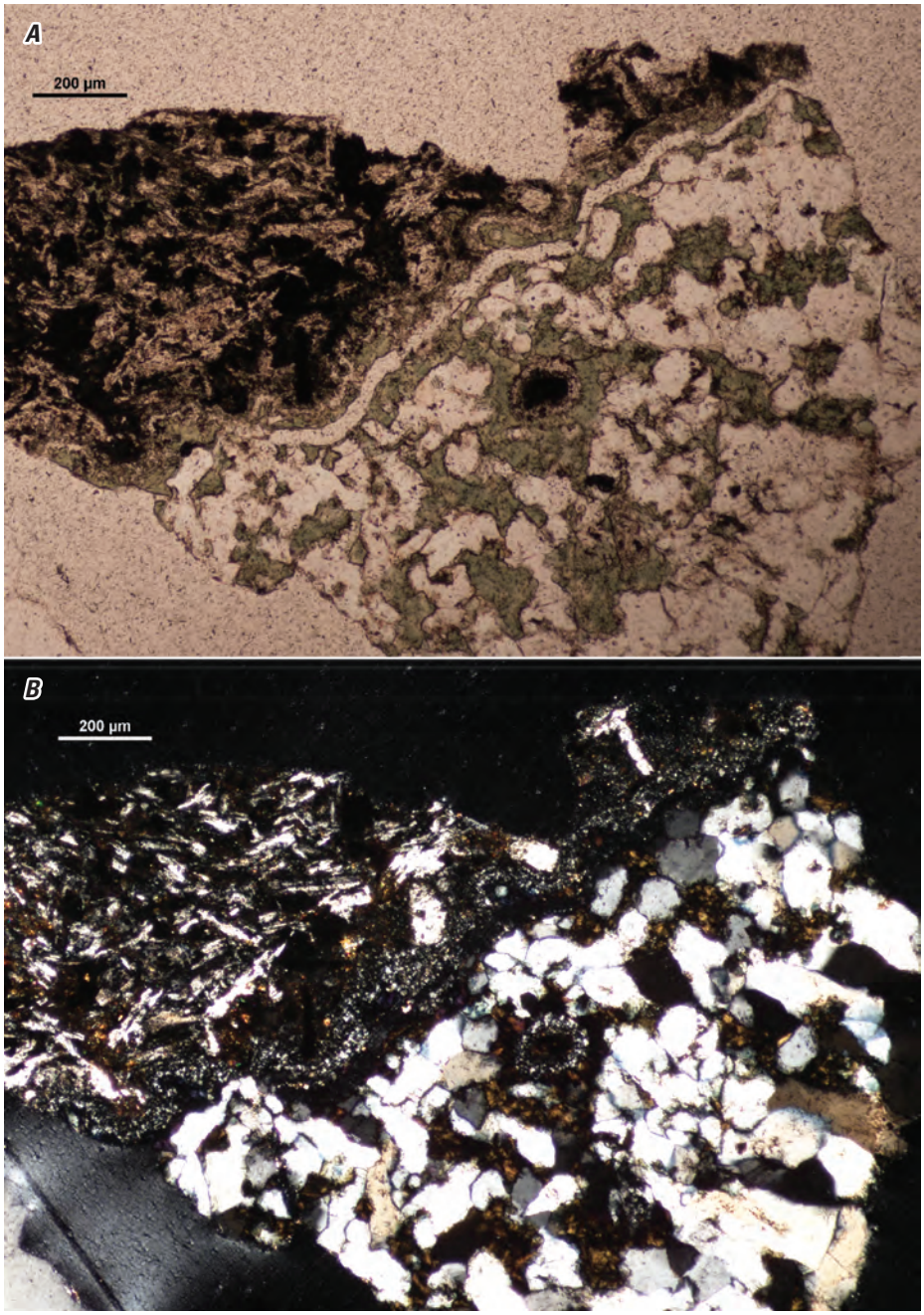

Figure 103. Pair of photomicrographs of a fragment from borehole W11499 from 5,300 to 5,310 feet depth showing the chilled contact between porphyry and sandstone country rock in plane-polarized light (*A*) and cross-polarized light (*B*). Term: µm, micrometer. Photomicrographs by Ryan Deasy, U.S. Geological Survey.

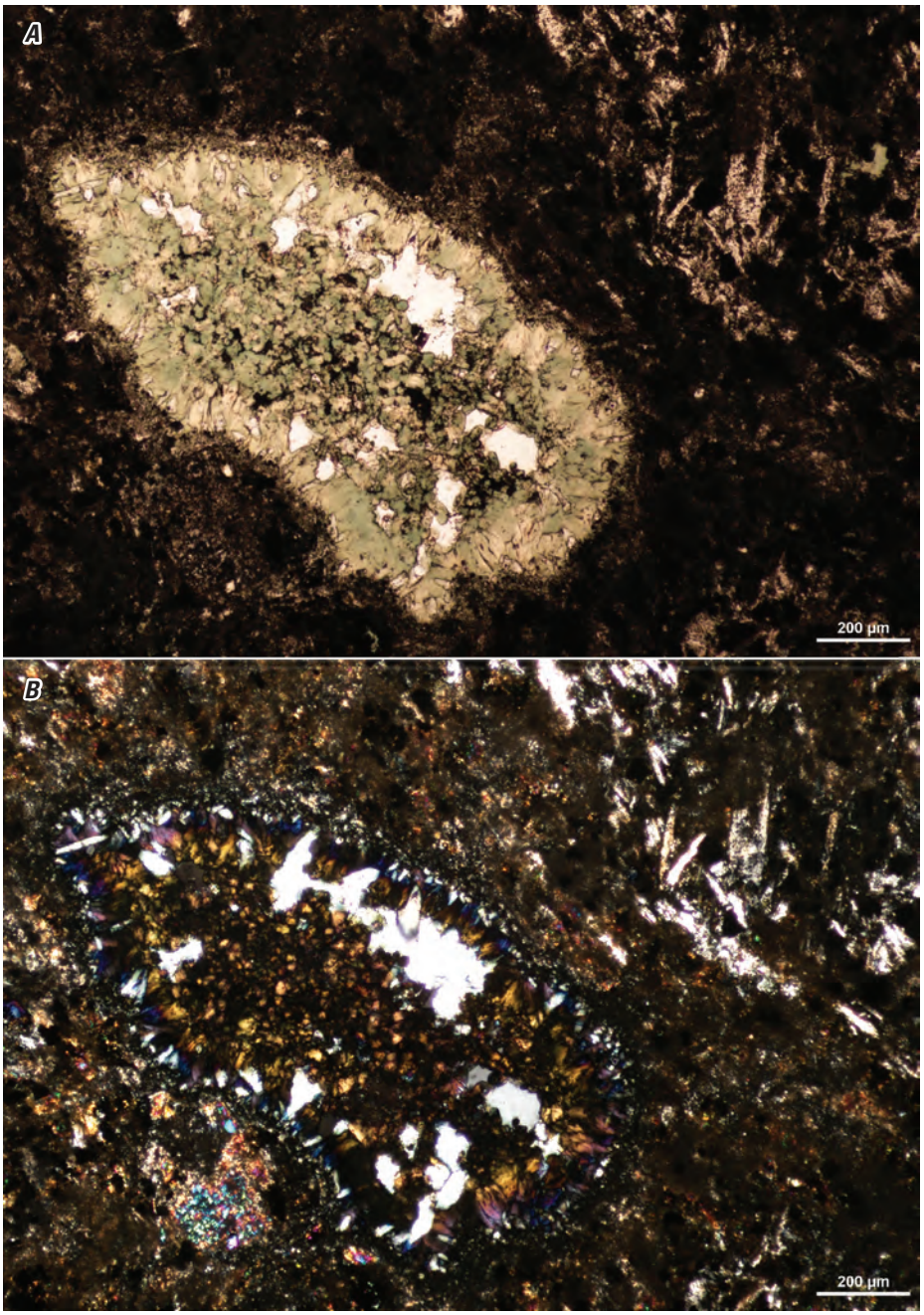

Figure 104. Pair of photomicrographs of a fragment from borehole W11499 from 5,310 to 5,320 feet depth in plane-polarized light (*A*) and cross-polarized light (*B*) showing a chlorite- and quartz-filled vug in altered volcanic porphyry. Term: µm, micrometer. Photomicrographs by Ryan Deasy, U.S. Geological Survey.

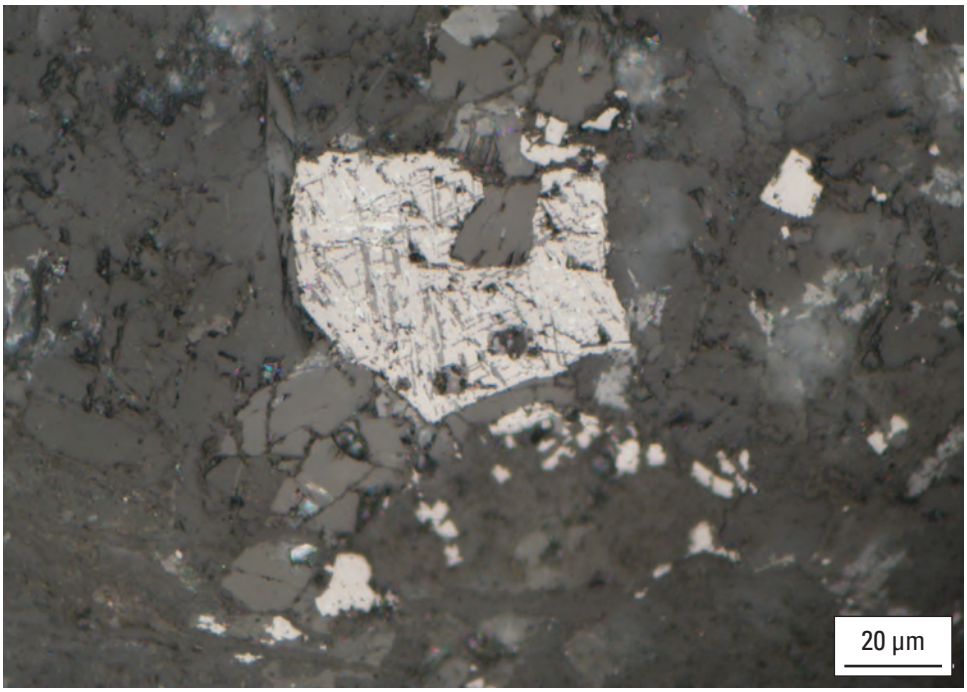

Figure 105. Photomicrograph in reflected light of a fragment from borehole W11499 from 5,330 to 5,340 feet depth showing exsolution of dark ilmenite/rutile(?) and bright hematite(?) in subhedral magnetite. Term: µm, micrometer. Photomicrograph by Ryan Deasy, U.S. Geological Survey.

Borehole W11771

This borehole encountered granitic basement rock at ~5,730 ft depth. Samples of cuttings from 5,740 to 5,770 ft depth were investigated in detail in this study.

Previous Work

Barnett (1975, p. 136) described basement rocks in this borehole as "Weathered igneous (drill cuttings)" and included the following remarks: "drill cuttings 5770-80: very coarsely crystalline, 70-75% orthoclase, 5-10% biotite and pyroxene 20% quartz." A U-Pb age from zircon of 551±6 Ma is given in Heatherington and others (1996), citing unpublished data.

Cuttings Log

Summary: The contact between granitic basement rock and overlying limestone occurs at ~5,730 ft depth. The bottom ~50-ft interval of sediment contains some lithic/feldspathic input, presumably from granite immediately below.

5,680–5,690 ft No granitic clasts. Limestone clasts contain a few percent very fine grained quartz.

5,690–5,700 ft Rare gray granitic clasts are subrounded with limestone cemented on margins. Limestone unit must be partly lithic/feldspathic.

5,700–5,710 ft AA.

5,710–5,720 ft Almost entirely limestone with minor well-rounded quartz grains present. Rare gray granitic clasts with pink-red K-feldspar. Granitic fragments have no reaction in HCl.

5,720–5,730 ft Micritic limestone is the dominant lithology. Granitic fragments more abundant than above, with pink, weathered granite more abundant than red. Well-rounded quartz grains are also present. Rare quartz grains 1 mm within micrite.

5,730–5,740 ft Roughly equal fractions of deep red fresh granite and pale, bleached clasts.

5,740–5,750 ft Less weathered material than above. Granitic fragments grade in color from red to orange to pink. Many orange K-feldspar cleavage fragments.

5,760–5,770 ft Deep-red granitic fragments with dark chloritized biotite splotches and gray quartz. Significant fraction of light pink weathered(?) granitic fragments. The color of granitic clasts is bimodal with pink and red.

5,770–5,780 ft AA, with fewer pink weathered fragments.

Thin Section Petrography

The observations below apply to samples from the following depth intervals:

5,740–5,750 ft

5,750–5,760 ft

5,760–5,770 ft

The basement rock here is a medium-grained (0.2–2 mm), idiomorphic granite. Feldspars are penetratively altered to sericite (illite), chlorite, and fine-grained oxides (fig. 106). K-feldspar grains include graphic quartz intergrowths. Carlsbad and penetration twins are common in plagioclase, but they are partially obscured by sericitization. Quartz grains are inclusion-free, and most have uniform extinction; undulose extinction is uncommon. Magnetite is a common accessory, occurring in most fragments as anhedral, commonly brecciated grains or as clusters of grains ranging from ~0.1 to 0.5 mm. Biotite is uncommon, occurring in only a few fragments as anhedral interstitial grains, and is pseudomorphically replaced by chlorite and stained with hematite.

Notes on XRD Methods and Results

Granitic cuttings fragments from 5,750 to 5,770 ft depth were handpicked under a binocular microscope to isolate the basement lithology from contaminants. The fragments were placed in an automated Brinkman grinder fitted with an agate mortar and pestle for initial grinding. The sample was continuously lubricated with acetone during grinding. The resulting coarse powder was further ground by hand in a corundum mortar and pestle, again lubricated with acetone, and allowed to air dry. An aliquot of the powder was placed in the 3×2×0.1-cm cavity of a Ti "front-pack" mount and scanned in a Bruker D8 diffractometer from an angular range of 2–80° 2Θ with a Cu anode and point detector. Semiquantitative mineral abundances (Deasy and others, 2024b) were obtained by Rietveld refinement modeling in TOPAS (Bruker AXS, 2011).

Because of the strong alteration that is evident in thin section, further analysis was performed to characterize the nature and abundances of clay minerals that are extant in the K-feldspar concentrates that were prepared for $^{40}Ar/^{39}Ar$ analysis; this analysis is described here. A small amount of the powdered sample was mixed in a slurry with distilled water on a quartz "zero background" plate, was allowed to air dry, and was then scanned on the Bruker D8 from 2 to 90° 2Θ at 6 sec/step. The mounted sample was then placed in an EG-saturated chamber for a minimum of 24 hours before being scanned again, immediately upon removal from the EG chamber, from 2 to 40° 2Θ at 4 sec/step.

Upon EG solvation of powdered K-feldspar concentrate, the broad, low-angle shoulder of the 6° 2Θ (d=1.4 nm) chlorite peak disappears and is replaced by a broad peak centered at ~5° 2Θ (d=1.74 nm), indicating the presence of a small amount of chlorite/smectite in the sample (fig. 107). There is no corresponding change in the shape or intensity of the ~9° 2Θ (d=1.0 nm) peak.

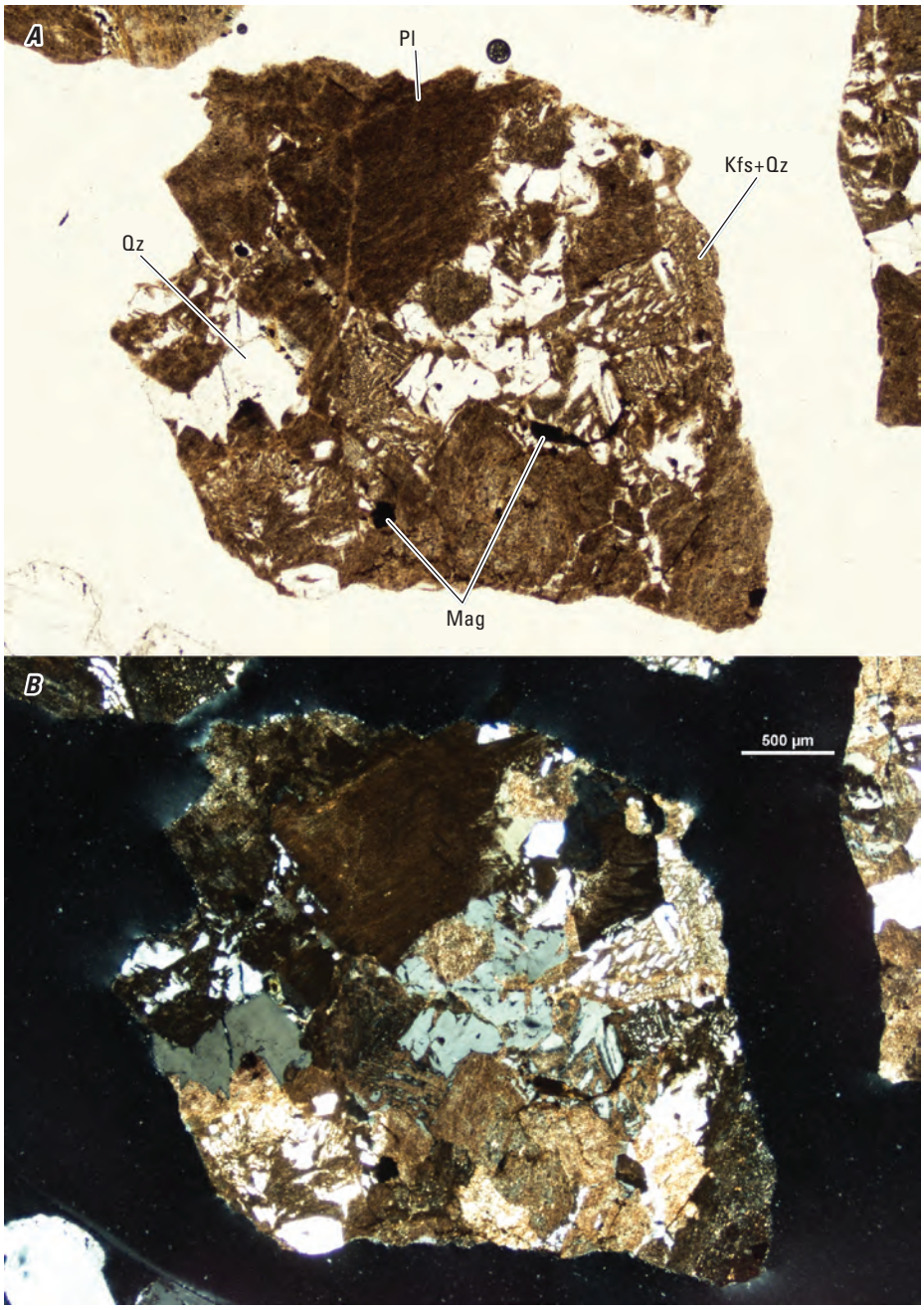

Figure 106. Thin section photomicrographs of a representative cuttings fragment from borehole W11771 from 5,740 to 5,750 feet depth in plane-polarized light (top) and cross-polarized light (bottom). Terms: Pl, plagioclase; Kfs+Qz, graphic intergrowths of potassium feldspar and quartz; Qz, quartz; Mag, magnetite; µm, micrometer. Photomicrographs by Ryan Deasy, U.S. Geological Survey.

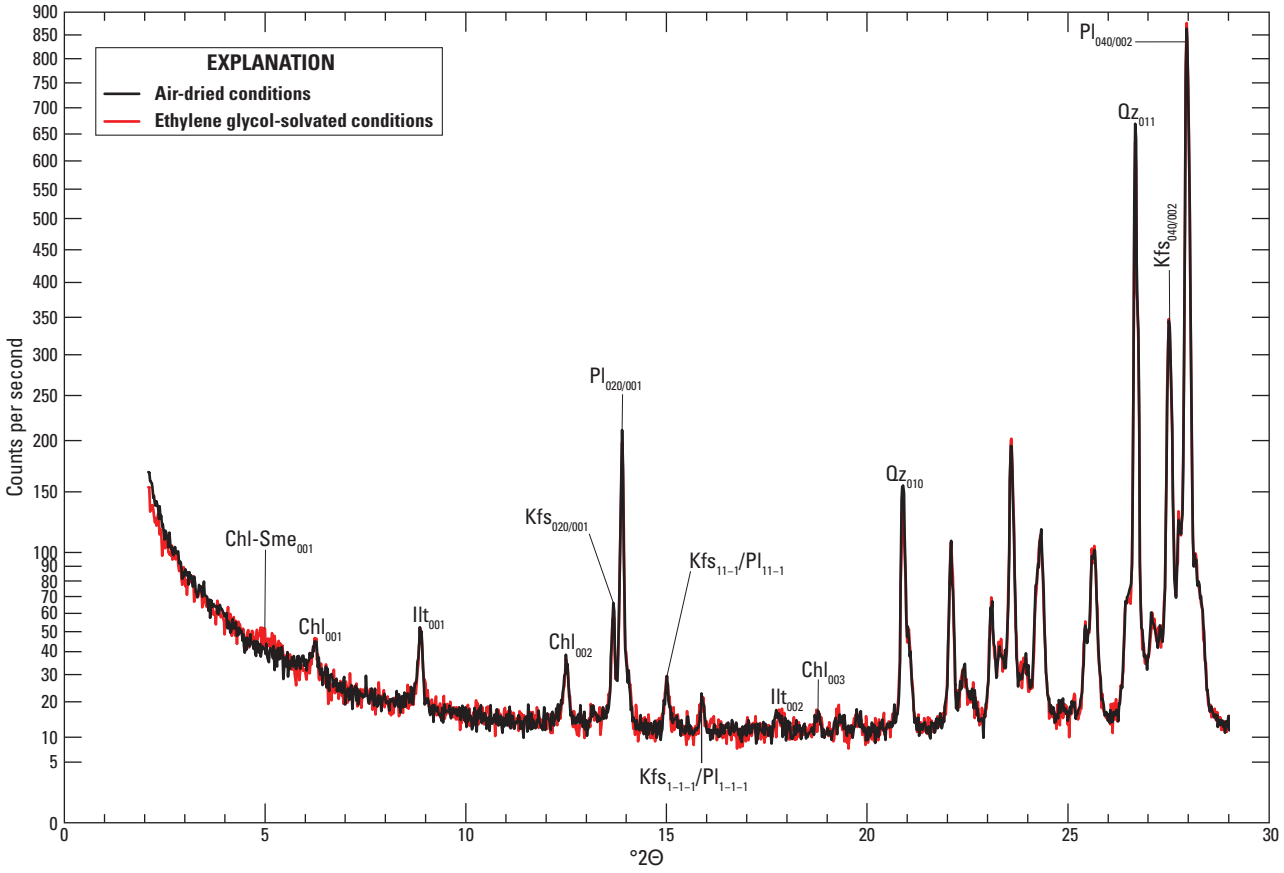

Figure 107. X-ray diffractograms of a potassium-feldspar concentrate from borehole W11771 from 5,710 to 5,740 feet depth under air-dried and ethylene glycol-solvated conditions. The *y*-axis is in square root scale. Selected peaks are labeled with mineral abbreviations; numbers in subscript denote Miller indices. Terms: °2Θ, degrees two theta; Chl-Sme, chlorite/smectite; Chl, chlorite; Ilt, illite; Kfs, potassium feldspar; Pl, plagioclase; Qz, quartz.

Borehole W1014

Drill core and cuttings of granodioritic basement rock were recovered from this borehole at 8,030–8,044 ft depth.

Previous Work

The ~14 ft of basement rock penetration in this borehole was first described in the scientific literature as an "altered and veined biotite granite" by F.F. Grout, as cited in Applin (1951, p. 19). A major element geochemical analysis of a sample from 8,034 to 8,042 ft depth is reported in Milton and Grasty (1969); a black-and-white, PPL photomicrograph of the sample is also included in the publication. Bass (1969) provides a detailed petrographic analysis of core from 8,042 to 8,044 ft depth, noting strong vein development and cataclastic zones, and estimates a crystallization age of ~530 Ma from rubidium-strontium (Rb-Sr) isotopic analyses of feldspar concentrates (n=4, with high scatter). A summary of the above, a brief core description, and a pair of black-and-white photomicrographs in PPL and XPL are included in Milton (1972). Dallmeyer (1989) inferred a cooling age of 527–535 Ma from $^{40}Ar/^{39}Ar$ analysis of biotite. U/Pb analyses by SHRIMP of six separated zircon grains returned two Archean ages and four Neoproterozoic ages and, from this, a somewhat older (~600 Ma) crystallization age for the granitoid was inferred by Mueller and others (1994). U/Pb analyses of zircon by laser ablation inductively coupled plasma mass spectrometry (LA-ICP-MS) returned an age of 554±13 Ma (n=15; Deasy and others, 2023), an age that is equivalent to the ages of other granitoids in the Osceola intrusive complex (unit €Zo of Mueller and others [2014]).

Core and Cuttings Log

Summary: The contact between granitic basement rock and overlying arkose occurs at ~8,030 ft depth. Weathered granitic regolith is a major component of the bottom ~10 ft of basal sediment. The sand grades upward into more evolved, quartz-dominated detritus. Recovered granitic material includes several bags of cuttings (fragments range from ~6 mm in maximum dimension to dust sized) and core chips.

7,990 ft Washed. Cuttings mostly 0.5–4 mm in maximum dimension. Lithologically diverse, comprising (in decreasing order of abundance) fine-grained (0.1–2 mm in diameter), well-rounded, translucent to white to yellow quartz grains, red and purple siltstone (including one large red clast, 8-mm in maximum dimension), greenish gray shale clasts (including one large elongate fragment 3×15 mm), and carbonate clasts. This interval contains finer grained and more lithologically diverse cuttings than below.

8,020 ft Washed. Dominantly subrounded to well-rounded, translucent to white to yellow quartz grains 1–4 mm with subordinate clasts of very fine grained red sandstone and siltstone. Red sedimentary grains contain a few percent muscovite grains and few percent pink to orange to white feldspar grains up to 0.5 mm. Muscovite grains are strongly aligned in bedding planes. Rare gray shale and marl clasts up to 5 mm are typically blocky to elongate and pencil-like (aspect ratios of 2:1–5:1) in habit and contain minor very fine grained, euhedral pyrite. Cuttings also contain rare (<1 percent) pink-orange feldspar cleavage fragments and rare sandstone lithics with opaques. Rare epidote clasts.

8,020–8,044 ft Washed. Cuttings are >90 percent fresh granitic clasts. Some oxide-red stained granite clasts are present. Minor components, interpreted as contaminant, include carbonate, redbed clasts, and rounded quartz grains.

8,020 ft Unwashed. Cuttings of red-orange quartz arenite, clasts up to 1.2 cm with 0.1–4-mm subrounded to rounded quartz grains. Individual, loose quartz grains are subrounded to well rounded, clear to white yellow to orange, all <3 mm. Includes ~5–10 percent gray shaley clasts. No conspicuous K-feldspar grains or granitic clasts.

8,020–8,044 ft Washed. Cuttings, 1–6 mm in diameter, are dominantly (>90 percent) angular oxide-red granitic lithic fragments and angular, white to translucent quartz grains, with subordinate "fresh" granitic fragments, rare platy shale clasts, and rare subrounded quartz grains.

8,034–8,042 ft Red, oxide-stained brown chips and cuttings, ~1–17 mm in diameter, of penetratively weathered, coarse-grained granitic rock.

8,042–8,042.5 ft Granitic chips, ~1–8 mm in diameter, comprise pink K-feldspar, glassy to gray quartz, white plagioclase, and green chloritized biotite. No apparent vein material.

8,042.5–8,043.5 ft Two large granitic chips AA, one with submillimeter quartz(?) veins (fig. 108).

8,043.5–8,044.5 ft Large chip (fig. 109). Coarse-grained, massive granitic chip with pink K-feldspar, white to dark gray plagioclase, translucent quartz (1–4 mm), and highly chloritized (green) biotite, all 1–4 mm in diameter, cut by pink dolomite vein (2 mm wide, tapers to <1 mm) and ~0.5-mm wide quartz veins.

Figure 108. Photograph of granodioritic core chips from borehole W1014 from 8,042.5 to 8,043.5 feet depth. The ruler scale is in centimeters. Photograph by Ryan Deasy, U.S. Geological Survey.

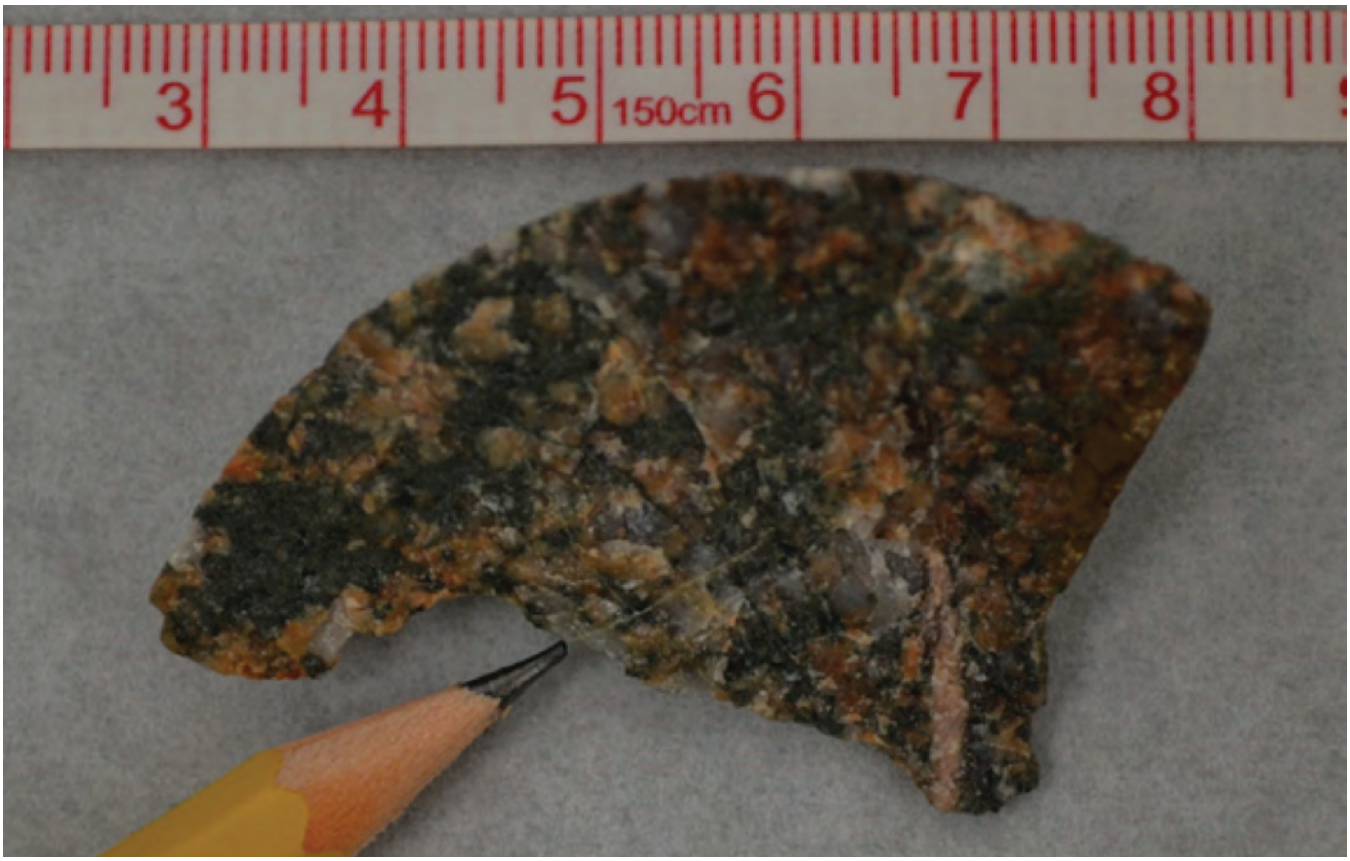

Figure 109. Photograph of a granodioritic core chip from borehole W1014 from 8,043.5 to 8,044.5 feet depth. Two pink dolomite veins are present in the chip: (1) on the right side of the chip, vertical in this view and tapering from bottom to top, and (2) parallel to and in line with the pencil tip and also thinner than the other vein. The width of the pencil is 7 millimeters; the ruler scale is in centimeters. Photograph by Ryan Deasy, U.S. Geological Survey.

Thin Section Petrography

8,034–8,042 ft Thin section of 3 core chips, each 0.5–1 cm in diameter, of weakly altered, coarse-grained (1–2 mm) granitic rock (fig. 110) with roughly equal amounts of quartz, plagioclase, and K-feldspar, with subordinate chloritized biotite and minor opaque(s). Feldspar grains are highly altered with fine-grained opaques, sericite in microcrystalline mats, isolated white mica (~50 µm), and chlorite throughout grains (fig. 111). Plagioclase is generally more thoroughly altered than K-feldspar. Deformation twins in plagioclase are present. K-feldspar grains commonly contain subgrain boundaries marked by strings of very fine grained feldspar. Biotite books (up to 0.5 mm thick) with stubby (1:1) to elongate (4:1) aspect ratios, are pseudomorphically replaced by chlorite; in most grains, replacement is >90 percent. Chlorite pseudomorphs are weakly pleochroic in green in PPL, have anomalous blue interference colors in XPL, and contain opaque inclusions everywhere. Euhedral apatite and zircon grains occur in close association with biotite. Quartz grains are mostly free of inclusions and show common subgrain boundaries in XPL. Subgrain rotation is demonstrated by differing lattice orientations in XPL with gypsum plate inserted. Other deformation microstructures in quartz include, in decreasing order of prevalence, grain boundary migration, undulose extinction, and bulging. One clast contains a ~50–100-µm thick quartz vein with an irregular, nonplanar wall. In the quartz vein, fibrous grains oriented at a high angle to the wall have recrystallized grain boundaries, suggesting slight ductile vein transposition. Discontinuous patches of opaques+carbonate along quartz vein walls suggest local (<0.5 cm) control on vein-fluid composition.

8,042–8,042.5 ft Thin section of 2 core chips, roughly 0.5 cm and 1 cm in diameter (fig. 112). Mineralogy and texture are similar to the sample from 8,034 to 8,042 ft depth, except that feldspars in this sample are replaced with fine-grained epidote/clinozoisite in addition to sericite. Veins are filled with epidote, epidote+quartz, or carbonate.

8,043.5–8,044.5 ft Thin section of a single core chip ~2 cm in diameter (fig. 113). Plagioclase grains in this sample have much more strongly developed and more common deformation twins than in other samples from borehole W1014 (fig. 114). Chlorite occurs in radial aggregates between feldspar grains. Biotite books are not present in this fragment. Veins are more abundant than in other intervals for borehole W1014 and are filled with epidote, dolomite, or quartz with or without chlorite. One vein is zoned with a core of fine-grained quartz and walls comprising fine-grained, radial, massive chlorite, green and weakly pleochroic in PPL and dark green to brown in XPL. Epidote vein is a submillimeter fracture, massive and microcrystalline.

Notes on XRD Methods and Results

Hand-picked core chips from two intervals (8,034–8,042 and 8,043.5–8,044.5 ft depth) were ground to a powder in an automated Brinkman grinder fitted with an agate mortar and pestle. The samples were continuously lubricated with acetone during grinding. The resulting powders were further ground by hand in a corundum mortar and pestle, again lubricated with acetone, and allowed to air dry. Aliquots of each powder were placed in 3×2×0.1-cm cavities of Ti "front-pack" mounts and scanned in a Bruker D8 diffractometer from an angular range of 2–70° 2Θ with a Cu anode and point detector. Semiquantitative mineral abundances (Deasy and others, 2024b) were obtained by Rietveld refinement modeling in TOPAS (Bruker AXS, 2011).

The strongly asymmetrical shape of the ~9° 2Θ (d=1.0 nm) peak in diffraction results from the sample from 8,034 to 8,042 ft depth (fig. 115) prompted re-analysis to characterize the nature and abundances of clay minerals, as follows. Small amounts of each powdered sample were mixed in a slurry with distilled water on quartz "zero background" plates, were allowed to air dry, and were then scanned on the Bruker D8 from 2 to 70° 2Θ at 6 sec/step. The mounted samples were then placed in an EG-saturated chamber for a minimum of 24 hours before being scanned again, immediately upon removal from the EG chamber, from 2 to 50° 2Θ at 2 sec/step.

The asymmetrical ~9° 2Θ (d=1.0 nm) peak in the sample from 8,034 to 8,042 ft depth becomes more symmetrical upon EG solvation by both a decrease in lower angle intensity and an increase in higher angle intensity, and there is a corresponding slight increase in the intensity of the peak at ~15.8° 2Θ (fig. 115). This is attributed to the presence of a small amount of illite/smectite. Although interference from other phyllosilicate peaks is strong, the positions of the illite/smectite peaks suggest ~50 percent smectite in the illite/smectite (Moore and Reynolds, 1997, table 8.3).

Ethylene glycol solvation has no effect on diffraction results from the sample from 8,043.5 to 8,044.5 ft depth (fig. 116), demonstrating the absence of expandable clays in this interval. To constrain the abundance of the smectitic component in the sample from 8,034 to 8,042 ft depth, an aliquot was spiked with corundum and reanalyzed on the Bruker D8 from 2 to 80° 2Θ. Modeling in TOPAS estimates the abundance of an "amorphous" component—interpreted here as the abundance of illite/smectite—of ~0.5 wt. pct.

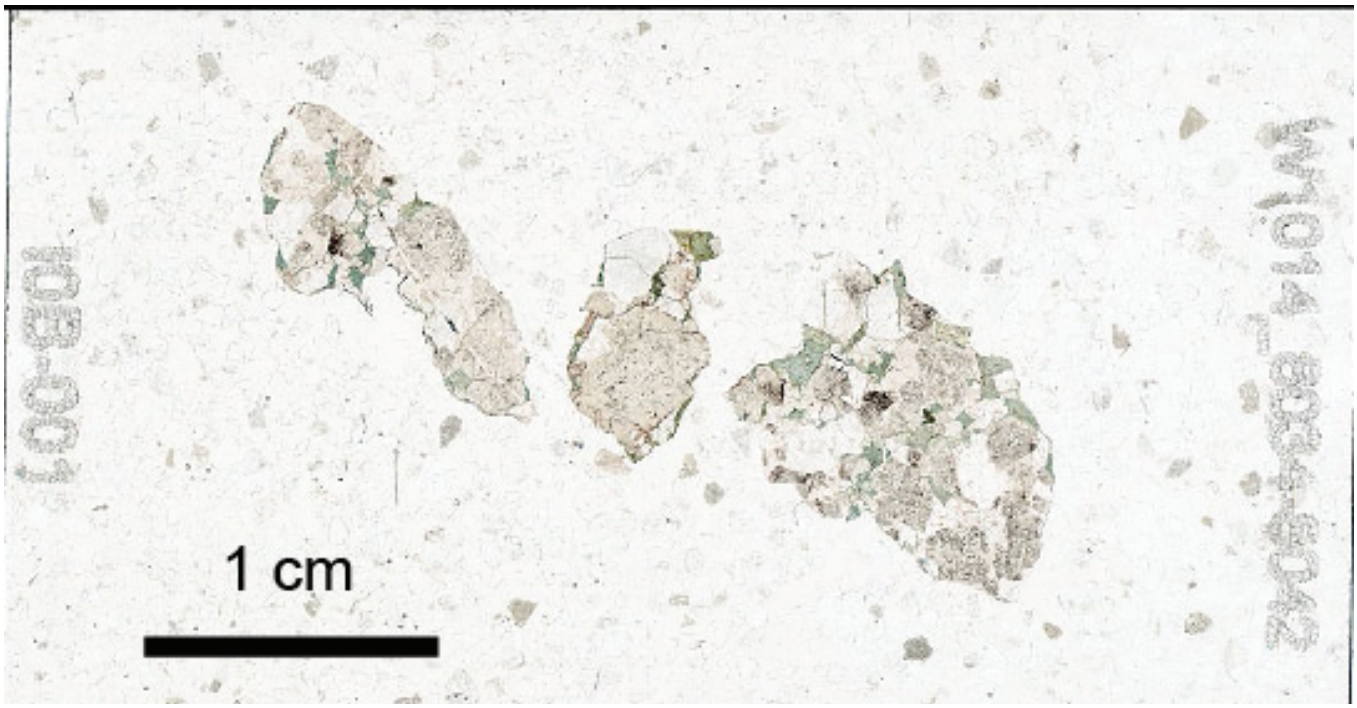

Figure 110. Scan of a full, standard-sized thin section in plane-polarized light of core chips from borehole W1014 from 8,034 to 8,042 feet depth. Term: cm, centimeter. Photomicrograph by Ryan Deasy, U.S. Geological Survey.

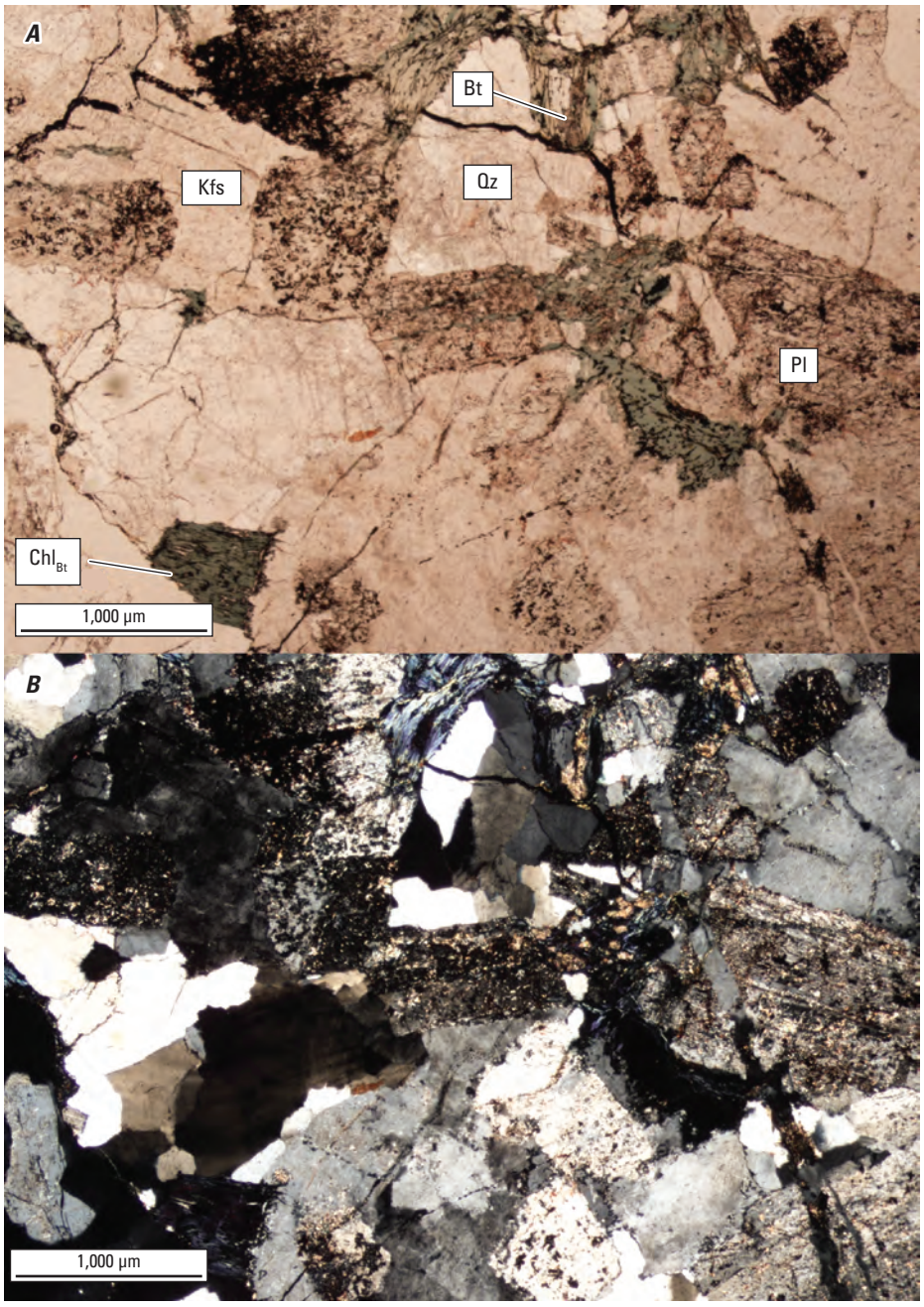

Figure 111. Pair of representative photomicrographs in plane-polarized light (*A*) and cross-polarized light (*B*) of granodiorite from borehole W1014 from 8,034 to 8,042 feet depth. Plagioclase (Pl) is strongly altered to epidote, carbonate minerals, and sericite. Potassium feldspar (Kfs) is less altered than plagioclase. Quartz (Qz) is divided into subequant subgrains. Biotite (Bt) is partially to completely pseudomorphically replaced by chlorite (Chl). A thin Qz vein crosscuts the right half of the image. Terms: Chl_{Bt}, chlorite pseudomorph after biotite; µm, micrometer. Photomicrographs by Ryan Deasy, U.S. Geological Survey.

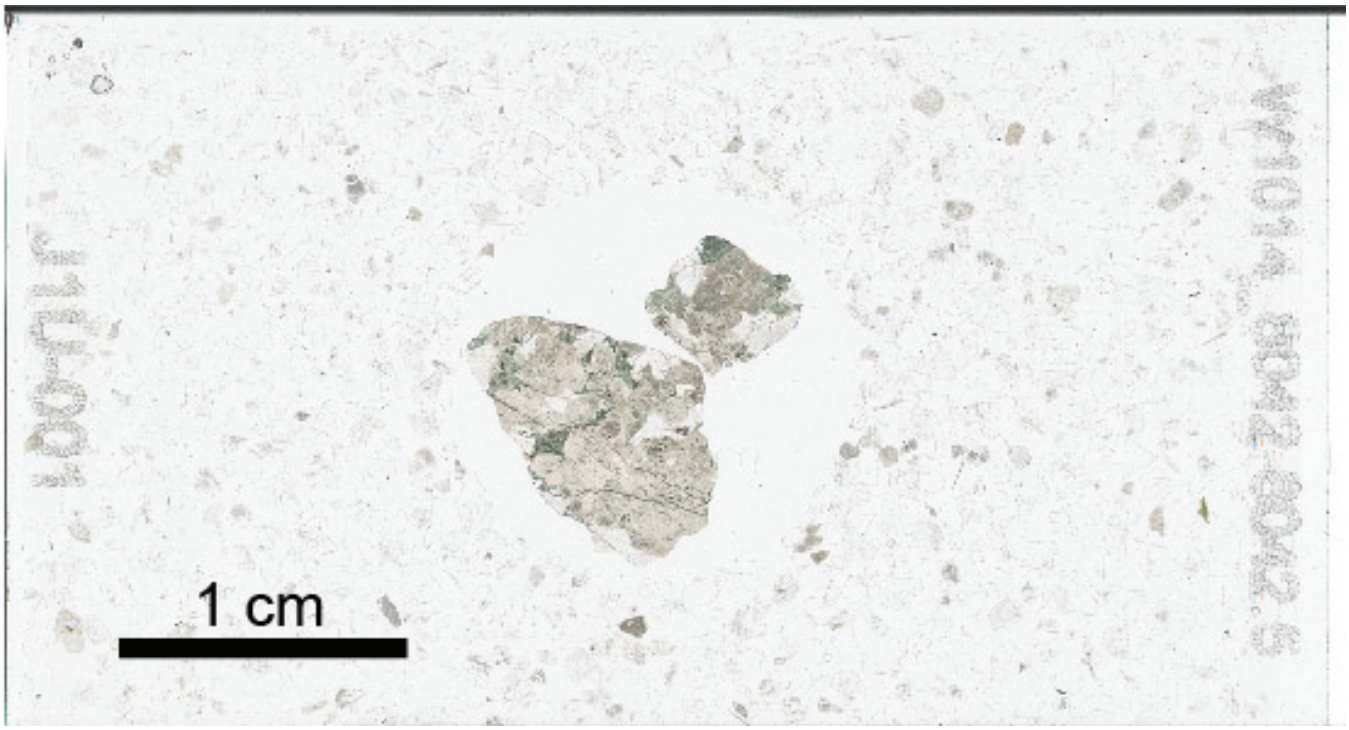

Figure 112. Scan of a full, standard-sized thin section in plane-polarized light of core chips from borehole W1014 from 8,042 to 8,042.5 feet depth. Term: cm, centimeter. Photomicrograph by Ryan Deasy, U.S. Geological Survey.

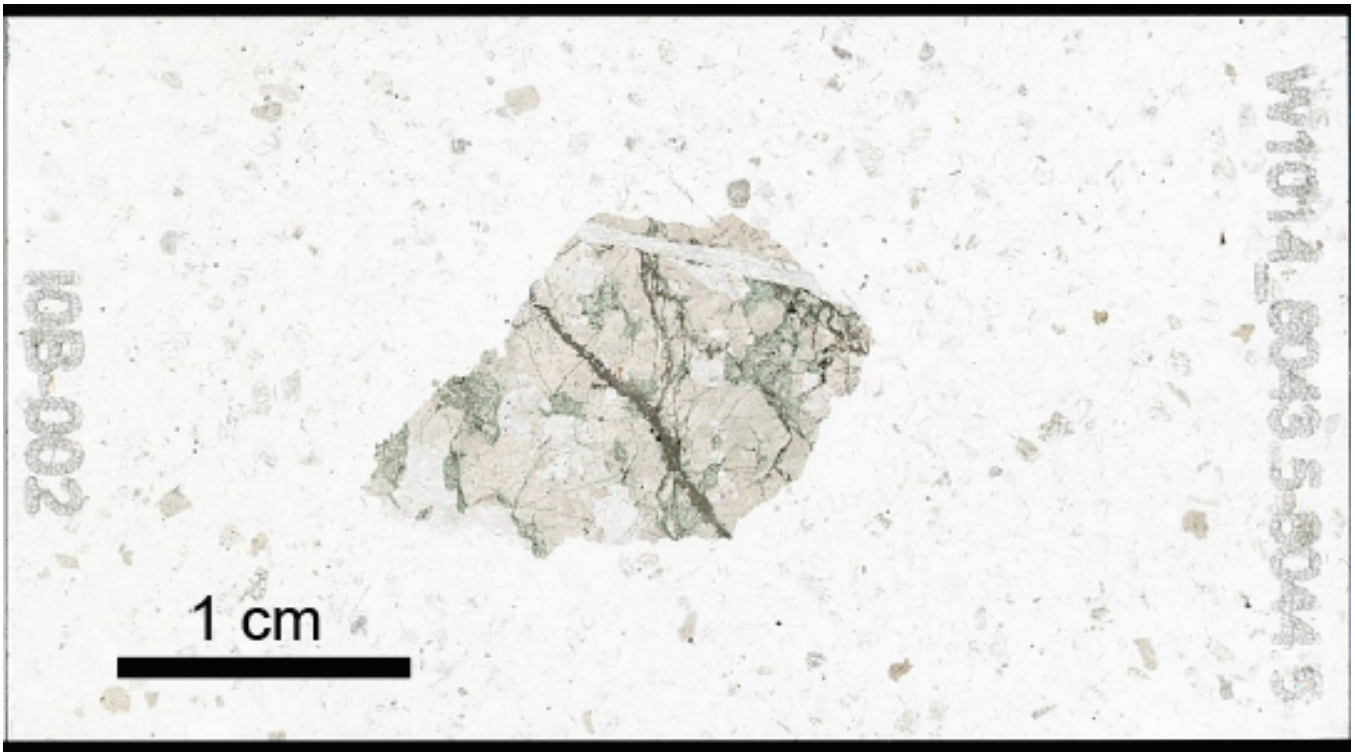

Figure 113. Scan of a full, standard-sized thin section in plane-polarized light of a core chip from borehole W1014 from 8,043.5 to 8,044.5 feet depth. Term: cm, centimeter. Photomicrograph by Ryan Deasy, U.S. Geological Survey.

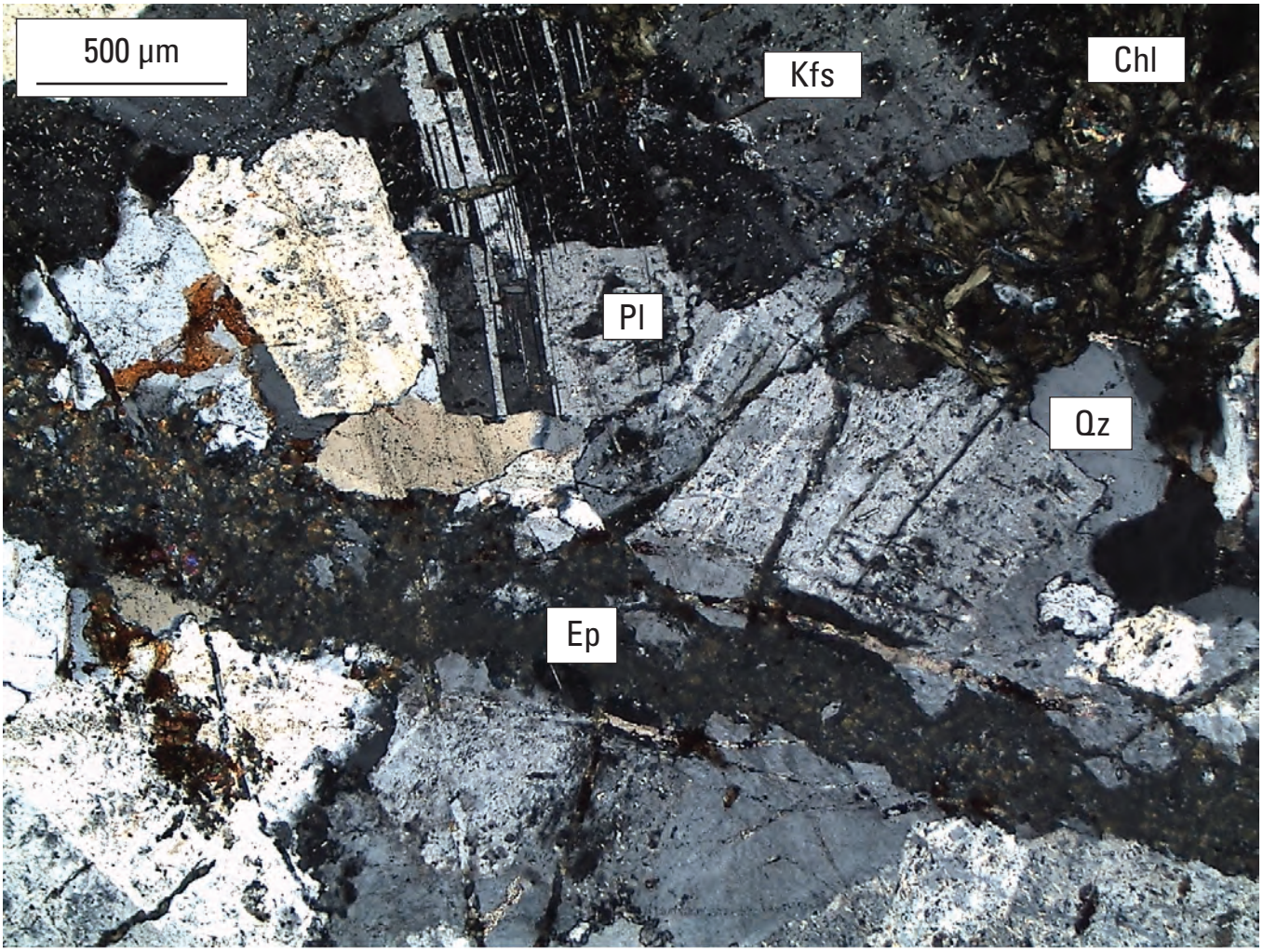

Figure 114. Photomicrograph in cross-polarized light of granodioritic rock from borehole W1014 from 8,043.5 to 8,044.5 feet depth. Magmatic feldspars are partially altered to epidote, carbonate minerals, and sericite, but plagioclase (Pl) is more strongly altered than potassium feldspar (Kfs). Chlorite (Chl) has pseudomorphically replaced biotite. Deformation features include subgrain development in feldspars and quartz (Qz) and deformation twins in Pl. A vein of fine-grained epidote (Ep) crosscuts the sample. Term: µm, micrometer. Photomicrograph by Ryan Deasy, U.S. Geological Survey.

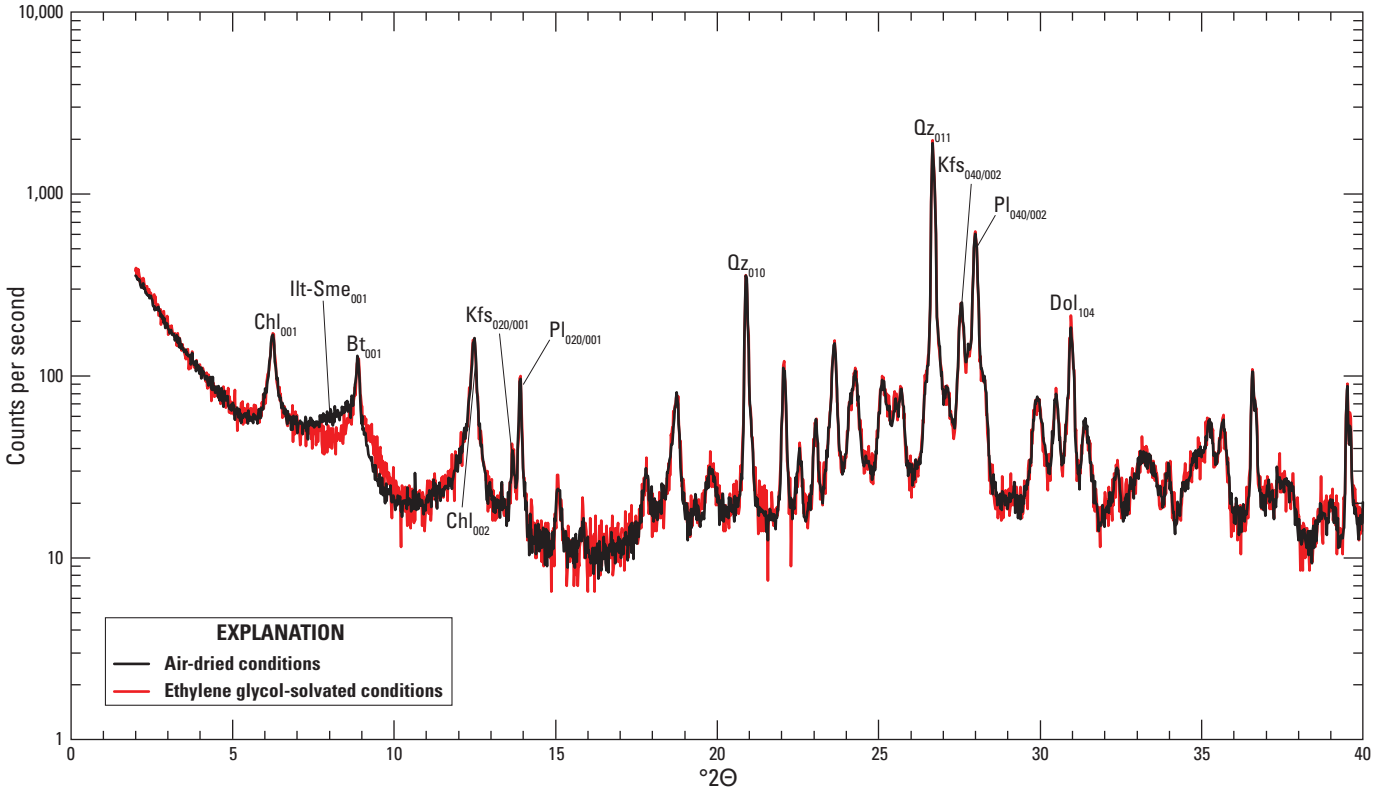

Figure 115. X-ray diffractograms of granitic rock from borehole W1014 from 8,034 to 8,042 feet depth under air-dried and ethylene glycol-solvated conditions. The *y*-axis is in logarithmic scale. Selected peaks are labeled with mineral abbreviations; numbers in subscript denote Miller indices. Terms: °2Θ, degrees two theta; Chl, chlorite; Ilt-Sme, illite/smectite; Bt, biotite; Kfs, potassium feldspar; Pl, plagioclase; Qz, quartz; Dol, dolomite.

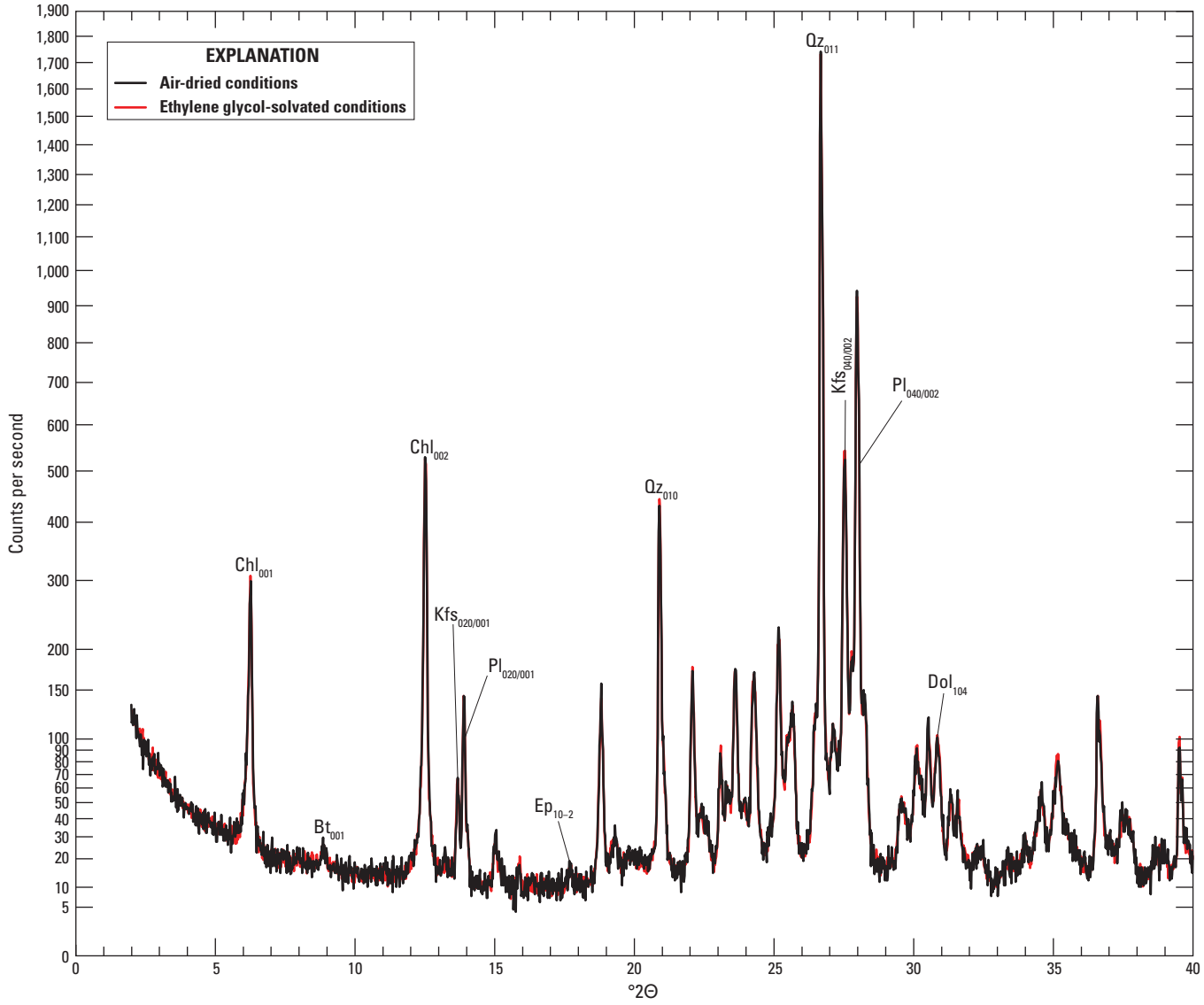

Figure 116. X-ray diffractograms of granitic rock from borehole W1014 from 8,043.5 to 8,044.5 feet depth under air-dried and ethylene glycol-solvated conditions. The *y*-axis is in square root scale. Selected peaks are labeled with mineral abbreviations; numbers in subscript denote Miller indices. Terms: °2Θ, degrees two theta; Chl, chlorite; Bt, biotite; Kfs, potassium feldspar; Pl, plagioclase; Ep, epidote; Qz, quartz; Dol, dolomite.

Borehole W1411

This borehole encountered rhyolitic basement rock at 8,740–8,798 ft depth. Core chips from 8,744 to 8,756 ft depth were investigated in detail in this study.

Previous Work

Applin (1951) reports 58 ft of rhyolite beginning at 8,740 ft depth. A sample from 8,781 ft depth returned a whole-rock K-Ar age of 173±4 Ma (Grasty and Wilson, 1967). Milton (1972) provides a core description and several photomicrographs.

Thin Section Petrography

The basement lithology in this borehole is a rhyolite porphyry dominated by a moderately indurated microcrystalline groundmass with randomly oriented quartz, plagioclase, and K-feldspar phenocrysts up to 2.5 mm across that compose 10–15 percent of the rock by volume (figs. 117 and 118). Ellipsoidal chloritic and opaque-rich lithic clasts are also randomly oriented and make up another ~2–5 percent volume. One lithic clast contains relatively coarse-grained chlorite and epidote. Opaque grains, making up another ~1 percent of total volume, include subhedral magnetite with ilmenite lamellae and round ilmenite-rutile symplectites (fig. 119). Zircon grains are rare, small (≤40×≤20 µm), subhedral to euhedral, commonly have broken edges, and have oscillatory zoning in BSE. The massive matrix comprises equant quartz and elongate feldspar grains up to 50 µm in diameter and 200 µm in length, respectively (figs. 119–122). Much of the rock is overprinted by Liesegang rings, leaving sharp contacts between red-orange hematite- and goethite-bearing domains and tan non-oxidized domains (figs. 117, 118, 121). All quartz grains have uniform extinction and many are equant and round, although some grains retain crystal faces (fig. 120). The round grains are uniformly dim in CL with quartz overgrowths that are bright in CL (fig. 123), whereas the quartz grains with subhedral to euhedral shapes have bright, oscillatory zoning in CL and lack overgrowths (fig. 124). It is likely, then, that at least some of the rounded grains are sedimentary xenocrysts. K-feldspar phenocrysts are subhedral to euhedral, are pervasively mottled with quartz lamellae (fig. 125), and are partially altered to illite (figs. 120 and 121). Although fine-grained, lath-shaped plagioclase composes a significant fraction of the groundmass (fig. 122), large plagioclase phenocrysts are uncommon. Rare large plagioclase grains are up to 2 mm in length, are euhedral with slightly rounded or resorbed corners, and have oscillatory zoning (figs. 122 and 126). In contrast to K-feldspar, plagioclase is unaltered except along fractures and contains only patchy domains of exsolved quartz+albite+K-feldspar (fig. 126). Vugs in the groundmass are rare, small (<20 µm across), lined with euhedral quartz, and locally contain REE-rich carbonates or other unusual minerals (fig. 127). Evidence of deformation is limited to the apparently in situ brecciation of many quartz grains (figs. 121 and 123).

Notes on XRD Methods and Results

Representative core chips from the following depth intervals were shattered in a steel percussion mortar to pea-sized or smaller fragments:

8,744–8,750 ft

8,750–8,753 ft

8,753–8,756 ft

These were placed in an automated Brinkmann grinder fitted with an agate mortar and pestle. The sample was continuously lubricated with acetone during grinding. The sample was then ground further by hand in a corundum mortar and pestle, again continuously lubricated with acetone. An aliquot of the resulting fine powder was loaded into the 2×3×0.1-cm cavity of a Ti "front-pack" mount and analyzed on a Bruker D8 diffractometer with a Cu anode and point detector from an angular range of 2–100° 2Θ at a scanning rate of 8–14 sec/0.02° step.

In order to characterize the clay populations in this sample, an aliquot of the sample from 8,750 to 8,753 ft depth was mounted on a quartz "zero background" plate in a slurry with distilled water and allowed to air dry before being analyzed on the Bruker D8 from 2 to 70° 2Θ at 9 sec/step. The mounted sample was then placed in a chamber with an atmosphere saturated with EG. After 24 hours, the sample was again scanned, immediately upon removal from the EG chamber, on the Bruker D8 from 2 to 40° 2Θ at 2 sec/step. There was no change in the diffraction pattern as a result of EG-solvation, indicating the absence of expandable clays in this sample.

Semiquantitative mineral modes in each sample were determined using TOPAS (Bruker AXS, 2011) and the Rietveld method and are available in Deasy and others (2024b). K-feldspar populations were modeled with a combination of microcline, orthoclase, and sanidine models. A major and trace element geochemical analysis of core chips from 8,744 to 8,756 ft depth is available in Deasy and others (2024a).

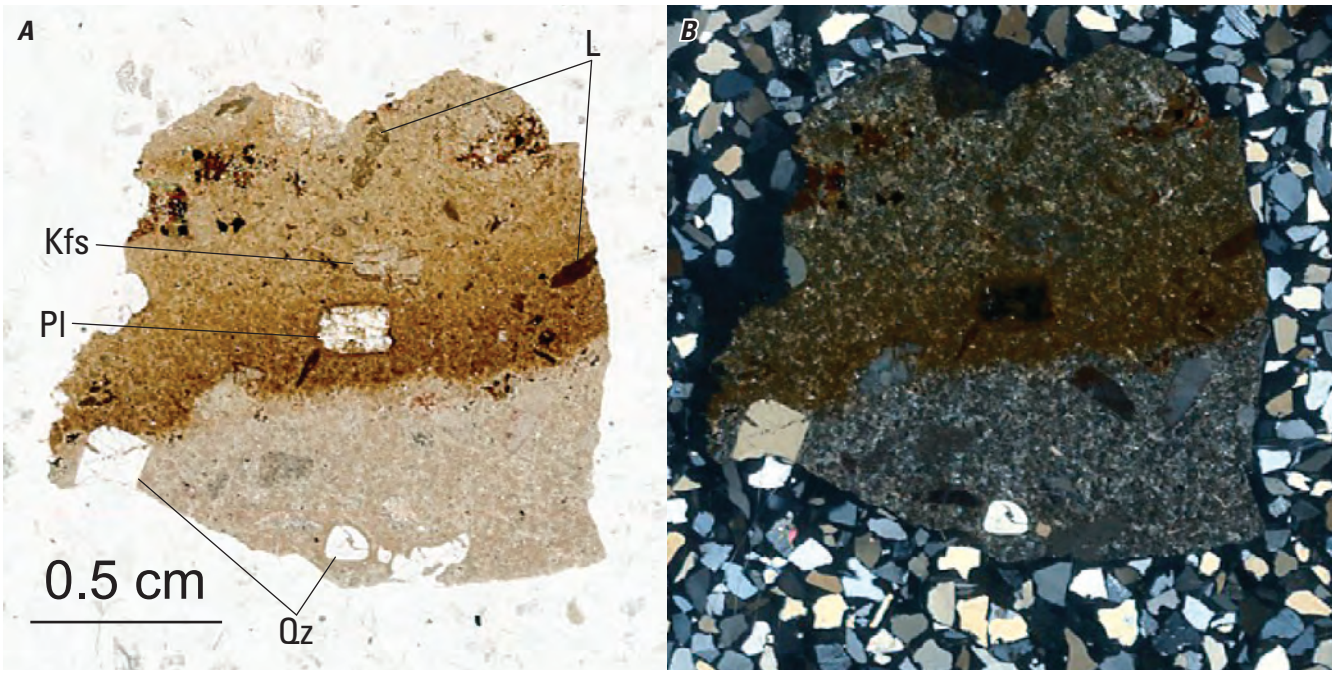

Figure 117. Pair of full thin section scans of a sample of rhyolite from borehole W1411 from 8,744 to 8,750 feet depth in plane-polarized light (*A*) and cross-polarized light (*B*). Terms: L, lithic clast; Kfs, potassium feldspar; Qz, quartz; Pl, plagioclase; cm, centimeter. Photomicrographs by Ryan Deasy, U.S. Geological Survey.

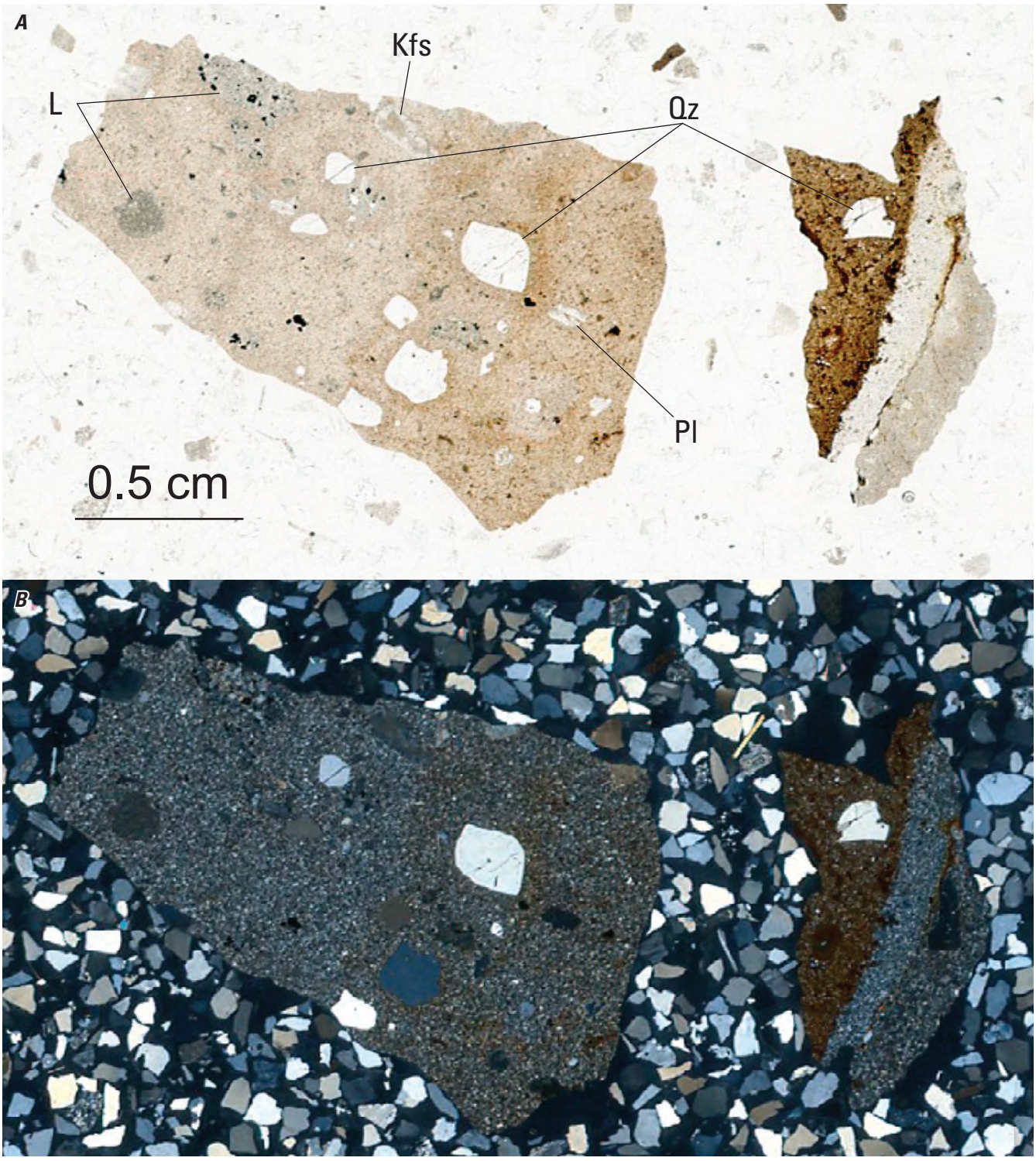

Figure 118. Pair of full thin section scans of a sample from borehole W1411 from 8,750 to 8,753 feet depth in plane-polarized light (*A*) and cross-polarized light (*B*). Terms: L, lithic clast; Kfs, potassium feldspar; Qz, quartz; Pl, plagioclase; cm, centimeter. Photomicrographs by Ryan Deasy, U.S. Geological Survey.

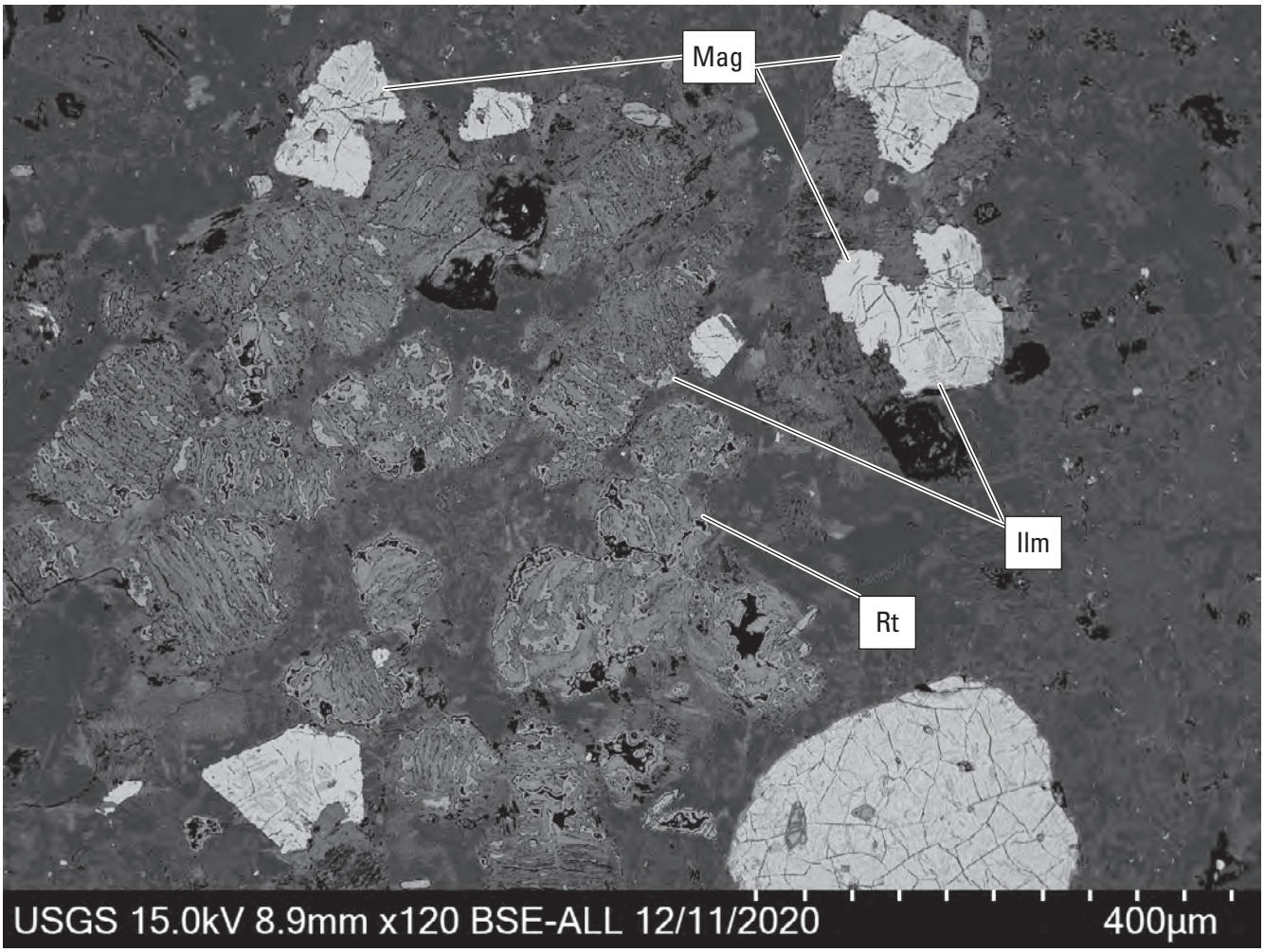

Figure 119. Back-scattered electron (BSE) image of symplectic magnetite (bright) and round ilmenite grains from borehole W1411 from 8,744 to 8,750 feet depth. Text in the bottom left identifies data source (USGS); operating conditions including beam potential in kilovolts (15.0 kV), working distance in millimeters (8.9 mm), and image magnification in multiples of actual size (120 times); and date of acquisition (12/11/2020). Terms: Mag, magnetite; Ilm, ilmenite; Rt, rutile; USGS, U.S. Geological Survey; kV, kilovolt; mm, millimeter; BSE-ALL, back-scattered electron, all energies; µm, micrometer. Photomicrograph by Ryan Deasy, U.S. Geological Survey.

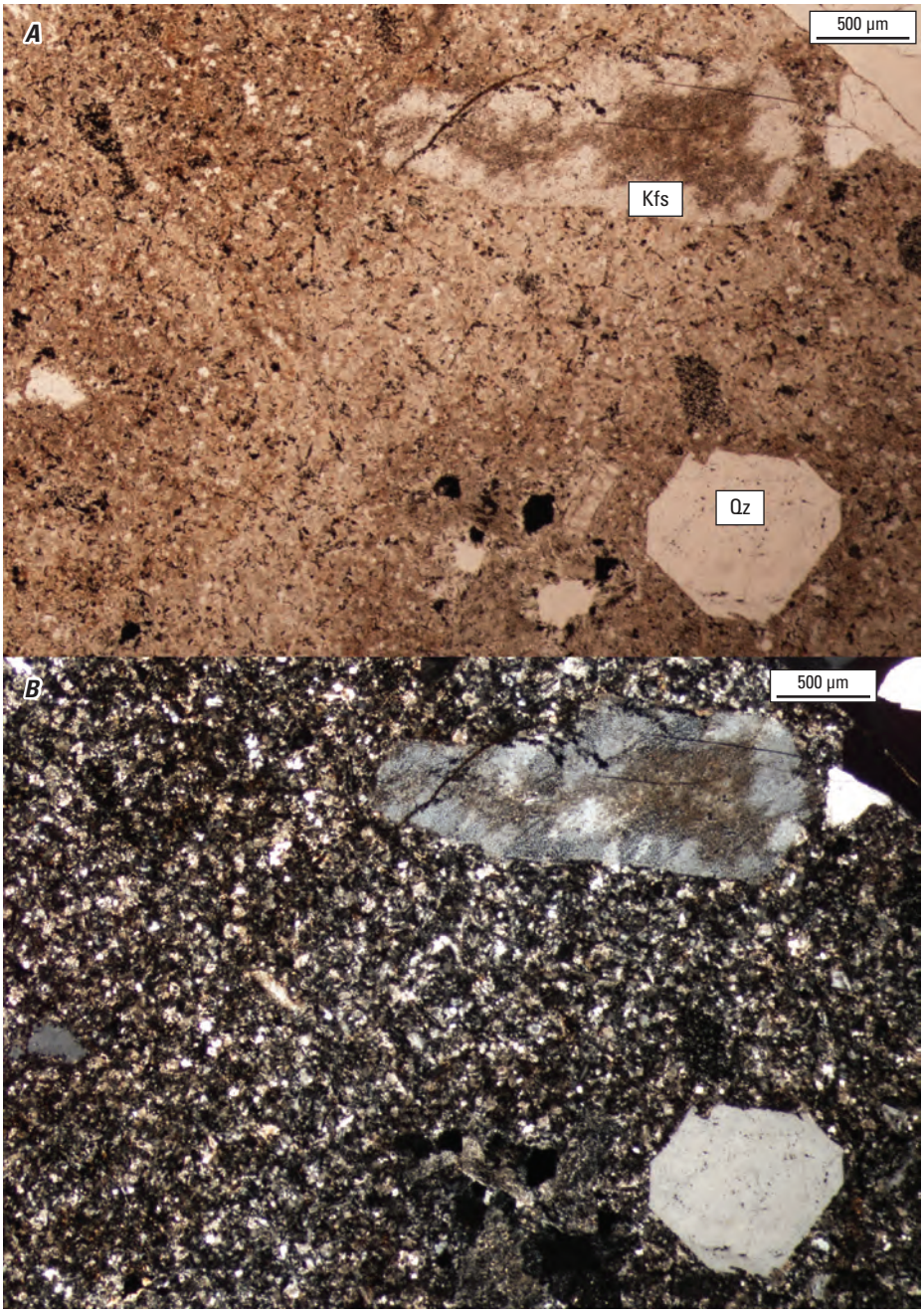

Figure 120. Pair of thin section photomicrographs of a sample from borehole W1411 from 8,750 to 8,753 feet depth in plane-polarized light (*A*) and cross-polarized light (*B*). Phenocrysts include potassium feldspar (Kfs) and quartz (Qz). Term: µm, micrometer. Photomicrographs by Ryan Deasy, U.S. Geological Survey.

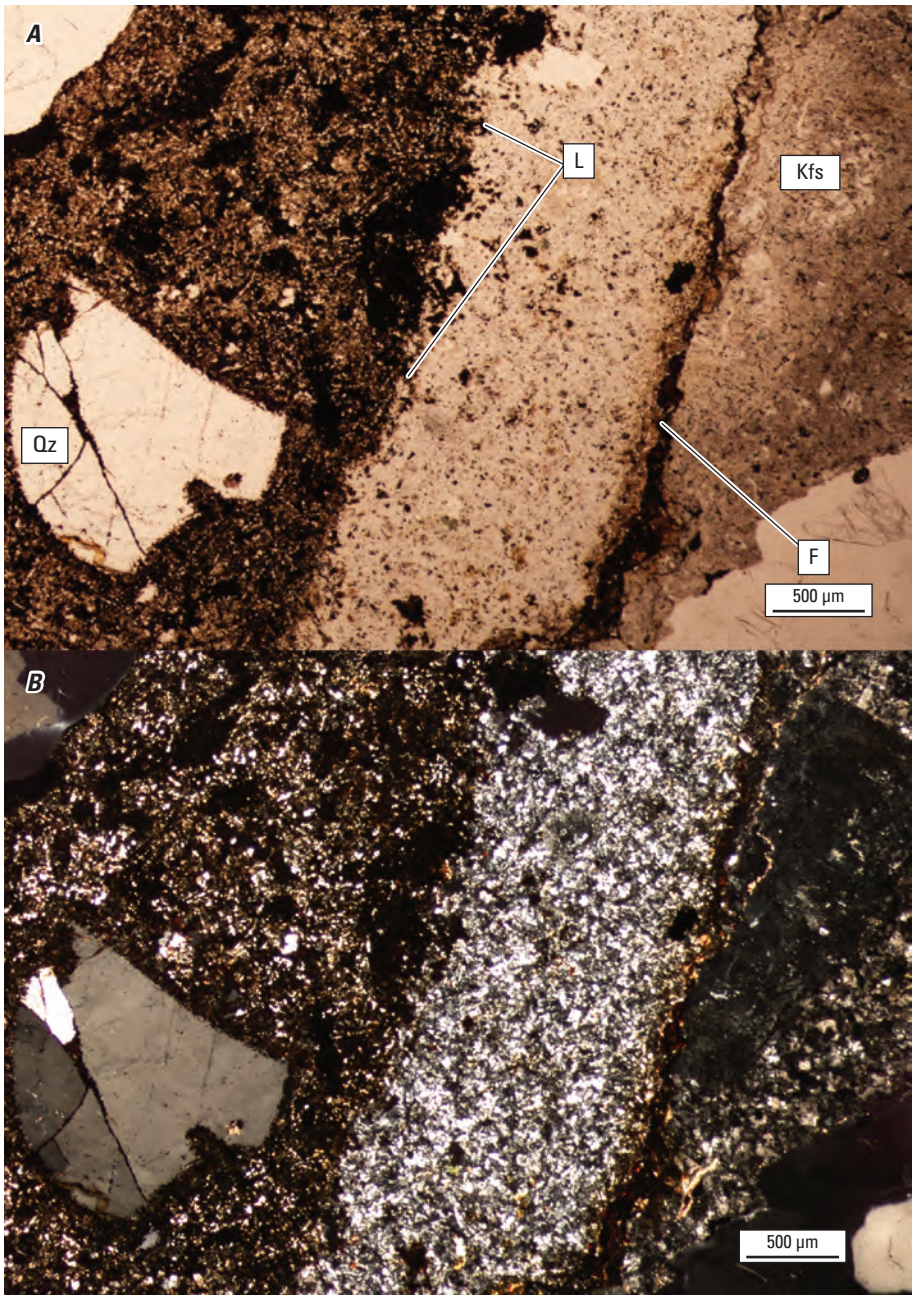

Figure 121. Pair of thin section photomicrographs of a sample from borehole W1411 from 8,750 to 8,753 feet depth in plane-polarized light (*A*) and cross-polarized light (*B*). A rounded and broken (probably detrital) quartz (Qz) grain is brecciated in place. Potassium feldspar (Kfs) is highly altered but not brecciated. Redoximorphic alteration occurs along fractures (F) and as Liesegang banding (L). Term: µm, micrometer. Photomicrographs by Ryan Deasy, U.S. Geological Survey.

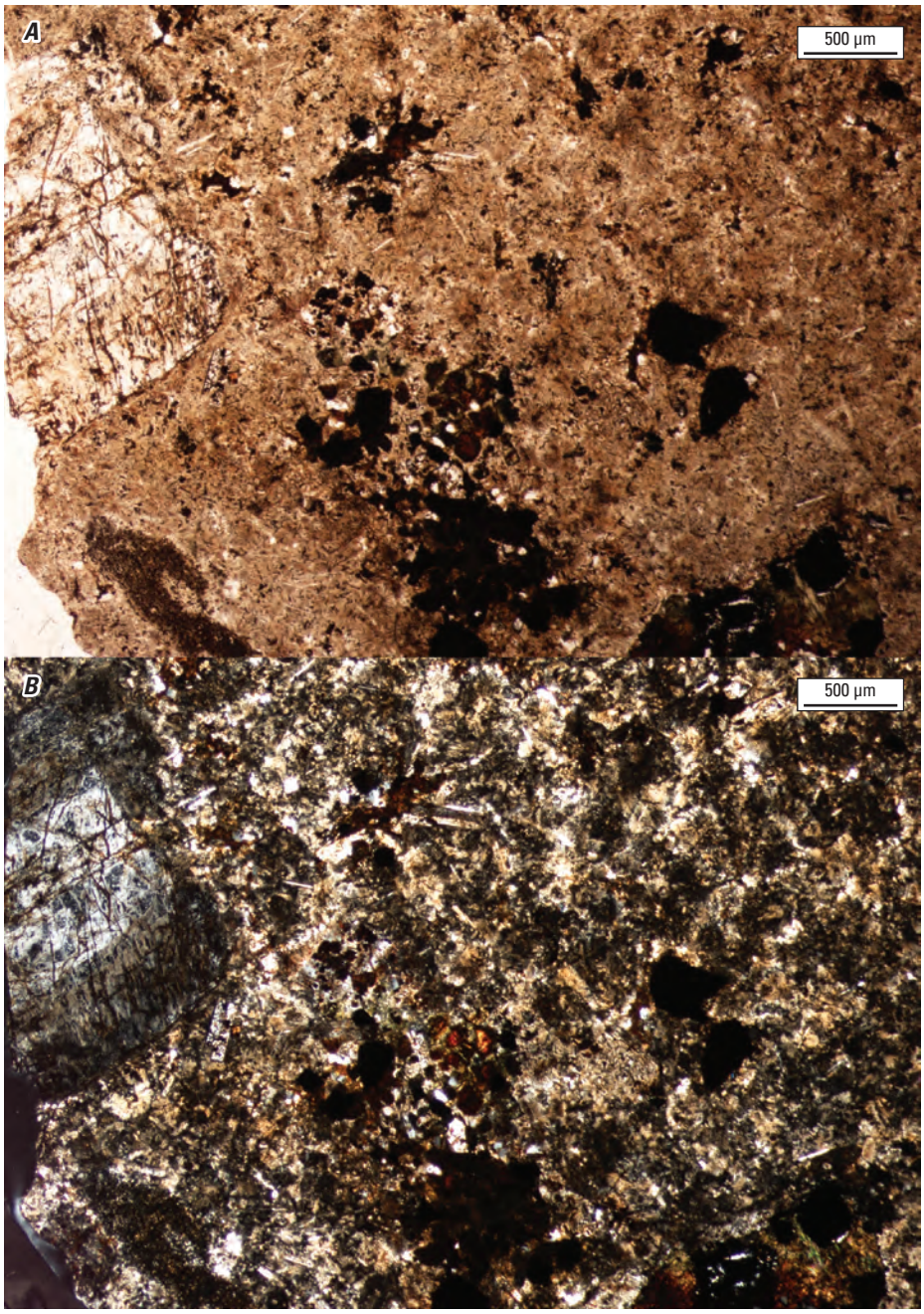

Figure 122. Pair of thin section photomicrographs of rhyolite from borehole W1411 from 8,744 to 8,750 feet depth in plane-polarized light (*A*) and cross-polarized light (*B*). Note the oscillatory zoning in the plagioclase phenocryst on the left side. Term: µm, micrometer. Photomicrographs by Ryan Deasy, U.S. Geological Survey.

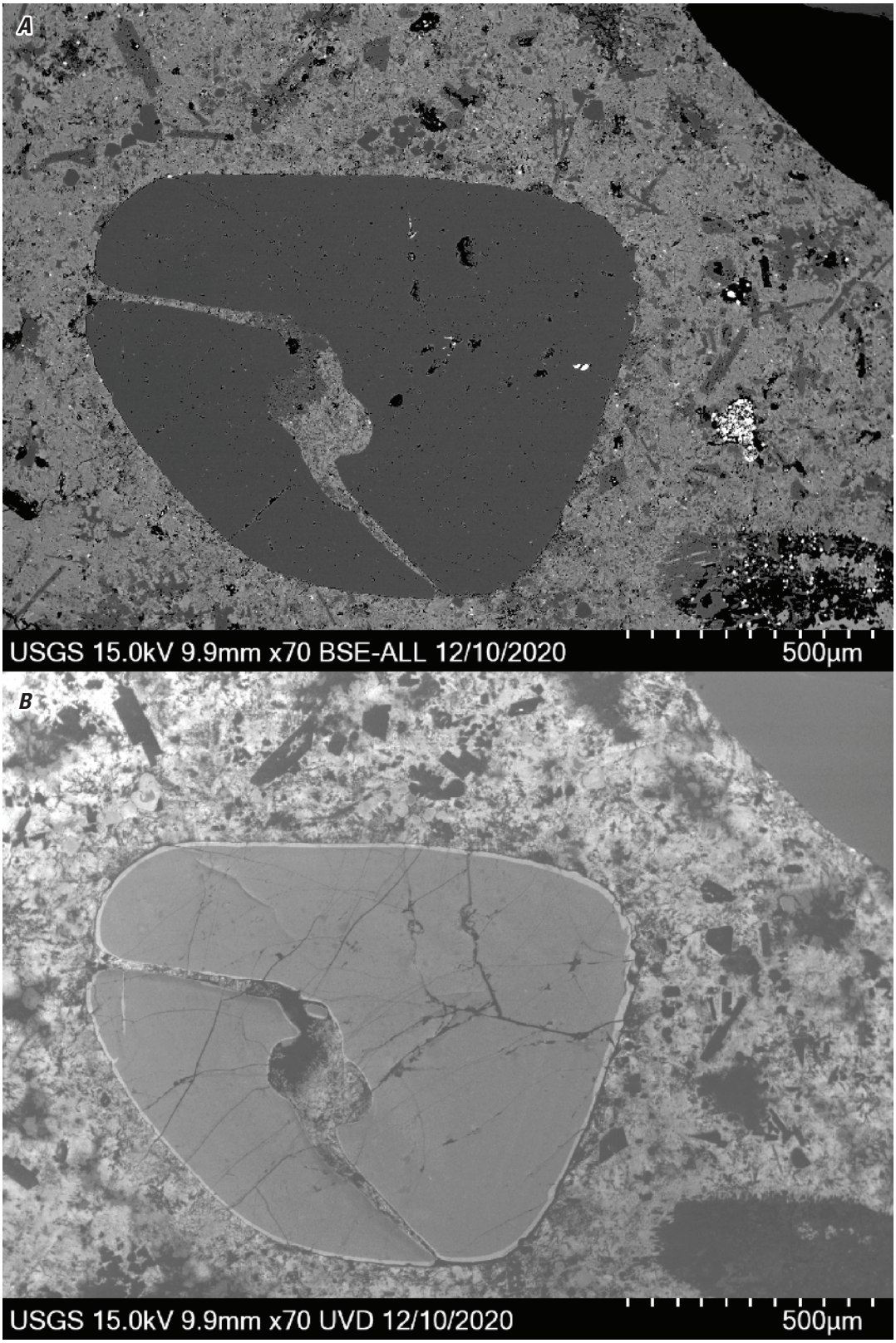

Figure 123. Pair of images of a xenocrystic/detrital rounded quartz grain in rhyolite from borehole W1411 from 8,744 to 8,750 feet depth in back-scattered electron (BSE) (*A*) and cathodoluminescence (*B*). Text in the bottom left of each image identifies data source (USGS); operating conditions including beam potential in kilovolts (15.0 kV), working distance in millimeters (9.9 mm), and image magnification in multiples of actual size (70 times); and date of acquisition (12/10/2020). Terms: USGS, U.S. Geological Survey; kV, kilovolt; mm, millimeter; BSE-ALL, back-scattered electron, all energies µm, micrometer. Photomicrographs by Ryan Deasy, U.S. Geological Survey.

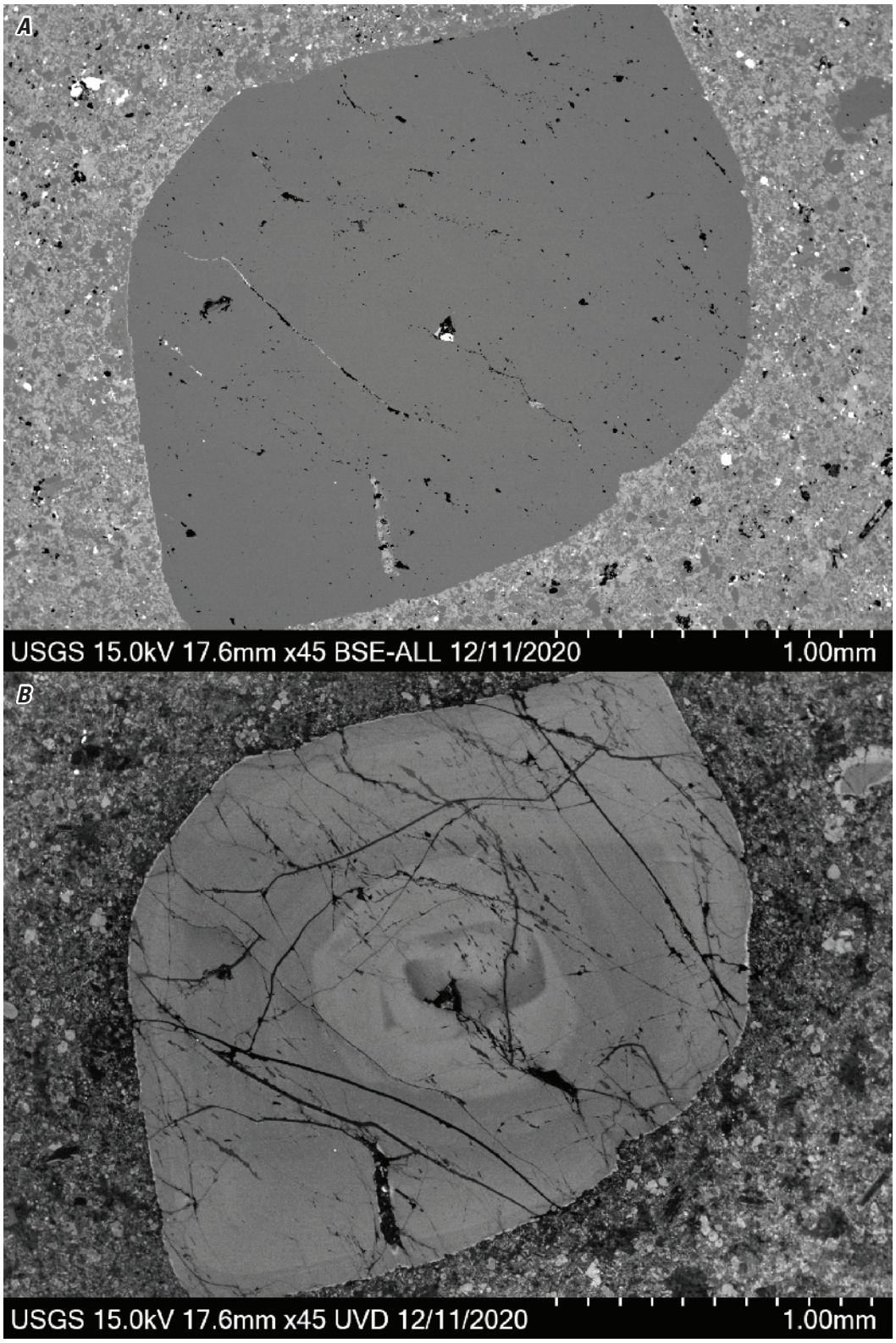

Figure 124. Pair of images of a subhedral, zoned magmatic quartz grain with oscillatory zoning in rhyolite from borehole W1411 from 8,750 to 8,753 feet depth in back-scattered electron (BSE) (*A*) and cathodoluminescence (*B*). Text in the bottom left of each image identifies data source (USGS); operating conditions including beam potential in kilovolts (15.0 kV), working distance in millimeters (17.6 mm), and image magnification in multiples of actual size (45 times); and date of acquisition (12/11/2020). Terms: USGS, U.S. Geological Survey; kV, kilovolt; mm, millimeter; BSE-ALL, back-scattered electron, all energies; UVD, ultra variable-pressure detector. Photomicrographs by Ryan Deasy, U.S. Geological Survey.

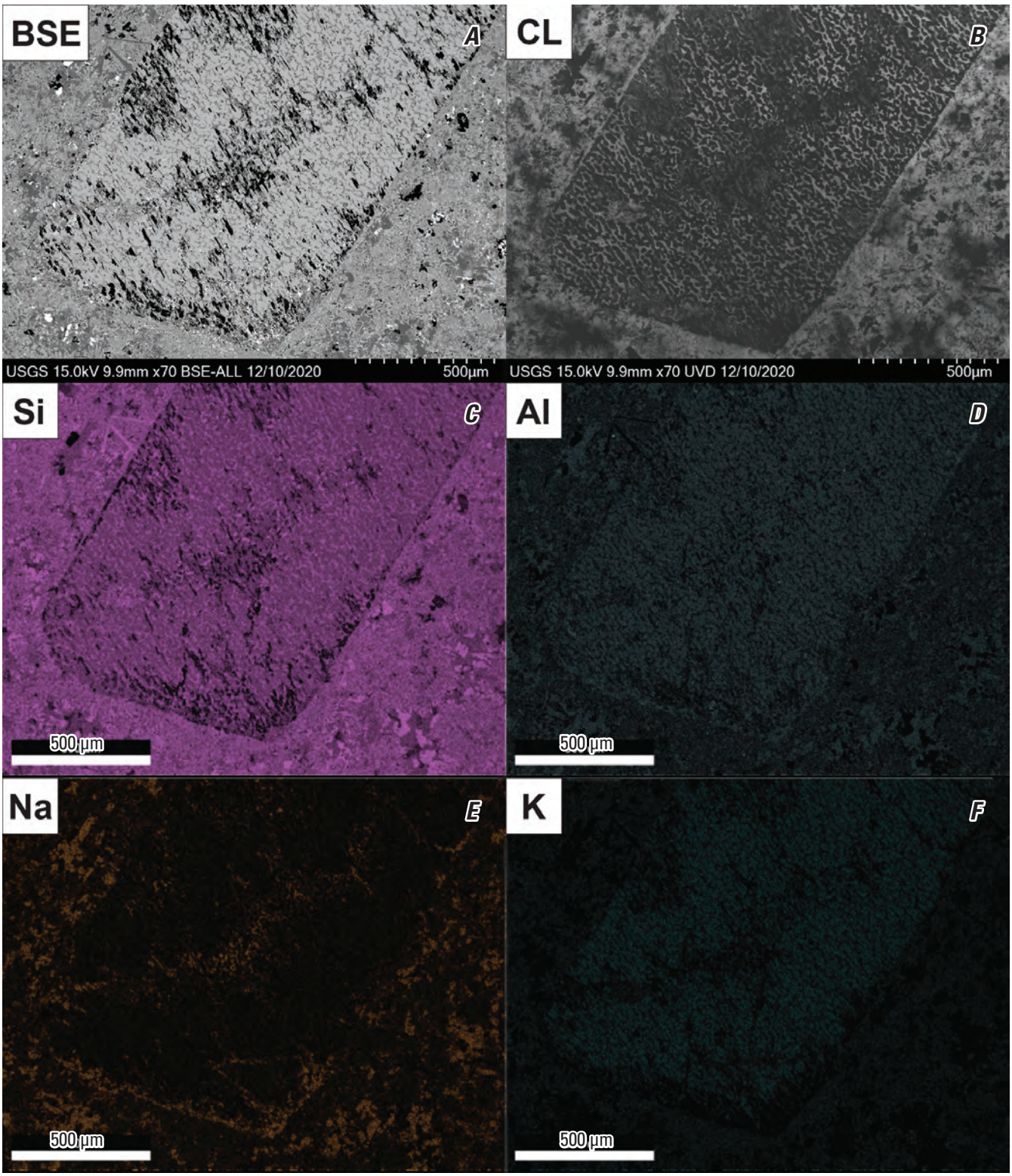

Figure 125. Back-scattered electron (BSE) (*A*), cathodoluminescence (CL) (*B*), and selected element maps from energy dispersive spectroscopy (*C*–*F*) of a potassium feldspar phenocryst from borehole W1411 from 8,744 to 8,750 feet depth. A network of quartz lamellae is dim in BSE (part *A*) and bright in CL (part *B*). Text in the bottom left of parts *A* and *B* identifies data source (USGS); operating conditions including beam potential in kilovolts (15.0 kV), working distance in millimeters (9.9 mm), and image magnification in multiples of actual size (70 times); and date of acquisition (12/10/2020). Terms: Si, silicon; Al, aluminum; Na, sodium; K, potassium; USGS, U.S. Geological Survey; kV, kilovolt; mm, millimeter; BSE-ALL, back-scattered electron, all energies; UVD, ultra variable-pressure detector; µm, micrometer. Photomicrographs by Ryan Deasy, U.S. Geological Survey.

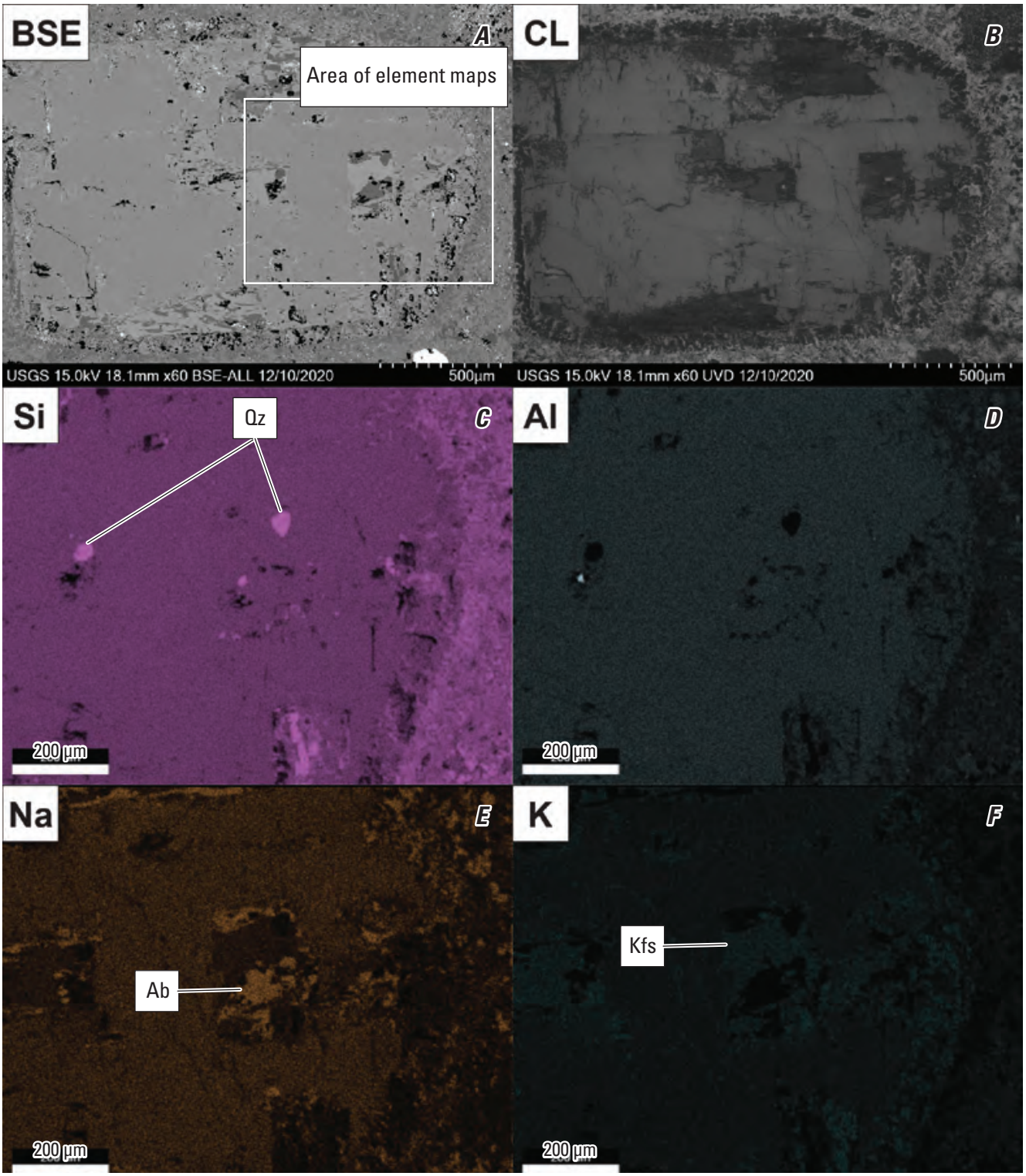

Figure 126. Back-scattered electron (BSE) (*A*), cathodoluminescence (CL) (*B*), and selected element maps from energy dispersive spectroscopy (*C*–*F*) of a plagioclase phenocryst from borehole W1411 from 8,744 to 8,750 feet depth. The extent of parts *C*–*F* are shown in part *A*. Patchy exsolved domains include quartz (Qz), albite (Ab), and potassium feldspar (Kfs); exsolved minerals are labeled where they appear brightest for clarity. Text in the bottom left of parts *A* and *B* identifies data source (USGS); operating conditions including beam potential in kilovolts (15.0 kV), working distance in millimeters (18.1 mm), and image magnification in multiples of actual size (60 times); and date of acquisition (12/10/2020). Terms: Si, silicon; Al, aluminum; Na, sodium; K, potassium; Qz, quartz; Ab, albite; Kfs, potassium feldspar; USGS, U.S. Geological Survey; kV, kilovolt; mm, millimeter; BSE-ALL, back-scattered electron, all energies; UVD, ultra variable-pressure detector; µm, micrometer. Photomicrographs by Ryan Deasy, U.S. Geological Survey.

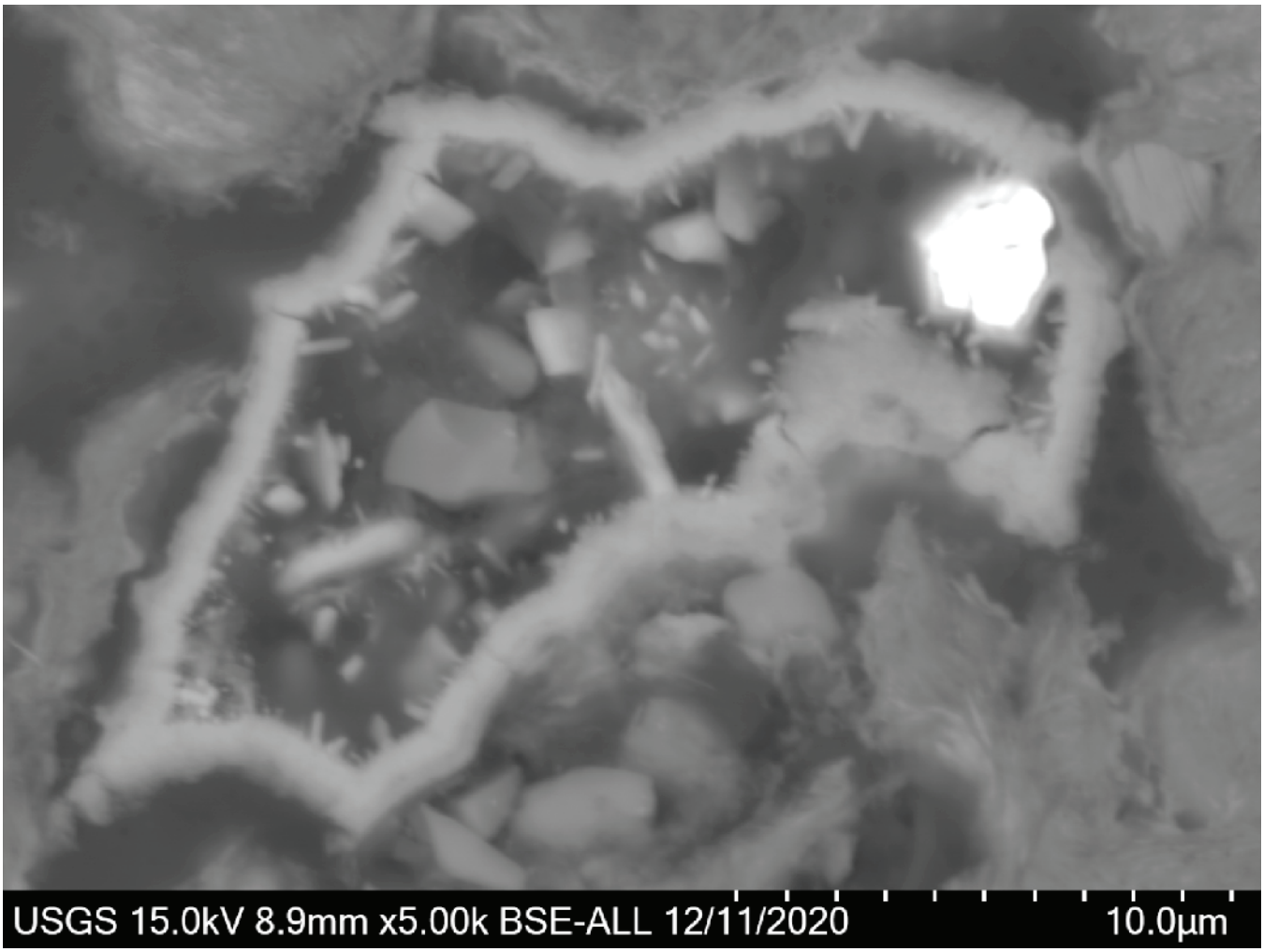

Figure 127. Back-scattered electron (BSE) image of a quartz-lined vug in a sample from borehole W1411 from 8,744 to 8,750 feet depth. The bright mineral is a rare-earth-element carbonate (bastnaesite?). Text in the bottom left identifies data source (USGS); operating conditions including beam potential in kilovolts (15.0 kV), working distance in millimeters (8.9 mm), and image magnification in multiples of actual size (5,000 times); and date of acquisition (12/11/2020). Terms: USGS, U.S. Geological Survey; kV, kilovolt; mm, millimeter; BSE-ALL, back-scattered electron, all energies; µm, micrometer. Photomicrograph by Ryan Deasy, U.S. Geological Survey.

References Cited

Applin, P.L., 1951, Preliminary report on buried pre-Mesozoic rocks in Florida and adjacent states: U.S. Geological Survey Circular 91, 28 p., accessed February 1, 2022, at https://doi.org/10.3133/cir91.

Arthur, J.D., 1988, Petrogenesis of early Mesozoic tholeiite in the Florida basement and an overview of Florida basement geology: Florida Geological Survey, Report of Investigation 97, 39 p., accessed September 29, 2021, at https://ufdc.ufl.edu/UF00001284/00001.

Barnett, R.S., 1975, Basement structure of Florida and its tectonic implications: Gulf Coast Association of Geological Societies Transactions, v. 25, p. 122–142, accessed September 29, 2021, at https://archives.datapages.com/data/gcags/data/025/025001/0122.htm.

Bass, M.N., 1969, Petrography and ages of crystalline basement rocks of Florida—Some extrapolations, *in* Bass, M.N., and Cebulski, D.E., eds., Other papers on Florida and British Honduras: American Association of Petroleum Geologists Memoir, v. 11, p. 283–310.

Bruker AXS, 2011, TOPAS, ver. 5.0: Karlsruhe, Germany, Bruker AXS software release.

Carroll, D., 1963, Petrography of some sandstones and shales of Paleozoic age from borings in Florida: U.S. Geological Survey Professional Paper 454–A, 15 p., accessed September 29, 2021, at https://doi.org/10.3133/pp454A.

Dallmeyer, R.D., 1989, Contrasting accreted terranes in the Paleozoic southern Appalachian orogen, basement beneath the Atlantic and Gulf Coastal plains, and West African orogens: Precambrian Research, v. 42, nos. 3–4, p. 387–409, accessed September 29, 2021, at https://doi.org/10.1016/0301-9268(89)90021-1.

Deasy, R.T., Holm-Denoma, C., McAleer, R., Horton, J.W., Jr., and Pianowski, L., 2023, New geo- and thermochronological constraints on the architecture and evolution of the Suwannee terrane, Florida, USA [abs.]: Geological Society of America Abstracts with Programs, v. 55, no. 2. [Also available at https://doi.org/10.1130/abs/2023SE-385536.]

Deasy, R.T., Horton, J.W., Jr., Glock, S.N., and Lupo, M.E., 2024a, Geochemical data from selected pre-Middle Jurassic basement rocks beneath the Atlantic and Gulf Coastal Plains in Florida and Alabama: U.S. Geological Survey data release, accessed May 30, 2024, at https://doi.org/10.5066/P13NBKKC.

Deasy, R.T., Horton, J.W., Jr., Glock, S.N., and Lupo, M.E., 2024b, Mineral abundances of selected pre-Middle Jurassic basement rocks beneath the Atlantic and Gulf Coastal Plains in Florida and Alabama from whole-rock powder X-ray diffraction analysis and the Rietveld method: U.S. Geological Survey data release, accessed November 5, 2024, at https://doi.org/10.5066/P133DRW5.

Deasy, R.T., Horton, J.W., Jr., Glock, S.N., Lupo, M.E., Crider, E.A., Jr., and Daniels, D.L., 2026, Geologic map of pre-Middle Jurassic basement rocks beneath the Atlantic and Gulf Coastal Plains in Florida: U.S. Geological Survey Scientific Investigations Map 3543, 1 sheet, scale 1:1,000,000, 31-p. pamphlet, https://doi.org/10.3133/sim3543.

Deasy, R.T., Lupo, M.E., McAleer, R.J., and Horton, J.W., Jr., 2024c, Photographs and photomicrographs of selected pre-Middle Jurassic basement rocks beneath the Atlantic and Gulf Coastal Plains in Florida (ver. 1.1, June 2026): U.S. Geological Survey data release, accessed June 3, 2026, at https://doi.org/10.5066/P13XYCUC.

Deasy, R.T., and McAleer, R.J., 2022, Basement infrastructure of northwest Florida revealed by $^{40}Ar/^{39}Ar$ age spectra of K-feldspar and muscovite, [video, 01:27:04–01:45:01], *in* Appalachian orogenies—When and how do they start and end?: Geological Society of America video, 01:45:01, accessed April 8, 2022, at https://gsa.confex.com/gsa/2022NC/videogateway.cgi/id/5090?recordingid=5090. [Abstract for this presentation is available at https://doi.org/10.1130/abs/2022NC-373769.]

Duncan, J.G., 1998, Geological history of an accreted terrane—Stratigraphy of the north Florida basin, Suwannee terrane: Tallahassee, Fla., Florida State University, Ph.D. dissertation, 259 p., 4 pls., accessed October 16, 2024, at https://www.proquest.com/openview/f22d1ca07bca737a96c494aed7d274f9/1?pq-origsite=gscholar&cbl=18750&diss=y.

Florida Geological Survey, 2023, GEOlogic Data Enterprise System (GEODES): Florida Department of Environmental Protection web page, accessed April 13, 2023, at https://geodes.kyrasolutions.com.

Grasty, R.L., and Wilson, J.T., 1967, Ages of Florida volcanics and of opening of the Atlantic Ocean: American Geophysical Union Transactions, v. 48, no. 1, p. 212–213, accessed February 1, 2022, at https://agupubs.onlinelibrary.wiley.com/doi/epdf/10.1029/TR048i001p00003.

Heatherington, A.L., Mueller, P.A., and Nutman, A.P., 1996, Neoproterozoic magmatism in the Suwannee terrane—Implications for terrane correlation, *in* Nance, R.D., and Thompson, M.D., eds., Avalonian and related peri-Gondwanan terranes of the Circum-North Atlantic: Boulder, Colo., Geological Society of America Special Papers, v. 304, p. 257–268, accessed September 29, 2021, at https://doi.org/10.1130/SPE304.

Heatherington, A.L., Mueller, P.A., and Wooden, J.L., 2010, Alleghanian plutonism in the Suwannee terrane, USA—Implications for late Paleozoic tectonic models, *in* Tollo, R.P., Bartholomew, M.J., Hibbard, J.P., and Karabinos, P.M., eds., From Rodinia to Pangea—The Lithotectonic Record of the Appalachian Region: Geological Society of America Memoirs, v. 206, p. 607–620, accessed September 29, 2021, at https://doi.org/10.1130/2010.1206(24).

Horton, J.W., Jr., Glock, S.N., Daniels, D.L., and Deasy, R.T., 2023, Borehole data for pre-Middle Jurassic basement rocks beneath the Atlantic and Gulf Coastal Plains, Florida and Alabama (ver. 1.1, June 2026): U.S. Geological Survey data release, accessed June 3, 2026, at https://doi.org/10.5066/P9VBO427.

Lloyd, J.M., 1985, Annotated bibliography of Florida basement geology and related regional and tectonic studies: Florida Geological Survey Information Circular, no. 98, 72 p., accessed September 29, 2021, at https://ufdc.ufl.edu/UF00001159/00001.

Malvern Panalytical, 2018, HighScore Plus, ver. 4.7: Almelo, The Netherlands, Malvern Panalytical software release.

Milton, C., 1972, Igneous and metamorphic basement rocks of Florida: Florida Geological Survey Bulletin, no. 55, 124 p., accessed September 29, 2021, at https://ufdc.ufl.edu/UF00000245/00001/5j.

Milton, C., and Grasty, R., 1969, "Basement" rocks of Florida and Georgia: American Association of Petroleum Geologists Bulletin, v. 53, no. 12, p. 2483–2493, accessed September 29, 2021, at http://archives.datapages.com/data/bulletns/1968-70/data/pg/0053/0012/2450/2483.htm?q=%2BtextStrip%3Amilton+textStrip%3Agrasty.

Moore, D.M., and Reynolds, R.C., Jr., 1997, X-ray diffraction and the identification and analysis of clay minerals (2d ed.): New York, Oxford University Press, 378 p.

Mueller, P.A., and Porch, J.W., 1983, Tectonic implications of Paleozoic and Mesozoic igneous rocks in the subsurface of peninsular Florida: Gulf Coast Association of Geological Societies Transactions, v. 33, p. 169–173, accessed September 29, 2021, at http://archives.datapages.com/data/gcags/data/033/033001/0169.htm?q=%2BtextStrip%3Amueller+textStrip%3Aporch.

Mueller, P.A., Heatherington, A.L., Foster, D.A., Thomas, W.A., and Wooden, J.L., 2014, The Suwannee suture—Significance for Gondwana-Laurentia terrane transfer and formation of Pangaea: Gondwana Research, v. 26, no. 1, p. 365–373. [Also available at https://www.sciencedirect.com/science/article/abs/pii/S1342937X13002232.]

Mueller, P.A., Heatherington, A.L., Wooden, J.L., Shuster, R.D., Nutman, A.P., and Williams, I.S., 1994, Precambrian zircons from the Florida basement—A Gondwanan connection: Geology, v. 22, no. 2, p. 119–122. [Also available at https://doi.org/10.1130/0091-7613(1994)022%3C0119:PZFTFB%3E2.3.CO;2.]

Warr, L.N., 2020, Recommended abbreviations for the names of clay minerals and associated phases: Clay Minerals, v. 55, no. 3, p. 261–264. [Also available at https://doi.org/10.1180/clm.2020.30.]

Whitney, D.L., and Evans, B.W., 2010, Abbreviations for names of rock-forming minerals: American Mineralogist, v. 95, no. 1, p. 185–187, accessed September 29, 2021, at https://doi.org/10.2138/am.2010.3371.

Winston, G.O., 1992, "African" Paleozoic sedimentary rocks of the west Suwannee basin—Florida, Alabama, and Georgia: Coral Gables, Fla., Miami Geological Society, 25 p.

For additional information, contact:
Director, Florence Bascom Geoscience Center
U.S. Geological Survey
12201 Sunrise Valley Drive
MS 926A
Reston, VA 20192

Or visit our website at:
https://www.usgs.gov/centers/fbgc

Publishing support provided by the
Reston Publishing Service Center

ISSN 2771-9448 (online)
https://doi.org/10.3133/dr1209